Deepwater Horizon Release Estimate of Rate by PIV

July 21, 2010

Plume Team - FRTG

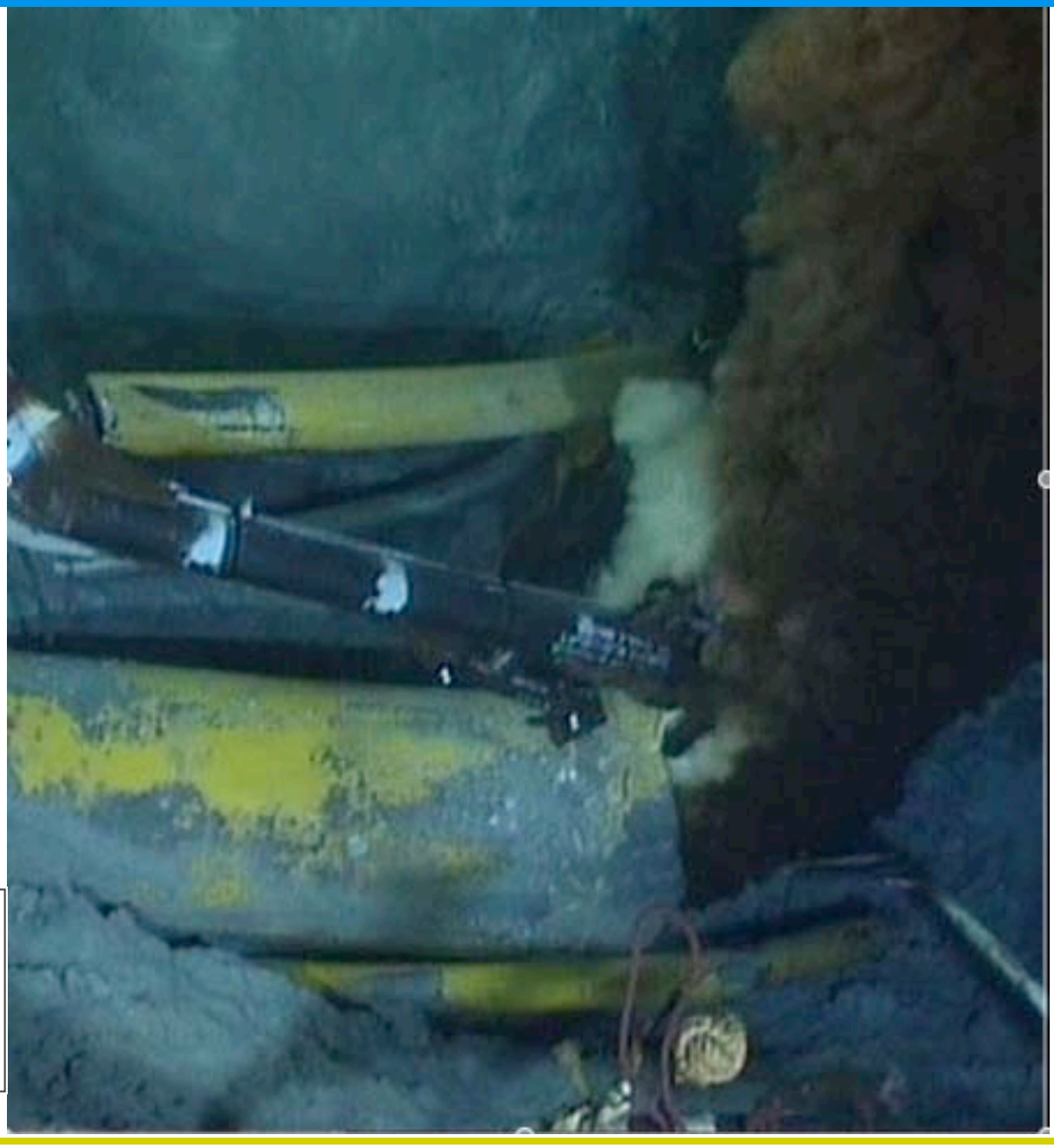

Report to

Dr. Marcia Mcnutt, USGS Director and Science Advisor to the Secretary of the Interior
Lead to the National Incident Command Flow Rate Technical Group

Prepared by

Plume Calculation Team

Aliseda, Alberto	Assistant Professor of Mechanical Engineering, University of Washington
Bommer, Paul	Senior Lecturer, Petroleum and Geosystems Engineering, University of Texas at Austin
Espina, Pedro	National Institute of Standards and Technology
Flores, Oscar	Department of Mechanical Engineering at University of Washington
Lasheras, Juan C.	Penner Distinguished Professor of Engineering and Applied Sciences, University of California at San Diego
Lehr , Bill (Lead)	Senior Scientist, National Oceanic and Atmospheric Administration Office of Response and Restoration
Leifer, Ira	Associate Researcher, Marine Science Institute and Institute for Crustal Studies, University of California, Santa Barbara
Possolo, Antonio	National Institute of Standards and Technology
Riley, James	PACCAR Professor of Mechanical Engineering, University of Washington
Savas, Omer	Professor of Mechanical Engineering, University of California at Berkeley
Shaffer, Franklin	Department of Energy National Energy Technology Laboratory
Wereley, Steve	Professor of Mechanical Engineering, Purdue University
Yapa, Poojitha	Professor of Civil and Environmental Engineering, Clarkson University

All the calculations and conclusions is this report are preliminary, and intended for the purpose, and only for the purpose, of aiding the response team in assessing the extent of the spilled oil for ongoing response efforts. Other applications of this report are not authorized and are not considered valid. Because of time constraints and limitations of data available to the experts, many of their estimates are only approximate, subject to revision, and certainly should not be used as the federal government's final values for assessing volume of the spill or its impact to the environment or to coastal communities. Each expert that contributed to this report reserves the right to alter his conclusions based upon further analysis or additional information. Note that this version of the report was modified post-July 21, 2010 to correct a typographic error on page 3 and clarify a point about the DOE team data on page 16.

Table of Contents

Executive Summary

The plume modeling team observed video both before and after the cutting of the riser pipe. The 'before' video looked at the end of the original riser leak and from the kink in the riser and from the kink leak above the Blowout Preventer (BOP). The later video examined the leakage shortly after the severing operation but before any capping operation.

The main method employed to make estimates was a common fluid dynamic technique called particle image velocimetry (PIV). While difficult in practice, it is simple in principle. A flow event, e.g., an eddy or other identifiable item, is observed at two consecutive video frames. Distance moved per time between frames gives a velocity, after adjustment for viewing angle and other factors. Repeated measurement over time and space give an estimated mean flow. Flow multiplied by cross-section area of the plume gives a volume flux.

Because of time and other constraints, only a small segment of the leakage time was examined, and assumptions were made that may through later information or analysis be shown to be invalid. For example, the Team assumes that the average flow between the start of the incident and the insertion of the Riser Insert Tube Tool (RITT) was relatively constant and the time frames that were included in the examined videos were representative of that average. If this were not true, then the actual spillage may differ significantly from the values stated below.

Most of the experts, using the limited data available and with a small amount of time to process that data, concluded that the best estimate for the average flow rate for the leakage prior to the insertion of the RITT was between 25 to 30 thousand bbl/day. However, it is possible that the spillage could have been as little as 20,000 bbl/day or as large 40,000 bbl/day. Further analysis of the existing data and of other videos not yet viewed may allow a refinement of these numbers.

The video of the post-cut was of higher quality than earlier video. The best estimate of the PIV experts was for a flow of 35,000 to 45,000 bbl with the possibility that the leak could be as large as 50,000 bbl/day. After consultation with groups from the Department of Energy that were using pressure readings from inside the Top Hat to estimate flow, a joint estimated range of 35,000 to 60,000 bbl was provided to the National Incident Command (NIC).

Deepwater Horizon, on fire after the explosion

Background

When the Deepwater Horizon drilling unit sank in the Gulf of Mexico, initial loss estimates were given as 1000 bbl/day. By April 26, it was obvious that this estimate was too low. Based upon visual observations of oil on the surface, a working number of 5000 bbl/day was adopted. However, the large amount of surface oil, the volume recovered or burned, and a re-examination of the pipe leakage, convinced the National Incident Command (NIC) that it was necessary to revisit the 5000 bbl/day number.

On May 19, the NIC Interagency Solutions Group established the Flow Rate Technical Group that has as one of its subgroups the Plume Team represented in this report. Experts on fluid dynamics, subsurface well blowouts, petroleum engineering and oil spill behavior were assembled as part of a larger effort to improve spill size estimation. The team consists of both government scientists and leading scholars at academic institutions throughout the United States.

On May 27, the Team issued an Interim Report that established an estimated range for the minimum possible spillage rate but did not issue an estimate for a possible maximum value because the quality and length of the video data could not support a reliable calculation. Instead, they requested, and received, more extensive videos from British Petroleum (BP). See Table 1.

Table 1: List of Video Segments on BP-Provided Hard-Drive

subsea 7 | DVR REGISTER

Project Title	Deepwater Horizon	Project No.	TC1024
Archive Name	BP_Deepwater_Horizon	Client	BP
Vessel	Skandi Neptune		

Transmittal: TC1024/BP/DW/TRANS/007 To S. Dietz 24/05/2010

Seagate 500Gb Drive Contents

Directory Name	Start KP	End KP	Dive	Date	Time Start	Time End	Remarks
On First RAID Drive, Retrieved from LTO4 tapes 4 and 5							
A.Plume_Monitoring	NA	NA	H14005	11/05/2010	07:22	08:22	Large Plume Monitoring, Measurment Ops
A.Plume_Monitoring	NA	NA	H14005	12/05/2010	08:03	08:33	Large Plume Monitoring
A.Plume_Monitoring	NA	NA	H14006	12/05/2010	10:04	11:04	Large Plume Monitoring
Retrieved from Second RAID Drive (In use on Skandi Neptune as of 24/05/10)							
A.Plume_Monitoring	NA	NA	H14006	13/05/2010	18:08	18:50	Large Plume Monitoring
A.Plume_Monitoring	NA	NA	H14006	13-14/05/2010	20:38	06:28	Large Plume Monitoring
D.Chemical_Dispersing_Ops	NA	NA	H14008	14/05/2010	15:27	16:30	Dispersion at Large Plume
D.Chemical_Dispersing_Ops	NA	NA	H8030	14/05/2010	15:54	16:17	Dispersion at Large Plume
J.Plume_Test_with_Oil	NA	NA	H14006	14/05/2010	16:30	20:25	Plume testing with Oil
A.Plume_Monitoring	NA	NA	H14006	14-15/05/2010	20:25	01:03	Plume Monitoring
I.Dredging_Ops	NA	NA	H8032	15/05/2010	01:22	02:52	Dredging Ops
D.Chemical_Dispersing_Ops	NA	NA	H8032	15/05/2010	02:52	03:42	Dispersion at Large Plume
D.Chemical_Dispersing_Ops	NA	NA	H14007	15/05/2010	03:45	14:38	Dispersion at Large Plume
I.Dredging_Ops	NA	NA	H8032	15/05/2010	03:53	06:26	Dredging Ops
I.Dredging_Ops	NA	NA	H8034	15/05/2010	06:32	10:11	Dredging Ops
I.Dredging_Ops	NA	NA	H8035	15/05/2010	12:45	14:31	Dredging Ops
H.Special Task/C.Hose Installation	NA	NA	H14007	15/05/2010	14:38	18:50	Second 600 hose installation
A.Plume_Monitoring	NA	NA	H14007	15-16/05/2010	16:50	01:15	BOP Monitoring (First 1/2 hour is debris)
K.Debris_Inspection	NA	NA	H8035	16/05/2010	18:56	19:31	Debris Inspection
A.Plume_Monitoring	NA	NA	H8035	15-16/05/2010	22:58	01:15	BOP Monitoring

After May 16, the Riser Insert Tube Tool (RITT) was placed into the riser at the main leak point, reducing the oil being released into the environment from this source. The recovery rate of gas and oil for the tube between the insertion and May 25 is shown below.

Table 2: Gas and Oil Flow Rates from the Riser Insert Tube Tool

Date	Oil (bo)	Gas (mmcf)	Oil + Gas (boe)	Gas Portion (%)	High Oil (bopd)	Low Oil (bopd)	High Gas (mmcf/d)	Low Gas (mmcf/d)
16-May-2010	290	0.9	440	34%				
17-May-2010	1,410	3.5	2,015	30%				
18-May-2010	1,930	10.4	3,721	48%	2,191	1,066	12.5	5.3
19-May-2010	3,014	17.5	6,025	50%	4,102	1,521	23.2	10.5
20-May-2010	2,185	15.6	4,882	55%	5,389	44	32.4	4.4
21-May-2010	2,173	4.9	3,025	28%	3,599	646	7.6	1.8
22-May-2010	1,361	7.1	2,586	47%	4,531	0	14.7	2.0
23-May-2010	1,120	2.9	1,616	31%	3,103	0	5.6	2.0
24-May-2010	6,078	9.8	7,771	22%	8,961	2,523	16.1	2.0
25-May-2010	2,596	15.8	5,316	51%	7,337	877	30.4	9.4
Total	22,158	88.4	37,397	41%	8,961	0	32.4	1.8
Average	2,430	9.7	4,106	40%				

As can be seen from Table 2, the amount of oil and gas fluctuated significantly. Part of this fluctuation was due to movement of the end of the RITT in the riser due to tidal effects and the natural separation of the oil from the gas in the riser (gas tends to rise to the top). However, examination of the videos also shows significant intermittency in the gas fraction of the flow.

During the time period of the videos examined by the Team, there were two main leak points, shown in Figure 1. The figure also displays the ultimate fate of the released fluid and gas. The main leak, until the most recent severing operation, came from the broken end of the riser, some distance away from the Blowout Preventer (BOP). The leakage was only from the annulus (inside pipe diameter of nineteen and a half inches) surrounding an interior drill pipe (pipe diameter of six and five eighth inches). According to BP, the mouth of the riser was damaged in the initial incident, reducing the cross-sectional area by 30%. Figure 2 shows the damaged riser. After May 1, and perhaps earlier, a second leak source appeared in the kinked riser above the BOP. The number of holes and leakage volume in the kink has increased over time, as BP has attempted to stop oil release by such operations as the RITT and Top Kill.

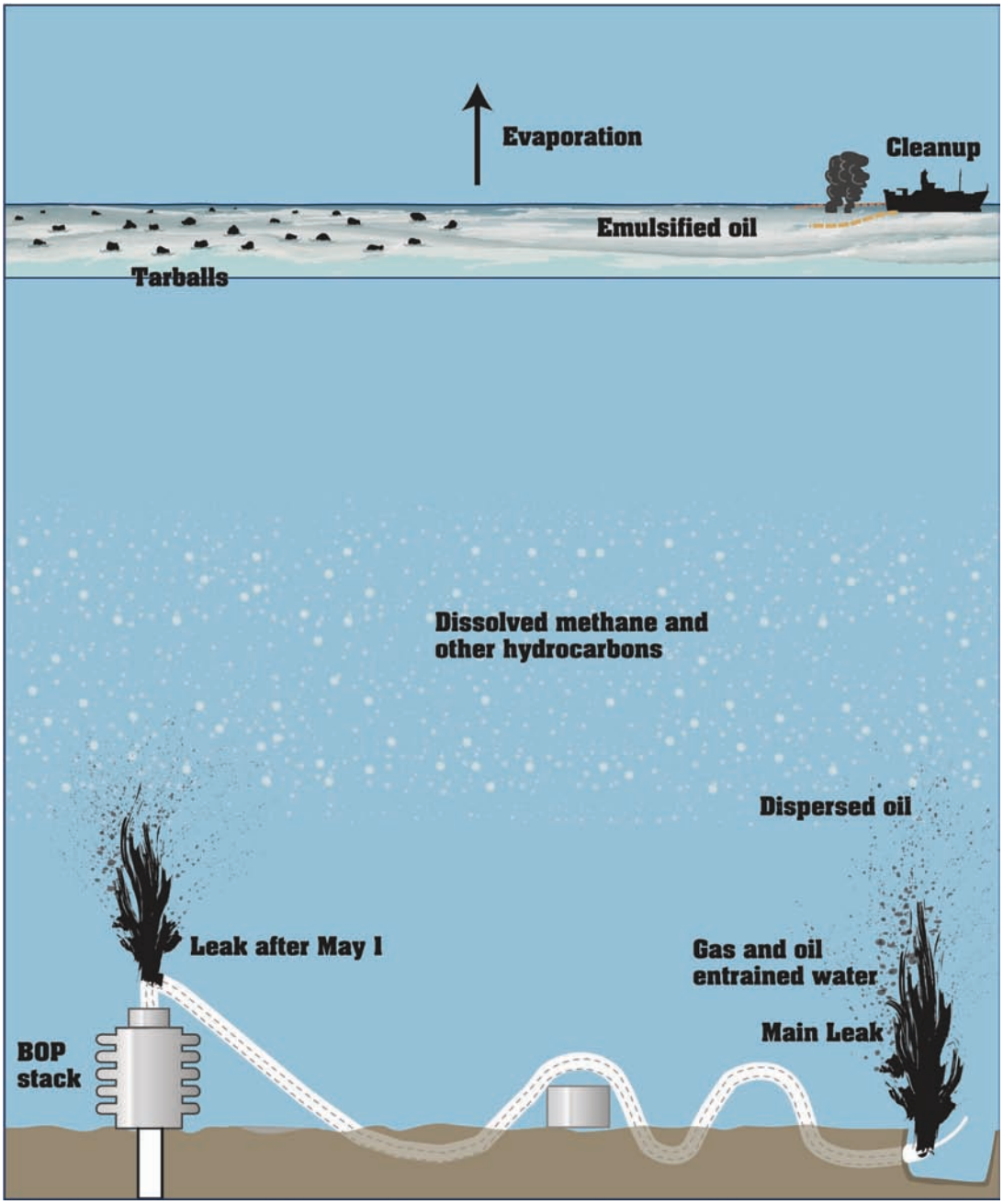

Figure 1: Graphic Showing Leaks and Oil Fate

At certain times, a dispersant wand was inserted in the plume and dispersant added. These chemicals are designed to lower surface tension and reduce the average oil droplet size. Unfortunately for flow rate estimation, they add an additional component to the flow and produce a less defined plume. Measurements were not done using video while dispersant was being applied

While particle image velocimetry (PIV), described in the next section, was the main approach to estimating the leak rate, alternative approaches were used to provide an additional credibility check on the results from the PIV method. These included looking at expected flow based upon properties of the reservoir and reservoir fluid, comparison of this release with a controlled experiment in the North Sea, using well-established similarity characteristics of turbulent jets, and calculating a possible release size, based upon surface oil and oil recovered or burned. Appendix 2 describes an estimate made using one of these alternative methods. Some of these same methods will be or are being examined by other Flow Rate Technical Group teams.

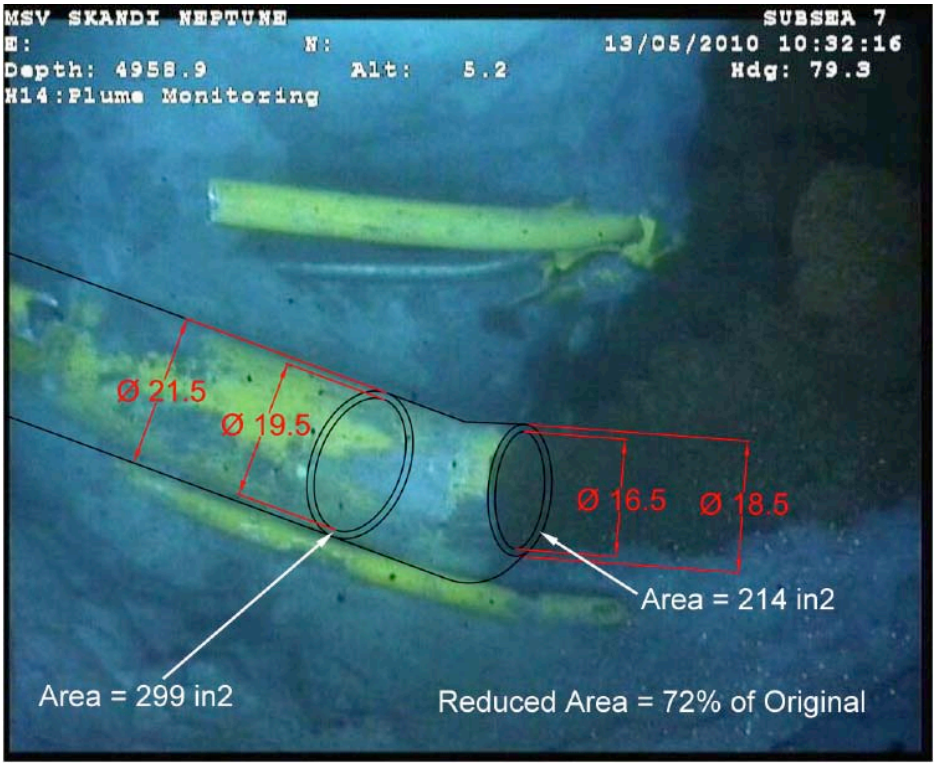

Figure 2: Riser Outlet Showing Its Reduced Cross-Sectional Area

Particle Image Velocimetry

The term particle image velocimetry was first proposed in 1984 by R. J. Adrian, a reviewer of this report. While difficult in practice, PIV is simple in principle. In this method a flow event, e.g., an eddy or other identifiable item, is observed at two consecutive video frames. Distance moved per time between frames gives a velocity, after adjustment for viewing angle and other factors. Repeated measurement over time and space give an estimated mean flow. Flow multiplied by cross-section area of the plume gives a volume flux.

Many researchers were drawn to PIV because it provided a new way to study turbulent flow structure. Turbulence is a phenomenon that is characterized by multiple length scales. To measure turbulent flow, therefore, the method must be able to operate at different scales with possible flow movement in all directions. True PIV uses small, solid particles illuminated by laser light and recorded under very short time exposures. In this instance, natural markers in the flow were employed. These markers themselves changed over time, increasing the complexity of the problem.

Figure 3 illustrates the approach. Because the flow velocity is not uniform throughout the plume, multiple locations, known as interrogation spots, must be sampled to estimate and average velocity. Similarly, the cross-sectional area is time and spatially dependent as well as having diffuse boundaries so that an average cross-section, dependent upon the location of the interrogation spots, needs to be calculated. A further challenge for measuring the flow in this case is that it is not spatially or temporally uniform in mixture of gas and fluid.

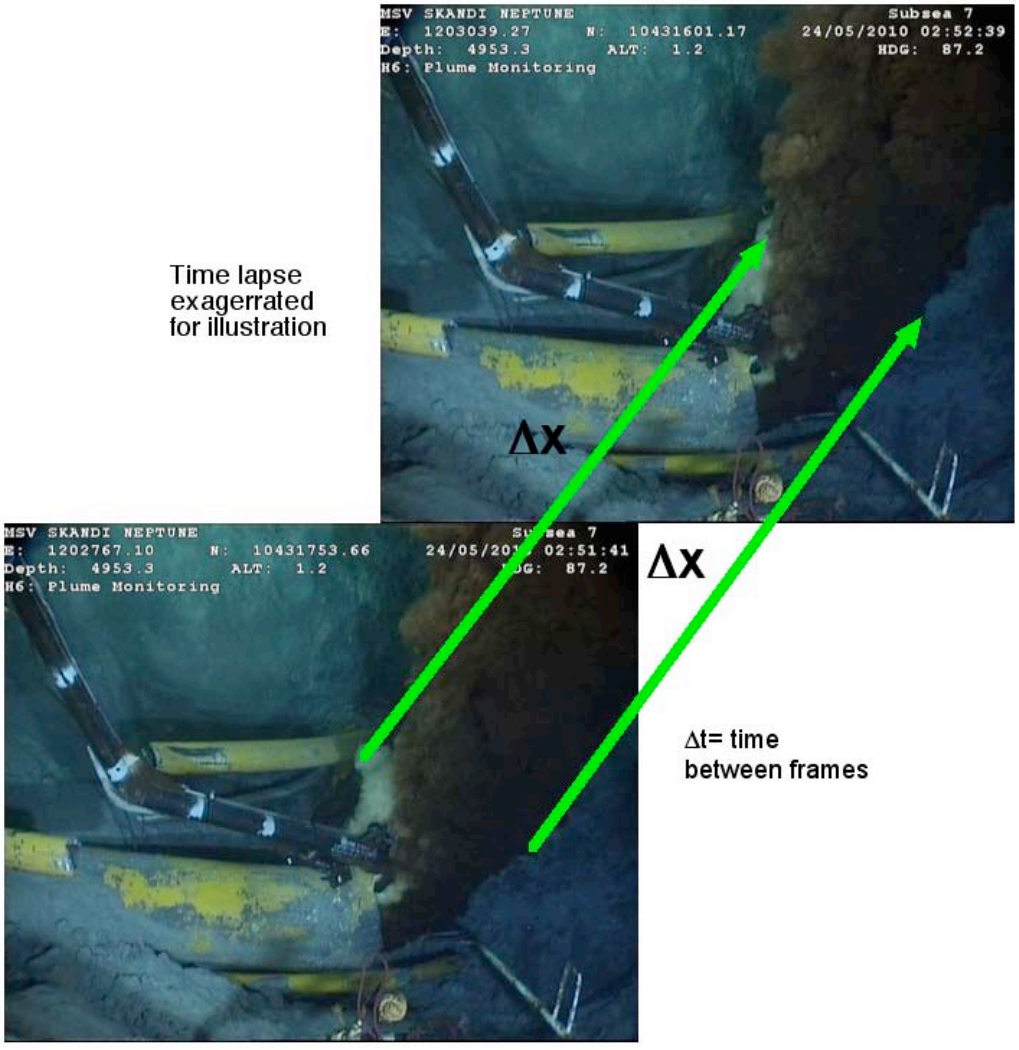

Figure 3: Illustration of Particle Image Velocimetry

For each of the interrogation sites a vector velocity $\Delta X/\Delta t$ is computed. The vector average of these velocities provides an average velocity. Combined with an average cross-section area, this yields a net flux of both gas and oil. A key parameter was this average ratio of gas to liquid. This term seemed to vary over the time period of the spill and during the time of the video clips. Increasing gas increased the velocity of the plume but decreased the mass flow. Analysis of the available short movies of the riser flow shows the existence of periods when the flow oscillates from pure gas to seemingly pure oil. This could be an indication of Slug Flow Regime. These periods of gas-oil flow fluctuation are in the range of minutes. Longer periods may also exist but would require examination of longer clips to determine.

Another key question was the fluid velocity at the interior of the jet, something that obviously could not be directly observed. The different PIV experts approached this problem in different ways. Most assumed a correction factor for the interior velocity, usually two or two multiplied by the square root of two. One expert chose larger scale structure that he believed would feel the interior flow directly so that no correction was necessary.

Kink Leak

The Kink leak began sometime around May 1. The Team has requested clarification of the exact date from BP. The number of holes in the riser pipe at the kink increased on or before May 15. The team believes that the amount of escaping oil from this source increased as the holes widened, increased in number, and as the RITT insertion placed more upstream pressure on the riser. Estimation of the flow from the kink was challenging because only one plume, labeled J1 below, was clearly visible and unobstructed in the video.

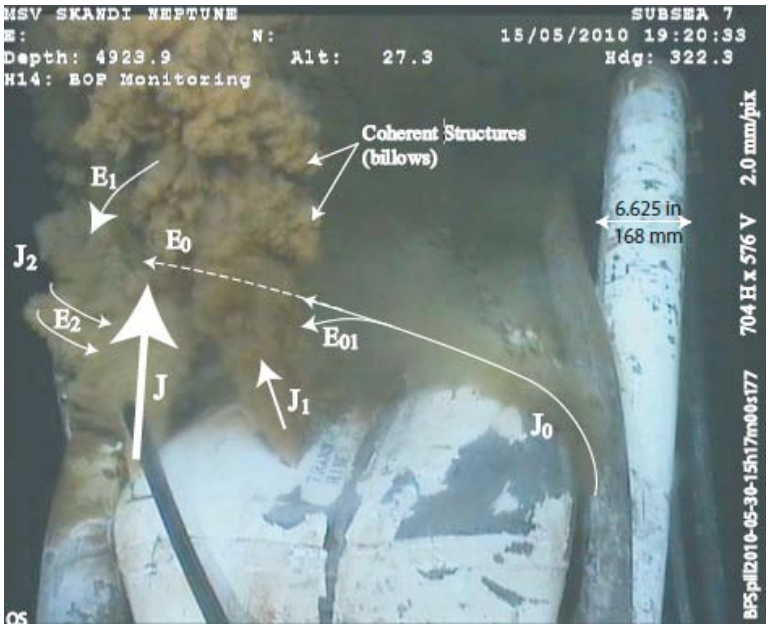

Figure 4: Kink Leak (Annotations by Savas)

New Leak at Severed Riser

By June 3, BP had severed the riser just above the BOP. According to the oil company estimates, this was expected to increase the total leak rate by approximately 20%. Surprisingly, the interior of the riser pipe contained not one, but two pieces of drill pipe inside (Figure 5). One team member speculated that the drill pipe snapped during the accident into several segments that would fit side by side inside the riser. The team requested from BP videos of the leak after the cut but before the installation of a dome designed to capture part of the flow. The damage to the riser during cutting complicated the task of estimating flow cross section.

Figure 5: Cut Riser Showing Two Pipes Inside

The quality of the video was much better for the severed riser flow than the video used for earlier estimates. This allowed for greater confidence in calculated flow. The PIV experts were able to use the visible flange and bolts as references although parallax adjustments were required. There was a noticeable difference in the color of the two distinct plumes emanating from the cut riser. BP attributed this to greater gas content in the lighter plume.

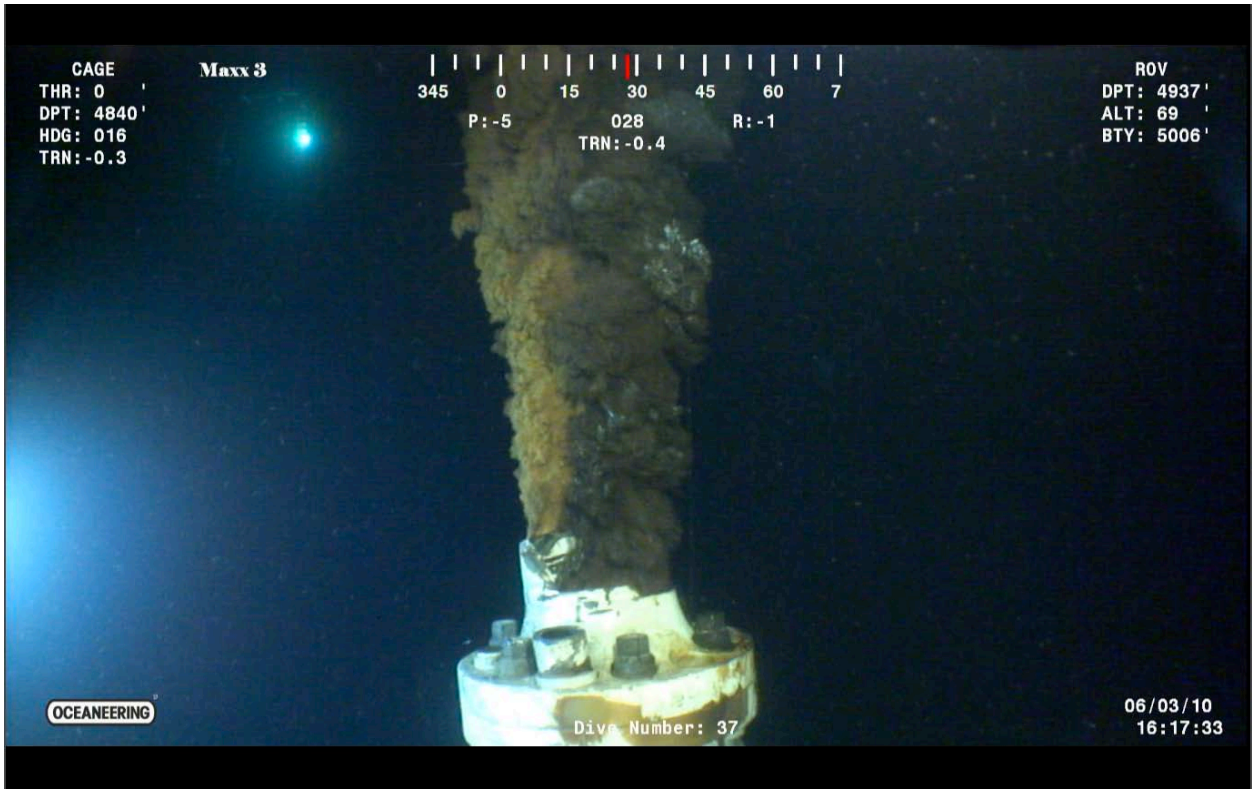

Figure 6: Cut Riser Leak

Shortly after the cut, BP placed a 'Tophat' over the riser stub, allowing the capture of some of the oil. This Tophat had vents that could be equipped with a pressure gauge, allowing an alternative method to estimate the flow. Teams affiliated with the Department of Energy, using the subsequent pressure readings to estimate flow, pooled their findings with the Plume Team results to produce a common estimate for operation purposes to the National Incident Command.

Conclusions

As with earlier estimates, the conclusions in this report are only to aid the Response, not to determine the final Federal estimate of spillage. Because of time and other constraints, only a small segment of the leakage time was examined, and assumptions were made that may through later information or analysis be shown to be invalid. For example, the Team assumes that the average flow between the start of the incident and the insertion of the RITT was relatively constant and the time frames that were included in the examined videos were representative of that average. If this were not true, then the actual spillage may differ significantly from the values stated below.

Most of the experts have concluded that, given the limited data available and the small amount of time to process that data, the best estimate for the average flow rate for the leakage prior to the insertion of the RITT is between 25 to 30 thousand bbl/day. However, it is possible that the spillage could have been as little as 20,000 bbl/day or as large 40,000 bbl/day. Further analysis of the existing data and of other videos not yet viewed may allow a refinement of these numbers.

For the time period after the riser cut, most of the experts concluded that the likely range for the flow was between 35,000 and 45,000 bbl/day but could be as high as 50,000 bbl/day.

The Plume Team then met with other experts from the Department of Energy, who employed non-PIV methods to estimate flow rate. The combined groups reached a consensus estimated flow range of 35,000 bbl/day to 60,000 bbl/day.

Appendices

Appendix 1 includes some statistical conclusions on the separate Particle Image Velocimetry (PIV) estimates, treating each estimate with equal weights. It does not necessarily represent the consensus of the Team, which has already been presented in the Conclusions. Team members who did not conduct PIV analysis—but instead served as experts to the Team on related subjects—provided Appendices 2 and 3. Appendices 4-8 describe the separate PIV results. Appendix 9 lists the biographies of the team members. Review comments are included in Appendix 10.

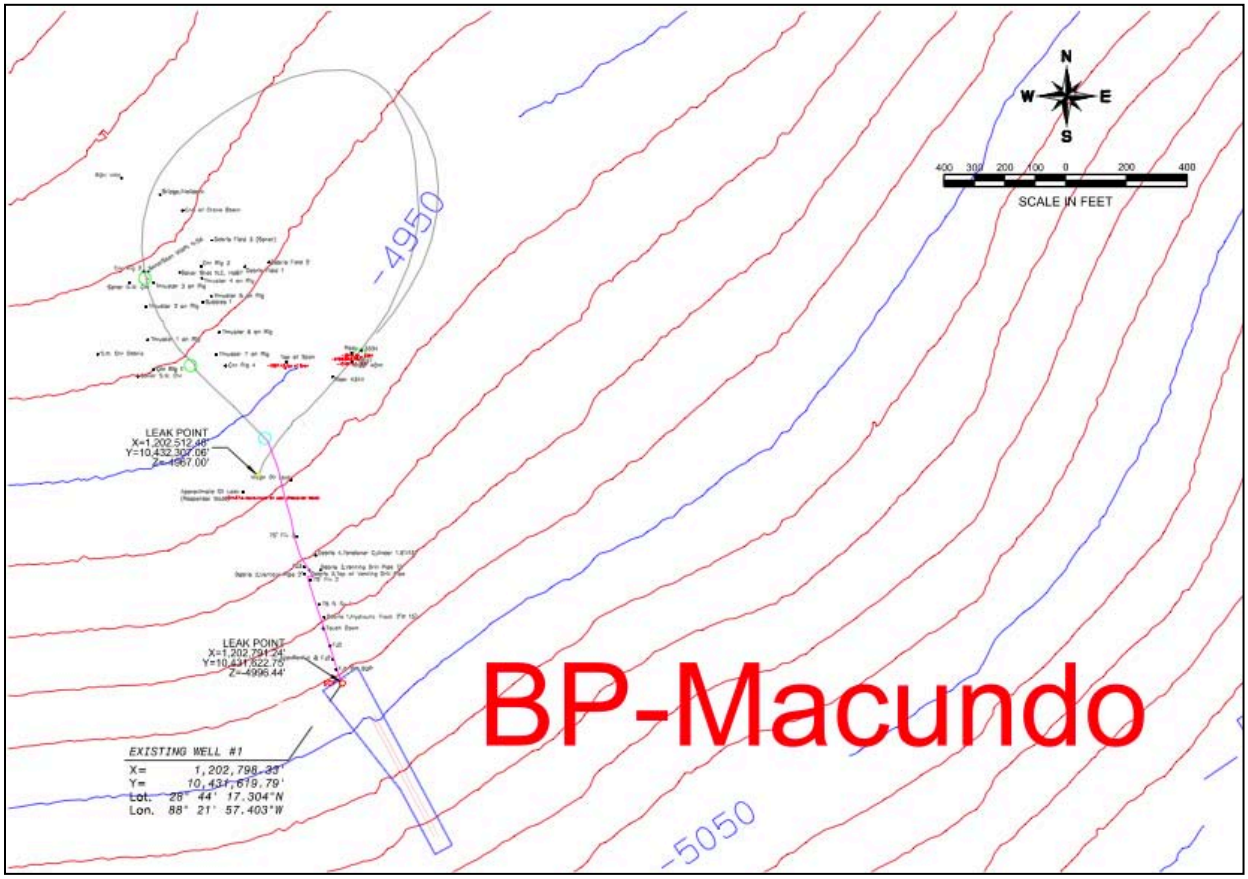

Appendix 1: NIST Statistical Analysis

Pooling Plume Team Expert Assessments

Antonio Possolo and Pedro Espina
National Institute of Standards and Technology

July 13th, 2010

Summary

In the course of the Plume Team meeting that took place in Seattle on June 13th, 2010, and subsequently during a teleconference co-chaired by U.S. Secretaries Chu and Salazar on June 14th, several members of the Plume Team produced or revised their independent measurements of the average daily volume of oil flowing from the stub left after the riser pipe was cut in preparation for deployment of the "Lower Marine Riser Package" (LMRP) containment system ("Top Hat"). More recently, two other Plume Teams produced additional, independent estimates for the same average daily volume.

A statistical method was used to reconcile the estimates produced by the Plume Team experts with one another and with the actual average daily volume being captured by the recovery vessels at the Deepwater Horizon incident site. The corresponding analysis yielded a best estimate of 46 000 bbl/day, a most likely value of 45 000 bbl/day, and an interval from 24 000 bbl/day to 123 000 bbl/day[1] that, with approximately 95 % probability, includes the true value of that average daily volume of oil.

Assessments

The following table summarizes the intervals that five experts, A–E, a subset of the Plume Team, provided during the June 13th, 2010, Plume Team meeting in Seattle, or during the teleconference co-chaired by U.S. Secretaries Chu and Salazar on June 14th. These are estimates of the average daily volume of oil flowing from the stub left after the riser pipe was cut.

Expert	Low (bbl/Day)	High (bbl/Day)	Confidence
A	24 000	40 000	Medium-High
B	24 000	40 000	Medium-High
C	24 000	40 000	Medium-High
D	42 000	49 000	Very High
E	30 000	40 000	Medium-High
F	4 375	120 625	Medium-High
G	46 000	76 000	Medium-High

[1] Standard barrels of crude oil per day.

Expert F's results were retrieved from his contribution to the Plume Team's final report, and were obtained by manual imaging velocimetry based on a video segment that is three seconds long. His estimate was 62 500 bbl/day, and he assessed the associated relative uncertainty at 93%. The low and high values in the corresponding line of the preceding table therefore are 62 500 × (1 + 0.93) = 4 375 bbl/day and 62 500 × (1 - 0.93) = 120 625 bbl/day. Expert G's results arrived on July 13th, in the form of 61 000 ± 15 000 bbl/day.

The fact that the low value for expert F, as well as some of the values simulated (as described below, under "Approach") for all the experts, was lower than the volume of oil actually being recovered from the Top Hat, is corrected in the reconciliation exercise.

The values listed above were multiplied by the factor 1.35 × (0.30 / 0.41) = 0.988 prior to reconciliation, for the reasons discussed during the teleconference of June 14th and relating to the proper conversion to barrels of oil at sea surface thermodynamic conditions, and to the use of the same volume fraction of oil in the total leak flow as used by other FRTG teams who also estimated the oil leak.

Approach

We use probability distributions to model the uncertainty implied in each expert's assessment, and apply a statistical method by Stone [1961][2] to reconcile these distributions. More specifically, we use Stone's [1961] linear pool, which is equivalent to asking each expert to cast a vote in favor of his work, where his vote is a random draw from the probability distribution that encapsulates the expert's assessment and that expresses his confidence in his results. The final result is a probability distribution that represents the Plume Team's collective state of knowledge about the average volume of oil flowing from the stub left after the riser pipe was cut.

Details

With the exception of expert D, who during the teleconference of June 14th expressed very high confidence in his assessment, the other members of the Plume Team expressed views of their work that were consistent with medium to high confidence in their assessments. We translated this "medium to high" confidence into a 65 % probability,[3] and took "very high" confidence to mean 90 % probability. This conforms to the Guidance Notes for Lead Authors of the IPCC Fourth Assessment Report on Addressing Uncertainties that have been used by the Intergovernmental Panel on Climate Change in the preparation of their fourth assessment report [Solomon et al., 2007, Table 3, *Quantitatively calibrated levels of confidence*], where "medium" is taken to mean confidence of about 50 %, "high" is taken to mean confidence of about 80 %, and "very high" is taken to mean confidence of about 90 %.

[2] Stone's [1961] method was further elaborated by Bacharach [1979], Lindley [1983], and Clemen & Winkler [1999], among others.

[3] The average of 50 % and 80 % probability.

Also assuming that the probability distributions implicit in the experts' assessments were Gaussian, and using the confidence levels just mentioned, we derived the means and standard deviations of these distributions: for example, expert A's implied mean is 31 600 bbl/day, and the implied standard deviation is 8 500 bbl/day.

We produced a statistical sample of size 1 000 000 by repeating the following two steps: (i) select one expert uniformly at random (each one with the same probability of being selected); and (ii) draw one value from the selected expert's distribution. Any values generated in this process that were less than the average daily volume of oil being recovered via the Top Hat at the time, were disregarded.

The figure depicts a smooth estimate of the probability density of the results, produced using a kernel density estimator.[4] The corresponding mean (blue dot) is 46 200 bbl/day: the interval from 24 000 bbl/day to 123 000 bbl/day (horizontal blue line) should include the true average number of barrels of oil exiting the stub of the riser pipe per day, with probability approximately 95 % (shaded area under the curve). The most probable value (where the probability density achieves its maximum), is 44 600 bbl/day (red diamond).

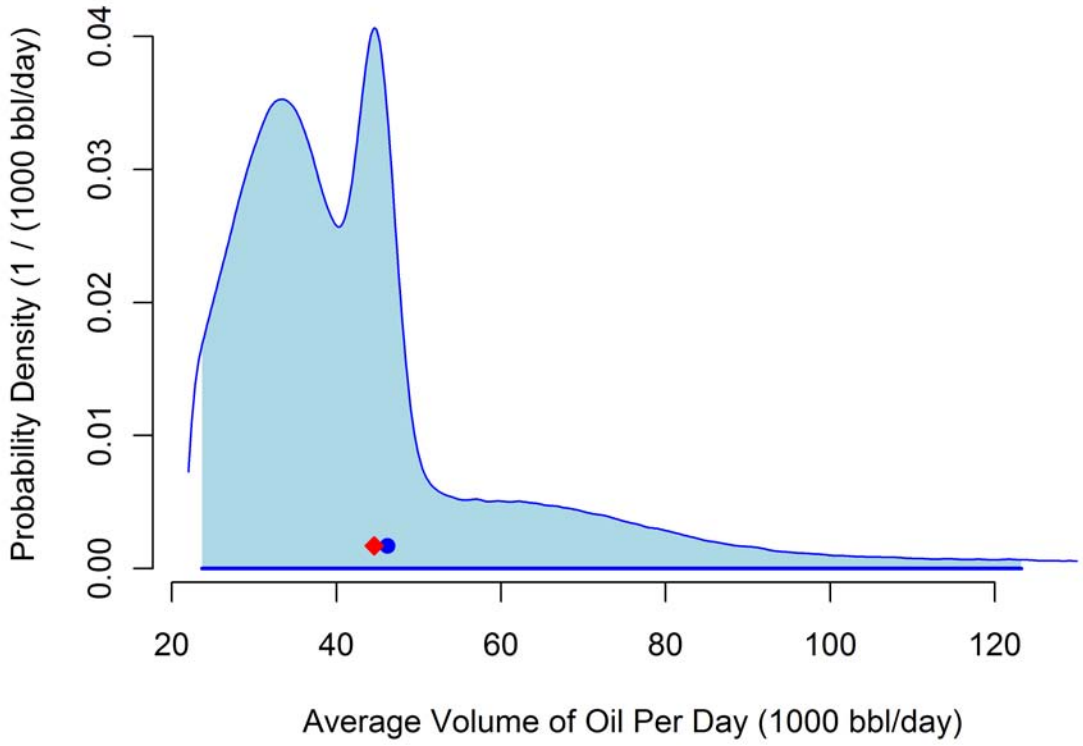

[4] As implemented in the function density of the R [R Development Core Team, 2009] environment for statistical programming, computation, and graphics.

Acknowledgments

The authors are much indebted to Dr. Blaza Toman (*Mathematical Statistician*, NIST Division 898), Dr. Michael Moldover (*NIST Fellow*, NIST Division 836), and Drs. John Wright and Aaron Johnson (NIST Division 836) for their guidance and review of this work.

References

Bacharach, M. (1979) Normal Bayesian Dialogues. *Journal of the American Statistical Association*, 74 (368): 837–846.

Clemen, R. T. and Winkler, R. L. (1999) Combining Probability Distributions from Experts in Risk Analysis. *Risk Analysis*, 19 (2), 187–203.

Lindley, D. V. (1983) Reconciliation of probability distributions. *Operations Research*, 31(5): 866–880.

R Development Core Team (2009) R: A language and environment for statistical computing. R Foundation for Statistical Computing, Vienna, Austria. ISBN 3-900051-07-0, URL http://www.R-project.org.

Solomon, S., Qin, D., Manning, M., Marquis, M., Averyt, K., Tignor, M. M. B., and Miller, H. L. (2007, editors) *Climate Change 2007 — The Physical Science Basis*. Working Group I Contribution to the Fourth Assessment Report of the Intergovernmental Panel on Climate Change (IPCC). Cambridge University Press, New York, NY, 2007.

Stone, M. (1961) The opinion pool. *Annals of Mathematical Statistics*, 32 (4): 1339–1342.

Appendix 2: Reservoir Fluid Study

Personal Work Report

To: Bill Lehr, NOAA
From: Paul Bommer, Ph.D.
Department of Petroleum and Geosystems Engineering
The University of Texas at Austin
June 2, 2010

Re: Reservoir fluid study and oil flow rate from the BP Mississippi Canyon 252 1-01 blow out.

Bill:

My approach to this problem, described in more detail below, is to determine what type of fluid is in the reservoir, construct a flow model in the reservoir, and construct a flow model through a conduit to the surface. In summary, I calculate the oil flow rate range at the top of the blow out preventers with the riser attached as between 9,200 and 22,000 stock tank (standard condition) barrels of oil per day. These results are based on the data currently available from BP and my selection of the most likely flow conduit.

The Reservoir Fluid

The reservoir is a gas – volatile oil reservoir. This is important because the reservoir fluid is actually a critical fluid in the reservoir at 11,856 psia and 243 deg F. A critical fluid is a fluid at the critical point in the reservoir meaning gas and liquid are indistinguishable from each other at this point. Two companies analyzed the reservoir fluid samples and came to only slightly different conclusions.

The first study was done by Core Labs (PENCOR) on April 22, 2010. In this study the fluid was characterized as a gas with a dew point. This can be seen in Appendix A, second page, where the percentage of liquid begins at zero at the dew point of 6,504 psia at 243 deg F. Below the dew point the liquid percentage increases rapidly to a maximum of 59.96% at 6,000 psia and 243 deg F. As pressure continues to be decreased the fluid shows a retrograde phenomena as some of the liquid vaporizes back into the gas phase with 49.63% liquid remaining at 1,000 psia and 243 deg F.

Once the gas leaves the reservoir and enters the flow conduit to the surface some cooling takes place due to the geothermal gradient and the Joule-Thompson effect if the gas is free to expand. To demonstrate the effect of cooling on the amount of liquid present a test was performed by PENCOR at 100 deg F. Using this data (see the first page of Appendix A) there is 67% liquid at 2,250 psia and 100 deg F. This pressure is chosen because it is the pressure at the ocean floor due to the weight of sea water.

The second study was performed by Schlumberger and reported on May 19, 2010. An excerpt from this study is shown in Appendix B. This study reported the reservoir as a liquid with a bubble point of 6,348 psia at 243 deg F. This means that there were gas bubbles that appeared in the test cell rather than liquid droplets as in the PENCOR test. This reinforces the notion that this is a critical fluid at reservoir conditions. The Schlumberger tests are the same type run by PENCOR except that the Schlumberger tests were all done at 243 deg F (none at 100 deg F). At the ocean floor pressure of 2,250 psia and the reservoir temperature of 243 deg F the percentage of liquid from the Schlumberger test of Appendix B is 59.7%. Please note that this compares favorably with the results form PENCOR, which under identical conditions recorded 53.8% liquid in the test cell. Therefore, I believe the fluid can be adequately described using either data set.

Both studies also performed a flash calculation from reservoir conditions to standard conditions. Partial results from the flash calculation are shown in Table 1. I have made an independent flash calculation using the base data from Schlumberger and arrived at very similar results.

Table 1: PENCOR Flash Calculation Results

Multi-Stage Separator Test

PENCOR ID No. 36126-53: 18,142 ft Depth

Separator Conditions Pressure (psia)	Separator Conditions Temperature (°F)	Liquid Density (g/cm^3)	Gas Density (g/cm^3)	Gas Gravity (Air = 1.0)	Solution GOR, R_s (scf/stb)	Solution GOR, R_s (scf/sep bbl)	Liberated GOR, R_l (scf/stb)	Separator Shrinkage (stb/bbl at P,T)
6,504	**243**	**0.528**		**N/A**	**2,554**		0	**N/A**
1,250	130	0.731	0.073	0.683	475	607	2,079	0.783
450	120	0.763	0.027	0.730	260	306	216	0.848
150	120	0.768	0.015	0.894	123	139	137	0.881
15	60	0.833	0.002	1.538	0	0	123	1.000

Summary Data

Total Solution Gas-Oil Ratio	2,554	scf/stb
Stock Tank Oil Gravity	38.2	°API at 60 °F
Formation Volume Factor	2.367	(Bbl at P_{sat} /stb)
Accumulated Gas Gravity	0.740	(Air = 1.00)
Color of Stock Tank Oil	Light Crude	

Notes:

- stb: stock tank barrel at 60 °F
- sep bbl: volume of separator liquid at P,T.
- Solution GOR is given as the gas volume per stock tank barrel (stb) and per separator barrel (sep bbl)
- Separator Volume Factor is the inverse of the Separator Shrinkage Factor
- Liberated GOR (R_l) is gas liberated from previous stage to current stage per stock tank barrel (stb)
- See following page for flash gas compositional analyses

Flash calculation results from the Schlumberger study, while not identical, are very similar to the results shown in Table 1.

The viscosity of the fluid is shown in Table 2. The average viscosity in the reservoir, between the original pressure and the flowing pressure at the bottom of the well is 0.165 cp.

Table 2: Reservoir Fluid Viscosity

Preliminary Viscosity at 243°F

PENCOR ID No. 36126-53: 18,142 ft Depth

Measured using Electro-Magnetic Viscometer

Piston used 0.2 - 2.0 cP

Pressure (psia)	Measured Viscosity Centipoise (cP)
14,500	0.190
14,000	0.186
13,000	0.178
11,856	0.168
11,000	0.161
10,000	0.154
9,000	0.146
8,000	0.139
7,000	0.139
6,900	0.140
6,800	0.134
6,504	0.162
6,430	0.172
6,300	0.182
6,000	0.205
5,000	0.266
4,000	0.330
3,000	0.405
2,000	0.475
1,000	0.595
150	0.879

The Reservoir

Data from BP shows that this reservoir is a sandstone. The average properties are shown in Table 3. The reservoir is estimated to cover 4,500 acres with one well estimated to drain 1,500 acres.

Table 3: Average Reservoir Properties from BP Data

MD Interval (ft)	Net Pay (ft)	Porosity (%)	Sw (%)	ko (md)
17,804-17,806.5	2.5	22.48	24	397.28
18,067-18,089	22	20.67	17.17	86.53
18,120-18,191	64.5	22.08	9.7	275.22
18,217.5-18,238.5	6.5	21.08	21.85	110.39
Total Net Pay (ft)	95.5			
	Wtd Avg	21.7	12.6	223.7

A flow model for the reservoir can be constructed using the radial single phase (liquid) version of Darcy's Law shown as equation (1).

$$\frac{q}{p_e - p_{wf}} = \frac{k_o h}{141.2 B_o \mu_o \left[\ln\left(\frac{r_e}{r_w}\right) + s \right]} \quad \text{..... (1)}$$

$q =$ liquid flow rate (STB/day)

$p_e =$ reservoir boundary pressure = 11,856 (psia)

$p_{wf} =$ flowing pressure inside, but at the bottom of the well (psia)

$k_o =$ permeability to reservoir fluid (md)

$h =$ net reservoir thickness (ft)

$B_o =$ liquid formation volume factor = 2.367 $(\text{reservoir bbl/STB})$

$\mu_o =$ viscosity of reservoir fluid = 0.165 (cp)

$r_e =$ radius to the well drainage boundary = 4,560 (ft)

$r_w =$ well bore radius = 0.254 (ft)

$s =$ reservoir skin damage = 0 (dimensionless)

$$\frac{q}{p_e - p_{wf}} = \frac{223.7(95.5)}{141.2(2.367)0.165\left[\ln\left(\frac{4,560}{0.254}\right) + 0 \right]} = 39.5 \text{ STB/day/psia} \quad \text{..... (2)}$$

Equation (1) is also called the reservoir inflow performance relation (IPR) with the result shown as volume of liquid at standard conditions flowing per day per incremental drop in pressure that is necessary to induce flow into the bottom of the well. Equation (2) is the IPR for this reservoir. So long as the reservoir pressure does not fall below the bubble (dew) point, this equation will apply to the critical single phase fluid in the reservoir. Equation (2) can be rearranged to solve for the pressure remaining at the bottom of the well $\left(p_{wf}\right)$ that is available to support a given flow rate (q) to the surface with a constant boundary pressure $\left(p_e\right)$.

The Flow Conduit

There are several possibilities for the flow conduit from the reservoir to the ocean floor. I will discuss three possibilities.

(1) I believe the most likely conduit is the annular space between the outside of the production casing and the inside of the various liners and casing strings that sealed the balance of the well. This belief is based on the rapidity of gas reaching the surface just before the blow out, but this is another subject that has been outlined in a forum at The University of Texas Energy Institute. A webcast of the forum can be seen at www.energy.utexas.edu. The entrance to this path is the reservoir outside the 7" casing. The exit from this path is past the well head seals. This path leads to the maximum flow rate calculated as a portion of this work.

(2) As a second possibility, the annular flow path of option (1) is used, except in this case the rupture discs in the 16" casing burst (see Appendix C and D for diagrams). Once the disc ruptures the reservoir fluids can enter the annular space between the 16" casing and the 18" liner. The shoe (end) of the 18" liner is exposed to open formation that was tested to a fracture pressure of 5,385 psi. The formation would fracture when exposed to the disc rupture pressure of 7,500 psi allowing reservoir fluids to exit the well. If a permeable sand is present in the open interval, reservoir flow will begin to charge this formation with reservoir fluids. The flow of reservoir fluid into the fracture diminishes the fluid escaping at the surface. This becomes the minimum flow estimate calculated in this work.

The fracture that is created in this scenario initiates 3,900' below the mud line. The vertical stress at this point is roughly 6,150 psi. This should cause the fracture to be a vertical fracture and if it is charging a permeable sand, it is unlikely that the fracture can escape beyond the sand boundaries to any large extent. This means the fracture is confined and will not grow to the mud line and erupt outside the well.

(3) The least likely conduit is through the bottom of the 7" casing and up the inside of the 7" and 9 7/8" casing to the surface. The entrance to this path is through the guide shoe, float joints, and float collar at the bottom of the 7" casing. The exit of this path is in the annulus between the 9 7/8" casing and a segment of 5 1/2" drill pipe and 3 1/2" tubing that was being used in the well at the time of the blow out. Although not completely conclusive there was a test on the check valves in the float collar that indicated they were not leaking at the end of the cement job. If this is true this path was sealed by the floats in the collar and by the 189 feet of cement that solidified in the float joints between the collar and shoe. For reservoir flow to enter through a leaking float collar, the reservoir gas bubble would be required to migrate down, against gravity. I think the natural path for a gas bubble is to rise through the cement and mud in the annulus.

It has been speculated that the production casing collapsed due to the gas pressure in the annulus and that this created an entry point to the inside of the casing. The collapse rating of the 7" should have been at least 12,000 psi (32 ppf, HCQ-125), which is more than the reservoir pressure. The collapse rating of the 9 7/8" is 10,695 psi (62.8 ppf, Q-125, corrected for axial load), which is more than the gas pressure should be at the depth the
9 7/8" casing was used. Therefore, the production casing should not have collapsed.

I have made flow calculations for this path, but I consider this pathway so unlikely that I do not present these results as a bound on the flow rate.

A well bore diagram from BP is shown in Appendix C. Although not shown on the well bore diagram, the well head and the blow out preventers attach at the mud line and extend above the ocean floor.

A well bore diagram showing the calculated gas bubble pressures in the annulus and the possible fracture point discussed as conduit (2) is shown in Appendix D.

Exit Pressure

The pressure exerted by the ocean water at the sea floor is roughly 2,250 psi. This pressure is exerted at every leak point where fluid can flow out of the well. BP measured flowing pressures above and below the blow out preventers. These pressures are shown in Figure 1. The flow restriction through the blow out preventers creates an 850 psi pressure loss. An additional 400 psi pressure loss is created by the various flow restrictions in the marine riser. There is also a pressure loss in the leaking well head seals, but this cannot be measured.

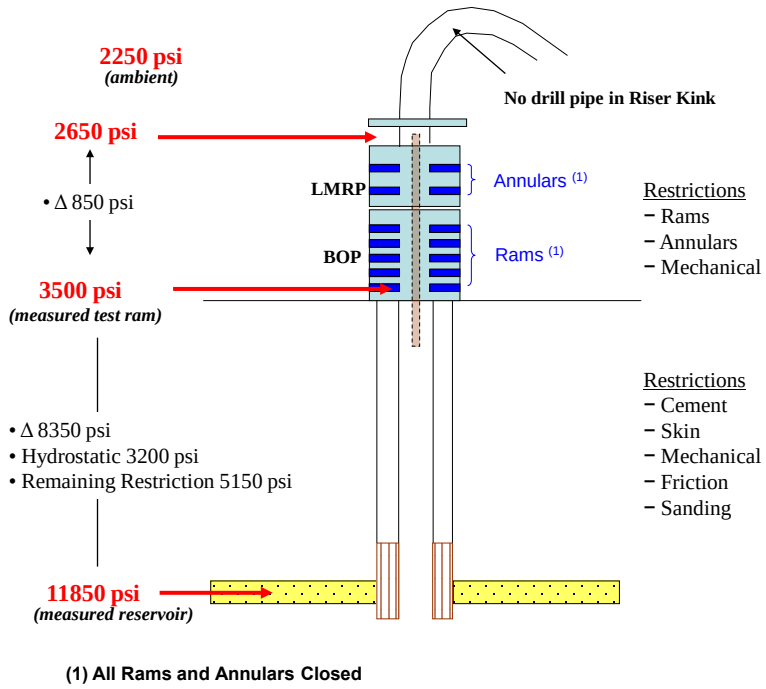

Figure 1: BP Flowing Pressure Measurements

Flow Calculation

The flow rate up a given conduit is computed using a nodal analysis approach and the modified Hagedorn and Brown two phase flow correlation. The basis for this correlation is the steady state mechanical energy balance neglecting any kinetic energy change. The method is an iterative one where the correlation predicts the flow regime and liquid hold up at any point in the flow conduit and uses this to compute the average flowing fluid density. The average flowing density is used to estimate the pressure gradient at a given point and another step is then taken along the flow path.

A number of flow rates are chosen and the correlation used to calculate the flowing pressure at the bottom of the well. This is the flowing bottom hole pressure $\left(p_{wf}\right)$ necessary to flow the fluid to the ocean floor up the flow conduit and still have the pressure required to exit the well head.

A graph of the flow rate versus bottom hole flowing pressure such as shown in the following figures is called the vertical lift performance (VLP) of the flow conduit in question. Also plotted on the figures is the inflow performance relation (IPR) that describes flow from the reservoir. Where these two lines intersect is the maximum rate the reservoir can flow into the bottom of the conduit with sufficient bottom hole flowing pressure remaining to flow up the conduit to the surface.

Flow Conduit (1) – The Annulus

The annulus is simulated using a conduit diameter described as a hydraulic diameter. The hydraulic diameter is the customary turbulent flow approximation equal to four times the computed hydraulic radius of the sections being considered. The average hydraulic diameter used in the simulation of the annulus is 3.67".

In order to simulate the flow restriction inside the blow out preventers and the marine riser (Figure 1) the exit pressure from the conduit is set at 1,250 psi more than the pressure of the sea water or 3,500 psia.

To simulate the pressure loss in the leaking well head seals a two phase choke flow equation from Ross is used. This equation is shown as equation (3).

$$p_1 = \frac{q\sqrt{GLR}}{235.4D^2} \quad \text{..... (3)}$$

$q =$ STB/day

$p_1 =$ upstream pressure $\left(\text{psi}\right)$

$D =$ choke diameter $\left(\text{inch}\right)$

$GLR =$ gas/liquid ratio $\left(\text{Scf/STB}\right)$

The leak diameter inside the seals is unknown at this time. An estimate based on hydraulic diameter between the well head housing and the seal case is 1.3". A better estimate of this restriction may be made in the future by a careful examination of the dimensions of the seals and well head. The gas-liquid ratio is as shown in Table 1.

No flow restriction other than the open annulus is assumed in the cemented area at the bottom of the well.

Figure 2 shows the results of several simulations of annular flow for various exit pressures.

The most likely flow rate occurs when the seal, well head, blow out preventer, and marine riser restrictions are considered. This flow rate is estimated to be 22,000 STB/day.

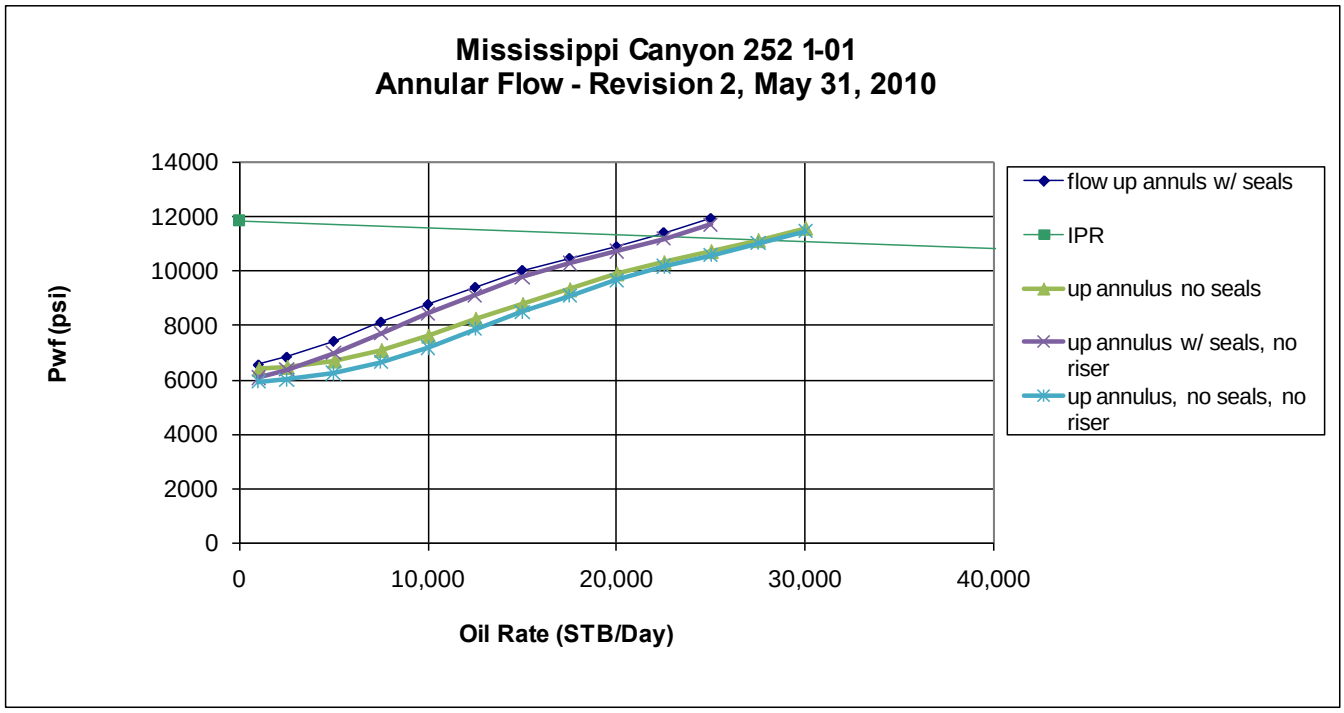

Figure 2: Annular Flow Rate Based on Reservoir Inflow and Annular Conduit Flow Performance

As an aside, Figure 2 shows that the loss of the marine riser above the blow out preventer has very little effect on flow rate because the back pressure due to flow in the riser is only 400 psi.

Flow Conduit (2) – The Annulus Coupled with a Fracture

The flow path is the same model described for option (1) except now a fracture has formed at 8,969' at the end of the 18" casing and the fracture is accepting part of the flow rate. The pressure necessary to hold the fracture open and inject part of the reservoir flow into the fracture is estimated to be 5,600 psi. The two phase flow model is used to predict the flow rate escaping at the ocean floor that is required to create this amount of pressure at the fracture point 3,900' below the mud line. The annulus hydraulic diameter in this section is 4.97". The same well head and seal pressure loss boundary conditions used in option (1) are used here.

The results of this simulation indicate that 9,200 STB/day are escaping at the surface. This means that roughly 12,800 STB/day are charging the permeable sand at 8,969'. This should not be a steady state condition. Flow probably fluctuates between the fracture and the ocean floor.

Flow Conduit (3) – Inside the Production Casing

This flow path is the inside of the 7" and 9 7/8" casing. The average diameter inside this conduit is 7.51".

The entrance to this conduit is through the float collar flapper, which must be damaged for flow to access this path. The diameter of the flapper is roughly 2.375" and the pressure loss though this short restriction is negligible.

The exit from this path is out the annulus between the 5 1/2" drill pipe and 3 1/2" tubing and the 9 7/8" casing and the inside of the 5 1/2" and 3 1/2" tubes. The 850 psi flow restriction in the blow out preventers remains the same as before as does the 400 psi flow restriction in the marine riser. Thus, the exit pressure is a constant 3,500 psi, including the pressure of the sea water.

Figure 3 shows the results of two simulations for pipe flow using exit pressures with and without the marine riser.

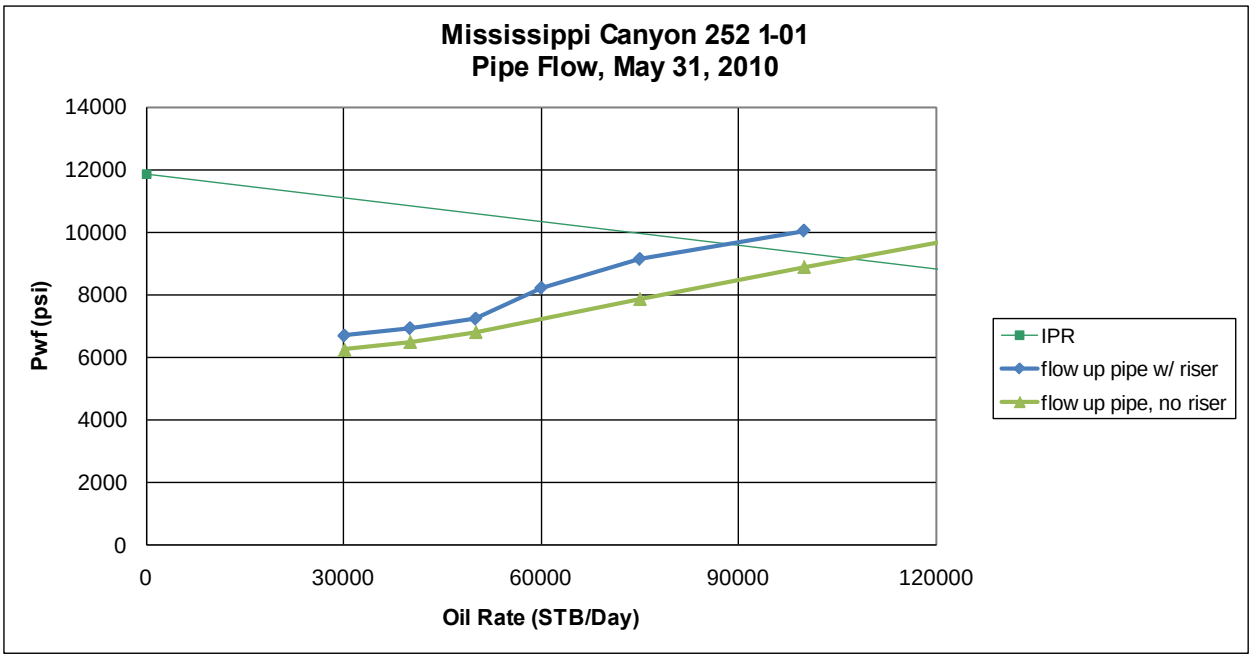

Figure 3: Pipe Flow Rate Based on Reservoir Inflow and Pipe Flow Performance

Using the estimates shown in Figure 3, the flow rate up the pipe is 90,000 STB/day with the marine riser attached. Without the marine riser the flow increases to 105,000 STB/day.

As I do not believe this flow path is likely (see the flow conduit section for discussion), I have not included these estimates in my minimum and maximum flow rate statement.

Results

From this process I believe the flow is up the annulus. The minimum flow up this pathway is 9,200 STB/day and the maximum flow is 22,000 STB/day. Confirmation of flow rate will occur when BP severs the riser and installs the soft seal that will capture the flow to a vessel.

Appendix A from Bommer Report: PENCOR Fluid Report at 100 deg F, April 22, 2010

Constant Composition Expansion at 100°F
Pressure-Volume Relations

PENCOR ID No. 36126-53: 18,142 ft Depth

Pressure (psia)		Relative Volume (V / V_{sat})	Oil Density (g/cm^3)	Relative Liquid Volume (%)	Oil Compressibility ($\Delta V/V/\Delta psi) \times 10^6$	Y-Function ($(P_{sat}-P)/P(V/V_{sat}-1)$)
11,856	**Reservoir**	**0.939**	**0.639**			
10,000		0.956	0.628		9.60	
9,500		0.962	0.624		10.76	
9,000		0.967	0.621		11.08	
8,500		0.973	0.617		11.77	
8,000		0.979	0.613		13.21	
7,500		0.986	0.609		14.23	
7,000		0.994	0.604		14.87	
6,710		0.999	0.601		17.54	
6,636	**Saturation**	**1.000**	**0.600**	**0.00**	**18.22**	
6,616		1.001		36.20		
6,500		1.003		57.07		6.99
6,000		1.015		68.53		7.15
5,500		1.030		68.78		6.98
5,000		1.048		68.76		6.83
4,500		1.072		69.09		6.58
4,000		1.105		68.90		6.25
3,500		1.153		68.37		5.84
3,000		1.230		68.32		5.27
2,500		1.360		67.70		4.60
2,000		1.597		66.55		3.88
1,500		2.058		64.51		3.23
1,000		3.073		61.58		2.72

Notes:

- Relative Volume (V / V_{sat}) is the fluid volume at the indicated pressure and temperature relative to the saturated fluid volume.
- Density (lb/ft^3) = Density (g/cm^3) x 62.428
- Compressibility is the average compressibility between the indicated and the next highest pressure.
- Relative Liquid Volume % is the volume of liquid relative to volume at saturation pressure

Constant Composition Expansion at 100°F
Data Presentation Figures

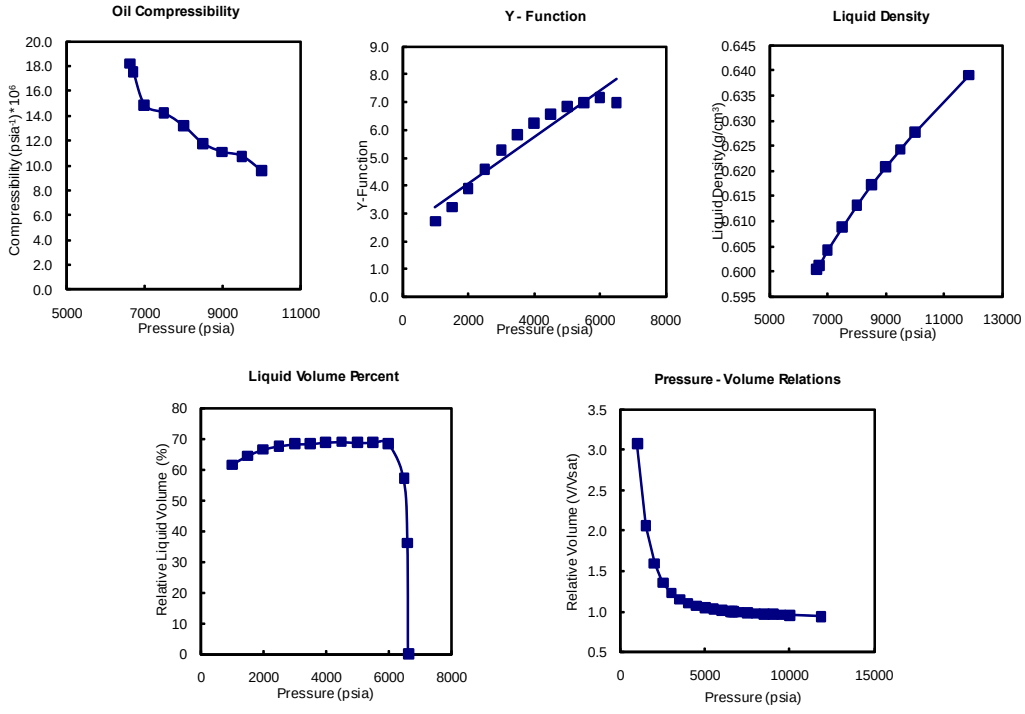

Appendix A from Bommer Report: PENCOR Fluid Report at 243 deg F, April 22, 2010

Constant Composition Expansion at 243°F
Pressure-Volume Relations

PENCOR ID No. 36126-53: 18,142 ft Depth

Pressure (psia)		Relative Volume (V/V_{sat})	Oil Density (g/cm^3)	Relative Liquid Volume (%)	Oil Compressibility ($\Delta V/V/\Delta psi) \times 10^6$	Y-Function $(P_{sat}-P)/P(V/V_{sat}-1)$
11,856	**Reservoir**	**0.900**	**0.587**			
10,000		0.927	0.570		15.30	
9,500		0.934	0.565		16.75	
9,000		0.943	0.560		17.66	
8,500		0.952	0.555		18.88	
8,000		0.962	0.549		21.42	
7,500		0.973	0.543		22.54	
7,000		0.986	0.536		26.60	
6,504	**Saturation**	**1.000**	**0.528**	**0.00**	**28.17**	
6,495		1.001		9.22		
6,475		1.002		31.23		
6,450		1.003		39.76		
6,400		1.005		50.10		
6,300		1.009		55.49		
6,200		1.013		56.82		3.64
6,100		1.018		57.80		3.63
6,000		1.023		59.96		3.63
5,500		1.052		59.75		3.50
5,000		1.090		59.37		3.36
4,500		1.139		58.57		3.20
4,000		1.208		57.60		3.02
3,500		1.303		57.11		2.83
3,000		1.442		55.39		2.64
2,500		1.645		54.10		2.48
2,000		1.982		53.45		2.29
1,500		2.573		50.99		2.12
1,000		3.812		49.63		1.96

Notes:

- Relative Volume (V/V_{sat}) is the fluid volume at the indicated pressure and temperature relative to the saturated fluid volume.
- Density (lb/ft^3) = Density (g/cm^3) x 62.428
- Compressibility is the average compressibility between the indicated and the next highest pressure.
- Relative Liquid Volume % is the volume of liquid relative to volume at saturation pressure

Constant Composition Expansion at 243°F
Data Presentation Figures

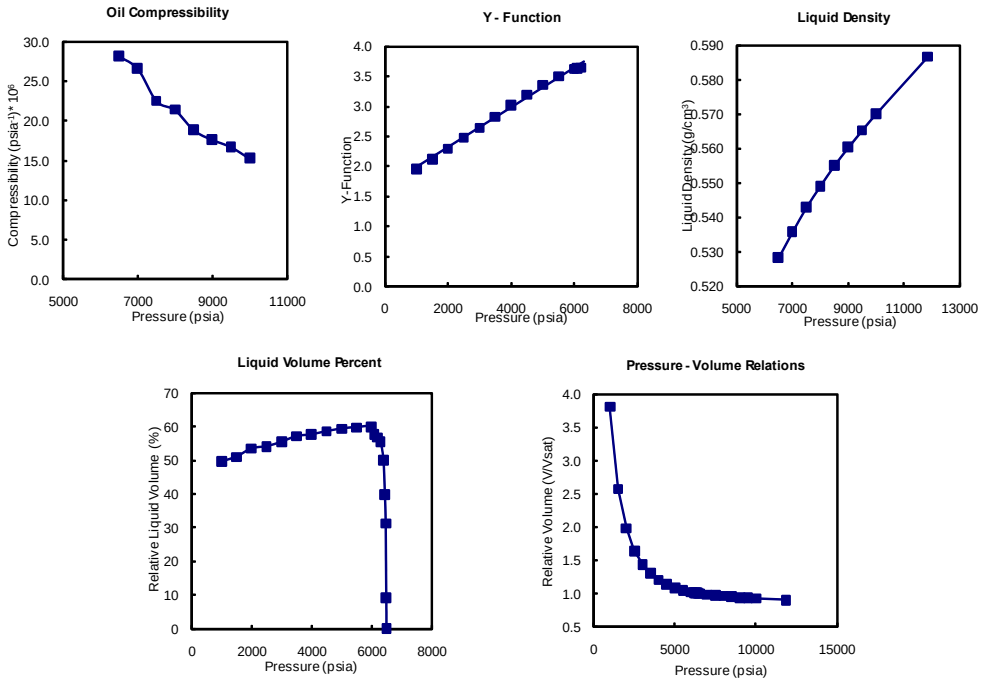

Appendix B from Bommer Report: Schlumberger Fluid Report Excerpt, May 19, 2010

Client: BP **Field:** Mississippi Canyon 252
Well: OCS-G 32306 # 1 **Sand:** -

Schlumberger

PVT Analysis on Sample 1.18; Cylinder 20D127; Depth 18142 ft. MD

Constant Composition Expansion at Tres

The CCE study was initiated by charging a sub-sample of live reservoir fluid into the PVT cell at a reservoir temperature of 243°F and at a pressure of 15,015 psia. Sequential pressure decrease in steps and the corresponding volume changes are presented in Table 21. The pressure-volume (P-V) plots of the CCE data are presented in Figure 11. The intersection of the single-phase and two-phase lines in the P-V plot and the visual observation was used to define the bubblepoint. For the subject fluid, the bubblepoint was determined to be 6,348 psia at the reservoir temperature of 243°F. Also, calculated relative volume and oil compressibility is presented in Table 21. As seen in the table, the compressibility of this oil is 25.0 x 10e-6 1/psia at the saturation pressure.

Table 21: Constant Composition Expansion at 243°F (Sample 1.18)

Sample 1.18; Cylinder 20D127; Depth 18142 ft. MD

	Pressure (psia)	Relative Vol (Vr=V/Vsat)	% Liquid (Vl/Vsat)	% Liquid (Vl/Vtotal)	Liquid Density* Measured Pyc Flash (g/cm3)	Liquid Density* Measured Anton Parr (g/cm3)	Compressibility (10^{-6}/psia)
1	15015	0.8783					8.4
2	14015	0.8862					9.5
3	13015	0.8951			0.598	0.598	10.7
Pi	**11871**	**0.9069**			**0.590**	**0.591**	**12.2**
5	10015	0.9303					15.4
6	9015	0.9457					17.5
7	8015	0.9635			0.555	0.556	19.9
8	7015	0.9842			0.543	0.544	22.8
9	6370	0.9995			0.535	0.536	24.9
Pb	**6348**	**1.0000**			**0.535**	**0.536**	**25.0**
10	6322	1.0000	70.7	70.7			
11	6265	1.0029	70.1	69.9			
12	6215	1.0047	69.6	69.3			
13	5880	1.0184	68.0	66.8			
14	5532	1.0369	66.9	64.5			
15	5039	1.0700	65.0	60.8			
16	4537	1.1148	64.5	57.9			
17	4037	1.1759	63.6	54.1			
18	3536	1.2607	62.5	49.6			
19	3025	1.3859	61.7	44.5			
20	2530	1.5709	60.6	38.6			
21	2027	1.8762	59.1	31.5			
22	1525	2.4202	57.7	23.9			
23	1098	3.3203	54.6	16.4			

Appendix C from Bommer Report: BP Well Bore Diagram

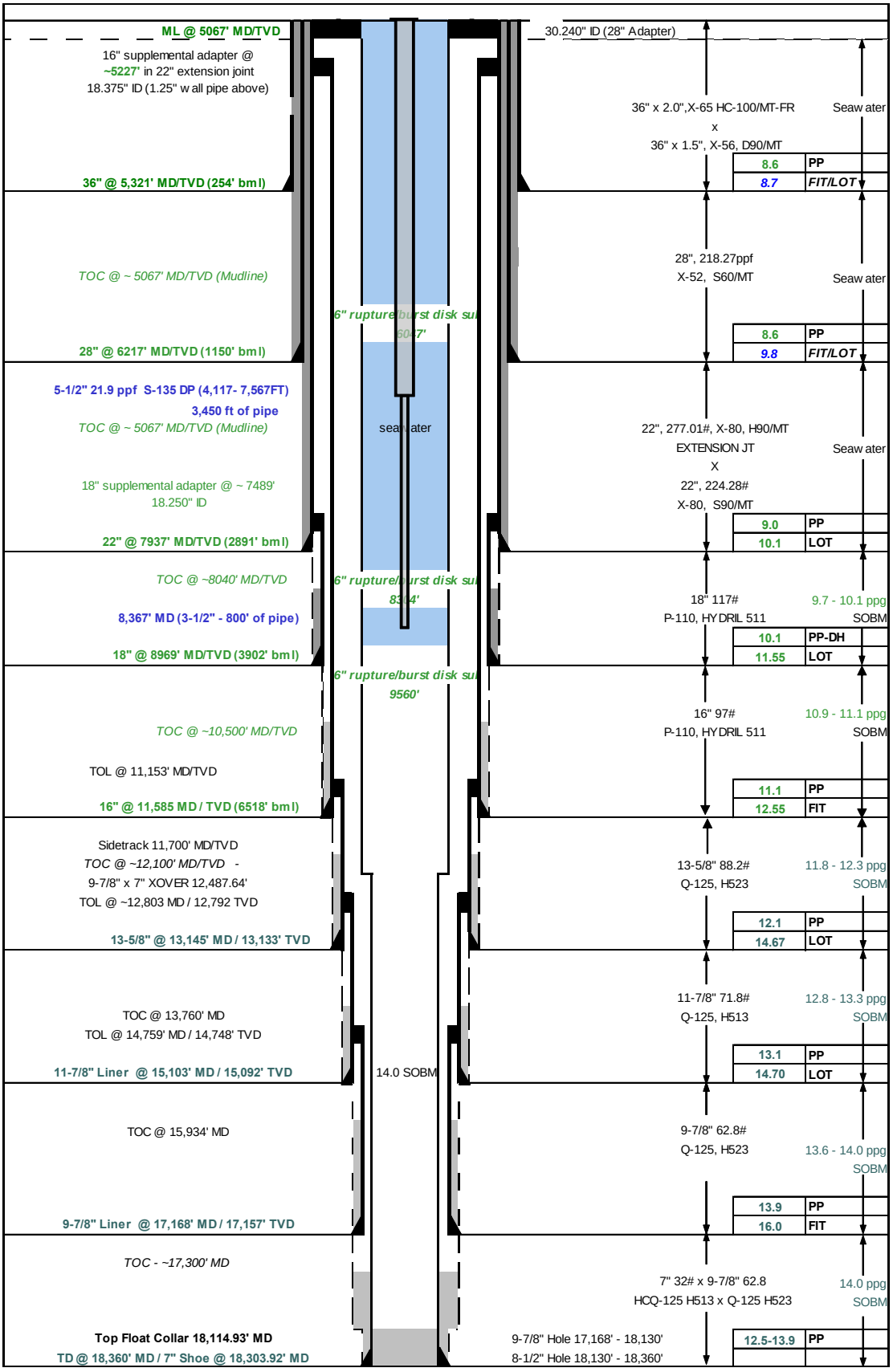

Appendix D from Bommer Report: Calculated Confined Gas Bubble Pressures

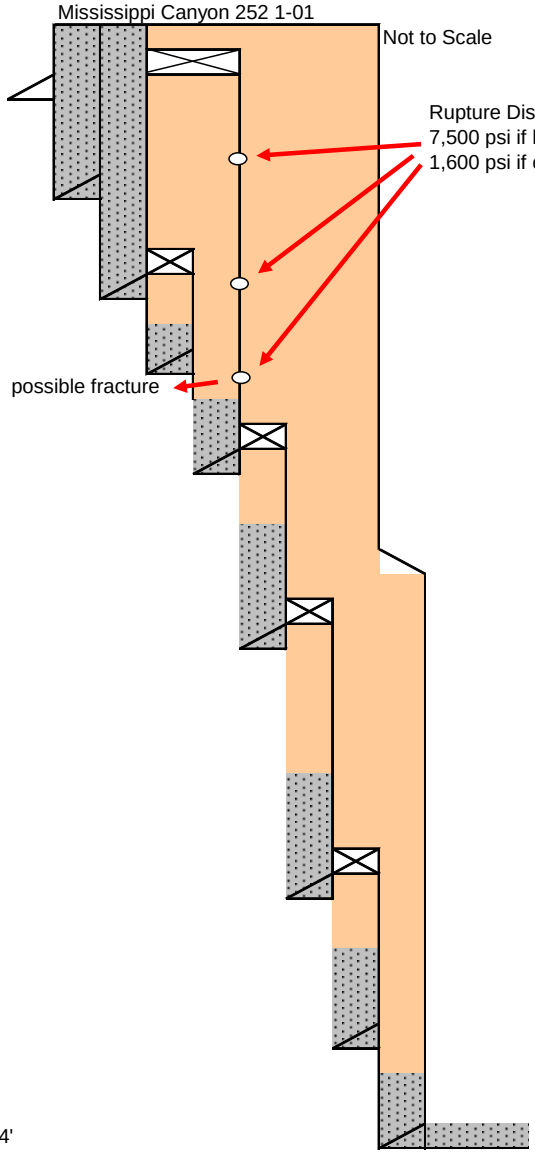

All depths from sea level.	Gas Bubble Psi	Temp deg F
5,067' mud line	7,460	100
36" conductor 5067-5321'		
28" casing 5067-6217', TOC=ML		
22" casing 5067-7937', TOC=ML	8,000	130
18" liner 7489-8969', TOC=8040'	8,215	142
16" caing from 5,227-11,585', TOC=10,500'	8,545	166
13 5/8" liner from 11,153-13,145', TOC=12,100'	9,000	184
11 7/8" liner from 12,803-15,103', TOC=13,760'	9,575	204
9 7/8" liner from 14,759-17,168', TOC=15,934'		
7" x 9 7/8" combination casing from 5,067-18,304' TOC=17,300'	11,856	243

Appendix 3: Description of Underwater Oil and Gas Release Behavior

Poojitha Yapa
Clarkson University

The report explains how oil behaves in general terms when released in deep water. This is not for a particular incident such as the recent Deepwater Horizon accident but applies to atypical subsurface well blowout. This description is based on the fundamentals of fluid mechanics, years of modeling experience, and the experience from observations of data from Deepspill - large scale field experiments conducted in Norway.

In general, when oil and gas are released from a deep water location, they are expected to breakup into bubbles or droplets of various sizes. Theses sizes can vary widely. But what was experienced in Deepspill was generally between 1 mm and 10 mm. However, they can be much smaller or much larger in different spill conditions. Let's consider oil. The larger droplets are going to move faster towards the surface, the smaller droplets are slower. Bubbles are subjected to cross currents which will move them laterally while it is moving upwards. The larger droplets will come to the water surface sooner and the smaller droplets will take a longer time. For this reason the larger droplets and the smaller droplets may not come to the surface at the same location, but quite a distance apart. If there are droplets of very fine scale, like 100 microns or 500 microns it may take weeks or even months for them to come to the surface. That is assuming that the ambient water doesn't have any downward component in the ambient velocity. If it has even a slight downward velocity, then that may negate the buoyant velocity of the smaller particles and they may stay under the water for a very long time.

Gas also has many bubble sizes. In many deepwater releases large amount gas bubbles will dissolve and may never make it to the surface. Gas bubbles move faster than oil bubbles if they are the same size. Because of this, gases can separate from the main plume and start going in a slightly different direction (Chen and Yapa, 2004). The schematic in Figure 1 depicts what has been described before. In this schematic we are using only three sizes of oil bubbles and one size of gas bubbles. In reality there will be many more sizes. Gas bubbles are in purple color and oil bubbles are in orange, pink, and green. Orange are the largest size and comes to the surface the fastest, the green are the slowest because they are the smallest bubbles. Gas bubbles, shown in purple color, in this case dissolve before they reach the surface. We are depicting here only with one size of gas bubble. A real spill may have many sizes and the bubble size distribution can be also continuous. Gases when released in deep water also have the potential to be converted into hydrates. Methane has a level of hydrate dissociation generally around 550 m of water depth as shown in Figure 2. But this is not a fixed value. It depends on parameters like water temperature and gas type. Natural gas can get converted to hydrates at a much higher level. Therefore, gases can get converted into hydrates as they travel up. Hydrates are still buoyant. It should be noted that no hydrates were observed during the Deepspill experiments.

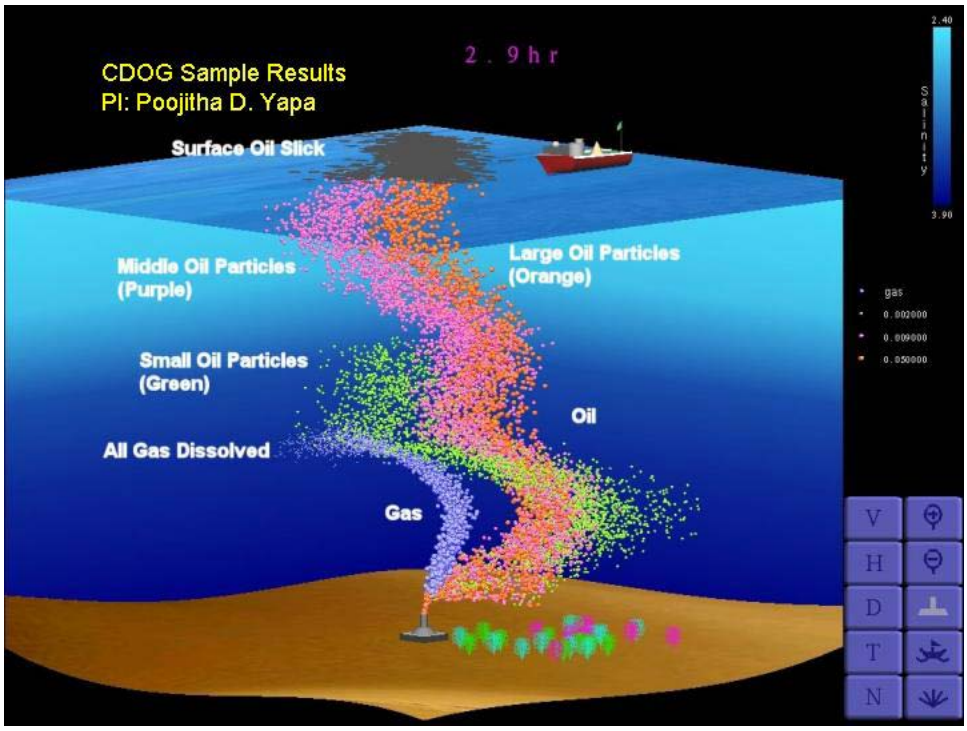

Figure 1: A schematic representation of how oil and gas behave when released underwater (from various projects under PI: Yapa).

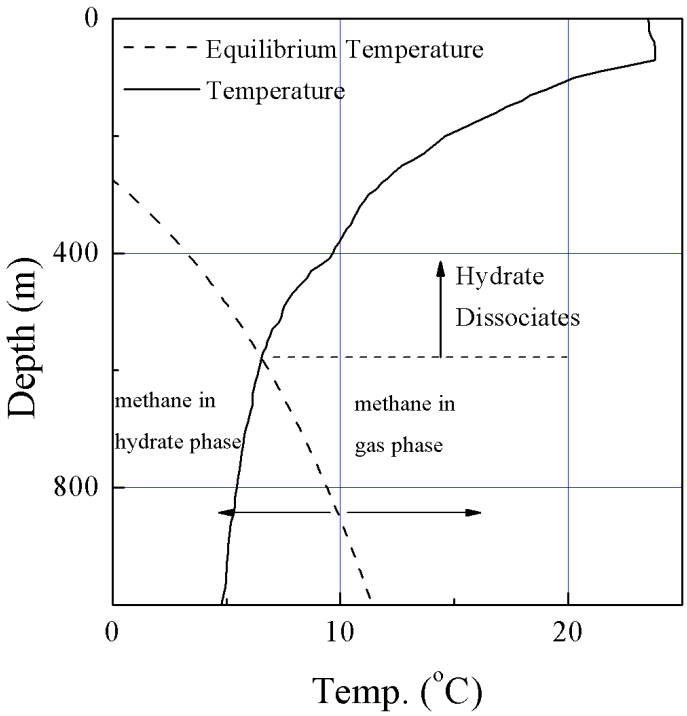

Figure 2: A typical ambient temperature and thermodynamic equilibrium curve for methane (Yapa and Chen 2004).

As hydrates travel towards the water surface they can get reconverted back into gas when they reach the lower pressure in the shallower regions. Figure 2 above, shows the thermodynamic equilibrium curve and the water temperature. This is for a location in Gulf of Mexico. Figure 3 shows schematically how the gases (shown in yellow) are converted into hydrates (shown in blue).

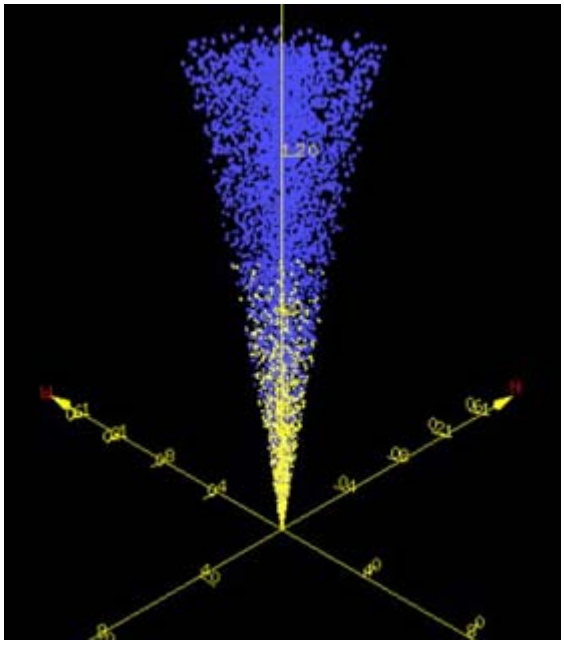

Figure 3 Schematic representation of gas (yellow) converting to hydrates (blue) as they travel upwards. Ambient current = 0.

In summary, it is important to understand that what has been described here is the general behavior of oil and gas when it is spilled in deep water and each individual spill may have different condition depending on the environmental factors, ambient factors like water temperature, salinity and the depth at which it was released, the type of oil.

References

Yapa, P. D. and Chen F.H. (2004). "Behavior of Oil and Gas from Deepwater Blowouts," *Journal of Hydraulic Engineering*, ASCE, June, 540-553.

Chen, F.H. and Yapa, P.D. (2003). "Three-Dimensional Visualization of multi-phase (oil/gas/hydrate) plumes," *Journal of Environmental Modelling and Software*, Elsevier, the United Kingdom, 19 (2004), 751-760.

Chen, F.H. and Yapa, P.D. (2004). "Modeling Gas Separation From a Bent Deepwater Oil and Gas Jet/Plume," *Journal of Marine Systems*, Elsevier, the Netherlands, Vol 45 (3-4), 189-203.

Zheng, L., Yapa, P. D., and Chen, F.H. (2003). "A Model for Simulating Deepwater Oil and Gas Blowouts - Part I: Theory and Model Formulation" *Journal of Hydraulic Research, IAHR*, August, 41(4), 339-351.

Chen, F.H. and Yapa, P.D. (2003). "A Model for Simulating Deepwater Oil and Gas Blowouts - Part II : Comparison of Numerical Simulations with "Deepspill" Field Experiments", *Journal of Hydraulic Research, IAHR*, August, 41(4), 353-365.

Zheng, L. and Yapa, P.D. (2002). "Modeling Gas Dissolution in Deepwater Oil/Gas Spills," *Journal of Marine Systems*, Elsevier, the Netherlands, March, 299-309.

Chen, F.H. and Yapa, P.D. (2001). "Estimating Hydrate Formation and Decomposition of Gases Released in a Deepwater Ocean Plume," *Journal of Marine Systems*, Elsevier, the Netherlands, Vol 30/1-2, 21-32.

Zheng, L. and Yapa, P.D. (2000). "Buoyant Velocity of Spherical and Non-Spherical Bubbles/Droplets," *Journal of Hydraulic Engineering, ASCE,* November, 852-855.

Zheng, L., and Yapa, P.D. (1998). "Simulation of Oil Spills from Underwater Accidents II: Model Verification," *Journal of Hydraulic Research, IAHR*, February, 117-134.

Yapa, P.D., and Zheng, L. (1997). "Simulation of Oil Spills from Underwater Accidents I: Model Development," *Journal of Hydraulic Research, IAHR*, October, 673-688.

Appendix 4: 2010 Gulf of Mexico Oil Spill Estimate

Ömer Savaş
Department of Mechanical Engineering
University of California Berkeley
Berkeley, CA, 94720-1740
savas@me.berkeley.edu
June 7, 2010

Observations

This report discusses the flow rate at the collapsed well head of the Deepwater Horizon drilling unit oil spill site in the Gulf of Mexico, which sank on April 22, 2010. The basis of the discussion is the four videos among the many downloaded from a secure ftp site set up by the USGS:

- Video 1: H14 BOP Plume May 15 1915-1920.asx (04:59),
- Video 2: H14 BOP Plume May 15 1920-1945.asx (25:14),
- Video 3: BOP.wmv (05:05), wide view of discharge at BOP , and
- Video 4: 20100514224719234@H14 Ch1-H264h.mov (09:40), RITT close up.

The first two seem to be a continuous stream of images divided into two parts. The flow in view is the discharge at the kink (collapsed pipes) immediately downstream of the blowout preventer (BOP). Only a limited discussion of the discharge at the broken end of the riser (for the discussion here, named riser insertion tube tool (RITT)) is presented. I tried numerous video players. In particular, the variable play speed play feature of openly available VLC Media Player was quite helpful (0.03×–4× on my computer). I found that playing the videos at 4× speed gave a better understanding of the flow patterns. I went over the files numerous times. I captured a random image and annotated it to describe my observations below.

Figure 1 summarizes my observations of the discharge flow pattern at the kink. The flow field has in the foreground one very clear, classic, turbulent jet J_1. There is a weak stream of discharge on the right side coming from the underneath of the buckled pipe and wrapping around it, labeled J_0, the origin of which is evidently under the bend. On the left side of the picture, I marked as J what I consider to be the main discharge jet which is pointing away from the camera. In fact, this jet is the dominant feature in the wide view Video 3 taken down stream of the jet at distance. The jet, judging from that view, seems to be discharging 30 – 45° from the horizontal. There seems to be a fourth jet J_2, obscured by J, which seems to be discharging somewhat toward J, but slightly to its left.

The jets J_1 and J_0 are clearly in the view and are the most amenable to direct analysis. J_1 shows all the characteristics of a classical turbulent jet e.g., linear growth, sharp intermittent interface. Fortuitously, the weaker jet J_0 acts as an exquisite marker of the entrainment field of J_1, marked as E_{01}. PIV may be used to estimate the entrainment velocity at the *edge* of J_1. J_0, however, oscillates back and forth, and at times its plume is entrained by J, behind J_1. This entrainment field into J is marked as E_0.

There is a strong inflow at the left edge of J, marked by E_2. This is especially clear when the video is played at high speeds. It is likely that the fluid in E_2 is the plume of a jet hidden from the view, marked as J_2. Velocities in E_2 seem to be much higher than in E_{01}. Lastly, the plume of J_1 itself is being entrained by J, which may be observed at the upper regions of the flow field. This entrainment field is labeled as E_1.

Figure 1: Summary of observations of the discharge flow field at the kink. J-jet, E-entrainment. The picture is 704 pixels wide and 576 pixels high; the length scale: 1 pixel = 2.0 mm.

Analysis

I have used numerous tools in my analysis of the flow field in Fig. 1. These include the self similar behavior of turbulent jets, our in-house Particle Image Velocimetry/Lagrangian Parcel Tracking software (PIV/LPT), Adobe Photoshop©, and numerous tools developed on the IDL© platform.

Turbulent Jet Self-Similarity

The discharge jet J_1 in Fig. 1 looks like a classical turbulent jet of a high Reynolds number. This is evident in the presence of sharp interfaces (intermittency), a multitude of cascading length scales (from the large coherent structures, billows, to the fine scales cut-off at the camera resolution), and a linear spread except for a slight tilt (~ 13°) to the left. The ratio of the largest and smallest lengths scales is a clear indicator of the jet Reynolds number

$$Re = \quad , \tag{1}$$

where J is the momentum flux, ρ the fluid density in the jet, and ν the kinematic viscosity of the fluid. In this case, since the camera resolution is low, and it is too far away, there is no way of capturing the smallest scales of the flow. In fact, it is even a big challenge to capture them in a controlled laboratory experiment.

To estimate the volumetric discharge rate of the jet Q_j, we first write the momentum of the jet

$$J = (\rho_j U_j)\,(U_j A_j) = \rho_j Q^2{}_j / A_j \tag{2}$$

where ρ_j is the density of the discharging fluid, U_j the velocity of the jet at its orifice, A_j the jet orifice area, and $Q_j = U_j A_j$. Combining Eqs. 1 and 2, the jet discharge flow rate is written as

$$Q_j = \nu\, Re \ , \tag{3}$$

where I did not attempt to distinguish ρ from ρ_j. Since the jet is developed in the ambient water, the kinematic viscosity $\nu \sim 2cs$ is that of the ambient sea water. From Fig. 1, I estimate the jet discharge orifice diameter as $D_1 = 12 \pm 1$ pixels, hence its area as $A_j \sim 4.5 cm^2$, using the length conversion factor of 2mm/pixel shown in the figure. Based on my experience with turbulent flows, I am guessing that

$$Re_{J1} \sim 10^6. \tag{4}$$

For comparison, the Reynolds number for candle light is ~100. The flow rate estimate from Eq. 3 is

$$Q_{J1} \approx 0.02 \times 10^6 \times \ \sim 4.2 \cdot 10^4 \text{ cm}^3/\text{s} \rightarrow 3{,}700 \text{ m}^3/\text{day} \tag{5}$$

This estimate is for the darker jet J_1 only. A higher value for ν may be used since the jet is a mixture of water and more viscous oil ($\nu \sim 5$ cs for oil). The Reynolds number remains uncertain, could be as low as half a million, or could be many millions. I present below an independent estimate for *Re* based on the velocity of the coherent structures shown in Fig.1.

Figure 2: Two successive images from a video sequence (24 fps), showing the advection of large structures downstream of J_1. Circles mark a group of *dark patches* that can be tracked individually. Individual frames are 880 pixels wide and 720 pixels high; the length scale: 1 pixel = 1.6 mm.

Image Analysis

Direct Image Analysis: The most straight forward technique is to analyze a few sample pictures visually, using Adobe Photoshop and ticker.pro. An indirect check of the guess in Eq. 4 can be done by estimating the speed of the coherent structures at the downstream of the jet in Fig. 2. By overlaying two successive images in Photoshop, and, independently using ticker.pro, I estimate the displacement of the coherent structures at about 70 cm downstream of the discharge to be about 40±10 pixels/step, or 150±40 cm/s at 24 frames/second video rate. (The images in Fig. 2 are converted to 880 × 720 resolution during extraction from the video stream, hence 1 pixel=1.6 mm.) This is about half of the centerline velocity in a uniform density, non-buoyant turbulent jet. This implies a centerline velocity of about U_o = 3.0 m/s at 70cm downstream of the discharge. Using the inverse decay law of centerline velocity for a turbulent jet, I estimate the velocity at the jet discharge to be about

$$U_{J1} = (70cm \,/\, 2.4cm) \times 3.0m/s \approx 85 \text{ m/s} \qquad (6)$$

(projecting a virtual origin at one diameter behind the wall). Along with $A_j = 4.5 cm^2$, this suggests a discharge flow rate of

$$Q_{J1} = \times Uo \times Aj = \times 300 cm/s \times 4.5 \text{cm}^2 \approx 39{,}600 \text{ cm}^3/\text{s} \rightarrow 3{,}400 \text{ m}^3/\text{day}, \quad (7)$$

which is somewhat lower than the above estimate in Eq. 5, yet well within the uncertainties. The Reynolds number is, from Eq. 3,

$$ReJ1 = \approx = 0.9 \times 10^6. \quad (8)$$

Again, somewhat lower than the guess in Eq. 4, yet comparable.

As a reference point, if the flow were lossless, it would take a pressure differential of about 36 atmospheres to accelerate water to 85 m/s, *a la* Bernoulli. If there were no leakage at the kink, the static pressure differential between the BOP and the sea floor would be about 340 atmospheres, assuming no restriction inside the well head.

PIV: PIV techniques may be employed in this case with *due* caution. These techniques are able to capture the phase velocity of large scale structures, and only at downstream when the jet is sufficiently slowed down. As the estimate above indicates, there are phase displacements as large as 40 pixels between successive video frames. Hence, one needs interrogation windows up to 128 pixels on the side to capture them. As the window size or time step is increased inordinately, the PIV approach degrades at turbulent interfaces, since the turbulence, by its very nature, will continually *re-granulate* the interface, hence *stressing* any PIV algorithm. In particular, it will underestimate displacements. Turbulence has by its nature has a cascades of time and lengths scales. If the time step is too large, the intermediate time and lengths scales will change completely between the successive PIV images, rendering any correlation algorithm helpless. This will result in only a handful of independent velocity vectors. Our PIV technique is no exception.

In our PIV/ALPT implementation, the largest displacement output was around 16 pixels per time step for the coherent structures tracked in Fig. 2, compared to 40 pixels that I deduced by examining it visually using Photoshop, and ticker.pro. I was able to get this value only after using tall interrogation window, 8 × 64 (64 pixels along the jet direction). Square windows of 32×32, 64×64, and even 128×128 yielded even lower values. In contrast, I was able to track few individual patches of *dark* material in the weak jet J_0 encircled in Fig. 2 using Photoshop in conjunction with ticker.pro. Their displacements are in the range 9-13 pixels/step (35-50 cm/s), comparable to what my PIV algorithm was giving for the obviously much stronger jet J_1. Therefore, I decided to use PIV results qualitatively only. Perhaps, we should develop a flow rate estimation scheme based on edge detection.

PIV promises the most for J_1 in Fig. 1, but only in an intermediate distance from the discharge point. The velocities are too fast closer to the discharge point, and the interface is too turbulently granulated farther downstream. For the high speed jet *J*, it provides no direct information. In the case of the faint jet J_0, we expect more vectors, since the flow is slow. Unfortunately that is the weakest of the leaks, and is of low interest.

Figure 3 shows a sample filtered result from our PIV/ALPT algorithm. The images in Fig. 2 are processed. The velocity vector field and some *selected* streamline segments are overlaid on one of the images in regions where I have some confidence in the results, either in the direction or the magnitude of the velocity vector, or both. It *qualitatively* captures some features of the flow: J_1, J_0, E_{01}, to some degree E_1, and a hint of E_2. With caution in mind, the results suggest that the velocities in E_2 are comparable to E_1, but certainly higher than in E_{01}.

Figure 3: Sample PIV/LPT results for J_1. The images in Fig. 2 are processed.

Discussion

Jet Strengths

It is now time to order the four jets; J, J_0, J_1, & J_2; identified in Fig. 1. First, we note here that the entrainment velocity v at the edge of a turbulent jet is indicative of its centerline velocity U_o,

$$v = 0.08 U_o. \qquad (9)$$

Therefore, based on our observations and the implications of the PIV results just discussed, we can use the relative entrainment strengths to put the four jets in an order. Clearly, J_0 is the weakest. Since part of J_1 is entrained into J, I conclude that J is stronger than J_1. The PIV results in the entrainment zones suggest that the phantom jet J_2 is stronger than J_1. However, to stay on the side of caution, I will assume that J_1 is comparable or stronger than J_2. The final ordering is

$$J > J_1 > J_2 >> J_0. \qquad (10)$$

Oil/Gas Ratio

This brings up a whole new question about the variability of the conditions between the kink at BOP and the opening at the RITT. The RITT discharge is evidently binary/ intermittent: almost unmixed (a better term is 'separated') light colored (gas) and dark colored (oil) fluids. The discharge at the kink is nearly uniform in color. I will go even further and say that the faint stream of J_0 warping around the collapsed tube on the right side at the BOP is all oil.

RITT

Flow at the RITT is an unrestrained discharge, that is, the pressure drop in the pipe is only that required to maintain the flow rate at an unobstructed (?) opening. The view of the discharge at the RITT oscillates between an almost white, apparently gaseous methane and dark liquid, presumably oil. The views with the details are essentially the shear layers at the discharge. What one sees at the edge of these shear layers primarily depend on the velocity profile of the discharge and the ratio of the density of the discharging fluid to that of the ambient fluid. For the same upstream pressure ignoring losses), to the first order, gas moves faster than liquid, since the pressure, potential energy, is converted to kinetic energy. For the same upstream pressure, gas being low in density, moves faster. This is evident in the video so the RTT discharge (Video 4). The lighter colored jet, presumably gas, shoots farther that the darker color fluid, presumably oil. The second important effect is the density ratio. Since the flow is at high Reynolds numbers, it is inertia dominated. The behavior of the visible interface is determined by the inertial effects (except when there is significant surface tension). In particular, the apparent velocity of the interface is determined by the pressure balance at the stagnation points of the large scale coherent structures in the reference frame moving with them, assuming quasi steady behavior. By accounting for this balance on streamlines extending to either side of the interface, one can deduce the apparent velocity (celerity) at the interface. Hence the density ratio becomes a factor. Intuitively, a light stream has to slow down considerably when pushing along a heavy fluid, as the case is here when the gas is trying to drag along the sea water. Consequently, our estimates base on the observed velocities of the interface must be corrected for the density ratio. This raises two points:

1. The speed estimates from the motion of the interface does not give the speed of the discharge. It has to be corrected for the density ratio. In the case of oil, whose density is close to that of the water, this correction is well within the uncertainty. For the gas phase, however, it is significant. If the velocity discharge profile at the exit of the broken pipe were uniform or close to it, we would expect to see the classical rolled up eddies at the interface. It, however, more that likely that the velocity profile there is a developed one akin to that of axial flow between to concentric cylinders.
2. The oil/gas ratio cannot be determined by simply relying on intermittency of the discharge. The result has to be corrected for differences in the discharge speeds of the gas and oil phase streams.

Entrainment

A fully developed turbulent jet entrains ambient fluid at a uniform rate with downstream distance. Even though (Eq. 9) for entrainment velocity at the edge of the jet is written for a fully developed turbulent jet, I will use it to estimate the jet velocity at the RITT.

Around 00:12 time mark in Video 4, an eel drifts into the view from above. It drifts toward the jet for 35 frames almost like a rigid vertical rod, evidently being entrained by the jet. It only starts swimming away from the jet after 36-37 frames in the view. During drifting, the eel moves (Δx, Δy) ≈ (24cm, 39cm) which translates to an entrainment velocity vector of (u, v) ≈ (16 cm/s, 27 cm/s), at 30 cm/s nearly normal to the discharge direction of the jet. Since the discharge jet is confined over the sea floor, the entrainment velocity will be higher that a free jet. Therefore, using Eq. 9 will yield high values for the jet velocity (in this case about 4 m/s). Nevertheless, we can conclude from the drifting eel that the discharge velocity is on the order of a meter per second at the broken end of the riser.

Comparison of BOP and RITT

Given the forensic evidence after the riser was cut off on June 3, 2010, showing two tubes instead of one at the kink, it is very uncertain, even impossible to even guess the pressure profile between the BOP and the RITT. The view of the discharge at the RITT oscillates between an almost white, apparently gaseous methane and dark liquid, presumably oil. At this depth (150 atm), the temperature of the discharge must be higher than the ambient temperature of 2^oC. Since the pipe between the BOP and the RITT is mostly horizontal, there is no hydrostatic pressure differential, between the BP and the RITT. The pressure drop is almost exclusively due to flow losses. Further, fluid had some time for heat exchange with ambient (cooling).

The situation at the BOP is quite different. The discharge is evidently homogeneous; the intermittency of the white/dark fluid of the RITT is absent. Methane has not separated into billows. It may well be in fine bubble form. Evidently, the pressure at the kink is so *high* that, even after the discharge, the methane stays in homogeneous distribution with oil within the camera view. This argument, although speculative, corroborates the high discharge velocity estimated in Eq. 6.

Uncertainty

- length scale in Fig. 1: 2.0 ± 0.02 mm/pixel
- length scale in Fig. 2: 1.6 ± 0.02 mm/pixel
- discharge diameter of J_1: D_1 = 12 ± 1 pixel = 2.4±0.2 cm
- speed of coherent structures at cm downstream of J_1 discharge: 40 ± 10 pixels/step = 150 ± 40 cm/s
- range of discharge in Eq. 7: [2300, 4800] m^3 / day

Summary

Table 1 summarizes the result of this report. To obtain limits for the total discharge rate, I summed the lowest and highest estimates in the table. The oil/gas ratio is another source of uncertainty in estimating the oil discharge ratio. The estimates range from 25% to 67% oil. The latest figure form the field is 41% oil. I have, therefore listed in the table *oil* discharge rates based on 25, 40, and 50% oil content.

The jets J and J_1 are clearly contributing the most discharge. Therefore, as a conservative estimate, I assumed equal discharges from J_1 and J to arrive at my estimate of volumetric discharge rate in the last row of the table. Given the images in Video 3, this assumption is indeed very conservative.

An estimate of the discharge at RITT remains elusive for me. The estimate in the Oil/Gas Ratio section, along 25% oil content stated in the preliminary report, suggest an oil discharge rate on the order of $\sim 10^3$ m^3/day. My confidence level on this figure, however, is low, and I will not consider it further until I have better tools to study the flow.

Table 1

Flow (Fig.1)	Fluid	Discharge Q (m^3 / day)	Remarks
J	Oil/Gas	2,000 - 5,000	The dominant discharge, gas/liquid ratio uncertain

Supplemental Report After the Cut-off at the BOP
2010 Gulf of Mexico Oil Spill Estimate

Ömer Savaş
Department of Mechanical Engineering
University of California Berkeley
Berkeley, CA, 94720-1740
savas@me.berkeley.edu
June 15, 2010

Introduction

The pipe immediately downstream of the BOP was cut off on June 3, 2010. The FRTG was asked to estimate the flow rate from the cut end. Numerous high quality HD videos (1920W×1080H pixels) were made available to the group. I have gone through 15 of them. I am writing this supplement based on the video clip

TOPHAT_06-03-10_14-29-22.avi (03:59)

which is composed of 7188 frames, that were extracted using QuickTime Pro©. During the teleconference on June 10, 2010, it was clear that I must provide details for my concerns and bases for my opinions. I first discuss my view of the applicability of conventional PIV techniques to the discharge problem at hand. Then, I present my approach and my final opinion. As was agreed by the members, I have looked at a 220 frame section of the video, in the frame number range of 2200-2420. The corresponding time stamps on the video are 06/03/10, 14:30:35 - 14:30:42.

Limitations of Conventional PIV

I see two problems with the application of conventional PIV techniques to the discharge rate estimate. The first one is mild and perhaps can be worked around. Figure 4 shows segments of two consecutive frames from a video clip that was recorded at 30 frames per second. The images are the green channel of the TIFF files. Evidently the flow is of high Reynolds number; the length scales vary from very large scale eddies, commensurate with the width of the jet, down to the resolution of the camera and image compression technique that may have been utilized. The features at the largest scales can be visually tracked between the frames. The smaller features are, however, independent between the frames. Closer visual examination employing various methods show that scales below about 10-30 pixels in size are independent. For reference, three square interrogation windows are shown; 32, 64, and 128 pixels on the side. A classical PIV technique using common correlation algorithms with 32×32 interrogation windows will not capture the motion of the larger scales. Windows of size 64×64 are also dubious. Perhaps, windows of 128 or larger can yield information, but only on the motion of the largest features. Small windows may be sufficient very close to the exit of the pipe, but will fall short in about a diameter downstream, as seen in the figure.

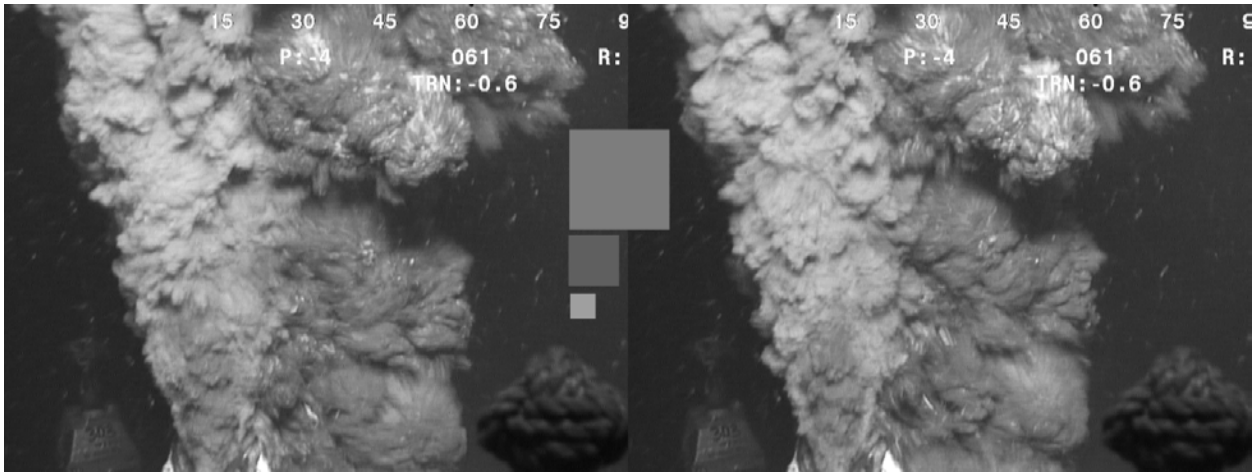

Figure 4: Cropped regions from TOPHAT_06-03-10_14-29-22, consecutive frames #2356 and #2357. The Green channel of the original TIFF image is shown. Images are 800W×600H and 1/30 second apart. The three squares at the center are 32, 64, and 128 pixels on the side.

The second limitation of PIV is more serious. The fluid that we are trying to measure is opaque. Optically we have access to the outermost *shell* of the discharge. As can be seen in almost all of the videos, the flow rolls into large eddies soon after leaving the pipe. Figure 5 shows an idealized cartoon of an eddy; it is rolled up, with interleaving layers of jet fluid and ambient sea water. In the figure the approximate light and camera directions are shown (see Figure 4). Overlaid are sketches of the mean velocity profile of the jet, and the velocity field of the eddy from its reference frame. Depending on the location of the eddy, one can even have a fluid element moving toward the exit of the jet (backward). The regions of the flow recorded by the camera are the outermost layers of the jet fluid. This layer, as explained above is constantly re-granulated by turbulence. Since the time between the images is too long to capture the same texture in both images, the camera records uncorrelated fine details on the jet fluid interface. In particular, if an interrogation window falls entirely on the surface of the structure (no large eddy shadow), then the correlation algorithm will yield not the velocity of the fluid parcel, but the length scale of the eddies. Any match with the local flow velocity is coincidental.

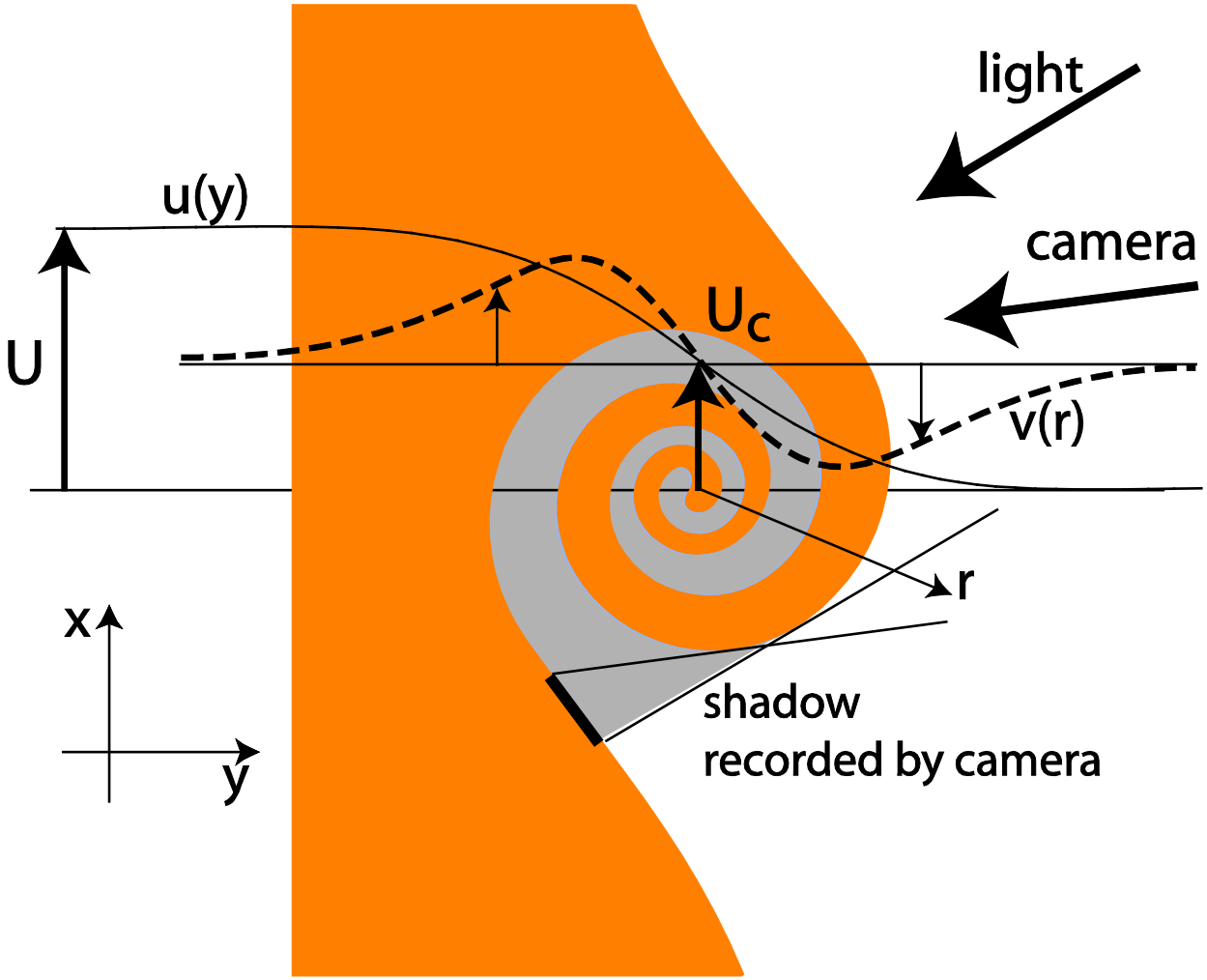

Figure 5: Flow field of a coherent eddy in the near filed of jet discharge. The jet fluid is discharging at velocity U, and is opaque. The eddy is translating at U_c. The mean profile of the jet is u(y) [solid line]. v(r) [dashed line] is the azimuthal velocity profile of the eddy in a reference frame moving with velocity U_c. Camera can only see the outer shell of the rolled up structure.

The shadows of the large eddies can be followed by the PIV if using commensurately large correlation windows (128 or larger, Fig. 6). Smaller windows will capture only smaller regions of shadow motion *and* the turbulence scales, biasing the PIV result toward the turbulence length scale. Therefore, a conventional PIV correlation algorithm will yield lower velocities for the motion the large eddies.

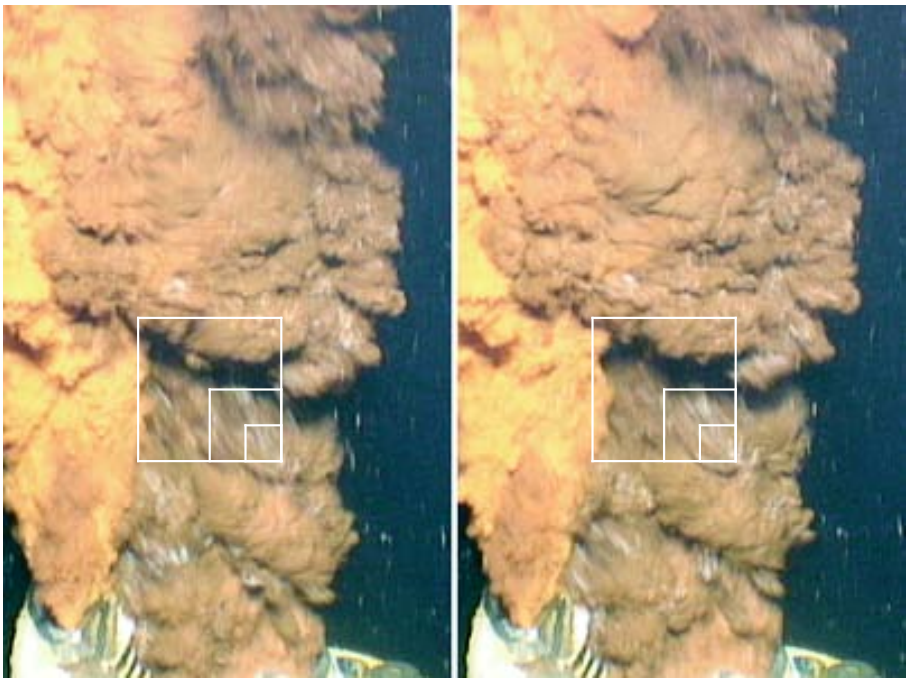

Figure 6: Cropped regions from TOPHAT_06-03-10_14-29-22, consecutive frames #2224 and #2225. Images are 400W×600H and 1/30 second apart. The three nested squares are 32, 64, and 128 pixels on each side.

Methods

I have used three independent approaches:

1. Direct visual tracking of large eddies,
2. Direct visual tracking of instability waves at the exit of the tube, and
3. Conventional PIV correlation on the green channel of the TIFF images.

Large Eddy Tracking

I have visually tracked large eddies using Photoshop. I used the central region of an eddy to mark its location and tracked it frame by frame for 10 steps (11 images). Figure 7 shows the beginning and the end of the first series of image frames where I marked the locations of the eddy with respect to a convenient reference on the edge of the pipe. The collective results for five series are plotted in the *xt*-diagram in Fig. 8 and tabulated in Table 2. The displacement results in the 4th column of Table 2, Δx, are the average displacements per step and are determined using the linear regression feature of MS Excel. The image calibration is done for each series separately, since the camera was moving. All measurements were done within 1.5 jet diameters.

The average large eddy velocity is 1.06 m/s, with a range of 0.47-1.61m/s. Part of this is due to the uncertainty in measurements, part is due to the uncertain conditions in the pipe. And some part is due to the dynamics of large eddies in the field of a jet; merging and leapfrogging of vortices cause variations in their trajectories.

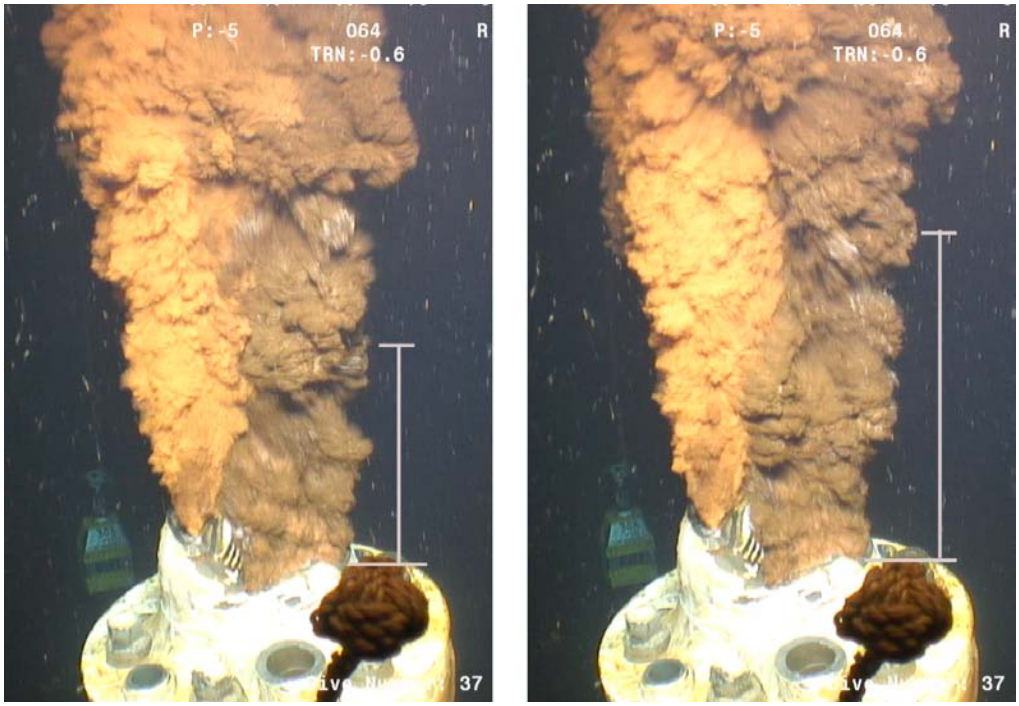

Figure 7: Visually following large eddies (coherent structures) in the flow field. Cropped images are from the first (2207) and the last (2217) images of Series 1 in Table 4. The vertical lines show the downstream position a tracked eddy with respect to a reference point on the edge of the pipe. Image segments are 700W×1000H.

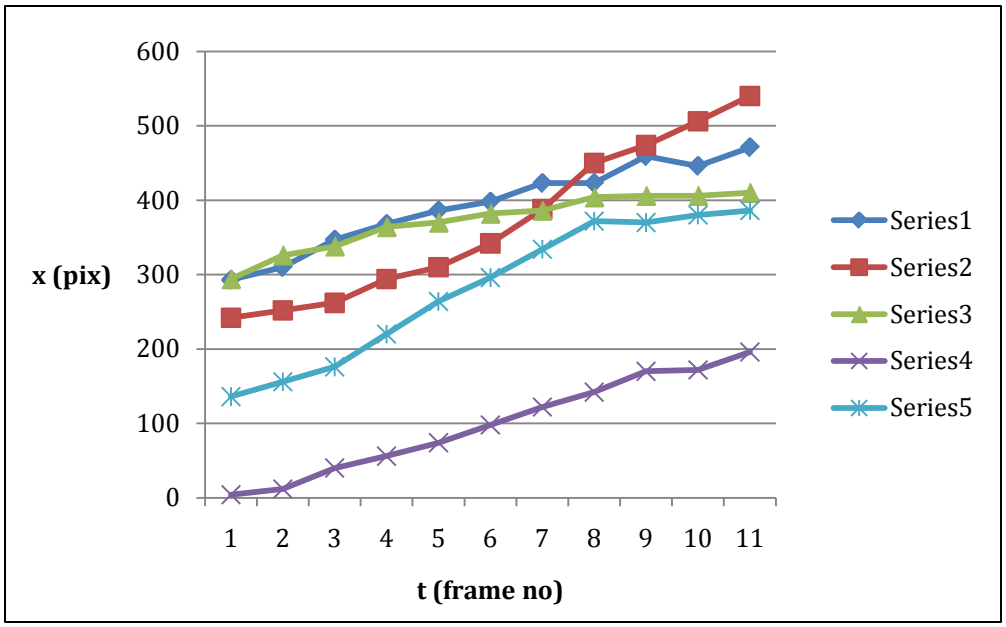

Figure 8: Trajectories of tracked large eddies in the discharge flow field.

Table 2: Manual large eddy tracking in the near field of the discharge.

Series	Image Sequence	Time Steps (1/30 sec)	Δx/step (pix)	Scale (mm/pix)	U (m/s)	Oil Discharge Rate (m^3/day)
1	2207-2217	10	17.4	2.04	1.06	7,100
2	2259-2269	10	32.1	1.67	1.61	10,800
3	2300-2310	10	10.9	1.46	0.47	3,200
4	2350-2360	10	20.1	1.49	0.90	6,100
5	2400-2410	10	28.2	1.51	1.28	8,600
	average				**1.06 ± 0.55**	**7,100 ± 3,700**

The discharge flow rates based on the large eddy tracking results are listed in the last column of Table 2. In these flow rate results, I assumed a cross sectional area of 0.19 m^2, ignoring probable distortions during cutting. I also have foregone extrapolating the large eddy velocity back to the exit plane of the discharge jet. The oil fraction is taken as 0.41. The discharge rate ranges from 3,200 to 10,800 m^3/day, with an average of 7,100 m^3/day. Sources of the variability were already noted above. Since no extrapolation to the exit plane nor any corrections for the density differences between the ambient sea water and discharge fluid were done, the discharge rates in the last column of Table 2 are conservative. They are likely to be higher.

Instability Wave Tracking

Right at exit of the cut pipe, I tracked the first signs of instabilities in successive image pairs I was able to detect. Figure 8 shows such a pair where I marked the location of the instability that was visually tracked using Photoshop. Since these are developing in the boundary layer of the exit flow, their phase speed is going to be slower than what the inviscid instability theory predicts. Furthermore, since the waves are just downstream of a solid wall where the no-slip condition is present (actually a stagnation point at lip), their speed will be further reduced. Nevertheless, that is much less than ½ of the bulk velocity inside the tube. Furthermore, buoyancy effects are negligible since the fluid has barely left the pipe.

The results are shown in Table 2. A close examination of the table shows that, when the waves are spotted near the exit, their velocity is slower, supporting the argument that the effect of the no-slip condition is present. It is assuring to see that the plot in the table suggests zero speed at the exit location where the there is a stagnation point. The average speed is 35 cm/s. Extrapolating these results to the bulk flow is a far stretch. It can, however, be used to established an exceedingly conservative lower limit for the discharge rate.

Figure 8: Visually following instability waves at their genesis. Sections from consecutive frames #2300 and #2301. The dashed line marks where the wave was tracked (see Table 3). Image segments are 450W×250H. The tracked displacement was 6 pixels.

Table 3: Manual wave tracking at the exit of the pipe.

Image Pair	Δx (pix) x_2-x_1=Δx	Scale (mm/pix)	U (cm/s)
2207-2208	39-32 = 7	2.06	43.3
2259-2260	22-18 = 4	1.90	22.8
2300-2301	39-30 = 9	1.45	39.2
2350-2351	23-17 = 6	1.49	26.9
2400-2401	47-35 = 12	1.51	54.3
5 samples			**35 ± 10**

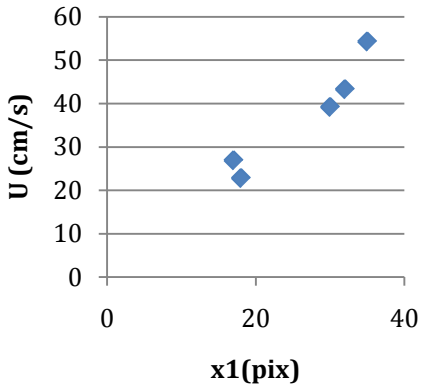

Taking the average value of 35 cm/s and multiplying by a factor of 2 to approximate the interior velocity (assuming iso-density), we obtain a volume flow rate of 0.133 m^3/s, or 11500 m^3/day. At 41% oil content, this gives an oil discharge rate of 4700 m^3/day. I have assumed here that the cross sectional area of the cut pipe is still 0.19 m^2. I consider this to be an exceedingly conservative lower limit for the oil discharge rate for two reasons: (1) density ratio will increase the velocity deduced at the center, and (2) the measured velocity of the waves is a lower fraction of the centerline velocity than the assumed value ½. Since the flow profile at exit is not known, (in fact it is known not to be uniform or top-hat), relating wave speed to the core speed is not obvious.

PIV Processing

After examining the **RGB** channels of the TIFF images extracted from the video, I have concluded that the Green channel had the best signal. The Red channel was saturated and the Blue channel was dim. After cropping the images to 1000H×1000V, I processed the five series listed in Table 2 at 32×32, 64×64 and 128×128 window sizes with no dynamic adjustment. The results for Series 1 are shown in Fig. 9. For the reasons stated above, only the results near the exit plane of the jet are deemed reliable, therefore the results presented in the table are averages over a one diameter across the jet and 1/3 diameter along the jet at the exit region. The results are summarized in Table 4. For each flow series, both the average flow speed (cm/s) and an average discharge rate (m^3/s) are shown. The speeds are comparable to the values of the instability wave speeds shown in Table 3 and the figure therein. This is expected, since, at their infancy, the instability waves are moving slowly, without changing their shapes radically. They are captured in successive images, unlike the flow feature further downstream. Therefore, it is obvious that any discharge rate calculation based on these PIV results near the exit will give values comparable to that obtained from wave tracking analysis above.

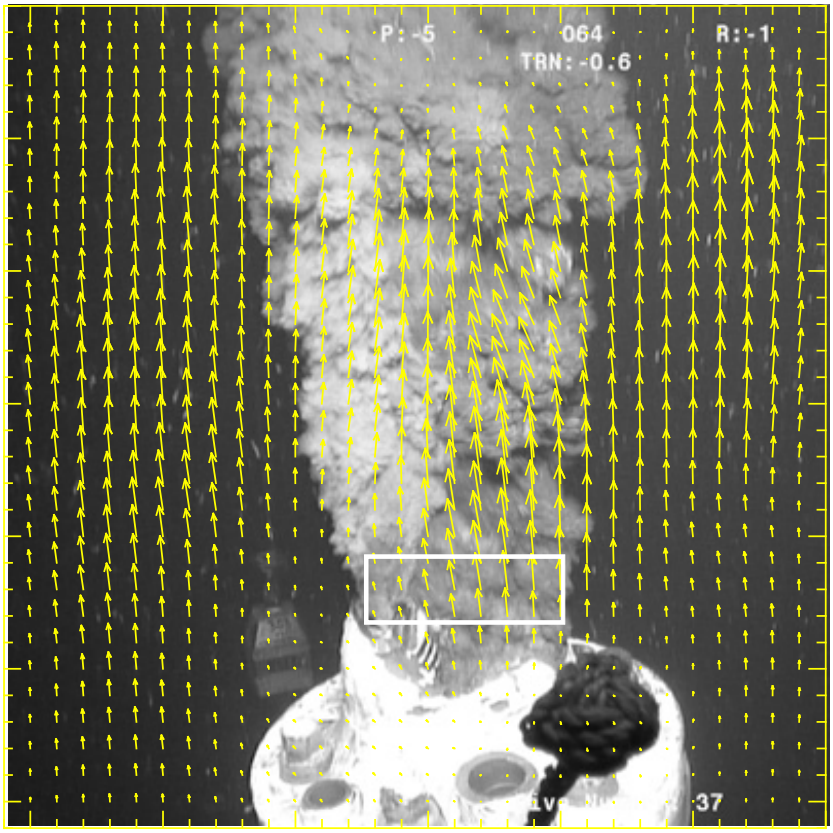

Figure 9: Sample PIV result. Average vector field of Series 1 is overlaid on frame #2207. Image processing is done at 64x64 windows. The vector field is filtered. The rectangular box over the pipe exit roughly marks the region where average velocity is determined.

The discharge rates in the table are calculated based on an exit area of 0.19 m^2 and an oil fraction of 0.41. Most important, the average speeds were multiplied by a factor of 2.9 (including density correction) to extrapolate for the *bulk* speed at the interior of the jet. This is necessary since what PIV is measuring are the speeds of the instability waves. The relation of these to centerline speed is a big source of uncertainty.

Table 4: PIV Processing Summary: Average wave speed (cm/s) at the pipe exit.

Series	Image Sequence	PIV @ 32×32	PIV @ 64×64	PIV @ 128×128	Remarks
1	2207-2217	30 cm/s	29 cm/s	32 cm/s	
		5,900 m^3/day	5,800 m^3/day	6,400 m^3/day	
2	2259-2269	25 cm/s	30 cm/s	29 cm/s	Excessive camera motion
		5,000 m^3/day	5,900 m^3/day	5700 m^3/day	
3	2300-2310	20 cm/s	22 cm/s	8 cm/s	
		4,000 m^3/day	4,400 m^3/day	1,600 m^3/day	
4	2350-2360	25 cm/s	29 cm/s	12 cm/s	
		4,900 m^3/day	5,700 m^3/day	2,500 m^3/day	
5	2400-2410	14cm/s	14 cm/s	3 cm/s	
		2,800 m^3/day	2,700 m^3/day	600 m^3/day	

Conclusion

Table 5 summarizes the findings of this supplemental report. All results are based on an oil fraction of 0.41 and a discharge area of 0.19 m^2. The results from eddy and wave tracking analysis are the basis of the conclusion of this supplement. The results from the PIV analysis are the highest discharge rates deduced subject to the assumptions stated and are presented to provide a perspective.

Table 5: Supplemental report summary.

Method	Oil Discharge Rate (m^3/day)	Remarks
Large eddy tracking	**7,100**	**Most likely**
Instability wave tracking	4,600	Conservative minimum
Image velocimetry @ 32×32	6,400	Maximum from Table 4
Image velocimetry @ 64×64	5,900	Maximum from Table 4
Image velocimetry @ 128×128	5,900	Maximum from Table 4

I consider the oil discharge rate of 7,100 m^3/day as the most likely value. It is doubtful that it is significantly lower that this value. However, it can easily be 10%, even 20% higher, since the assumptions made in calculating the flow rate from eddy tracking were on the conservative side.

Respectfully presented,

Ömer Savaş
June 15, 2010
Berkeley, CA

Appendix 5: Gulf Oil Spill PIV Analysis

Professor Steve Wereley
Mechanical Engineering and
Birck Nanotechnology Center
Purdue University

Abstract

The Flow Rate Technical Group (FRTG) was tasked with arriving at several estimates of the oil release into the Gulf of Mexico (GoM) subsequent to the April 20, 2010, blow out of the British Petroleum Deepwater Horizons well. We were initially instructed to arrive at a scientifically defensible estimate of the oil flow rate out of the end of the broken riser pipe during the period before the RITT was installed. We were to consider both the flow from end of the riser as well as the flow from multiple jets at point where the riser was kinked on top of the Blow Out Preventer (BOP). Using several different videos, I calculated flow rates ranging from 15,000 to 35,000 barrels per day. On June 3 BP cut the kinked riser pipe just above the BOP and installed a cap called the Lower Marine Riser Package (LMRP) cap to capture some fraction of the flow. There was a considerable time (on the order of hours) between the cutting and capping of the riser during which time videos were acquired showing the oil flowing vertically upwards out of the riser stub. The cutting operation accomplished two things in addition to making the LMRP cap operation possible. First, it changed the flow from several independent flows emerging from multiple locations to a single large flow emerging from one location. Second, it increased the flow rate. Simple consideration of the physics dictates that the flow must increase to some undetermined degree when the flow resistance from the kink and a considerable length of riser pipe is removed. The FRTG was also tasked with determining the oil flow rate during this period. I calculated a flow in the range of 30,000 to 40,000 barrels per day.

Introduction

The jet issuing from the broken riser pipe lying on the ocean floor could be classified as a buoyant, immiscible jet with different physical properties from fluid it is issuing into. Most notably, the density is lower and the viscosity of the oil is higher than the sea water. The reader is referred Panton (2005) for a general discussion of jet behavior. The analysis of the jet is difficult because it is opaque. It is not possible to see the interior motion of the jet as with conventional Particle Image Velocimetry. In fact, this approach would be more properly classified as correlation-based feature tracking. Basing my analysis on the features that I see—and track—at the oil/water interface introduces some complexity into the analysis and requires assumptions about how the motion of the visible structures relates to the average velocity of the jet. These issues are well-described in other reports from the FRTG so I will not repeat them here.

Pre-Riser Cut Flow Rate

Initial Individual Measurements (a Bit of History)

On May 12, 2010, British Petroleum released the video *Crater_plume_gassing_11_may_2010_2333.wmv* that shows oil and gas emerging from the broken riser pipe lying on the ocean floor subsequent to the Deepwater Horizon accident on April 20, 2010. Frames from the video were extracted and analyzed using the particle image velocimetry code EDPIV (custom written by Lichuan Gui and available at edpiv.com) as well as manual feature tracking. This was the first video released to the public and was of very poor quality. It had a number of compression artifacts in it. It seemed to be a screen capture at 30 Hz of a video originally recorded at 25 Hz. Nonetheless, it was possible to make a preliminary determination of the oil flow rate. I selected two images from around 23 seconds into the video (Fig 1) to analyze because they seemed representative of oil flow and I could see many flow features with my eye that I expected my custom-written PIV code, EDPIV, to be able to track.

These two images were analyzed by **EDPIV** using the following settings:

- initial displacement (10,-6) pixels
- window size 128x128 pixels
- grid size 32x32 pixels
- regional renormalization with 37 pixel kernel
- 5 iterations

A very small vector field measuring only 3 vectors horizontally by 2 vectors vertically was chosen. Quite large interrogation windows were needed (128x128 pixels) in order to have sufficient signal to noise ratio for **EDPIV** to successfully compute velocity vectors. These large interrogation regions span the horizontal extent of the jet and so fully sample the velocity of the flow features. The average displacement for these 6 vectors has a magnitude of 10.2 pixels. Since the vectors are calculated slightly downstream of the elliptical volume of fluid used in the manual feature tracking approach, the displacement has decreased slightly. It is also apparent that the plume has broadened at this location. The velocity field calculated is plotted on top of the first image of the pair used to calculate it and shown in Fig. 2.

Figure 1a: Filename and time index: 22890000 (22.89 secs). The pipe is seen running horizontally in this image with the flow issuing out of the break at approximately the horizontal center of the image. The darker colored material is crude oil. The arrow indicates the location of the lower right edge of the elliptical volume of fluid used in the manual tracking approach.

Figure 1b: Filename and time index: 22957000 (22.957 secs).

Figure 2: PIV calculated vector field (average displacement 10.2 pixels).

Turning this displacement calculation into a volume measurement requires two additional parameters: a length scale and the time between images. The length scale was provided by British Petroleum. The outer diameter of the pipe visible in the pictures is 21 inches. Measurements in the images show that the pipe is 124 pixels across. The time between frames is given by the time index of the images. For these two images that works out to: 22.957 - 22.890 = 0.067 sec. However, the properties information for the video says it was recorded at 25 Hz, i.e., an interframe time of 0.04 sec. I will use the 0.067 sec interframe time to come up with a *more conservative* estimate of velocity. With these parameters the velocity can be calculated from the displacement according to

$$10.2\,\frac{pixels}{frame}\times\frac{1\,frame}{0.067\,sec}\times\frac{21in}{124pixels}=25.8\,\frac{in}{sec}$$

To turn this into a volume flow rate measurement, one must multiply by the cross-sectional area of the pipe. British Petroleum has informed me that the inner diameter of the pipe is 20 inches. The volume flow rate is calculated according to

$$25.8\,\frac{in}{sec}\times\frac{\pi}{4}\times(20in)^2=8105\,\frac{in^3}{sec}$$

Units conversion to barrels per day:

$$8105\,\frac{in^3}{sec}\times\frac{60\times60\times24sec}{day}\times\frac{1gal}{231in^3}\times\frac{1bbl}{42gal}=72179\,\frac{bbl}{day}$$

On the flow analysis side, this estimate is doubly conservative because after the jet of oil issues out of the pipe, it slows and expands. By using a PIV velocity measurement from the plume area (where the speed is slower than in the pipe) and the cross-sectional area of the pipe (which is smaller than the diameter of the plume), we get a *conservative estimate* of the velocity.

I calculated an oil flow rate of 72,179 barrels per day (0.129 m^3/s) and estimated the uncertainty to be +/- 20%, meaning that the likely flow rate is in the range of 56,000 to 84,000 barrels per day. BP had released very little information to the public at the time these calculations were made. In particular, the Gas to Oil ratio or GOR was not released. After these initial measurements were made, a GOR of 3000 scf of gas per barrel of oil was announced by BP. This translates to a volume fraction of oil at the sea floor conditions of 0.29. Another factor to take into account is the variation in oil density as the temperature and pressure change from the area where the videos were recorded to sea surface conditions. The density change is estimated to increase by 35% as the oil cools and floats to the surface (Sec Chu). My original measurements above can then be adjusted by these two factors to give:

$$\left(72{,}179\,\frac{bbl}{day}\right)_{sea\ floor} \times 0.29 \times 1.35 = \left(28{,}258\,\frac{bbl}{day}\right)_{std\ conds}$$

BP also announced that the end of the riser was deformed to a considerable extent resulting in the exit area of the riser pipe being reduced by approximately 30%. Further, a drill pipe protruding from the end of the riser further reduced the cross-sectional area. Since the measurements were made approximately one diameter downstream of the riser exit, it is expected that these effects will not influence the flow rate calculation.

A few days later BP released four more videos. One of these was *H14 BOP Plume May 15 1920-1945*. From this video it was possible to calculate the flow out of one of the two apparent leaks at the riser kink location immediately on top of the BOP. Based on visual inspection and feature tracking, an initial flow rate calculation of 25,000 bbl/day was calculated. Making the same adjustments as above, the actual flow rate in stock barrels per day at standard conditions is

$$\left(25{,}000\,\frac{bbl}{day}\right)_{sea\ floor} \times 0.29 \times 1.35 = \left(9{,}788\,\frac{bbl}{day}\right)_{std\ conds}$$

A total initial estimation of the flow rate based on the poor quality videos available at the time would be 38,046 bbl/day.

Phase 1 FRTG Measurements

After the formation of the Flow Rate Technical Group, we began to analyze the pre-riser cut videos made available to us by BP. Initially these were very poor quality videos that appeared to be a screen capture at 30 Hz of a 25 Hz video. Compression artifacts, most notably pixelization, were clearly observable as were temporally non-uniform frames. After a couple of iterations with BP, full resolution videos were finally made available. These videos were shot with a variety of lighting conditions and magnifications. Several of the videos were suitable for correlation analysis. The video *20100514221717125@ H14_Ch1-H264h.mov* was suitable for correlation analysis. The ROV was stationary during this video. In order to increase the accuracy of the PIV measurements, an ensemble of 1000 images was used to calculate the jet displacement. The time index (as seen by the clock in the video) of the beginning of this ensemble was 17:30:05 and the end was at 17:30:48. This video segment was chosen because it showed mostly liquid oil flow and not gas. Using procedures similar to those described above as well as correlation averaging (Raffel, 2007), an average velocity of 7.52 in/sec and a plume diameter of 24.53 in is calculated along the yellow line (Fig 3). These numbers can be used to calculate the daily flow rate. Assuming oil to gas ratios from 0.29 to 0.5 and jet outer velocity to jet average velocity ratio of 1.5 to 2.0, a range for the oil flow rate is found to be 13,771 to 31,658 barrels per day. The combinations of these values are shown in Table 1.

Figure 3: Displacement (or velocity) field and plume diameter measurement area. The average velocity is 7.52 in/sec and the plume diameter is 24.53 in along the yellow line.

Table 1: Phase 1 riser exit flow calculations.

Jet Displacement	2.155	2.155	2.155	pix
Jet Ratio	1.50	1.75	2.00	
Jet Velocity	7.52	7.52	7.52	in/sec
Jet Flow	5332	6221	7110	in^3/sec
GOR	0.29	0.40	0.50	
	13771	**22161**	**31658**	bbl/day

Of the multiple leaks in at the kink point of the riser, only one was suitable for image analysis. The video *H14 BOP Plume May 15 1920-1945* shows these leaks. Because the ROV was hovering during the acquisition of these images, an ensemble of only 25 images could be found where the ROV was relatively stationary. The average velocity at the location indicated by the arrow in Fig 4 was 6.95 in/s while the jet diameter at that location was 7.61 in. Combining these measurements into a flow rate calculation, the flow rate was found to range from 1225 to 2815 bbl/day. These values are shown in Table 2. Because of the presence of two jets in the kink location, only one of which was measurable, the total flow rate from the two leaks was taken as twice the flow rate from the measurable jet. The total flow rate from the two locations, the kink point and the riser end, range from 14,996 to 34,473 bbl/day.

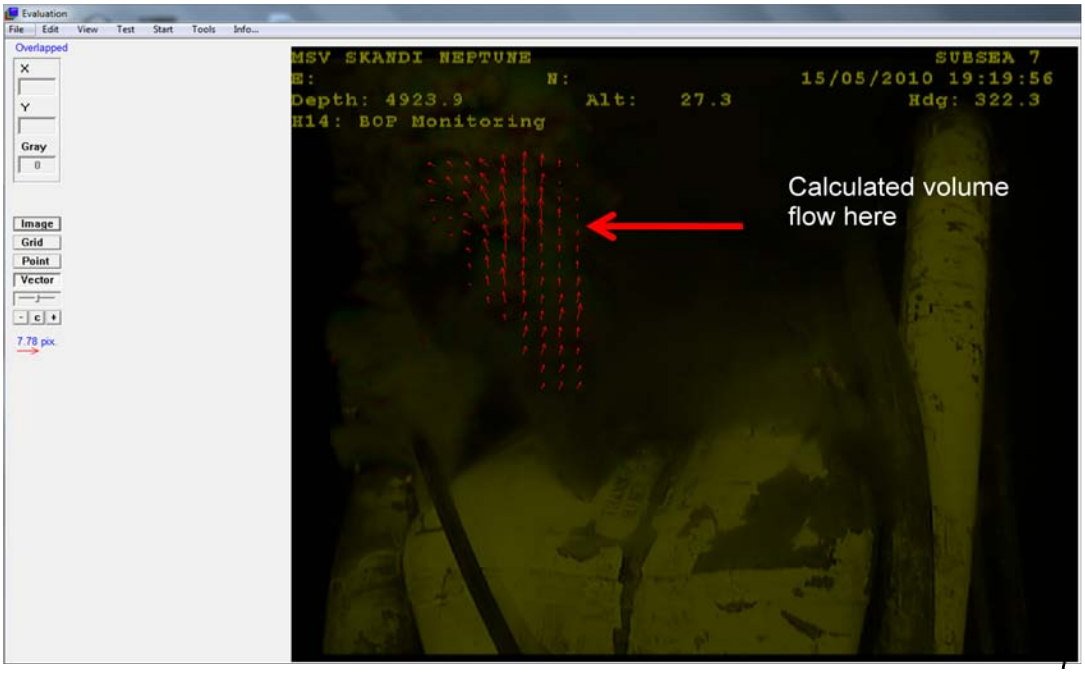

Figure 4: Velocity field for one of the jets at the location of the kinked riser and location where volume flow rate is calculated.

Table 2: Phase 1 velocity of kink point jet and location of flow rate calculation.

Jet Velocity	6.95	6.95	6.95	in/sec
Jet Diameter	7.61	7.61	7.61	in/sec
Jet Ratio	1.5	1.75	2	
Num Jets	2	2	2	
Jet Flow	474	553	632	in^3/sec
GOR	0.29	0.4	0.5	
	1225	**1971**	**2815**	bbl/day

Post Riser Cut Operation

Phase 2 FRTG Measurements

The kinked riser was cut on June 3 and a tophat was clamped on top of the riser stub. The tophat featured a riser to a surface collection ship, ethanol injection points, and several vents. During the time frame between cutting and removing the riser and installing the tophat, a ROV was tasked to acquire images of the oil flowing out of the riser stub. All of the videos have the same problem as kink jet measurements above—the ROV was afloat and hence the field of view is continuously moving. The video most suitable for correlation analysis is *TOPHAT_06-03-10_14-29-22.avi*. This video shows several well-lit views of the jet. The cross section of the riser contains two sections of drill pipe within it. At least one of these drill pipes is flowing oil as well. The color of the oil coming out of the drill pipe is lighter than that coming out of the riser. Because correlation averaging is such a versatile method for increasing the signal-to-noise ratio, a time period during which the ROV motion is minimal was found. The time index (as seen on screen) was 14:30:35. At this time frame, an ensemble of 51 images could be used because the motion of the ROV was very small compared to the size of the jet. A jet outer feature velocity of 20.24 in/sec calculated using a framing rate of 30 Hz and a scale factor based on the flange of 43 in = 527 pix (Fig 5). Instead of using the actual jet cross-sectional area which is difficult to use because the significant entrainment of the sea water, the riser cross-sectional area was used instead. Of course, there was a slight reduction in riser cross-sectional because of the shears used to cut the riser as well as the presence of two drill pipes in the riser pipe but we also know that at the area where the velocity was calculated, the actual jet diameter would have increased from its exit diameter. These two factors offset each other and the cross-sectional area of the riser is a good approximation for the cross-sectional area of the jet. That area is 298.6 in^2. Using a oil to gas ratio of 29% and an expansion of the oil from sea floor conditions to atmospheric conditions of 135%, the oil flow can be calculated as 30,000 to 40,000 bbl/day with an expected value of 35,000 bbl/day.

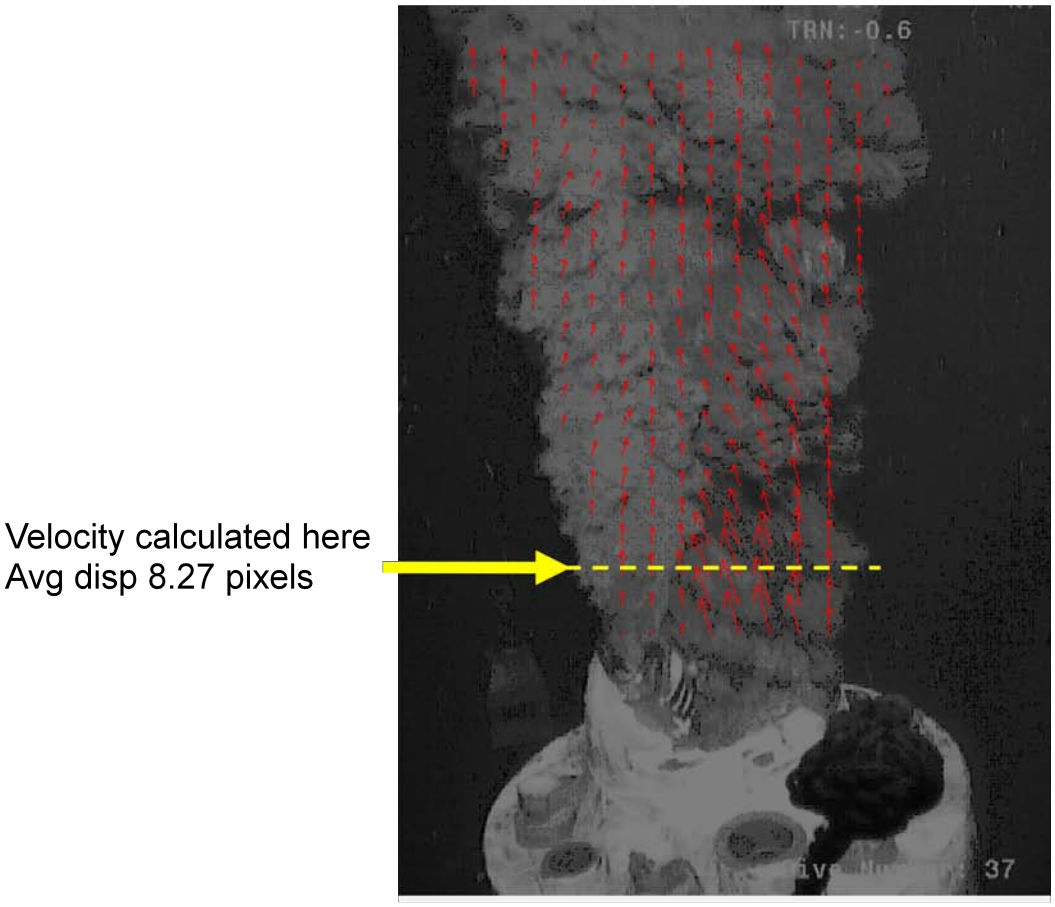

Figure 5: Phase 2 measurements made during the cut and cap operation June 3.

References

M. Stanislas, K. Okamoto, C. J. Kähler, J. Westerweel and F. Scarano, "Main results of the third international PIV Challenge," Exp Fluids, Vol. 45, pp 27-71 (2008).

M. Raffel, C. Willert, S. Wereley, J. Kompenhans, Particle Image Velocimetry: A Practical Guide, Springer, New York (2007). ISBN: 978-3-540-72307-3

L. Gui, Methodische Untersuchungen zur Auswertung von Aufnahmen der digitalen Particle Image Velocimetry, Shaker Verlag, Aachen, Germany (1998). ISBN 3-8265-3484-0.

Appendix 6: Riser Pipe Flow Estimate

Dr. Ira Leifer
University of California, Santa Barbara

Overview

Our goal was to estimate the amount of oil issuing forth from the pipeline leaks of the Macondo incident based on BP provided (and BP selected) data for use in coming up with representative flow rates for spill response issues, not damage assessment. As a result, we were tasked to use the data at hand to provide our best possible guidance under the understanding that the results were unlikely to be accurate due both to the large number of uncertainties for a high volume, oil-gas-hydrate-tar bubble flow at these depths, and because of the demonstrated variability on a range of time scales even with the data provided, as well as our understanding of natural hydrocarbon migration systems which exhibit significant variability. As a result, the approach used did not seek to quantify oil flows with a second digit, and all values herein must be considered as probably with large uncertainty as to whether they are representative for the data herein, much less for extension to other times when no data was available or was analyzed, and far less to other times, particularly times extending to periods prior to or after various BP operations to mitigate the oil leak.

Temporal Variability of Emissions, Pre – Top Kill

The oil-gas-water flow from the riser pipe exhibits clear temporal trends. Specifically, the flow shifts from a largely, buoyancy-driven gassy flow (primarily methane bubbles) to a flow that is predominantly oil – a conclusion based on the greatly reduced buoyancy of the flow. There also was a transition flow between these two cases, which is very abrupt in the case of shifting towards oily, and far slower for the shift to gassy (Fig. 1). This behavior is common in multiphase pipe flow, where the flow is no longer a well-mixed flow to what is best characterized as "slug flow." The flows are discrete indicating significant phase separation during flow through the pipe. Specifically, the oily phase can be seen "riding" under the gassy phase. During transitions, the flow color shifts towards brown rather than the white and black observed in the two extremes indicating that the fluid most likely is an emulsion (mixture of oil/gas/water in microscopic droplets) formed by turbulence at the "boundary" between the driving gassy flow and advected oily flow layer. Of course this is a significant oversimplification of the actual multiphase flow, which clearly includes hydrate flakes (most clearly visualized during the oily phase), likely oil globules, and a varying emulsion factor for all but the clear "white" gassy phase, where the buoyancy flow is best characterized as oily bubbles.

To characterize the variability in the flow, I created an intensity interrogation window (Fig. 1) and analyzed the time variability of the oil-gas ratio through the variations in the image intensity.

Figure 1: Plume of oil and gas escaping the riser pipe sowing the three flow types, gassy, transition, and slightly oily. Also shown is the location of interrogation window.

The interrogation window intensity variations (Fig. 2) clearly characterize greater variability during gassy flow, a rapid switch to oily flow and a slower return to gassy flow.

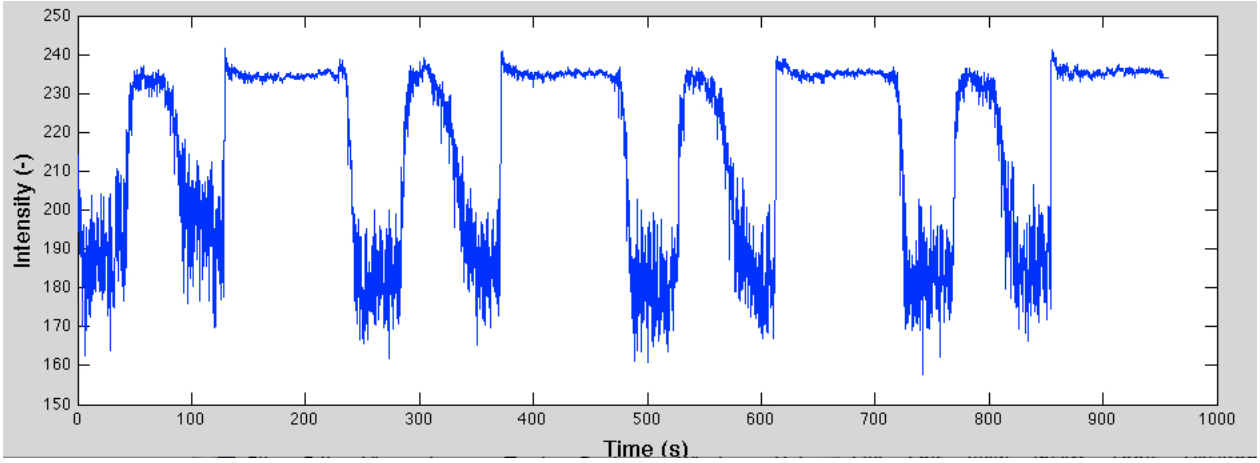

Figure 2: Interrogation window intensity trends. Higher value is darker.

Intensity variation of the riser pipe emissions (Fig. 2) then were evaluated by using a moving Hanning window and a spectral approximation approach (pburg, 128 pole). This analysis showed different spectral characteristics for the oily and gassy phases (Fig. 3). Thus, extrapolation of variability in the gassy and oily phases to longer time scales need to be considered separately.

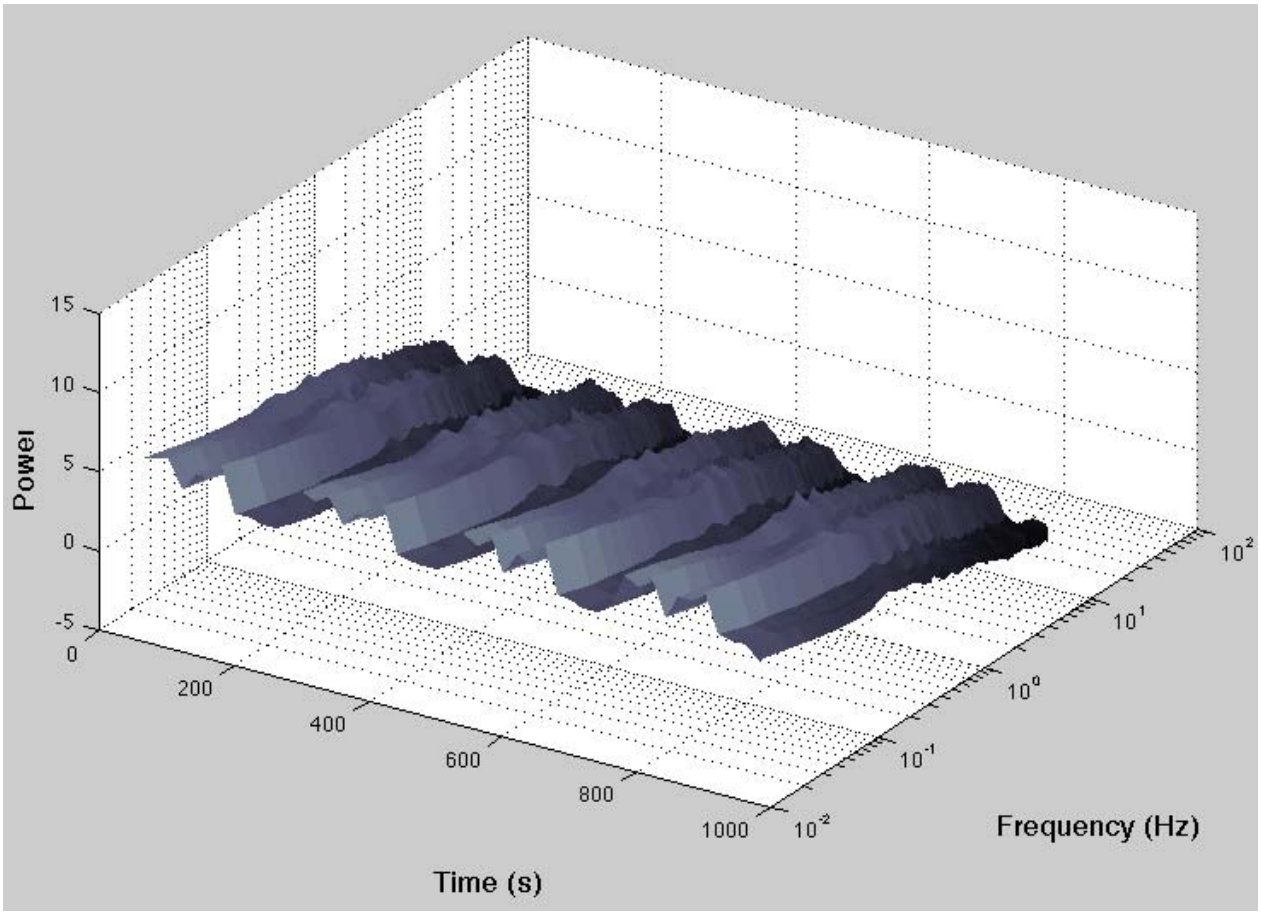

Figure 3: Spectragram of time varying spectra of the intensity variations, representative of oil-gas flow dynamics.

Spectragram of Gassy-Oily Phase

Because of the difference in spectra from the oily and gassy flow regimes, it is inappropriate to analyze a spectra for the entire data set (Fig. 4) and interpret quantitatively, thus the following qualitative interpretation is presented. Of significance, the spectra for the low frequency components is highly distinct from higher frequency components. These two behaviors likely relate to turbulence in the pipe (0.2 Hz to 1 Hz), and variability in the flow associated with slug flow behavior (>1 Hz). Because the interrogation window is close to the pipe mouth, turbulence structure development in open ocean flow has a relatively smaller effect on the intensity particularly for the oily phase – a conclusion that clearly is not valid further from the pipe entryway. Extrapolating variability to longer time scales, which could represent migration processes to the well within the reservoir rock layer, and the effect of possible breaches in the well pipe structure thereby allowing fluid migration into the surrounding rock formations above the reservoir formation cannot be done from the analysis of this data set.

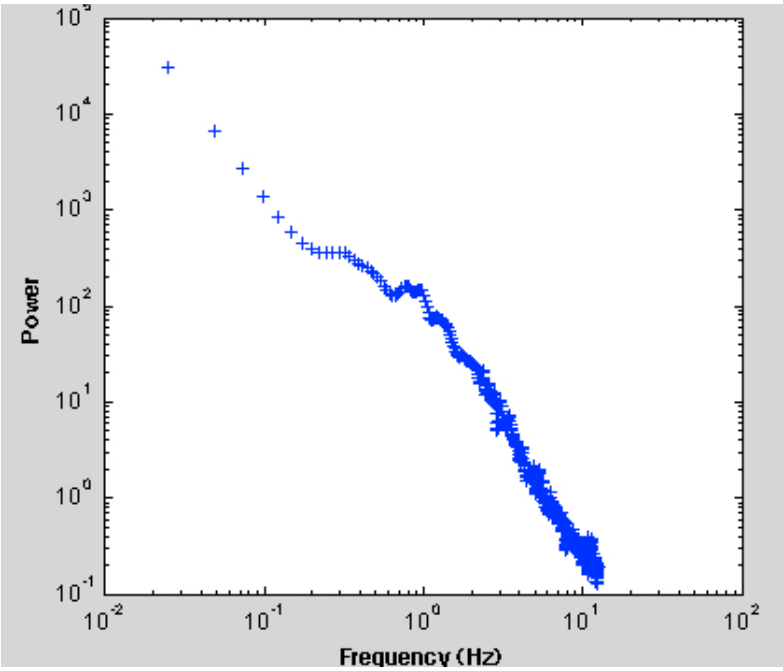

Figure 4: Entire data set spectrum of intensity in the interrogation window (from pburg spectral approximation approach).

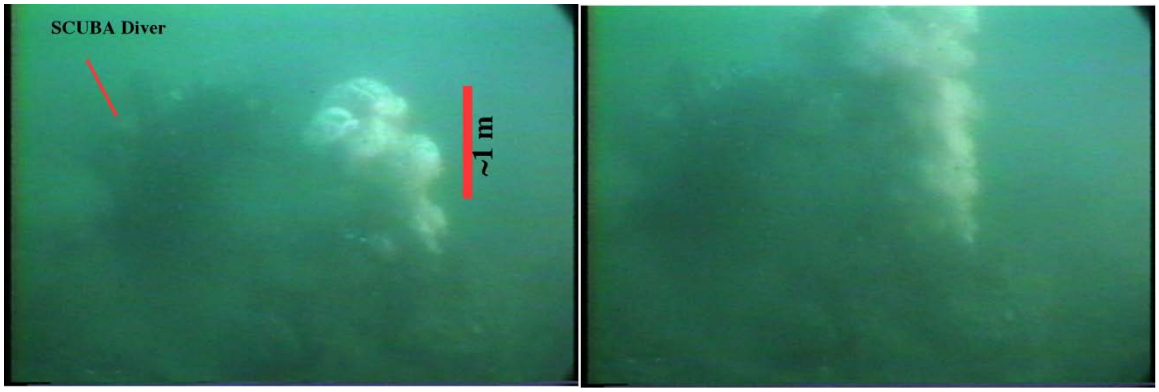

Figure 5: Images showing initial blowout in the Coal Oil Point seep field (20 m depth), and bubble plume one second later. Size scale based on an assumed standard spherical SCUBA diver head (25 cm diameter).

Flow Estimate by Similarity

Based on simple velocity and size scaling estimates, a rough buoyancy flow of 400 L/s was estimated for the plume during the gassy phase. This value was, coincidentally, similar to a blowout observed in the Coal Oil Point seep field [*Leifer et al* 2006] at 20-m depth. In the Coal Oil Point seep field plume (Fig. 5), a gas flow rate of 0.4 m^3/s STP (buoyancy flux 0.13 m^3/s or 11,000 m^3/day buoyancy flux, or 34,000,000 L/day gas buoyancy flux). Note, this natural blowout lasted only ~5 minutes. The emission flow was determined from back trajectory calculation using a Gaussian plume flux model of an atmospheric plume, thanks to the fact that the methane plume (fortuitously) drifted over an air pollution monitoring station a few minutes later.

Velocities of vertical features for the Coal Oil Point blowout plume (Fig. 5) were similar to feature velocities for the gassy phase of the Gulf Spill plume. Specifically, velocities were ~1.5 m s^{-1} versus 1.2 m s^{-1} for the Coal Oil Point blowout and Gulf spill plumes, respectively. It is important to note, though, that a dye injection in the Coal Oil Point blowout plume, a few seconds later, showed the centerline upwelling flow actually was 3-5 m/s in this depth range, with a water column average (based on time for the dye to arrive at the boat) of 3 m/s – the lower rise velocity arises from the effect of stratification [*Leifer et al* 2009]. **This demonstrates that in intense, large-scale bubble jets in the acceleration phase, centerline velocities can be elevated by significantly more than a factor of two compared to edge feature velocities, which is relevant for various image correlation analyses of plume surface features**.

Based on assuming these two flows are comparable, and that the gassy phase represents the dominant gas transport phase, an uncorrected flux of 33,500 barrels of oil per day for a 50:50 oil to gas ratio (gassy phase), or 19400 barrels of oil per day for a 29:71 oil to gas ratio can be calculated. Here, the difference between the plume surface feature velocities, ~20% higher for SB Channel, approximately balances the fact that the buoyancy flux is ~26% lower at the Macondo depth due to the effect of methane compressibility [*Rehder et al* 2009].

This approach makes several assumptions, one of which is that the effect of hydrate skins on the bubbles is negligible. This assumption may be reasonable because most of the bubbles appear to be very small (r < 150 μm) based on their behavior, thus, their surfaces area immobile whether due to oil or hydrates or ocean surfactants.

Assigning an uncertainty to this approach is difficult; around 20-40% seems likely. However, for the purposes of this report, this flux is used as a guide for comparison with the imaging velocimetry measurements.

Video showed bubble expansion at a rate for greater than hydrostatic suggesting that the below the orifice the bubbles were above hydrostatic equilibrium. While in the deep sea it is unlikely that there would be significant growth due to pressures significantly above hydrostatic, the probability of gas evasion from oil droplets is another issue. This effect could be very large at the kink, or where in the cut riser the gas escapes from a narrow restricted tube as a strong jet.

- - - - - - - - - - - - - -

There are two dominant flow regimes, or phases observed with radically different oil to gas ratios. For this portion of the analysis I consider the oil to gas ratio to be based on what is clearly visible. Thus, while the gassy phase suggests minimal oil, the oily phase is clearly a mixture. Specifically, different portions of the plume have more vertical trajectories (Fig. 6) suggesting greater buoyancy flux and thus lower oil to gas ratios. Consistent with this interpretation are white objects interpreted as hydrate flakes, and thus associated with higher gas to oil ratios, are in the portions of the plume whose trajectory is more vertical. Also affecting the flow is the trench seabed, which forces a vertical component into the flow. Interaction with the seabed causes a blow back of oil in the background. This oil does rise buoyantly, indicating a non-negligible buoyancy contribution from gas phase, creating a vertical motion, which is independent of pipe inertia and wall effects. These plumes are illustrated in Hierarchical Digital Imaging Velocimetry (HDIV) analysis shown in Fig. 6. This analysis uses custom written HDIV software in Matlab, with two passes, and an initial, 96-pixel interrogation window, the second window being 48 pixels, and 75% overlap. Because of the low contrast in this plume, the HDIV software has significant problems, and so the results are only considered indicative.

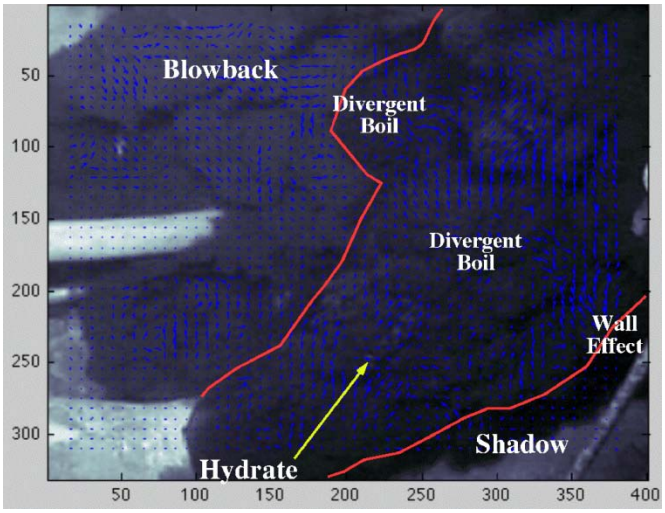

Figure 6: Hierarchical Digital Imaging Velocimetry-derived velocity vectors and flow image illustrating oily flow characteristics.

Based on manually tracking the hydrate tinged boils, ~ 17 cm s^{-1} and assuming a 1.4 momentum – centerline velocity (top hat velocity profile within), the flow is 92 L s^{-1}. Assuming 0% produced water, and 80% oil to 20% gas ratio, a 25% fluid entrainment growth rate, and a mean plume diameter of 70 cm, the oil flow is 44 L/s, or 3800 m^3 day (23000 bbl/day) for the oily phase. The entrainment factor is less than a pure geometric factor because, based on the observations of *Leifer et al* (2006), it is assumed that the gas phase is above equilibrium for the first few seconds of rise and the bubbles are expanding. This process requires several seconds for these kind of flows, studies of individual bubble formation show this arises due to the added mass force which is significant (the growing bubbles must push the water aside), e.g., [*Vazquez et al* 2010].

Key is the estimate of 17 cm/s from surface feature motions to internal fluid motions. In this case, a 1.4 factor likely is highly conservative (e.g., by comparison with the Coal Oil Point seep field observations, or the data presented in [*Milgram*, 1983]). Observations of the entrainment and advection of an eel by the flow (Fig. 7) suggests the fluid motion is 45 cm s^{-1}, or a factor of 2.6. This too likely is somewhat conservative due to the acceleration time of the oil flow on the eel's body. The eel shows no sign of attempting to swim into or out of the plume.

Figure 7: Fluid velocity estimate by eel advection. Ideally, a dye injection study would have allowed a proper scientific value to be determined; however, never was green-lighted by BP, although was proposed.

This value is increased by a geometric correction factor due to the wall effect, illustrated in Fig. 8. Unfortunately, this correction factor is not known, video from overhead is at an unknown but highly oblique angle with an unknown zoom setting, and at a different time (the geometric correction factor depends on the flow and the oil to gas ratio – where the flow is gassy, its rapid conversion from momentum driven to buoyancy driven allows the plume to remain distant from the wall such that wall effects on the plume proper (not the momentum plume) are minimal for the gassy phase. The likely correction factor could be 2 – 3 for the geometry shown in the image in Fig. 7b. Applying the momentum correction factors 2.6 and geometric correction factor of 2 suggest 89000 bbl/day for the oily phase. If one was to further assume no oil transport during the gassy phase, a best guess, conservative estimate based on a 50% duty cycle is ~45000 bbl/day for this plume. The precise duty cycle, while known for this data period, is not known for longer time periods, on the order of a day. An oil to gas ratio for the oily phase of 0.8 was assumed, which averaged with an oil to gas ratio for the gassy phase of near zero and a duty cycle of 50% yields a mean oil to gas ratio of 0.4.

2*2.6*17* pi*35* 35/1000 (*0.8*1.0*0.75*3600*24) / (159)

GeoCorr * MomCorr * velocity * pi * radius* radius / (cm3/liter) * (oil ratio * produced water ratio * entrainment efficiency) * (sec/hr*hrs/day)/(liters/bbl)

Figure 8: Top view schematic illustrating geometric correction due to wall effects.

In addition, the overview video (Fig. 8) shows that there was a second plume some of the time, which is not the blowback plume. The two plumes in the overview image could represent the same flux divided into two plumes, or because the darker plume would be obscured by the browner plume from the view used in the flow analysis, could be in addition. It is also important to note that the darker (oilier) plume is deeper than the browner (emulsion) plume suggesting the same phase separation observed in the analyzed video. To some extent, this secondary plume is accounted for in the geometric correction factor. What is not corrected for in the geometric correction factor is that the brown plume at this point clearly has a source behind the end of the riser, which is also observed in some of the videos. The amount this secondary emission mechanism could contribute is unknowable from this video, it could be 10 to 30 percent more or 10 to 30 percent less.

The estimate however, only accounts for what is observed. However, the video data provides strong evidence that the flow is not purely oil and gas. Firstly, there clearly are flakes of hydrate, which appear in the more turbulent vortices. Here, vortical (centrifugal) forces likely are pushing these flakes to the edge where they become visible (against the dark contrast of the oily plume). These particles are too large to have formed in the distance since exiting the pipe, and thus clearly indicate the pipe has internal hydrate formation. These hydrate flakes could have formed in the flow; however, particle formation in a flow generally happens on wall surfaces suggesting portions of the pipe were partially blocked by hydrates (see below) with the highly turbulent flow periodically removing chunks and flakes. In addition, it is very common in natural seeps and also production wells for paraffins and tar and also liquid oil globules to be transported within the flow.

At one point in the video, an expulsion of oil droplets occurs during a transition from the gassy to oily phases (Fig. 9). It is impossible to determine how much oil was expelled in this event, but several liters to tens of liters seems likely. Thus, I add a 10% factor for hidden oil globules, most of which likely are obscured. Thus the infrequency of the globule ejection event likely reflects the fact that an exceptionally large globule was in the plume at that moment. Because globule transport can occur at any time, it would be true for both gassy and oily plumes, pushing the steady state best guess estimate of ~50,000 bbl/day. Emissions from the kink would still need to be added. If the oil to gas ratio is 0.3 instead of 0.5, then ~30,000 barrels is a best estimate. However, given the other uncertainties, each of these numbers has a significant uncertainty. Best guess probably lies between these two oil to gas ratios, likely towards the 50,000 bbl/day***.

Although this estimate sought to quantify what is known, water column data, which was requested, has not been provided to eliminate the possibility of other leaks outside the area of inspection by the ROVs.

Figure 9: Oil Globule Expulsion

***Deriving uncertainty limits on this number are challenging and to some extent largely misses the bigger picture. For example, reasonable uncertainties in the many assumptions could be +/-50% (25k – 75k) or larger. These uncertainties then would represent the flow at the time of the video. However, given the "geyser-like" nature of hydrocarbon migration through reservoir formations, it is impossible to state whether the flow one minute before and one minute afterwards are similar, significantly higher, or significantly lower. Thus, extrapolating from the 46 minutes of data to a daily rate is highly problematic. Natural hydrocarbon migration systems show variability of factor of two and larger on time scales from seconds to months with large eruptions where emission increase by factors of tens or hundreds commonly observed. In fact, the blowout was one such example. Also, I observed a similar occurrence on streaming internet video after the pipe was cut and before the cap was put on, which appeared to push the ROV away, and appeared to represent a short term (minutes) very significant increase.

This level of uncertainty has led me to use the more qualitative approaches outlined herein to estimate flows. An example of HDIV analysis is provided below. The more detailed HDIV analysis is very useful for better understanding better the fluid dynamics of this complex, multiphase flow, however, the additional accuracy in the HDIV techniques is far less than the many other uncertainties.

Current Velocimetry by Eel Advection

Interpretation of the buoyancy drive on the oil plume (which relates to the oil to gas ratio) depends on interpreting the plume motions as due to momentum flux from the pipe, and this requires knowledge of the currents. ADCP data was (requested) but not provided, thus it was initially assumed that because this is the deep sea, currents were small. However, because this is a trench, current amplification cannot be neglected.

Eel analysis (the eel was advected towards the blow back plume, video on 5/14/2010), allowed a very rough estimate of currents of ~20 cm/s in the trench in the direction the oil plume is advected. This velocity is not due to plume entrainment, shortly afterwards, the eel is accelerated towards the camera and towards the main plume within which it then was entrained. This implies that 1 – buoyancy fluxes need to be calculated along a vector direction that considers the current, i.e., are likely greater, and 2, the oil to gas ratio likely is slightly lower.

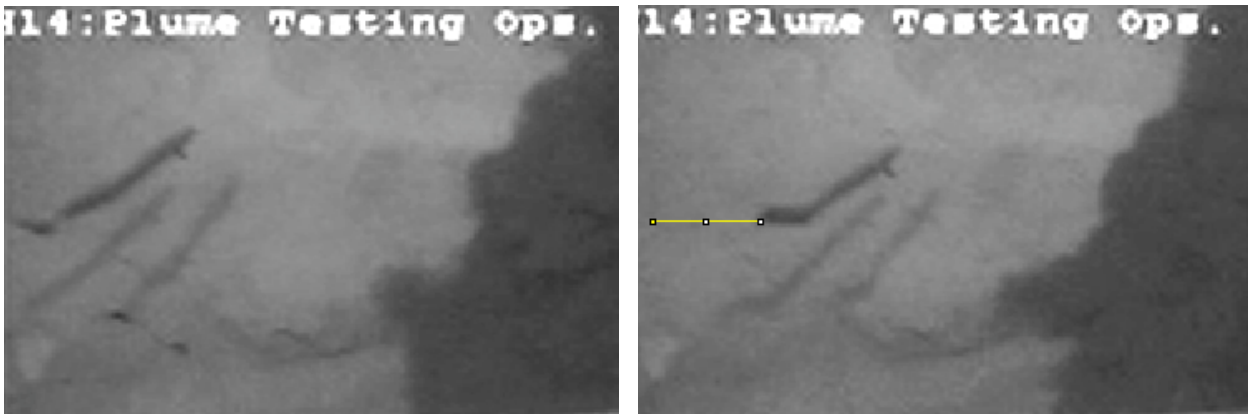

Figure 10: Eel advection in 1 second was ~20 cm, suggesting significant currents played a role in plume trajectories.

Unfortunately, BP did not provide velocities at the site, i.e., despite a request for such data, they claimed ADCP data was unavailable, which is strange given how knowledge of currents can improve safety of ROV operations. We were advised to assume currents of 0 cm/s; however, as the eel video shows there apparently was some current. Investigation of currents measured at nearby NOAA station shows that there can be a strong near seabed current layer, for example, see Fig. 11. These currents are not always present, likely having a tidal component and also relating to the loop currents, and local topography. Moreover, the riser pipe is in a trench, which could have accelerated local currents.

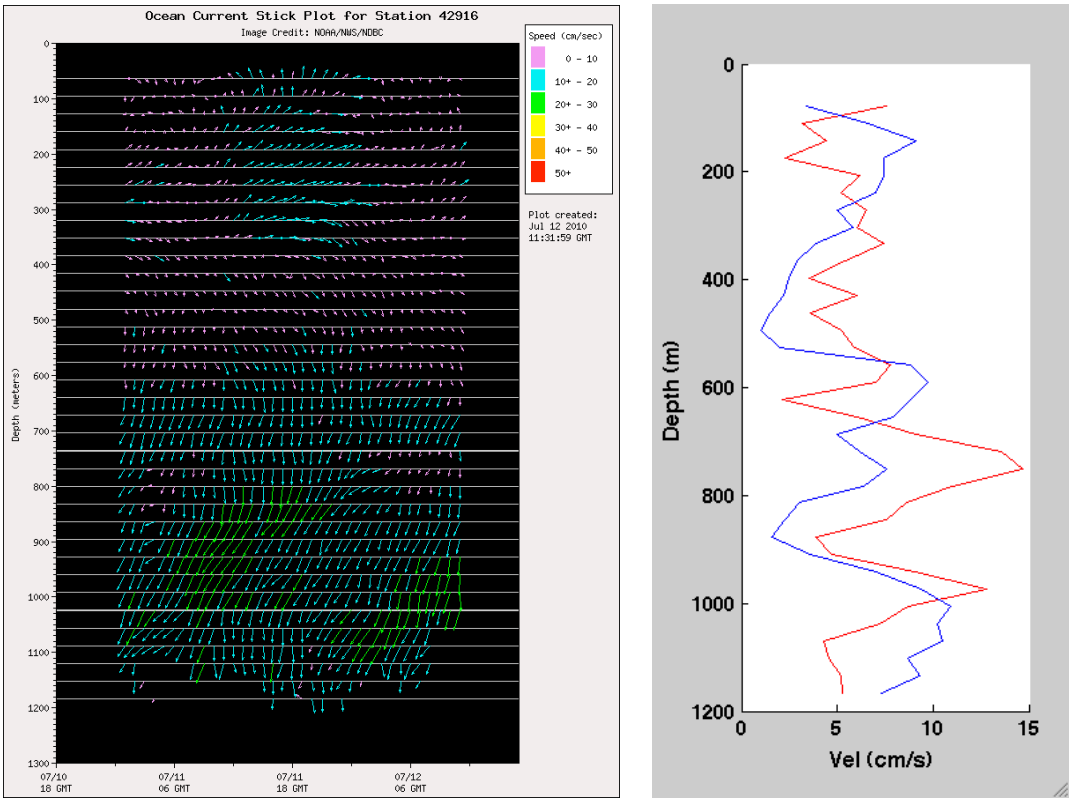

Figure 11: ADCP data for near the incident site shows currents of 10+ cm/s near the seabed on July 12. Right shows a plot of currents at station 42868 for 5/14/2010 at 12:29 (red) and 17:05 (blue).

Hierarchical Digital Imaging Velocimetry Applied to Gassy Plume

Mean velocities of 50 seconds of data all for during the gassy plume phase were calculated and show the plume core rises close to vertically (Fig. 12). Some bubbles detrain rather rapidly, being segregated downcurrent due to lower buoyancy (oiliness most likely). However, these bubbles generally experience a tendency towards re-entrainment into the main plume. This is a process that in an area plume is termed necking and is due to acceleration of the main plume. Re-entrainment of the blowback plume also is visible. Although immediately out of the pipe, the plume is primarily in an acceleration phase, by the top of the image, the outer-edge of the plume has begun to slow down as entrainment and pressure equilibration increase the plume dimensions. Horizontal velocities from turbulence are completely averaged away. Analysis of the remaining horizontal component for the upper reaches of the plume suggest currents of ~10 cm/s; however, deriving currents from bubble plume velocities is inaccurate due to processes such as flow separation, and entrainment.

Looking at the normalized mean velocities (normalized because the point of these figures is to illustrate what we can learn from HDIV of bubble plumes not to perform a mass estimate. The figure shows a rapid acceleration of the flow (at the edge of the plume), which largely reached equilibrium after ~20 cm, decreasing thereafter as the plume broadens. There also is a standing wave feature in the velocity structure with a node at ~175 cm. Above 250 cm, velocities decrease faster as the plume broadens further. Note the shadow shows up as having small velocities due to the scene illumination angle.

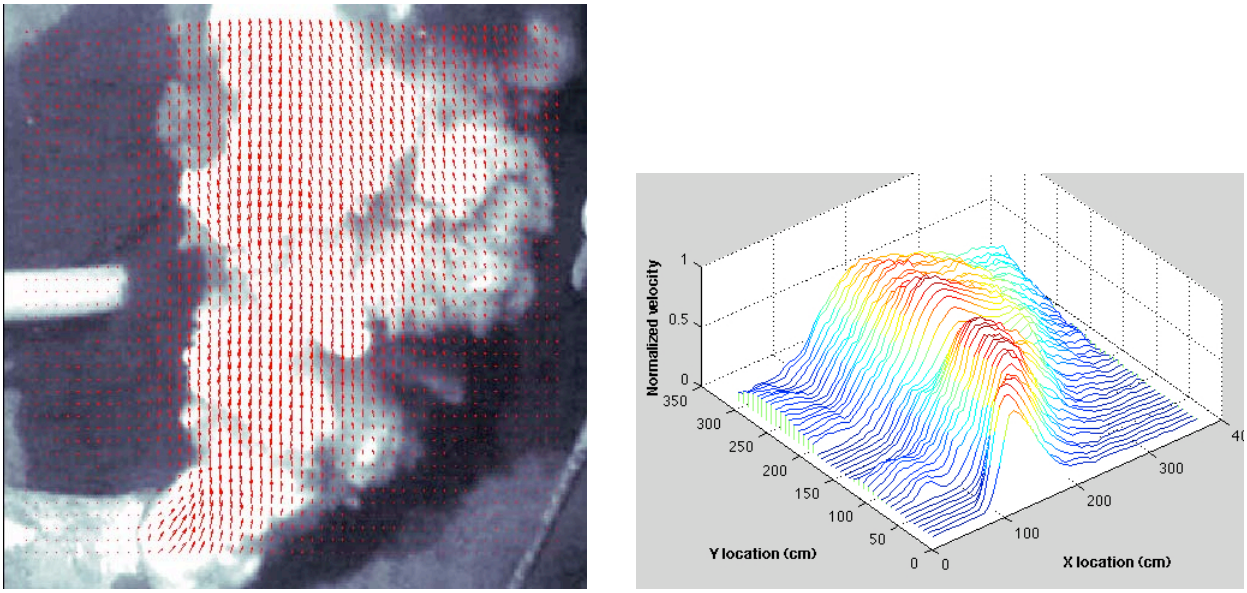

Figure 12: HDIV velocity analysis showing 90 second averaged velocities and illustrating the trajectory of the plume.

Post Top Kill, Post Riser Cut

Top kill sand-blasted clean the inside of the well pipes, almost certainly leading to increased flow by reducing resistance in the pipes, as well likely clearing away fragments of pipe annular material, and potentially creating new migration pathways external to the shattered and fragmented casing.

Key to imaging velocimetry is the size scale. Because volume (or volume flux) varies cubically, a scale variation of 10% leads to a 30% volume flux error. The flange diameter is 109 cm, while the bolt diameter is 10.5 cm. Comparison of bolt sizes around the flange shows a 20% increase from the front of the flange to the middle. The size scale at the center of the flange, likely is about 10% less than that of the bolt and flange, or about 1.85 pixels per cm; however, at the front of the plume, the scale is about 10% larger. Where the plume grows to a diameter comparable to the size of the flange, the size scale at the plume center is ~20% larger than at its edge – i.e., representative of a flow that is 73% larger. For frame 2115, the best guess scale is 1.8, for frame 2260, it is 2.0.

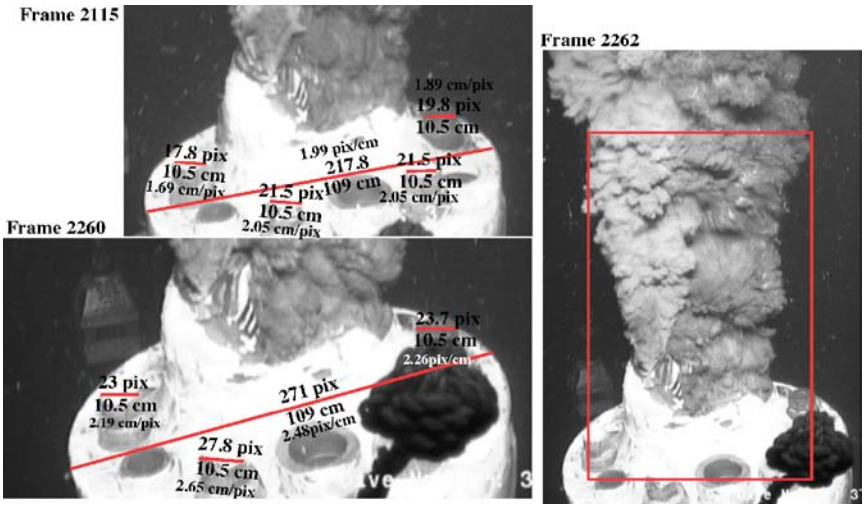

Figure 13: Two images from 14:30:32 to 14:30:36, file TOPHAT_06-03-10_14-29-22.

The flow is extremely rapid, with very strong eddies, whose velocities are large enough to cause the outer surface flow motion to be downwards, even though the overall flow continues to move upwards. Flows are rapidly pulsed, with ***strong turbulence jets that visibly penetrate through other turbulence structures***. As a result, automated HDIV analysis techniques can be significantly challenged.

Thus, a preliminary investigation used a hand tracking approach of clearly visible structures (Fig. 14). The size scale here was estimated from the position on the plume (center or edge) and the time, and has an uncertainty of ~5%. Note, this assumes that the plumes are radially symmetric, which seems approximately accurate from video where a ROV viewed the plume from a variety of angles. The mean velocity of the darker plume from the hand analysis is 130±20 cm/s, and of the lighter plume is 190±20 cm/s, i.e., the lighter plume, which likely has a greater of emulsion as might be expected of a more turbulent, higher flow plume. In contrast, the darker, lower flow plume exhibits hydrate flakes, suggesting a higher gas composition.

This translates into a flow of 50000 bbl oil day if the full plume was all made of the dark flow,

1.2*1*pi* mean([57 97]).^2*135 * 0.41 * 1 * 0.75 * (3600 * 24) /(159/1000)

Mom Corr* GeomCorr * pi * radius* radius * velocity * oil ratio * produced water ratio * entrainment efficiency) * (sec/hr*hrs/day)/(liters/bbl) (cm3/liters)

And 87500 bbl/day if the full plume was all made of the lighter plume.

1.2*1*pi* mean([57 114]).^2*190 * 0.41 * 1 * 0.75 * (3600 * 24) /(159/1000)

Here, the features being tracked are assumed to movie at close to the plume velocity, and thus the calculation uses a low value of 1.2 for the plume centerline/momentum velocity ratio. Assuming the faster plume is one third the total plume, the mean plume flow for these three seconds of data, based on the hand analysis is 62500 bbl/day. Moreover, as with the horizontal riser plume, it seems likely that the flow contains a similar quantity of tar and large oil droplets. This could possibly account for an additional 5 - 10%, or a total of 68000 bbl/day.

Uncertainty on this number is significant and includes the oil to gas ratio (±25%), the tar globule fraction (±5%), the size scale (±5%), the effect of the ratio between the two plumes 80:20 to 66:33 (±2%), the momentum correction (±10%), uncertainty in the velocity (±15%- ±10%), which also implies a change in the plume area of ±15%, and uncertainty in the entrainment rate (±10%).

A significant unknown is whether the momentum correction used of 1.2, which in a plume in the acceleration phase can be in the range 2.8 – 5, is correct for this manner of manual tracking. Evidence that it may be correct is provided by [*Leifer et al* 2009] who measured upwelling flows for a range of engineered bubble plumes at a range of depths. Interpretation of the upwelling flow suggested that upwelling data for the blowout in [*Leifer et al* 2006] implied an unreasonably large flux ~ 10^{15} L/min! As a result, the upwelling flow was interpreted as acting as a super bubble equivalent to 25-cm diameter with mass transport primarily by wake advection. In the case, here, such a super bubble would be as 8 to 10 cm with 0.7-0.8 eccentricity, which is approximately comparable to dimensions of the turbulence eddy boils.

Although this interpretation appears appropriate for the darker plume, it is unclear whether it is appropriate for the lighter plume.

However, the largest uncertainty is the extrapolation from 3 seconds of data to a daily rate. Natural seep systems can vary by orders of magnitude on short time scales from minutes to days to weeks [*Bradley et al* 2009] – and this is a well pipe tapping into a natural hydrocarbon migration system. As a result, it is unknown <u>whether these values are representative at all</u>.

S1 – 0.33 sec 40.47 cm =122.63 cm/s

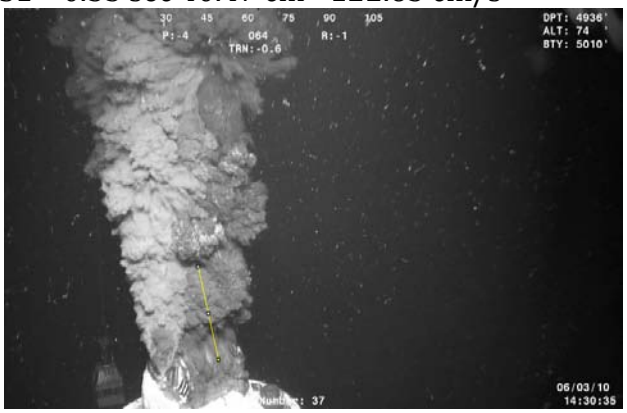

S2 – 0.66 sec, 74.53 cm = 112.9 cm/s

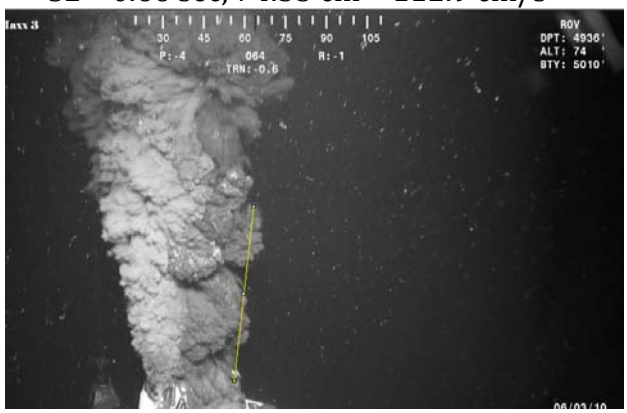

S3 – 0.1333 s, 22.3 cm, 167 cm/s

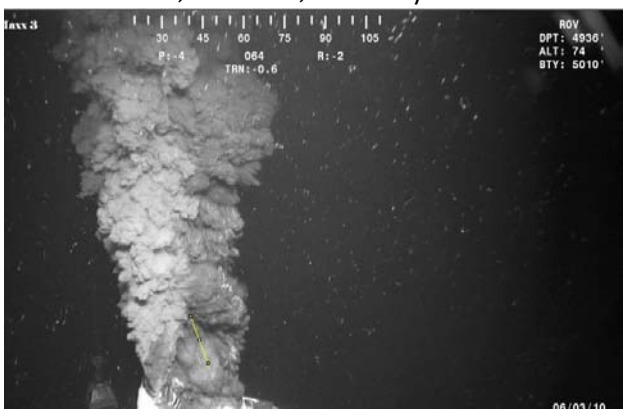

S4- 0.2 s, 31.5 cm, 157.5 cm/s

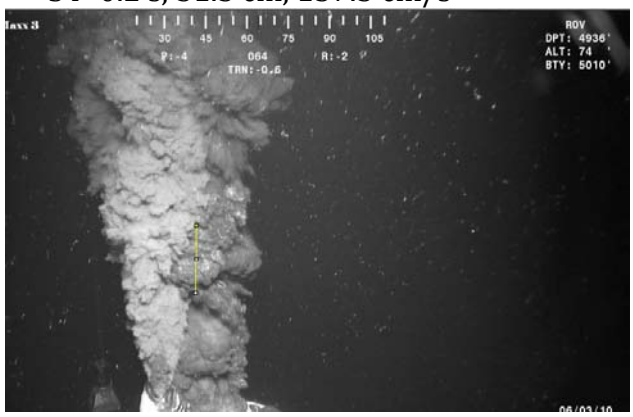

S5 – 0.267 s, 45.4 cm, 170 cm/s

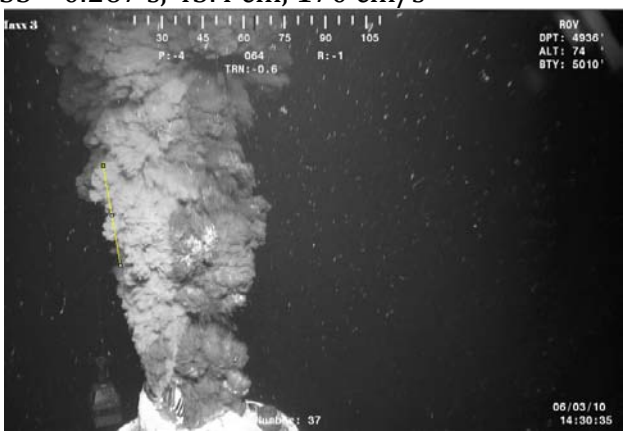

S6-0.1 s, 21.7 cm, 217 cm/s

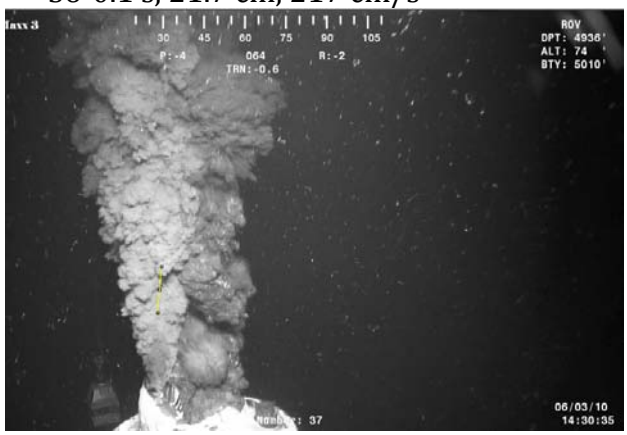

S7 – .233 s, 44.7 cm, 189 cm/s

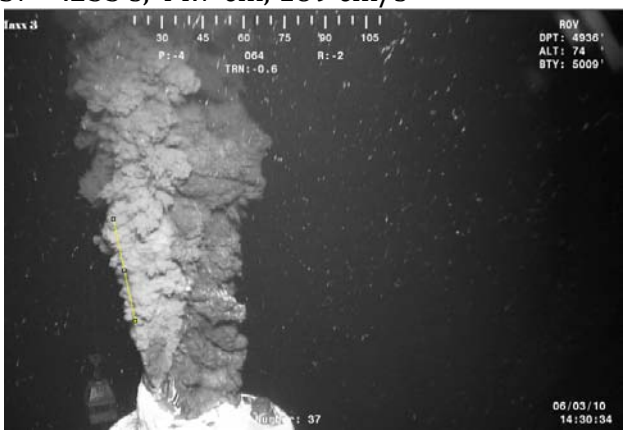

S8 – 0.267 s, 46.23 cm = 173 cm/s

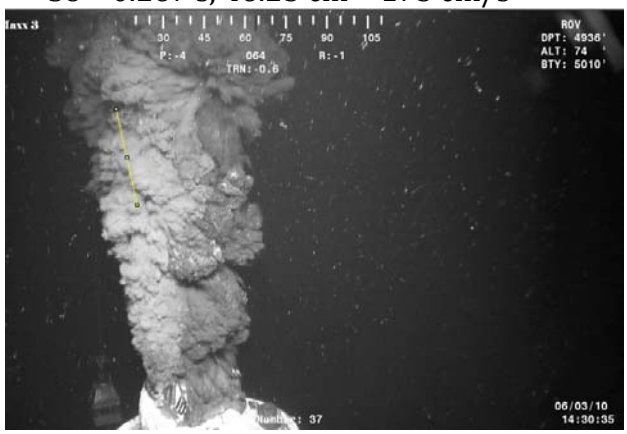

S9 – 0.333 s, 55.84 cm, 166.6 cm/s

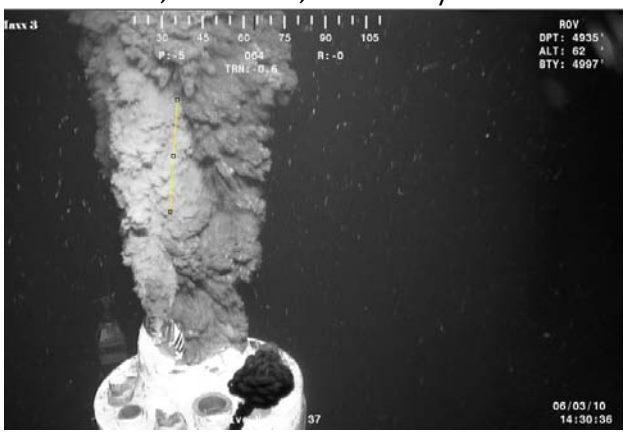

S10 – 0.267 s, 53.5 cm, 200 cm/s

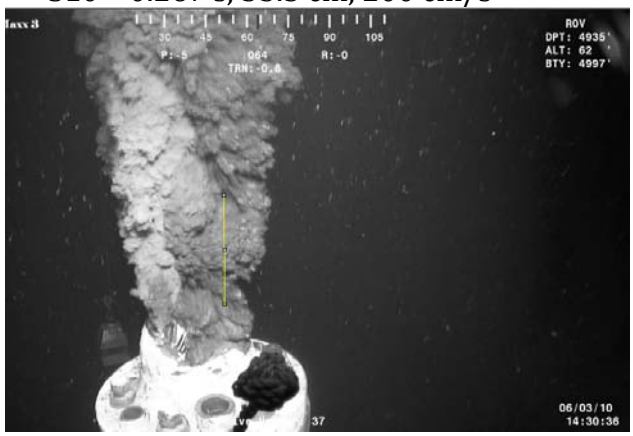

S11- 0.3 s, 37 cm, 123 cm/s

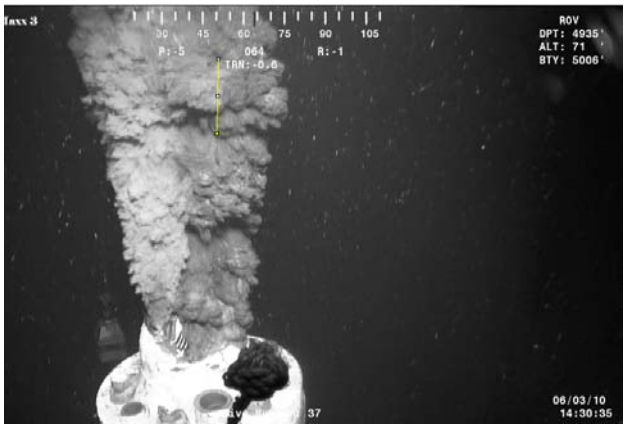

S12- 0.2 s, 44.2 cm, 221 cm/s

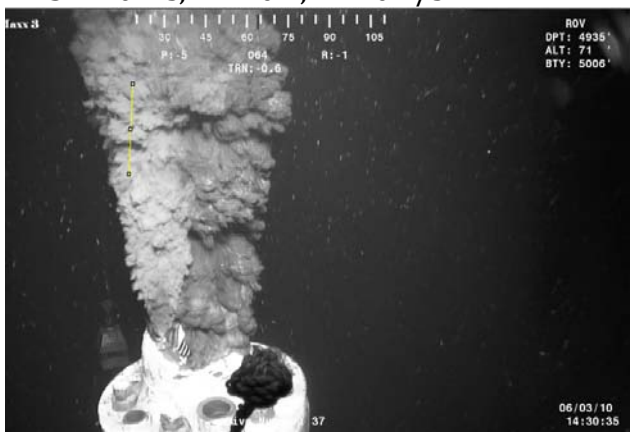

Figure 14: Hand analysis of features in the post riser cut plume. Yellow line shows feature tracked across a number of frames, which is noted above each figure as the delta time.

HDIV Analysis

Because the flows were so fast, a large initial interrogation window, 128 pixels was used with a 75% overlap, and a sensitivity filter of 3 standard deviations. Two subsequent passes at 50% the original window brought final window size to 32 pixels (or ~16 cm).

Analysis shows some of the complexity of the surface flow, with highly divergent flows in some portions, and negative velocities in others (due to rolling vortices). The HDIV analysis generally showed lower velocities in the paler plume, likely due to the lower contrast, higher velocity, and rapid evolution of features rendering them difficult to impossible for the routines to track. Evidence that velocities in the light colored plume are actually higher is provided by velocity data, showing an acceleration of darker colored plume near the interface between the two, which would only occur if the lighter color plume was moving faster, in agreement with the hand analysis.

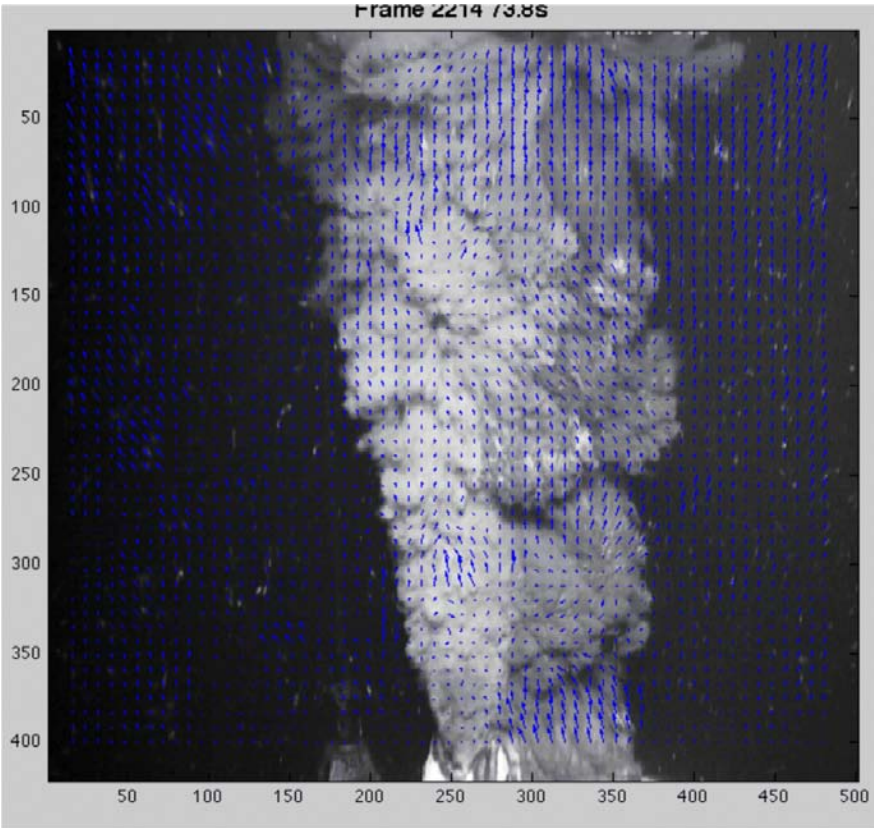

Figure 15: HDIV velocity vectors showing areas of highly divergent boils, strong upward flow, and strong entrainment.

Vertical velocities averaged over 0.33 s (over which the size scale changes minimally) show strong velocities near the pipe entryway, and near the upper plume edge. A uniform size scale of 2 cm/pixel was used, leading to errors on the order of approximately 10-20%. This upper higher velocity area, comparable to the tracked velocities in the hand analysis, likely correlates to segments where clear features are being advected. Other areas actually show negative velocity excursions, due to boils rolling, such as the feature at 350 vertical pixels in the darker plume. Visual inspection reveals that although the plume appears to be sinking, the entire vortex is rising. As a result, a mean surface velocity might be in the range of 20 – 30 cm/s, or about a fourth to a fifth of the hand analysis. One interpretation is that the difference is between the momentum plume and the main plume velocity, suggesting a ratio of 4-5, rather than 2.3. Note, however, the velocities are not really in the momentum plume, but are on an undulating surface of the bubble plume itself – which is far more distinctly defined because this plume is in the acceleration phase than a normal plume. Large-scale (50 m depth) studies by *Milgram* [1983] for bubble flows in fresh, quiescent water suggest a high ratio momentum/core plume velocity ratio. Given the uncertainty in the ratio between momentum and velocity plumes, and the challenge of tracking the light plume, which transports significant mass, HDIV was not used to estimate a flux.

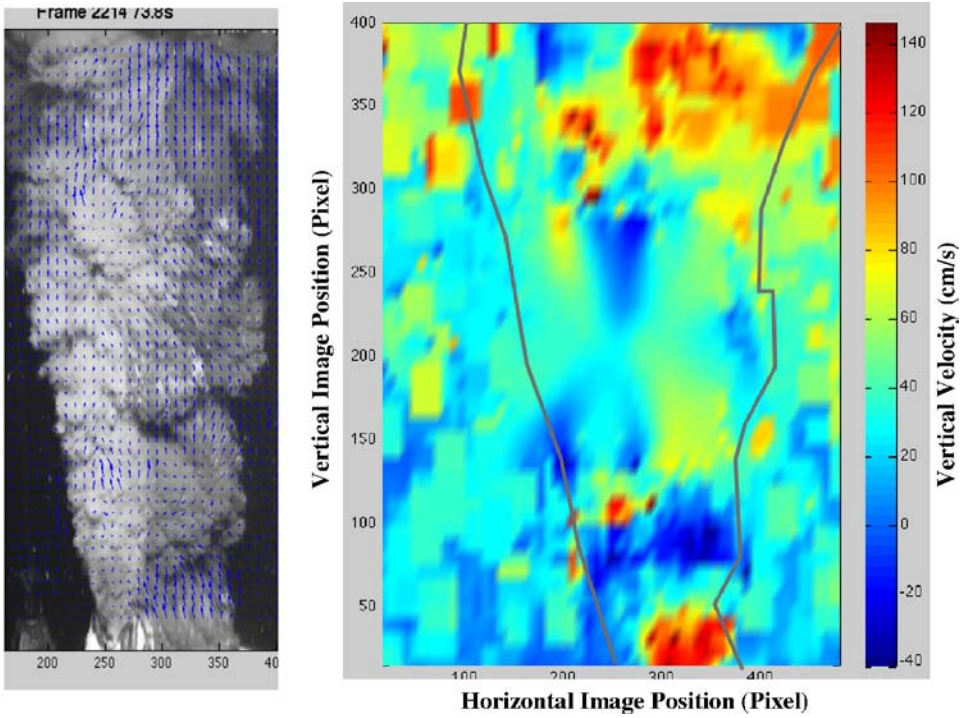

Figure 16: A) velocity vectors as in Fig. 14. B) mean of 0.33 s of vertical velocity data. Lines highlight approximate edge of the plume.

Final Words on Flow Analysis

The flows herein have large uncertainties attached, but the dominant uncertainty arises from variability in hydrocarbon migration systems, as well as the many unknowns. For example, we have been assured that there is no produced water issuing from the pipe, implying hydrate flakes could not form because of an absence of water in the system, (transport time is too short for hydrate flakes of centimeter size to form after exiting from the nozzle exit). This clearly implies that water was entering the system at some point. Possibilities include from the thief zone, through the BOP, or the reported absence of produced water (during a telecon in response to a direct question) is a sampling artifact. Should reservoir water be entering the hydrocarbon flow, it implies a greater fluid density, which would affect the fluid dynamics behavior of the plume in the first dozens of meters. BP could have resolved this immediately by simply collecting a plume sample; however, data were not provided.

The biggest unknown arises from temporal variability and that only a few seconds of video (or tens of minutes prior to the riser cut that) have been analyzed. More video was not analyzed due to BP not providing the video suitably fast. Had hard drives been fed-ex-ed overnight, then several additional days would have been available for analysis.

Moreover video streamed and available on *youtube* suggest much larger flows have occurred at different time periods. Given that the current system is best described as a leaky pipe stuck into a natural hydrocarbon migration system, such variability, as is commonly observed in natural seeps is expected. Thus, the possibility that BP specifically selected video for availability with lower flows or did not record video for higher flows, cannot be ruled out.

Natural seep systems are examples of hydrocarbon migration systems where faults and fractures serve the analogous role to the well pipe. As a result, similar variability can be anticipated from the leaking well pipe. This variability can be orders of magnitude on a whole range of time scales and can include blowouts (*Leifer et al.*, 2006). As a result, extreme caution must be used in applying these numbers for mitigation strategies. A healthy safety margin MUST be engineered for activities to be conducted safely.

Given the variability in the seep – well system, the importance of the flow rate numbers to response and safety, and the numerous calculation uncertainties due to poor knowledge of processes at these depths and the precise nature of the flow, the call for an experiment to directly measure the flow makes enormous sense to provide confidence in the flow team analyses, and to calibrate the HDIV analysis techniques. I provide the initial study plan below, which was presented to the team (twice).

Whether variability in the light and dark plumes (pre top kill) could occur due to positional shifts in the plumes. There is no indication from the overlooking video that such shifting occurred, and close inspection suggests that the main plume appears to issue from the same location in the pipe.

Scaling from plume edge velocities to interior velocities. As noted by one of the reviewers, justification is not provided for how to scale edge plumes to the centerline. The literature provides guidance, reviewed in *Leifer et al.* (2009) for large-scale bubble plumes. Some sources based on small-scale bubble plumes in the laboratory suggest 1.2 for well-developed bubble plumes (0.8 for continuum plumes). Analysis of the blowout plume with a comparable buoyancy flux suggests 3-5. The effect of oil on this scaling is unknown, but cannot and should not be ignored. Moreover, it is unclear exactly where the visible plume edge that is being analyzed likes in terms of the momentum and bubble plumes. The shift is observed statistically, while the visual edge shifts between the two due to large structured turbulence where upwards velocities can locally become negative. This illustrates the importance of an experiment to directly measure the flux, see below. As a result, default values were used, but there is no great faith in their applicability until critical experiments are in fact performed. In effect, *this approach remains uncalibrated*.

Eel swimming in the current estimation. As someone who has watched eels out a submarine window at other seep sites (550 m), I contend that with minimal observational experience, the eel body motions leading to swimming are easily detectable, and are not clearly evident in the relevant video. Further, the probability that there are strong (and unsteady) accelerations of fluid into the plume seems self-evident. The plume grows, so by continuity, there must be significant entrainment of ambient fluid. However, the main reason for bringing up the acceleration in the discussion was to illustrate how prior to when the eel began to be accelerated towards the plume, there was no evidence during when it was drifting. Being forced to use eels to study fluid motions clearly is less than ideal; however, there is an underlying reason, specifically, the difficulty in getting BP to collect and provide the critical data needed to analyze the flow from the well.

Theory of Deep Sea oil-gas-hydrate bubble plumes. Reviewer 4 provides a very thorough and detailed theoretical discussion of fluid plumes. What is unclear to me is whether they are appropriate at all for this particular flow at these depths where hydrate formation clearly plays a role. Further, studies of sewage outflows are largely inapplicable to bubble plumes (see work of *McDougall* (1978), and many further more recent, such as [Leifer et al., 2009]). Applying continuum plume theory to bubble plumes must be used with *extreme* caution, because they approximate the buoyancy as distributed rather than point sources. This can lead to completely wrong conclusions regarding for example, when a bubble plume encounters stratification.

Comparison of Seabed Mass Flux with Surface Integrated Mass Balance

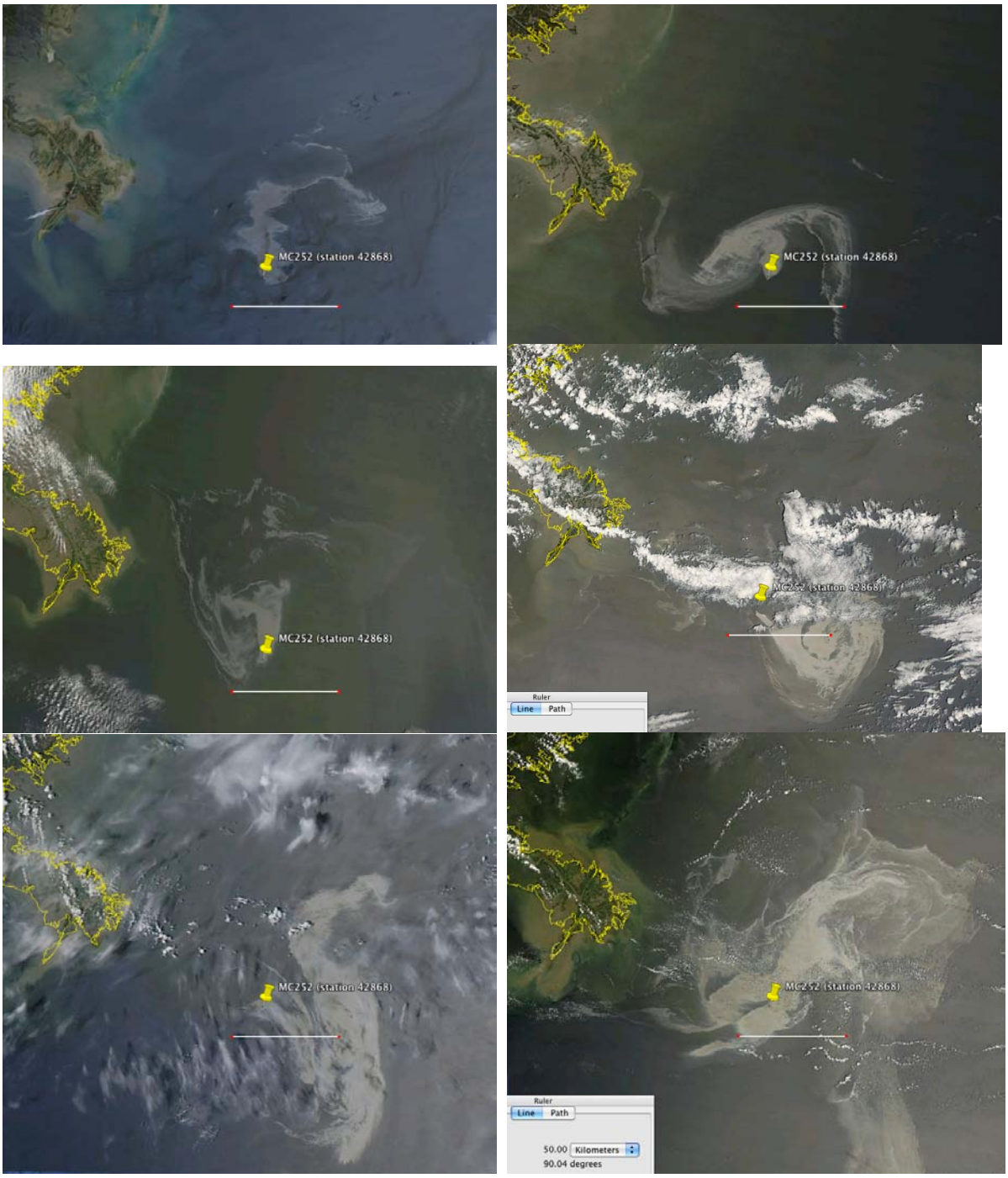

Figure 17: MODIS imagery for April 25th (Aqua), April 29th (Terra), May 1 (Terra), May 8th (Terra), May 22 (Aqua), and May 17th (Terra). Line is 50 km.

MODIS Satellite Imagery of Slick – Unsteady Emissions?

The Deepwater Horizon explosion occurred 20 April 2010 and sank two days later. Initial official estimates were 1000 and 5000 barrels per day. Examination of the MODIS satellite images shows an extensive slick shortly after the sinking of the rig, which appeared to have grown significantly in extent by four days later (April 29th), although the spatial extent of the densest portion of the slick remained similar. Even such that May 1st, the densest portions appeared to have shrunk. However a week later, the change is significant with the area of thick-oil-appearance slick having grown dramatically in spatial extent. One interpretation is that after an initial high flow burst associated with the sinking of the rig, the amount of oil escaping from the seabed decreased significantly until sometime early May. Afterwards, the slick proceeded to grow rapidly such that by May 11th, it has expanded significantly further. On May 17th, although the denser area of the slick remained approximately similar in spatial extent, thinner portions of the slick had expanded dramatically with oil feeding into the loop current (Fig. 18).

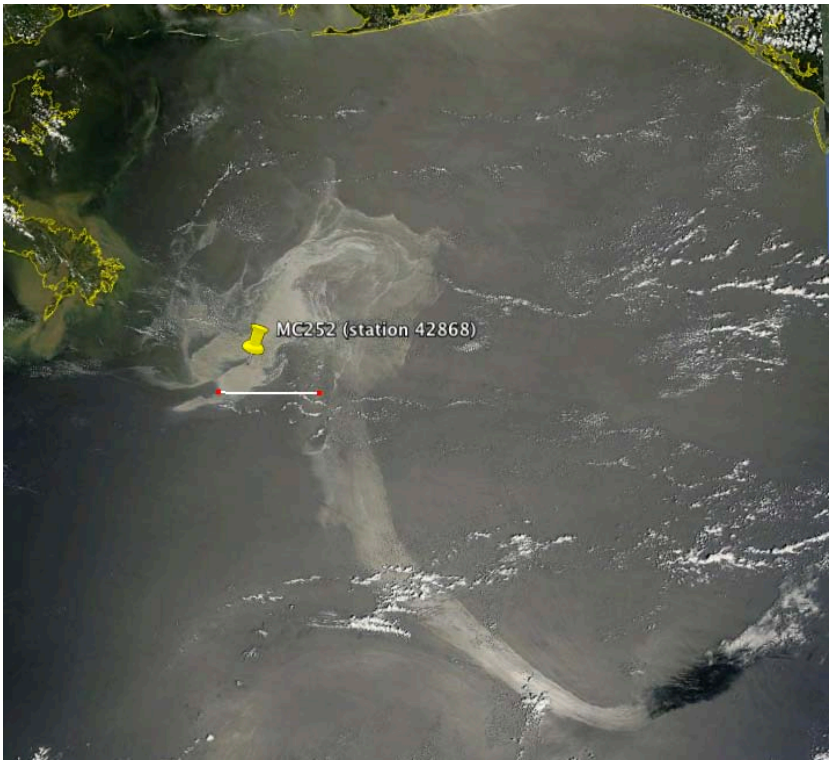

Figure 18: May 17th 2010 MODIS (Terra) imagery showing oil feeding from slick into the loop current. Line is 50 km long.

May 17th 2010 also was a clear sky day during which a series of NASA ER-2 AVIRIS flightlines were flown over the slick near the incident (Fig. 19). AVIRIS is the Airborne Visual InfraRed Imaging Spectrometer, which collects hyperspectral (224 bands) image data.

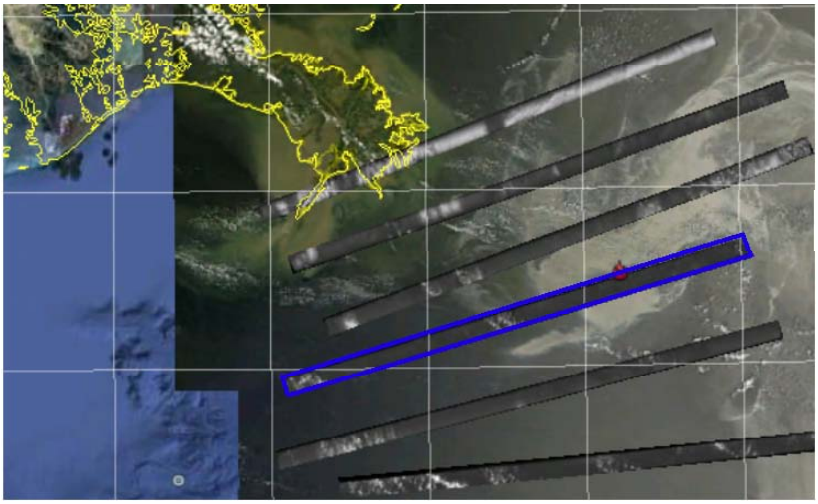

Figure 19:. Overlay of AVIRIS quicklook images of flight data for May 17th, 2010, showing flightlines with MODIS data.

The NASA response to the Deep Horizon Oil Spill had two primary missions: (1) to establish baseline observations before oil arrived at threatened coastal sites and (2) to provide synoptic observations that had rapidly grown larger than conventional aircraft could observe, at spatial resolution not available to satellite, and to leverage the hyperspectral imaging spectrometry unavailable on satellite platforms. AVIRIS was deployed for the Deep Horizon spill aboard the ER2 aircraft, allowing, for example, surveying with 8-m pixel spatial resolution, order 1000 km2 of coastline and/or sea surface in a day. Despite the ER2's unparalleled capabilities, coverage was small compared to the spill size (MODIS satellite data analysis indicated ~12,000 km2 of oil slick of significant (non-sheen) thickness). Surveys have been closely coordinated with NOAA and USGS to maximize data collection utility.

Although the relationship between color and oil thickness in the visible is minimal for oil thicker than sheens, absorption features in the IR are related to oil thickness and oil to water ratios (Clark et al., 2010). The underlying reason for the complexity in deriving abundances is partly illustrated in Figure 20, which shows reflectance spectra of a sample of oil emulsion made from oil collected in the Gulf of Mexico, Deepwater Horizon 2010 spill, which contained ~40 percent water. In the visible electromagnetic spectrum (approximately 0.4 to 0.7 microns) the oil emulsion color changes little for different thicknesses. Note, these oil emulsions are significantly thicker than the wavelength of light. In contrast, large changes in reflectance are observed in the near infrared (Fig. 2) because the oil is less absorbing at those wavelengths. At infrared (IR) wavelengths, both the reflectance levels and absorption features due to organic compounds vary in strength with oil thickness and the oil:water ratio.

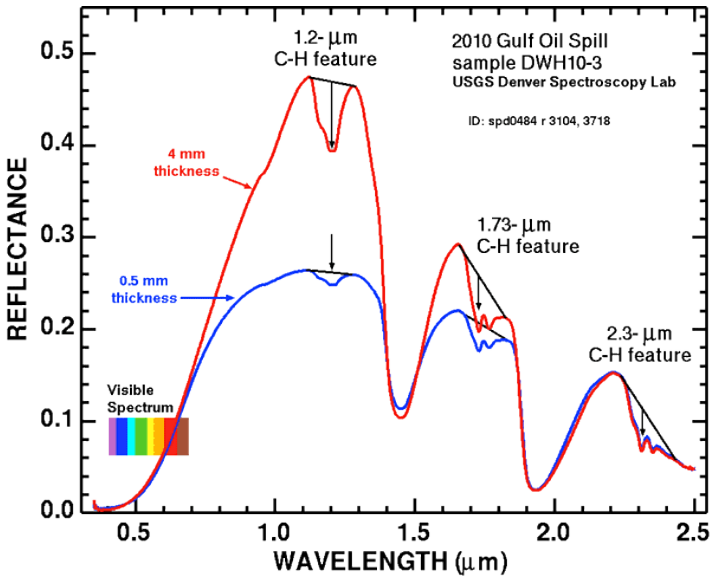

Figure 20: Spectra of oil emulsion from the Gulf of Mexico oil spill. Sample collected May 7, 2010. At visible wavelengths the oil is very absorbing and does not change color significantly with depth. At infrared wavelengths, both reflectance levels and absorptions due to organic compounds vary in strength with thickness. This sample contains slightly less than 50% water as determined by heat separation. Controlled sample depths were created in a cell on a glass window placed over a black substrate and a water substrate. The reflectance was measured over each of these substrates (no difference was observed). From *Clark et al.* (2010), http://pubs.usgs.gov/of/2010/1101/.

Figure 21: Overlay of AVIRIS Quicklook images of flight data for May 17th, 2010, showing flightlines with MODIS data illustrating similarity and evolution of spatial features.

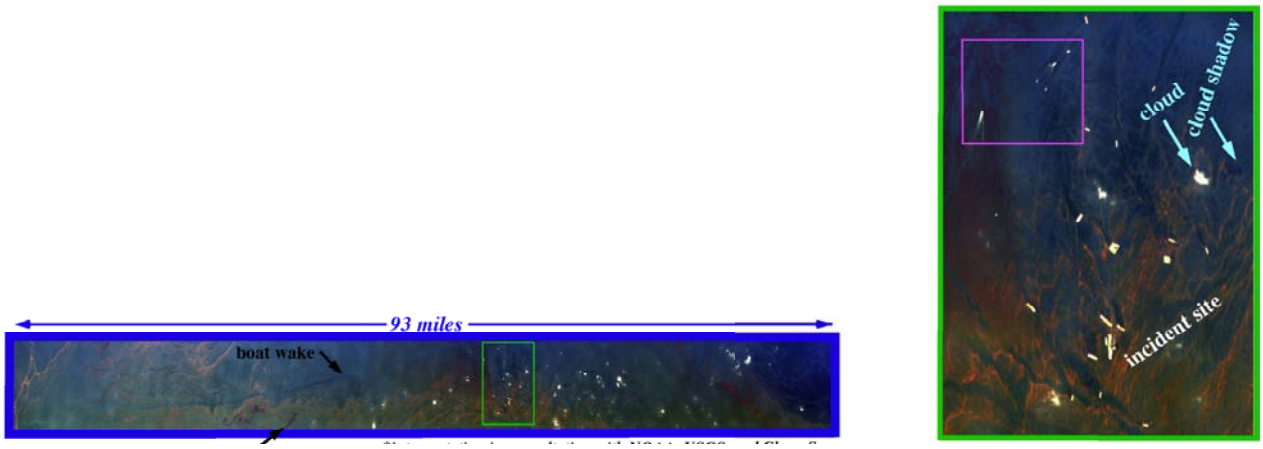

Figure 22: Overlay of AVIRIS Quicklook images of flight data for May 17th, 2010, showing flightlines with MODIS data illustrating similarity and evolution of spatial features. Lower left arrow highlights freshly surfaced oil (based on oil to water ratio, Roger Clark, pers. comm.).

The first step to analysis of the AVIRIS data is conversion of radiance data to surface reflectance data accounting for atmospheric effects, validated by calibration site data for each flight. Using laboratory spectra for a range of oil thicknesses and oil to water emulsion ratios, the Tetracorder algorithm (Clark et al. 2003) allows derivation of a mean oil thickness, oil coverage fraction, and mean oil to water ratio for each pixel.

As shown in Fig. 19, the total area of the oil slick is significantly larger than could be covered by AVIRIS, and moreover while MODIS acquires a snapshot image, AVIRIS requires hours to survey the slick, during which time the slick changed notably (Fig. 21). Thus, while many of the spatial features are highly similar between the MODIS and AVIRIS data for some lines, on others, significant differences are apparent. As a result, extrapolation from the AVIRIS surveyed area using MODIS data is critical, but requires validation that such extrapolation is appropriate. Specifically, there are regions in both the AVIRIS and MODIS data that appear to exhibit distinct spatial distributions from other areas. Closer inspection of the AVIRIS data for the blue outlined flight line in Fig. 19, shows structure on a range of smaller scales than visible in the MODIS data (Fig. 22).

To evaluate whether extrapolation is valid, MODIS data were investigated for self-similarity (Fig. 23). Self-similarity assumes that oceanographic and meteorological processes create a "fractal" oil spatial distribution, which is replicated over a wide range of size scales spanning AVIRIS to MODIS data. As the AVIRIS data shows, areas in MODIS that appear uniform are actually comprised of a mixture of thick and thin slicks and largely oil free surfaces. Specifically, that the processes that control the spatial distribution: turbulence, winds, waves, currents, etc., operate on a range of scales and that therefore the spatial probability oil thickness distribution in areas of MODIS that are similar, are representative of oil slick with similar spatial of oil slick thickness distributions.

Probability distribution functions (PDFs) were calculated for pixel areas where MODIS-scale images appeared similar (Fig. 23, green and yellow). Both are very well described by dual Gaussians ($R^2 = 0.995$ and $R^2 = 0.983$, calculated by a least squares, linear regression analysis (MatLab Curve Fit Toolbox, Mathworks, MA), which are highly similar, suggesting that on these scales, the pixel spatial distribution of oil thickness is self-similar.

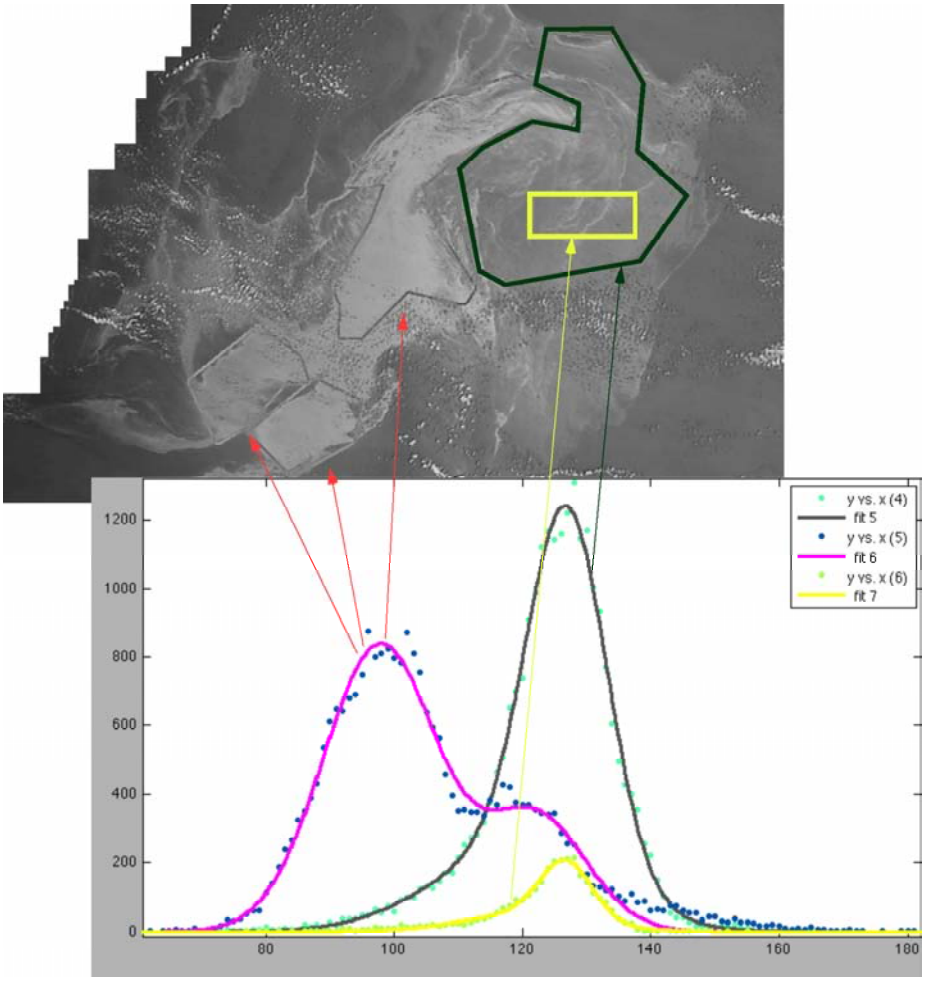

Figure 23: Probability distribution functions (PDFs) for the main slick. The main slick has two areas with dominantly distinctive patterns, one of which is whispy (yellow), and one that appears uniform (red) (uniform histogram combines pixels from three areas).

Unlike PDFs for the main slick, PDFs for the non-slicked water are quite different. Probability distributions on the upwind side of the oil slick (to the southwest) are narrower and spikier (less heterogeneous) than PDFs for the oil slick's downwind side (more heterogeneous). This is consistent with spreading of sheens from the slick tail in the downwind direction. Specifically, the sea surface to the downwind side has a wider range of albedos than to the upwind side where a contribution from oil is unlikely. Also note, clouds produce a highly distinct PDF from that of oil slicks. As a result, if significant fraction of the main MODIS pixels contained clouds on a sub-pixel size-scale, then one would anticipate a PDF significantly different from that for the slicks (Fig. 24, brown PDF). In fact, AVIRIS revealed that areas suspected of being cloud free in the MODIS data were cloud free on AVIRIS pixel size-scales, too.

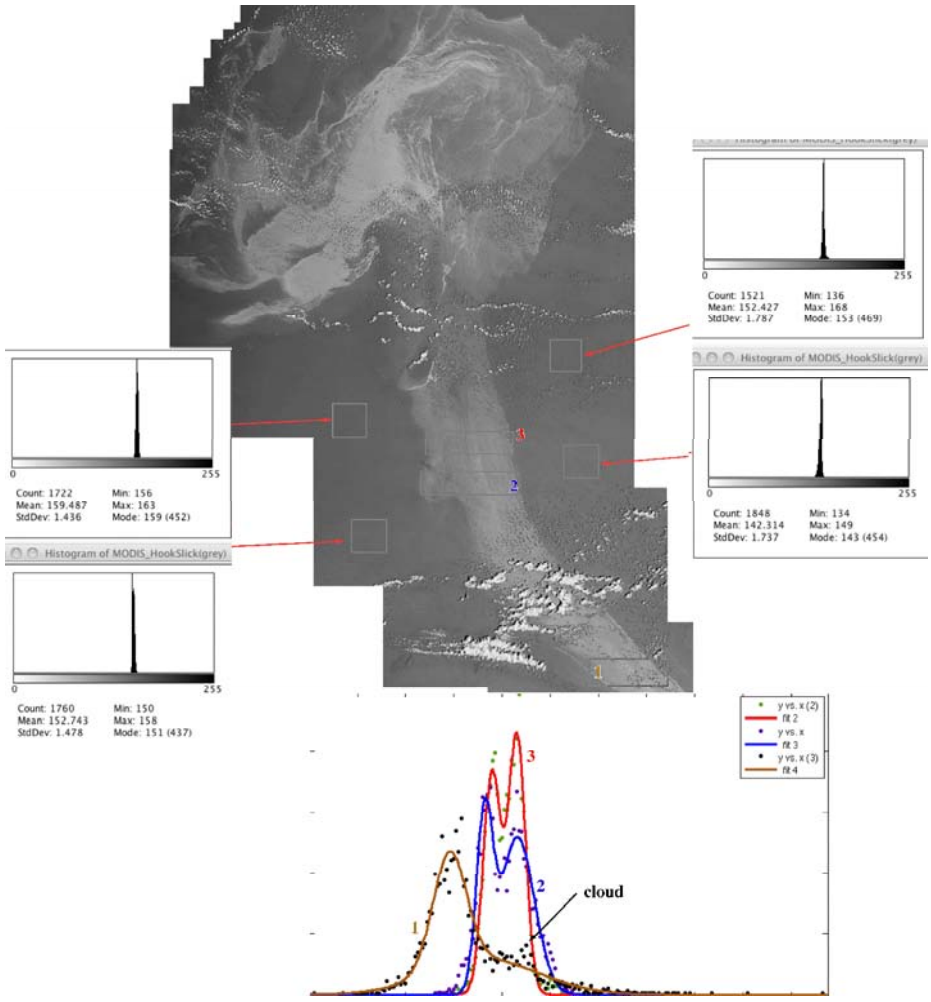

Figure 24: Probability distribution functions (PDFs) for largely or completely oil-slick free water and for "tail" in the loop current. PDFs labeled on figure by color-coded numbers.

Investigation of PDFs for the tail shows two separate plumes (2,3) that merge towards the South (1), with the half-width of the merged plume similar to that of a single Gaussian fit to dual plumes. Here, two plumes does not mean two physical thick plumes, but rather two different types of spatial distributions, co-located, indicating different controlling processes. Thus, their merging to the south, suggests that a single controlling process begins to dominate for the entire tail oil slick. For example, there could be a dominant plume controlled by current convergence associated with the Loop current, and a secondary plume associated with turbulence and winds. Then to the south, perhaps weakening of winds would lead to current processes dominating. The implication here is that the spatial PDF of oil slick thickness is distinct in each plume.

The tail also showed a PDF indicative of thicker oil in the main slick, and was interpreted as such. Subsequent analysis of AVIRIS flight data collected on May 19 (two passes, one midway and one most of the way towards the Southern edge of slick's tail) showed thick oil slicks (Fig. 25) in the "tail region."

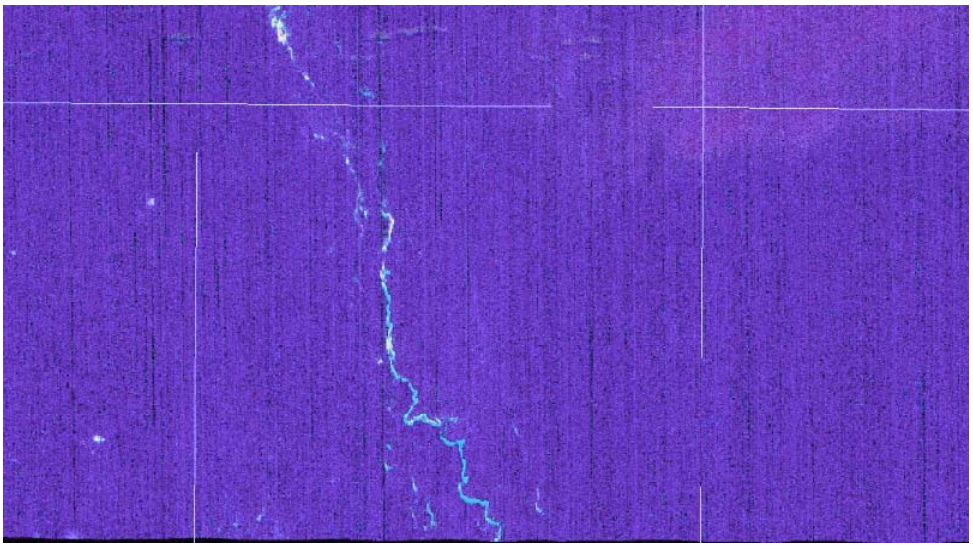

Figure 25: False color image from oil slick "tail" showing a primary, thick, surface oil slick, and several fainter thick slicks. The fainter slicks likely have size scales smaller than the 8-m AVIRIS pixel resolution. Image is normalized difference ratio of AVIRIS bands 144,145,146 and 135, 136, 137.

Oil Slick Thicknesses

Interpolation and extension to the entire slick is based on identifying regions of similar PDF and assuming that the spatial distribution of oil slick thickness is similar throughout those pixels. This estimate is based on AVIRIS imagery to estimate slick thicknesses according to the conventional formulation and analysis of spectral absorption features in the infrared, which vary with the oil thickness and the oil to water ratio (Fig. 20).

Table 1: Sheen Color and Maximum Thickness, from Taft et al. (1995)

Sheen	Max Thickness (μm)	Description
V Light	0.05	Pearly blue gray.
Silver	0.1	Mirror like, Reflects Sky.
First Color	0.15	A few light colors.
Rainbow	0.3	Vivid luminescent rainbow of colors.
Dull Colors	1.0	Dull Greasy rainbow. May damp capillaries.
Yellow Brown	10	Dull yellow brown. Can calm surface water.
Light Brown	100	Light brown, appears thick on water.
Brown Black	1000	Like thick black motor oil. Calms sea.

The Bonn Agreement Color Code 2003 describes the appearance of oil slicks with respect to slick thickness, although we use the formulation of *Taft et al* (1995). The thinnest slicks have a silvery-gray appearance due to improved reflectance. Rainbow slicks appear as such due to oil having a thickness near to, or a few integer multiples of the wavelength of light (accounting for viewing and illumination angle). Metallic color slicks have color but also begin to have a mirror effect reflecting the sky. Finally, slicks thicker than 50 μm are sufficiently thick to allow the oil's true color to show through. Note, that the category "brown-black," often appears as a reddish brown where the oil is in an emulsion (a mixture of oil and water), while thin sheens (mirror like) tend to contain very little of the total slick mass due to their relative thinness. Unfortunately, slicks thicker than 50 μm appear in the visible to be similar despite thickness variations of one to several orders of magnitude (e.g., Fig. 26); hence the importance of using spectral absorption features in the infrared reflectance to quantify the thicker oils.

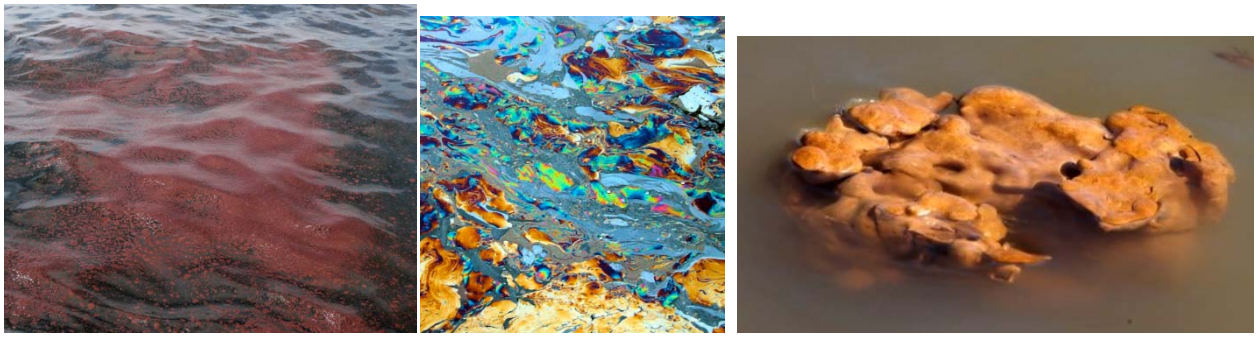

Figure 26: Oil slick images. Left - Thick (~1 cm) emulsion from Gulf of Mexico spill (from Clark et al, 2010). Center - Coal Oil Point seep field slick (photo Leifer). Right - Floating tar ball in Gulf of Mexico showing weathering air pockets, and loss of volatile components. (http://i.huffpost.com/gadgets/slideshows/6519/slide_6519_91561_large.jpg?1279031406134)

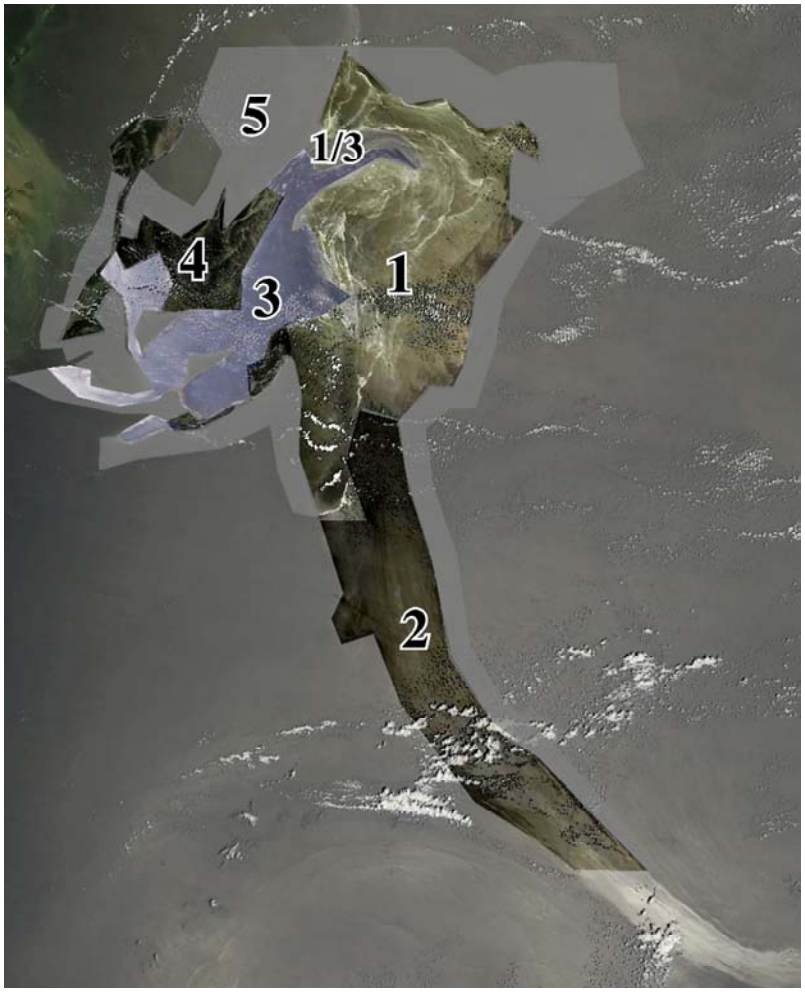

Figure 27: Slick class analysis on AVIRIS data of MODIS Terra image for May 17, 2010. The extent of the sheen (Class 5) is unknown, but is not significant to the oil budget.

The slick on 17 May 2010 was segregated into regions based on the PDF analysis approach. And pixel areas in each class summed in the program ImageJ. A summary of the analysis is provided in Table 2. AVIRIS analysis will be described in a manuscript in progress (*Green et al.* 2010) through personnel communications with colleagues on the mass balance and remote sensing teams.

AVIRIS imagery and boat observations (e.g., Fig 26A) demonstrate that each slick region contains a range of oil slick thicknesses. Outside the range of oil that can be observed by AVIRIS, there is significant other oil. Both media and reports from colleagues indicate significant floating near subsurface oil globules (Vernon Asper, personal communications, Ian MacDonald, personal communications), and dispersed oil in the near surface water column (i.e., in a dispersion too fine for visual identification as separate globules). At the sea surface, there also are large areas of thick oil (Ian MacDonald, personal communication, Gregg Swayze, Personal Communication) to many centimeters thick, as well as tar balls. Also, there are dissolved oil components in near surface waters and volatile components in the atmosphere.

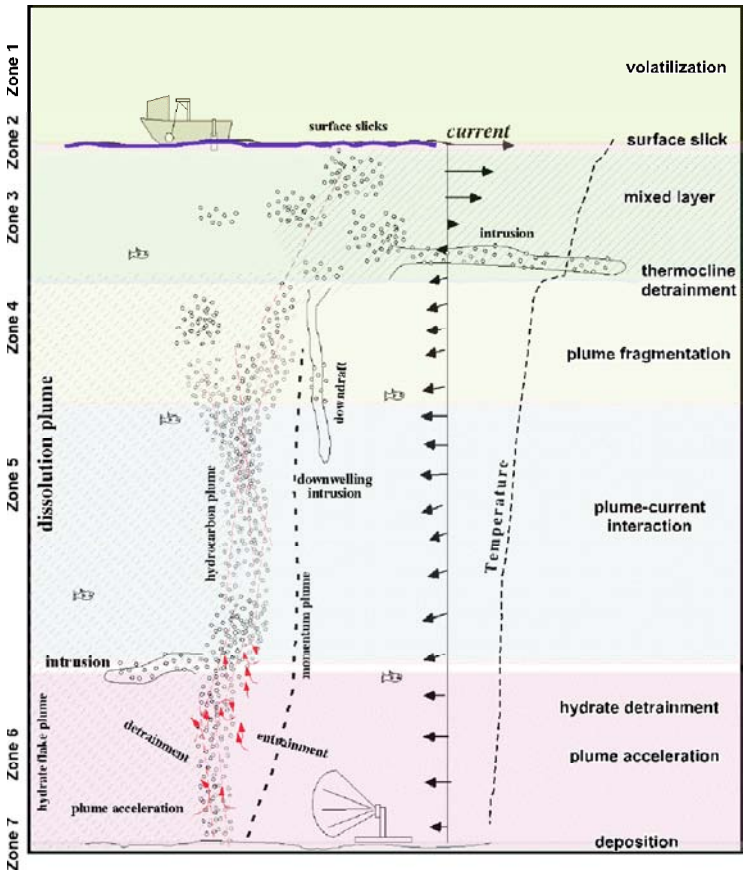

Figure 28: Schematic of different depth zones and relevant processes.

The underlying mechanisms of oil partitioning into these areas are known, if generally poorly understood even for conventional oil spills. Finally, during the oil's rise in the water column, many processes will occur that cause oil partitioning into different portions of the water column. Based on a range of theoretical and observational concerns, seven key depth zones are proposed where distinct processes govern the fate of seabed hydrocarbons from the Macondo Well (Fig. 28). Within these depth zones, the primary changes in the composition of the plume with time are associated with hydrates (formation, dissociation), hydrocarbon dissolution, and plume entrainment (plume growth) and detrainment. Details of these processes are hypothesized to be distinct in each of the depth zones. For example, hydrate-related processes only occur in the deep sea within the hydrate stability field, although they persist to somewhat shallower due to time required for hydrate dissociation. These processes were considered while deciding how to partition the oil into the different compartments in the mass balance calculation.

Zone 7 – Benthic-Water Interface

There are natural processes of deposition and sedimentation of organic material from the upper mixed layer photic zone to the deep sea and benthos – marine snow and conversion of dissolved organic material to particulate organic material, which settles. The processes are complex, only partially understood, and include biological cycling. In the case of a large oil gas plume, droplet detrainment in the deep sea leads to a plume of dispersed oil droplets, which diffuse towards the seabed (against their slight buoyant rise), that also interact with sinking marine snow (organic particles and detritus), leading to seabed deposition. Most of the oil here will arrive from plume losses in shallower zones, unless there is oil migrating along the outside of the casing and then through pathways in the seabed and mud, as in the 1969 Platform A blowout in Santa Barbara.

Zone 6 – Deep-Sea Plume

Unlike natural gas plumes at shallow depths, in the deep sea, hydrate (water-methane crystals stable at low temperature and high pressure) formation can strongly affect plume behavior [*Sauter et al.*, 2006]. Key initial plume processes are the acceleration phase when there is rapid plume growth and entrainment absent detrainment, which approaches quasi steady state behavior after a distance of tens of plume diameter length scales – e.g., [*Milgram*, 1983], in steady state, plume entrainment and detrainment are balanced, and the driving buoyancy flux changes slowly due to bubble gas exchange, negligible hydrostatic pressure changes, and phase (hydrate) changes. Dissolution losses are small because of hydrate skins [*Rehder et al.*, 2009]. Also, hydrate bubble skins separate the methane from the fluid, preventing rapid formation of hydrate crystals. Summer 2009 observations (*Leifer*, *Kastner*, *Solomon*, *MacDonald*, 2010, unpublished) during the HyFlux mission tracked intermediate size bubbles (1 – 3 mm radius) at MC118 (~1000 m, near the Macondo well site) across most of the water column, only losing them near the mixed layer. Their survival is best explained by hydrate skins, although oiliness likely also played a role [*Leifer and MacDonald*, 2003]. Despite multiple repeat bubble plume following experiments, there were no observations of spontaneous hydrate flake formation. Thus, the underlying mechanism behind the observed formation of hydrate-like particles in the deep sea (Vernon Asper, personal Communication, remains unknown. However, the rate of dispersion due to hydrates appears to be non-negligible and likely explains the deep vast plumes of oil moving in the deep sea (Samantha Joye, personal communication).

In general, in the deep sea, changes in the water column are slow and subtle; leading to general steady state plume behavior (*Solomon et al.,* 2009). However, relatively abrupt changes associated with for example, deep loop currents, can be observed. In the schematic, this is illustrated by a current shear, which leads to an intrusion in the hydrate stability field (HSF). Observations (*Asper*, 2010, unpublished) suggest increased hydrate particles with height above the seabed until several hundred meters altitude. This could result from progressively greater work required by the plume against the stratification (density gradient) leading to progressively greater detrainment, or could also have sharp characteristics due to the effect of water-column changes. There also is significant evidence for a deep-sea plume of oil (*Samantha Joye*, 2010, pers. comm.), which could be related in part to hydrate processes, as well as bubble plume processes.

There have been some deep-sea studies in the vicinity of the well site. The *R/V Brooks McCall* conducted field sampling during 4, EPA cruises May 8-25, during which ~230,000 of dispersants were applied. Oil transit to the surface as ~3 hours (~10 cm/s), implying the flux is not gas-driven across the entire water column. Rosette samples and standard Seabird suite measurements showed peak fluorescence at 1000 m (to 34 ppm) correlated with CDOM data while particle sizing data suggested small oil droplets.

Zones 4 and 5 – Deep to Upper-Water Column (Above Hydrate Stability Field)

In the absence of water column changes, the dominant evolution of the plume in the mid water column arises from bubble dissolution and fluid mixing with the ambient water column. Due to the buoyancy flux loss from bubble dissolution (mid-water hydrostatic pressure changes are relatively minimal, as is air uptake), the plume is increasingly unable to support the upwelling flow with gradually increasing detrainment. Total dissolution is feasible if the bubbles are small enough, however, sonar and direct ROV evidence suggests bubbles can survive against dissolution during transit of the mid-water column. Here, losses are primarily likely to be through dissolution of volatile components.

Zone 3 – Thermocline and Mixed Layer

For a bubble plume, the thermocline represents a significant challenge due to the rapid stratification at the base of the mixed layer. Here, massive plume detrainment is highly likely [*McDougall*, 1978], which, coupled with common current shear, should lead to plume disruption. Sonar observations often show bubble plumes disappearing abruptly at the thermocline or levels of current shear, e.g., [*MacDonald et al.*, 2002] for bubbles from 550 m.

Analysis of AVIRIS data indicates that oil reaches the surface not as a stream or plume as large boils. Specifically, several kilometers to the SE of the incident site (Fig. 29), down current, large oil patches are observed with very low water content (oil in non-sheen slicks almost always is in the form of an emulsion – a mixture of tiny oil and water droplets), and spatial patterns distinct from most of the scene oil which has high water content (Rob Green, personal communication). The best explanation is that these are patches of freshly surfaced oil and their spatial distribution suggests that the transport mechanism in the upper water column is as boils.

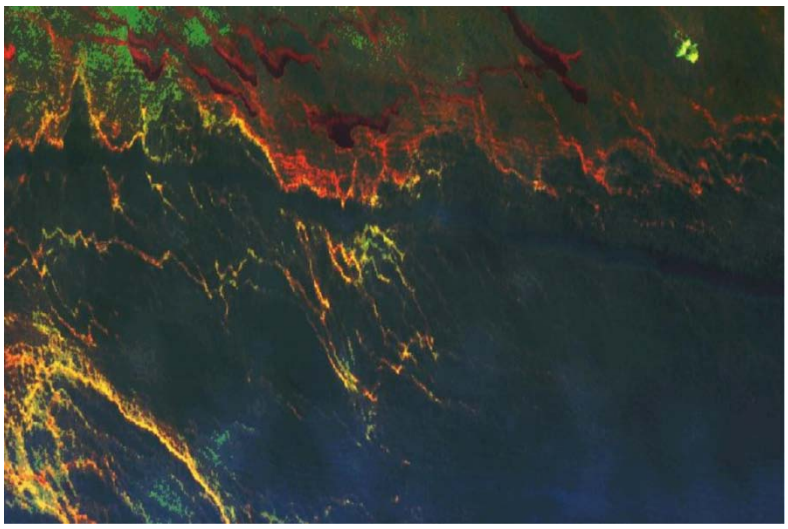

Figure 29: Band ratio (550 nm to 650 nm) with false color from AVIRIS flight 17 may 2010. Dark brown patches are freshly surfaced oil based on analysis. Image courtesy Eliza Bradley, UCSB.

Other observations with sonar suggest significant oil is submerged in the shallow subsurface (*Eric Maillard*, 2010, unpublished), which matches visual observations (*Asper*, 2010, unpublished). These oil globules (to tens of centimeters) and oil droplets (sub millimeter) are affected by surface mixing processes related to wind stress, turbulence, wave breaking, currents, and interaction with algae and density stratification due to fresh water lensing from the Mississippi outflow – at MC118, we measured salinities of 20 ppt or lower, summer 2010 in the upper few tens of centimeters. Here, also, weathered sinking oil (or tar balls) also may be found.

Zone 2 – Sea surface

Spilled crude oil changes due to numerous processes, shown schematically in Fig. 30, including advection from currents and winds, wave and current compression (into wind rows or narrow slicks), spreading and surface diffusion, flocculation and dissolution into the water column, evaporation, as well as photochemical and biological degradation [*NRC*, 2003].

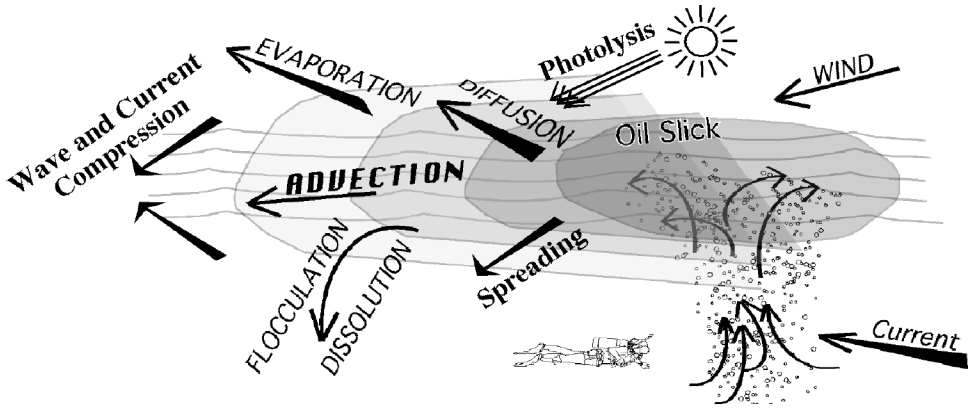

Figure 30: Major initial processes affecting surface oil slicks. After [Leifer et al., 2006b].

Chemically, oil slicks where there are multiple sources can be complex in terms of stages of weathering. Fresh oil becomes intermixed with more aged oil, although the two tend not to become intimately mixed barring wave action (boat wakes, etc). In addition, while volatilization occurs on hour time-scales for thin sheens and slicks [*Leifer et al.*, 2006b], where oil is in thick emulsions, slicks, or tarballs, evaporation proceeds far more slowly. In addition, while volatilization is highly efficient for lighter alkanes (decane, C10 and lighter) – as well as photolysis of larger molecules into lighter volatile components, dissolution is much less efficient than volatilization. Thus, oil at the base of an emulsion or slick loses volatile components at far slower rate. Thus, thick emulsions will preserve their volatile components better than thin emulsions or sheens.

Zone 1 – Atmosphere

The balance of volatile oil components entering the atmosphere depends significantly on the extent of dissolution during transit of the water column. For a deep spill, these dissolution losses can be significant. Preliminary analysis of gulf air samples showed significant higher carbon number alkanes and aromatics present while the lower carbon oil components were missing. This would be consistent with significant volatile component water-column dissolution. Total hydrocarbon (non-methane) loads were high, > 2 ppm, which is very unusual (*Blake*, 2010, unpublished), and has significant health implications (manuscript in prep). These observations were confirmed during a mid June NOAA flight (*David Parrish*, NOAA, 2010, personal comm.).

Mass Balance Calculation

The area in each slick class in terms of pixels was calculated (Table 2). Class 3, "Serious" is for oil such as often observed in the vicinity of the incident site, which appear to be solid gray in the MODIS data and which AVIRIS shows has many slick lines of thick oil slicks. This also includes large patches of recently surfaced oil, which appears not to be organized into lines, but rather fills an area. Here, all water is assumed to have some level of oil slick, but that most of the surface is partitioned between strong rainbow and brown oil, with "non-AVIRIS" black oil, only 1%, yet contributing comparable amounts to that of brown oil. Note, black, the thickest category covers oil too thin for the AVIRIS analysis approach, but thick enough for this thickness category. As a result, its area is significantly underestimated to avoid double counting. The "brown" category is estimated from AVIRIS data, while the thinner categories are based on general observations of partitioning for weathered oil slicks in the Coal Oil Point seep field.

Class 1 slicks were located to the Northeast, and have a generally whispy appearance in MODIS data with clear evidence of thick slick structures, borne out in AVIRIS data. These slick structures are assumed to have a significant brown thickness component, but the structures only cover a small fraction of the total area.

The Tail (Class 2) is assumed to have a different spatial distribution due to its spatial distribution being controlled by the loop current fluid dynamics, which should be distinct from those of the main slick. Two estimates were performed for the "tail", one the low estimate assumed that the tail was oily for only about half its length, and determined that the slick was 3143 km^2. However, given loop surface currents of ~1 m/s, or ~ 85 km/day, and some indications from the MODIS (Terra) May 12, 2010 data that the oil had entered the loop current, it seems feasible that oil slicks had reached the edge of the Gulf Current, thus the calculation assumed 5067 km^2 for the tail (the difference is ~8500 barrels). Most of the slick is assumed to be sheen or thin rainbow slick, it was too faint for AVIRIS detection, with brown and black percents derived from AVIRIS data.

Some of the slick was located between areas classified as serious, and the Northeast whispy area, and were assumed to share the characteristics of both. Class 4 was not observed well by AVIRIS due to sunglint, occupied a small portion of the total non-sheen slick (only 1500 km2 out of a total non-sheen area of 17279 km^2). This class was assumed to have more thick oil than the whispy, Class 1 area, due to prevailing currents driving oil from the "serious" oil class into this area. Finally, the sheen slick area was estimated at almost 7000 km^2, however because of its thinness only contributed an estimated 2000 barrels. This area could easily extend an additional 50% in areas not clearly visible in the MODIS data; however, it would not change the total oil significantly.

As noted, surface slicks do not count a significant fraction of the released oil which partitions elsewhere in the water column. EPA guidelines were used for dispersant application on the theory that BP would want to ensure that their application was legal, and it was further assumed to be 50% effective at the sea surface and 100% effective at the seabed, with a 15:1 application. Sea surface effectiveness may have been less due to interference from the Mississippi river outflow creating freshwater lensing.

Table 2: Oil budget calculation.

MODIS Class	Pixel	Area km2		Class	Lo	Uncert	Mean L/km2	Area L/km2	Area Liters	Area Barrels
class 1	76521	4783		**Silvery**	68%	5%	*110*	75		
NE				**Faint Rainbow**				0		
				Strong Rainl	30%	5%	*331*	99		
				Brown	2%	0%	*11050*	221		
				Black*	0.05%	0.01%	*552486*	276		
							TOTAL	**672**	**3212772**	**19124**
class 2	81065	5067		Faint						
Tail				**Silvery**	71%	5%	*110*	78		
				Faint Rainbow			*166*	0		
				Strong Rainl	27%	5%	*331*	90		
lo estimate	50286	3143		**Brown**	2%	5%	*11050*	221		
				Black*	0.02%	1%	*552486*	110		
							TOTAL	**499**	**2530370**	**15062**
class 3	35529	2221								
Serious				**Silvery**	5%	5%	*110*	6		
				Faint Rainbow			*166*	0		
				Strong Rainl	40%	5%	*331*	133		
				Brown	54%	5%	*11050*	5967		
				Black*	1.0%	1%	*552486*	5525		
							TOTAL	**11630**	**25824774**	**153719**
Class 1/3	9221	576		Faint						
				Silvery	36%	5%	*110*	40		
average of Class 1 & 3				**Faint Rainbow**			*166*	0		
				Strong Rainl	35%	5%	*331*	116		
				Brown	28%	5%	*11050*	3094		
				Black*	1%	1%	*552486*	2901		
							TOTAL	**6151**	**3544784**	**21100**
Class 4	23842	1490								
Misc										
				Silvery	44%	85%	*110*	8		
				Faint Rainbo	20%		*166*	0		
				Strong Rainl	30%	5%	*331*	116		
				Brown	5%	10%	*11050*	3043		
				Black*	1.0%	1%	*276243*	1450		
							TOTAL	**4617**	**6880096**	**40953**
Class 5	110552	6910		Faint	50%	20%	*55*	28		
sheen				Silvery	50%	20%	*110*	22		
							TOTAL	**50**	**343566**	**2045**
total non-sheen area		17279								
	total Area	24189						**GRAND**	**TOTAL**	**252002**
									AVIRIS	120000
									BBls Applied	
						Dispersed Surface**			16667	125000
Taft et al						Dispersed Subsurface***			3095	46429
		mm thick	mic	L/km2 (1 g/c	**L/km2**					
Faint		5.0E-05	#	50	**55**				tarballs	130201
									Beached	25110
Silvery		1.0E-04	#	100	**110**			Water col dissolution		55800
Faint Rainbow		1.5E-04	#	150	**166**			Surface Evaporation		55800
Strong Rainbow		3.0E-04	#	300	**331**		Natural Subsurface Dispersion			74400
Brown		1.0E-02	#	10000	**11050**		Natural Surface Dispersion			74400
Black*		5.0E-01	#	500000	**552486**			**Lower Bound Total**		**959143**
* value purposely cut off at lower Tetraquad limit										
								Lower Bound Day Rate		45673
	**	Assuming 50% safety margin on legal limit. Assuming a 50% effectiveness rate								
	***	Assuming 100% effectiveness with respect to removing from plume								
	^ assuming all first week slick is now a tar ball									

Tar ball formation takes about 1 week, so the total slick oil was assumed to have surfaced at a constant rate, with oil from the first week having been converted into tar balls, which would have lost their volatiles due to dissolution or volatilization (30%). Thus, the oil at the sea surface was assumed to represent primarily oil from the previous two weeks only. Some fraction of the oil at the sea surface (not dispersed, not volatilized, and not dissolved) had been reaching area beaches and wetlands for several weeks, this was assumed to be 5% as observed wind and advection patterns appeared to largely "slosh" the mass of oil back and forth (with a synoptic time scale).

For this calculation, it was assumed that half of the volatile components dissolved and half evaporated (total 30%); although data suggests a greater fraction may be entering the water column. In either case, the total mass budget is not affected by this partitioning, although the ecological impact of the dissolved oil fraction is far greater than that of the volatilized component as photolysis breaks these components down far faster than their loss in the water column.

Natural subsurface dispersion is a huge uncertainty, and includes hydrate effects where nothing is known other than there certainly seems to be an effect, thermocline losses, and plume turbulence. These loss values depend on currents and thus will have a strong tidal component. Thus, the 20% for natural sub-surface dispersion may be accurate or a gross underestimate.

Similar uncertainty arises regarding dispersion from surface processes which include waves and wave breaking and boating activities. Winds were calm, so wave breaking would not have been a significant contribution on May 17 2010; however, there are reports suggesting significant near-sea, suspended oil globules. These globules have not been quantified or mapped (or at least reported), even using existing technologies. Absent any information, a dispersion rate of 20% was assumed.

For this calculation the AVIRIS derived volume, termed *aggressive*, was used of 120,000 barrels, which yielded approximately 960,000 barrels of oil released as of May 17th. Assuming that for some of the first week, when the oil slick appeared not to grow rapidly in the satellite data, relatively little oil was released, then one could estimate oil emissions having arisen over 21 days, leading to a release rate of 46,000 barrels oil per day. If the *conservative* AVIRIS estimate was used (66,000 barrels), a release rate of 40,000 barrels per day is estimated; however, this assumes a maximum oil thickness that is significantly less than observations and is unrealistic. In contrast, if one assumes a *possible* oil thickness of up to many centimeters, the total oil emission rate is 84,000 barrels per day. Reality may lie between the possible and aggressive AVIRIS estimates.

Independent Validation Study of the Flow Rate

My experience on the TFRT strongly highlights the need for independent data for flow rate verification to assure public confidence in our work. This can be done quickly and accurately, using field-demonstrated, published, techniques on a two-track approach:

- **Prioritize collection of independent data**, to make the measurements needed to provide a non-BP value based on solid science.
  - A simple monitoring experiment, as detailed *below*, could be performed on a week time scale of the decision to proceed.
  - Readily repeatable to provide data until well emissions stabilize.
  - Includes monitoring capability
- **Investigate the BP-provided data** to estimate reasonable and scientifically defensible uncertainty bounds on the emission range.

Proposed Experiment

a. Measure the plume's "work" (physics' sense). Dye injection and fluorometer/video measurement of plume fluid velocity (*hydrates clog paddle-velocimeters, bubbles prevent ADCP usage*), not plume structures (*avoid deriving phase speed from HDIV on "crests"*) to provide the mass flux. The difference between mass and buoyancy fluxes (latter from plume's work) yields oil flux.

b. Multibeam scanning sonar (250 kHz) to measure plume growth and derive net entrainment rate. Also provides long-term monitoring of variability.

c. CTD measurements and hydrocasts downcurrent of the plume to measure plume detrainment rates. Temperature, salinity, and O_2 measured during casts will identify detrainment zones (intrusions). Niskin bottle samples from these zones will be sub-sampled for C_1-C_5 and DOC concentration analyses to trace and quantify mass fluxes from the plume to the water column. This will provide critical data for validating mass balance calculations in (a) and identifying the hydrocarbons' fate.

d. High quality, size-calibrated, plume video above the plume acceleration phase, observations from multiple angles.

e. Several repeats to "calibrate" the monitoring sonar allowing sonar return to be related to flux variability. Note, sonar does not penetrate dense bubble plumes, sonar only shows the plume outlines. However, plume dimensional-growth (*net entrainment*) directly relates to the buoyancy flux.

f. Directly and repeatedly sample the flow to measure the oil to gas ratio. A Niskin bottles on ROV will work fine, followed by video observation and shipboard.

g. Multibeam site survey to confirm that the study leak is the dominant leak.

This study should be coordinated with airborne remote sensing data. Development of a remote sensing approach to spill quantification is a NASA/NOAA/USGS effort under Dr Leifer's leadership. Coordination would leverage the value and accuracy of both efforts.

References on the marine application of the destratification strategy available on request.

Regards,
Ira Leifer, Ph.D.
+1(805)893-4931
Cell +1(805)252-3636
Email ira.leifer@bubbleology.com

References

Bradley, E. S., I. Leifer, and D. A. Roberts (2009), Atmospheric long-term monitoring of temporal trends in seep field emissions *Atmospheric Environments*, Submitted.

Clark, R.N., Swayze, G.A., Leifer, I., Livo, K.E., Lundeen, S., Eastwood, M., Green, R.O., Kokaly, R., Hoefen, T., Sarture, C., McCubbin, I., Roberts, D., Steele, D., Ryan, T., Dominguez, R., Pearson, N., Airborne Visible Infrared Imaging Spectrometer (AVIRIS) Team (2010), A method for qualitative mapping of thick oil spills using imaging spectroscopy: U.S. Geological Survey Open-File Report, Open File Report 2010-1101.

Clark, R.N., Swayze, G.A., Livo, K.E. , Kokaly, R.F., Sutley, S.J., Dalton, J.B., McDougal, R. R., Gent, C.A. (2003) Imaging spectroscopy: Earth and planetary remote sensing with the USGS Tetracorder and expert systems, *J. Geophys. Res.* 108 (E12) 5131, doi:10.1029/2002JE001847.

Green, R., et al., (2010) Quantitative analysis of oil slick thickness using SWIR AVIRIS absorption features. *Geophys. Res. Lett.*, In progress.

Leifer, I., B. P. Luyendyk, J. Boles, and J. F. Clark (2006), Natural marine seepage blowout: Contribution to atmospheric methane, *Global Biogeochemical Cycles*, *20*(GB3008), doi:10.1029/2005GB002668.

Leifer, I., B.P. Luyendyk, K. Broderick (2006b) Tracking an oil slick from multiple natural sources, Coal Oil Point, California. M*arine and Petroleum Geology*, 23(5), 621-630.

Leifer, I., I.R. MacDonald, (2003) Dynamics of the gas flux from shallow gas hydrate deposits: Interaction between oily hydrate bubbles and the oceanic environment, *Earth and Planetary Science Letters*, 210, 411-424.

Leifer, I., H. Jeuthe, S. H. Gjøsund, and V. Johansen (2009), Engineered and natural marine seep, bubble-driven buoyancy flows, *J. Phys. Oceanography*, *39*(12), 3071-3090.

MacDonald, I. R., Leifer, I., Sassen, R., Stine, P., Mitchell, R., Guinasso, N. (2002) Transfer of hydrocarbons from natural seeps to the water column and atmosphere, *Geofluids*, 2, 95-107.

McDougall, T. (1978) Bubble plumes in stratified environments, *J. Fluid Mech.* 85, 655-672.

Milgram, J. H. (1983) Mean flow in round bubble plumes, *Journal Fluid Mechanics*, *133*, 345–376.

NRC (2003) Oil in the Sea III: Inputs, Fates, and Effects. National Academy of Sciences, The National Academies Press, Wash DC, 245 pp.

Rehder, G., I. Leifer, P. G. Brewer, G. Friederich, and E. T. Peltzer (2009), Controls on methane bubble dissolution inside and outside the hydrate stability field from open ocean field experiments and numerical modeling, *Mar. Chem.*, *114*(1/2), 19-30.

Solomon, E., m. Kastner, I.R. MacDonald, I. Leifer (2009) Considerable methane fluxes to the atmosphere from hydrocarbon seeps in the Gulf of Mexico, *Nature*, 2, 561-565.

Taft, D.G., Egging, D.e., Kuhn, H.A. (1995) Sheen surveillance: An environmental monitoring program subsequent to the Exxon Valdez shoreline cleanup. ASTM STP 1219. Peter G. Wells, James N. Butler, and Jane S. Hughes, Eds., American Society for Testing and Materials, Philadelphia.

Vazquez, A., I. Leifer, and R. M. Sanchez (2010), Consideration of the dynamic forces during bubble growth in a capillary tube, *Chemical Engineering Science*, *65*(13), 4046-4054.

Appendix 7: Estimate of the Maximum Oil Leak Rate from the BP Deepwater Horizon

Estimate of the Maximum Oil Leak Rate from the BP Deepwater Horizon Based on Velocity Measurements, Theoretical Analysis, and CFD Simulations of Oil Leak Jets

Franklin Shaffer, Nathan Weiland[5], Mehrdad Shahnam, Madhava Syamlal, George Richards
US DOE National Energy Technology Laboratory

Prepared for the Phase II Report of the Plume Analysis Team
of the U.S. Flow Research Technology Group (FRTG)

Submitted on July 12, 2010

Introduction

The U.S. government's Deepwater Horizon Unified Command, led by Admiral Thad Allen, established the Flow Rate Technical Group (FRTG) to develop scientific estimates of the amount of oil leaking from the BP Deepwater Horizon well site. The FRTG is led by Dr. Marcia McNutt, Director of the U.S. Geological Survey (USGS). The Plume Modeling Team is one of the teams of the FRTG. The Plume Modeling Team is led by Dr. Bill Lehr of National Ocean and Atmospheric Administration (NOAA). The mission of the FRTG Plume Modeling Team is to develop an independent scientific estimate of the oil leak rate by analyzing videos of oil leak jets taken by BP's Remotely Operated Vehicles (ROVs).

In Phase I of the Plume Team's work, the team estimated a minimum value for the total average oil leak rate, primarily based on Particle Image Velocimetry (PIV) measurements of jet velocities using BP videos of the oil leak jets. The Phase I analysis was intended to provide a lower limit for the estimate of the total average oil leak rate during the period from the BP Horizon accident until the riser cut procedure (around 27 May 2010). The Plume Modeling Team concluded that the minimum oil leak rate was in the range of 12000 to 25000 barrels per day (bpd).

In Phase II of the Plume Team's work, the team had more time and information, so a more thorough and detailed analysis was conducted. The Phase II estimate started out to be an estimate of the *maximum* oil leak rate, but the estimate is now considered to be a "*best estimate of the average*" oil leak rate. The Phase II estimate of the Plume Modeling Team and an estimate by a team led by Secretary of Energy Stephen Chu were used to establish the U.S. government's official estimate of 35,000 to 60,000 bpd[6]. The estimates of oil leak rates by the NETL, as described in this report, are towards the high end of this range.

[5] Also Research Assistant Professor of Mechanical Engineering, West Virginia University
[6] "U.S. Scientific Team Draws on New Data, Multiple Scientific Methodologies to Reach Updated Estimate of Oil Flows from BP's Well," Deepwater Horizon Incident Joint Information Center, June 15, 2010 16:00:16 CST.

The estimates in this report are based on three different analysis approaches conducted by three separate teams of researchers at the USDOE National Energy Technology Laboratory (NETL) as follows:

Analysis Approach 1: This approach estimated oil leak rates by measuring oil jet velocities using manual Feature Tracking Velocimetry (FTV).

Analysis Approach 2: This approach estimated oil leak rates by analyzing the velocity profile and trajectory profile of oil leak jets using established theory of turbulent jets.

Analysis Approach 3: This approach estimated oil leak rates by simulating the trajectory of a buoyant oil leak jet using computational fluid dynamics (CFD).

In this report, we present an integrated assessment based on these three approaches, including an assessment of assumptions and uncertainties embodied in each approach. Analysis Approach 1 provides NETL's estimate for use by the Plume Modeling Team. Analysis Approaches 2 and 3 confirm the estimate of Analysis Approach 1.

Background

On April 20, 2010, the BP Deepwater Horizon oil well failed catastrophically and the Blowout Preventer (BOP) failed to seal the oil well. The riser pipe bent in a >90 degree kink approximately one meter above the top of the BOP and a section of about 500 feet of riser fell to position horizontally on the sea floor as shown in the schematic below (Fig. 1). The riser pipe was severed about 500 feet from the well with the end of the riser pipe open to the ocean. Pressurized oil and gas produced a turbulent, buoyant jet emitting from the end of the riser (hereafter called the Riser End Jet). The inner diameter of the riser is 19.5", but near the end of the riser, the riser is slightly deformed, reducing the inner diameter of the end of the riser to about an effective diameter of about 14 inches. It is estimated that considerably more than half of the oil is leaking from the Riser End Jet. At the kink in the riser just above the BOP, the riser developed small holes in several places with oil/gas jets emitting from the holes. These are referred to as Riser Kink Jets. In late May, the riser was cut just below the Riser Kink Jets and just above the top of the BOP. This resulted in all oil being emitted from one vertical jet at the top of the BOP. This is called the Post Riser-Cut Jet.

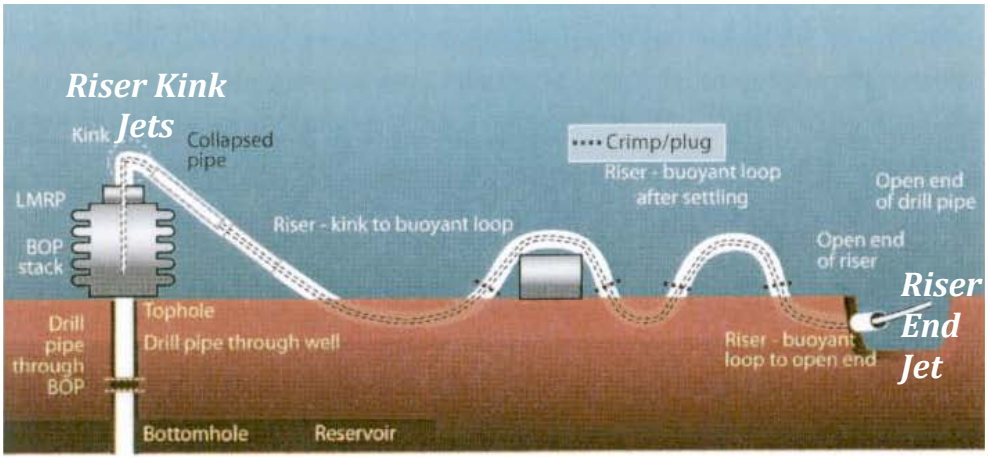

Figure 1: Schematic diagram of BOP and riser, showing positions of the jets analyzed in this report.

Example screenshots of videos showing jets emitting from many openings on the top side of the riser kink area above the BOP are shown below (Figs. 2 and 3). The main jet in the center of the image (J_1 in Fig. 3) is a classical, momentum driven turbulent jet with a 26 degree total divergence angle. The brown-orange color of the Riser Kink Jets suggests that the fluid is a mixture of oil and water. Entrainment of water into this turbulent jet is discussed in the section of this report on jet theory.

Figure 3 has an analysis of the complex flow patterns drawn onto the jets. This image was provided by one of the Plume Modeling Team experts, Professor Ömer Savas from the University of California at Berkeley. Because of the main jet labeled J_1 is the only jet that has an unobstructed, clear view, velocity measurements were made only for the main jet J1. Several team members made the assumption that the other jets produce (in total) about the same flow rate as the J_1 jet. So we assumed the total oil flow rate from the Riser Kink Jets could be represented by twice the value estimated for the J_1 jet.

Figure 2: Several jets emitting from openings in the Riser Kink area above the BOP.

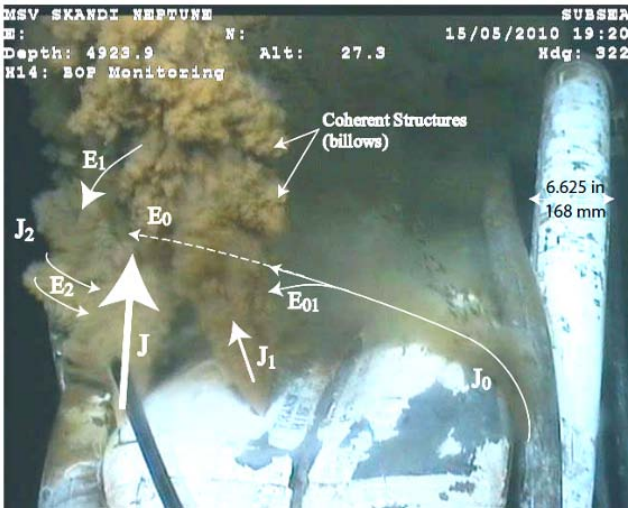

Figure 3: Schematic of complicated flow patterns of several jets emitting from the Riser Kink. Courtesy of Professor Ömer Savas of U.C. Berkeley.

Screenshots of a BP video of the Riser End Jet are shown below (Figs. 4 and 5). The screenshot in Figure 4 was captured when the jet was dominated by oil (dark), whereas the screenshot in Figure 5 was captured when the Riser End Jet was dominated by gas. The goal of this analysis is to estimate only the leak rate of oil, not methane, so velocity was measured only on images showing oil-dominated jets.

Figure 4: Riser End Jet when oil dominates the flow.

Figure 5: Riser End Jet when gas dominates the flow.

Assumption on Cross Sectional Area of the Exit of the Riser End Jet

On June 3, 2010, the riser was cut just above the BOP and before the Riser Kink Jets. On June 12, BP provided the Plume Team with photos of the actual cross section of the riser end, after oil had stopped flowing. The original photo from BP is shown in Figure 6. Figure 7 illustrates the outline of the Riser End Jet exit drawn using NIH's Image J software. The total area inside the polygon was measured to be 150 in^2 (0.096 m^2) using this image analysis software.

Figure 6: Photo supplied by BP on June 12 showing the exit of the end of the riser after oil had stopped flowing because the riser was cut above the BOP.

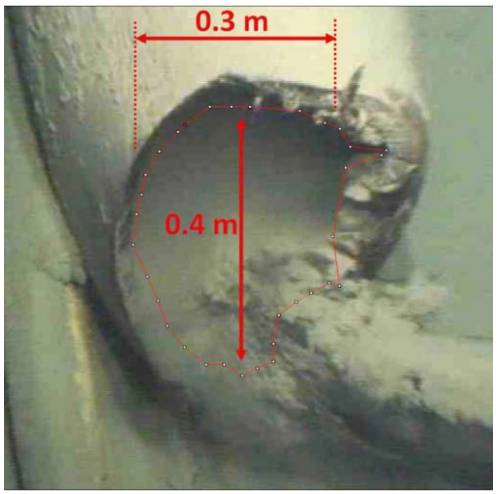

Figure 7: NIH's ImageJ software was used to measure the approximate cross sectional area of the actual riser exit.

The actual cross sectional area is not circular, but an assumed circular cross section was used in the analyses in this report. An equivalent diameter of 13.75" (0.35 m) was chosen to generate an equivalent cross sectional area of 150 in^2.

A screenshot of the sole oil leak jet after the riser was cut on June 3, 2010, is shown below in Figure 8. In this report this jet is referred to as the Post Riser-Cut Jet.

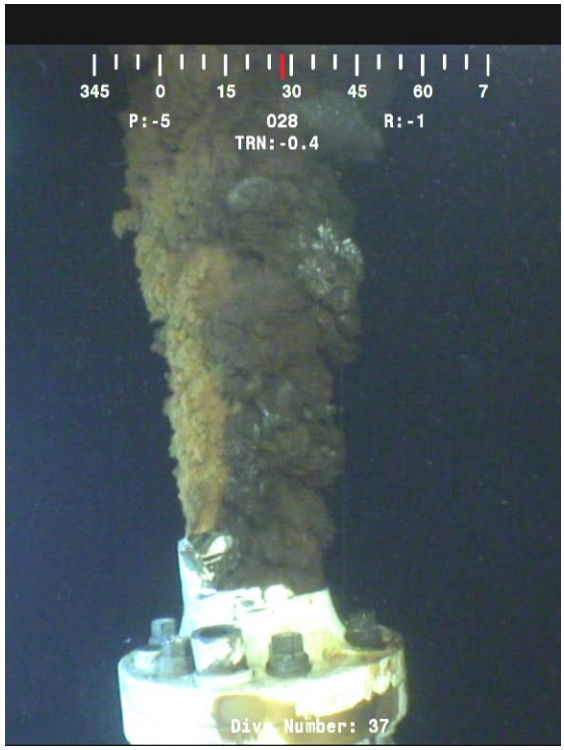

Figure 8: Vertical Post Riser-Cut Jet emitting from the riser pipe just above the BOP.

As mentioned above, NETL employed a multiple analysis approach. Three separate analyses by three different teams used different approaches to understand these oil leak jets. Analysis Approach 1 estimated oil leak rate from all three oil leak jets, before and after the riser was cut. Analysis Approach 2 estimated oil flow rate from the Riser Kink Jets and the Riser End Jet, both before the riser was cut. Analysis Approach 3 estimated oil flow rate from only the Riser End Jet, before the riser was cut. Analysis Approaches 2 and 3 were done to provide alternate methods to estimate oil leak rate, and to confirm the estimate of Analysis Approach 1. Both Analysis Approaches 2 and 3 are in agreement with the estimate of Analysis Approach 1 using manual Feature Tracking Velocimetry (FTV). Since most of the Plume Team's estimates were done using jet velocity measurements from automatic PIV or manual FTV, Analysis Approach 1 is considered to be NETL's estimate of oil leak rate.

The following sections discuss each of three separate NETL analysis approaches.

Analysis Approach 1: Manual Feature Tracking Velocimetry

Several videos taken by BP Remotely Operated Vehicles (ROVs) of the oil leak jets, both before and after the riser was cut on June 3, were used in this analysis. The videos were selected by BP and delivered to Bill Lehr of NOAA, the Plume Team Leader. The first major assumption made in this analysis is that the short video clips provided by BP before the riser was cut, less than five hours in total, are statistically representative of the total average oil leak flow rate over the period from the start of the oil leak until the riser was cut on June 3, 2010. The members of the Plume Modeling Team using automatic PIV or manual FTV were able to analyze a total of less than 30 minutes of the videos for the pre riser cut jets. Based on experience with other sea-floor oil leaks, one expert on the Plume Modeling Team, Dr. Ira Leifer (University of California at Santa Barbara Marine Science Institute) indicated that oil leaks similar to the BP Horizon leak can vary significantly with time. Dr. Leifer recommended that estimates of the total average oil leak rate be accompanied by a statement that the actual total average flow rate could be as low as one half of the estimate and as high as twice the estimate because of natural variability in oil leak rates from deep wells below the sea floor. After the riser was cut, BP provided high definition videos of much longer periods.

The file name of the video clip used by NETL to measure jet velocities are listed below.

Riser Kink Jets:

- H14_BOP_Plume_May_15_1920-1945.asf

Riser End Jet:

- 20100514224719234@H14_Ch1-ProRes.mov
- 20100514221717125@H14_Ch1-H264h_ProRes.mov

Post Riser-Cut Jet:

- TOPHAT_06-03-10_14-29-22.avi

In this analysis, manual feature tracking velocimetry (FTV) was used to measure the velocity of jet features. Jet velocity is used to calculate oil leak rates. For the Plume Team's Phase I estimate of minimum oil leak rate, NETL used its proprietary automatic feature tracking software (Patent Pending, U.S. Patent Application No. 12765317) to measure jet velocities. In this Phase II analysis, more time was devoted to studying the BP videos of oil jets in order to determine if automatic PIV software would be reliable for these videos. It was determined that automatic PIV/FTV software could produce unreliable and erroneous velocity values for the BP videos of oil leak jets. The reasons for this conclusion are listed below.

Reasons for not using Automatic PIV/FTV Software in the Analysis

Several characteristics of the BP videos, and of turbulent jets in general, indicated that automatic PIV software would not be reliable for detecting frame-to-frame feature displacement (and thus jet velocity) in these BP videos of oil leak jets. The reasons are listed and discussed below.

1. Automatic PIV software has not been tested and proven to be reliable for tracking large flow features in a turbulent oil jet. Automatic PIV software was developed for a different application, namely detecting the motion of very small particles (usually of diameter around 10 microns) in a transparent fluid. The small "seed" particles are illuminated with a thin laser sheet. Analyzing BP videos of oil leak jets is an entirely different application. The fluid is opaque, there are no small seed particles, and illumination is not from a thin laser sheet. The jet features that must be tracked in BP videos are primarily vortices and turbulent eddies. The size of these flow features is much larger than the 10 micron particles that automatic PIV software was designed for. The larger vortice features that are most easily tracked in the BP videos are of a size on the order of ten centimeters -- five orders of magnitude larger than the 10 micron particle.

2. Vortices in jets are known to have reverse spin, leading to velocities pointing upstream on the outside surface of a vortice. Since only the outside surface of these oil jets will be detected by automatic PIV software, the reverse spin velocity of vortices will be detected, leading to an underestimate of fluid flow velocity.

3. Vortices often appear to slow down and pause momentarily in the BP videos of oil jets. This may be because vortices have momentarily detached from the jet core or are moving in the direction of the camera. Only the fastest moving vortices are representative of the jet core velocity. But automatic PIV software will detect all vortices, including those that have paused or are moving slowly. This can cause automatic PIV software to generate velocity values much lower than the actual velocity of fluid flow in the jet core. This is discussed in detail in a section below.

4. As discussed by Professor Savas in his final report (see Appendix 4 section of this report), instability waves are present close to the exit of these oil jets. Instability waves propagate at a much lower speed than the fluid in the jet core. Automatic PIV software will detect these instability waves, leading to a significant underestimate of jet fluid velocity.

5. The following statement is from Professor Savas' final report (statements in parentheses were added):

   "As the window size or time step (of automatic PIV software) is increased inordinately, the (automatic) PIV approach degrades at turbulent interfaces, since the turbulence, by its very nature, will continually re-granulate the interface, hence stressing any PIV algorithm. In particular, it (automatic PIV software) will underestimate displacements (and thus underestimate velocity). Turbulence by its nature has a cascade of time and lengths scales. If the time step is too large, the intermediate time and lengths scales will change completely between the successive PIV images, rendering any correlation algorithm helpless."

6. There are visible objects moving slowly just outside of the jet boundary. Automatic PIV software could detect this motion, even though it is not part of the oil jet.

7. The pre riser-cut videos had poor resolution (704 x 576 pixels) and large compression artifacts. This will lead to high noise levels that will make motion detection difficult with automatic PIV software. A magnified screenshot showing the compression artifacts in video "20100514224719234@H14_Ch1.mov" is shown below. The compression artifacts appear in 8x8 pixel blocks and produce a high level of pixel-to-pixel noise. Our analysis of the BP videos indicates a compression level of 75% using Apple Pro Res codec. Compression artifacts cause flow features to be blurred and superimposed with noise. This makes automatic frame-to-frame tracking of flow features much more difficult.

Figure 9a: Magnified area shown in Figure 9b. Snapshot of video 20100514224719234@H14_Ch1.mov

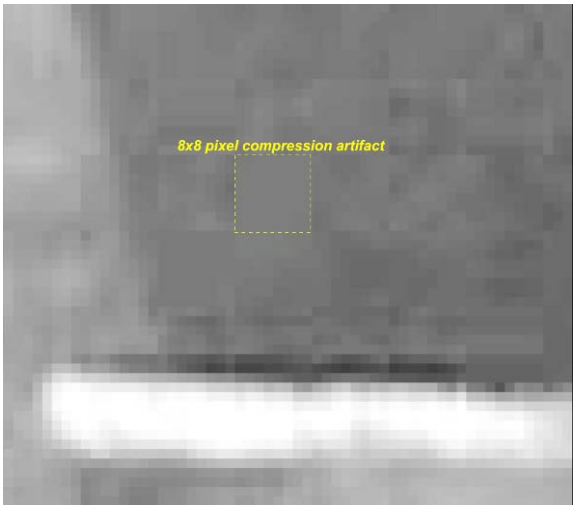

Figure 9b: Compression artifacts that appear as pixel noise in 8x8 pixel blocks.

For the reasons stated above, automatic PIV software was not used in this analysis. Rather, manual feature tracking velocimetry (FTV) was used to measure jet velocity. Manual FTV is much more time consuming, but because this estimate is a national priority of critical importance, the additional time required to do manual FTV is warranted. The details of the manual FTV method used in this analysis are discussed below.

Discussion of Manual Feature Tracking Velocimetry (FTV)

The turbulent oil leak jets shown in BP videos are completely opaque, so the flow inside these oil jets cannot be seen or measured. The figures below from a report by Hu et al. in 2003[7] show the general features inside of a turbulent jet. These figures show a vertical jet of water injected into still ambient water a Reynolds number of 6000. This Reynolds number is lower than the Reynolds numbers of the BP oil jets, but the general features of this jet are similar to features close to the exit of the Riser End Jet and the Post Riser-Cut Jet. These figures are presented only for the purpose of explaining the manual FTV technique used in this analysis. These figures are not intended to be an exact quantitative representation of the internal features of the oil jets seen in the BP videos.

[7] From "Analysis of a Turbulent Jet Mixing Flow by PIV-PLIF Combined System," H. Hu, T. Saga, N. Kobayashi, and N. Taniguchi, Journal of Visualization, Vol. 7, No. 1, pg 33-42, 2003.

Close to the jet exit, the jet has a strong potential core of velocity directed upstream. Most of the large structures seen in the BP videos are vortices in the outer mixing layer and turbulent eddies. In these figures, the internal morphology of jet flow field is visualized with Planar Laser Induced Fluorescence (PLIF). Jet velocities are mapped with PIV and jet concentration is mapped with PLIF.

It should be noted that the automatic PIV done by Hu et al. was done using the type of flow field for which automatic PIV was designed. The jet fluid was transparent and was seeded with small (10 - 20 micron) particles. The jet was illuminated with a thin laser sheet with a thickness of a few mm. This is the type of flow field that automatic PIV was designed for. For this type of flow field, automatic PIV has been extensively tested and proven reliable and accurate. However, automatic PIV software has not been tested and proven reliable for measuring the velocities of the flow fields shown in BP videos.

Shearing action between the high velocity jet core and the still ambient seawater sets up a mixing zone shown approximately as green and blue PIV map shown below. The shearing action causes vortices with reverse rotation to form in the mixing zone. Several sets of vortices can be seen along the sides of the jet Figures 10a and 10c.

Figure 10a: Planar Laser Induced Fluorescence (PLIF) of a water jet injected into still water at Re=6000. Image shown is a negative.

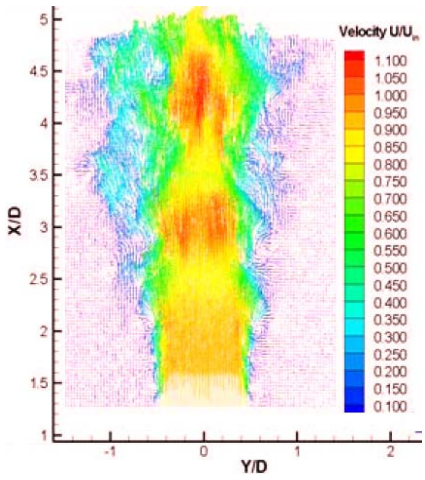

Figure 10b: Simultaneous measurement of jet velocity with PIV. Hu et al. 2003.

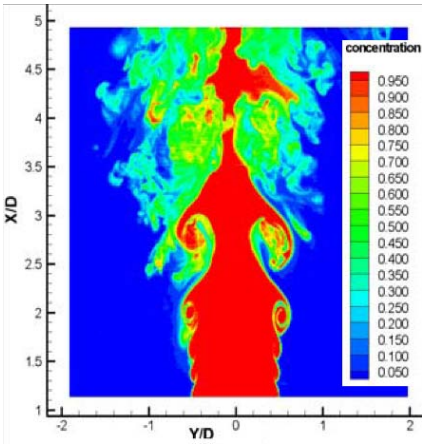

Figure 10c: Simultaneous PLIF measurement of jet concentration. Hu et al. 2003.

The schematic below in Figure 11 also represents the general features of a turbulent jet injected vertically into a still ambient fluid. This schematic will be used only to illustrate the details of how manual FTV was done in this analysis. The schematic shows an idealized oil jet emitting from a vertical pipe into ambient seawater. This schematic is also intended to be qualitative in nature -- it is not intended to capture the exact quantitative values of the oil jets seen in BP videos. The schematic only shows the jet features necessary to explain the manual FTV method used in this analysis.

The flow field inside the riser pipe of the BP Deepwater Horizon has a high Reynolds number and is turbulent, so the velocity profile inside the pipe will be closer to a "top hat" profile than a Gaussian profile. The velocity profile in the jet just downstream of the exit will also be close to a top hat profile. As the jet propagates downstream the velocity profile evolves into a Gaussian profile.

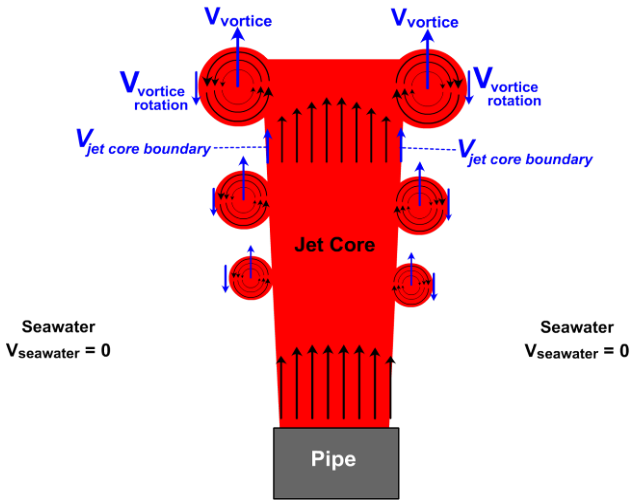

Figure 11: Schematic of the general features of a turbulent jet into still ambient water. This is not intended to be an exact quantitative representation of the oil jets seen in BP videos; rather it shows only the qualitative features necessary to explain the manual FTV method used in this analysis.

Again, the oil jet is entirely opaque, so automatic PIV or manual FTV can only measure velocities of the outer surface of the jet. As shown in the schematic, there are at least three different velocities that can be detected on the outer surface of the oil jets shown in BP videos. These velocities are shown in blue on the schematic and are listed below:

- $\mathbf{V_{jet\_core\_boundary}}$: This is the velocity on the surface of the jet core. In the BP videos, there are times when the outer surface/boundary of the jet core can be seen between vortices.
- $\mathbf{V_{vortice\_outer}}$: This is the rotational velocity at the outer surface of a vortice.
- $\mathbf{V_{vortice}}$: This is the propagation velocity of the entire vortice.

The boundary of the jet core in BP videos can sometimes be seen between vortice structures. The velocity $\mathbf{V_{jet\_core\_boundary}}$ can be measured by tracking small methane hydrates which appear bright white against the dark oil. Methane hydrates on the surface of the jet core often appear as dashed (streaked) while lines because of the higher speed of the jet core. Both the frame-to-frame displacement of the hydrate streaks and the length of the streaks is a measure of velocity.

The propagation speed of vortices, $\mathbf{V_{vortice}}$, ranges from zero to a maximum. In the BP videos, vortices often appear to pause, with their propagation velocity approaching zero. A momentary pause could be caused by the vortice momentarily propagating in the direction of the camera. A momentary pause could also be caused by the vortice momentarily detaching from the jet core, then soon being entrained back into the jet.

Some vortices propagate at high speeds. Large frame-to-frame displacements of the entire vortice, and motion blurring of the entire vortice, indicate a vortice is propagating at high speed. The maximum vortice propagation velocity, $\mathbf{V_{vortice\_maximum}}$, should approach the jet boundary velocity, $\mathbf{V_{jet\_core\_boundary}}$. $\mathbf{V_{vortice\_maximum}}$ is unlikely to be faster than $\mathbf{V_{jet\_core\_boundary}}$.

The goal of this analysis is to calculate total oil flow rate of an oil leak jet. The velocity of the jet core is most representative of the oil flow rate. So in this manual FTV analysis, an effort is made to measure only the jet core boundary velocity, $\mathbf{V_{jet\_core\_boundary}}$, and the maximum vortice propagation velocities, $\mathbf{V_{vortice\_maximum}}$.

In measuring the maximum vortice propagation velocity, only the fastest moving vortices were tracked. Vortices moving at slower speeds were not measured. To avoid detecting the reverse rotation of vortices, care was taken to track only the upstream and downstream edges of the vortices.

The velocity due to reverse rotation of vortices, $\mathbf{V_{vortice\_outer}}$, was not measured because it is considered to be a poor indicator of jet boundary velocity, and because it will bias the average jet velocity towards lower values. The propagation velocity of slower vortices was also not measured. Slower vortices, and vortices that have paused, are considered to be poor indicators of the jet core velocity. Measurement of slow or paused vortices can cause major underestimates of jet core velocity. So again, in this manual FTV analysis, only the jet core boundary velocity and the propagation velocity of the fastest moving vortices were measured.

Prior to analysis, the BP videos were enhanced using the ImageJ software package from the Research Sciences Branch of the National Institute of Health (NIH). The Bandpass Fast Fourier Transform (FFT) tool of ImageJ proved useful in removing variations in background level due to uneven illumination by ROVs. Brightness and contrast enhancements improved the visibility of dark jet features. Following image enhancement, jet features were tracked, recorded, and analyzed using the MTrackJ tool of ImageJ.

Velocities Measured for Riser Kink Jet

The Riser Kink has several jets, but only one of the jets has a clear, unobstructed view. Figure 12 shows the feature tracks manually identified in the main jet of the Riser Kink Jet. In Figure 12, color is used only to make the tracks easier to see. Color does not indicate magnitude of velocity. Velocities were measured only for the unobstructed main jet. An average velocity of 1.7 m/s was measured at a distance of 0.6 meters downstream from the jet exit. The jet exit diameter was measured to be 0.75 inches.

Figure 12: Feature tracks manually identified in the main jet of the Riser Kink Jet. (The trajectories of features shown in this image were pseudocolored randomly so they are easier to see. The colors do not represent velocity magnitude.)

Velocities Measured for Riser End Jet

For the Riser End Jet, velocities were measured at two locations on the bottom edge of the jet (Figures 13-15). One location was 0.8 meters downstream from the jet exit and the other location was further downstream at 1.5 meters from the jet exit. Jet velocity was measured only when the jet was dark in color and assumed to be all oil. Gas velocities were not measured in this analysis.

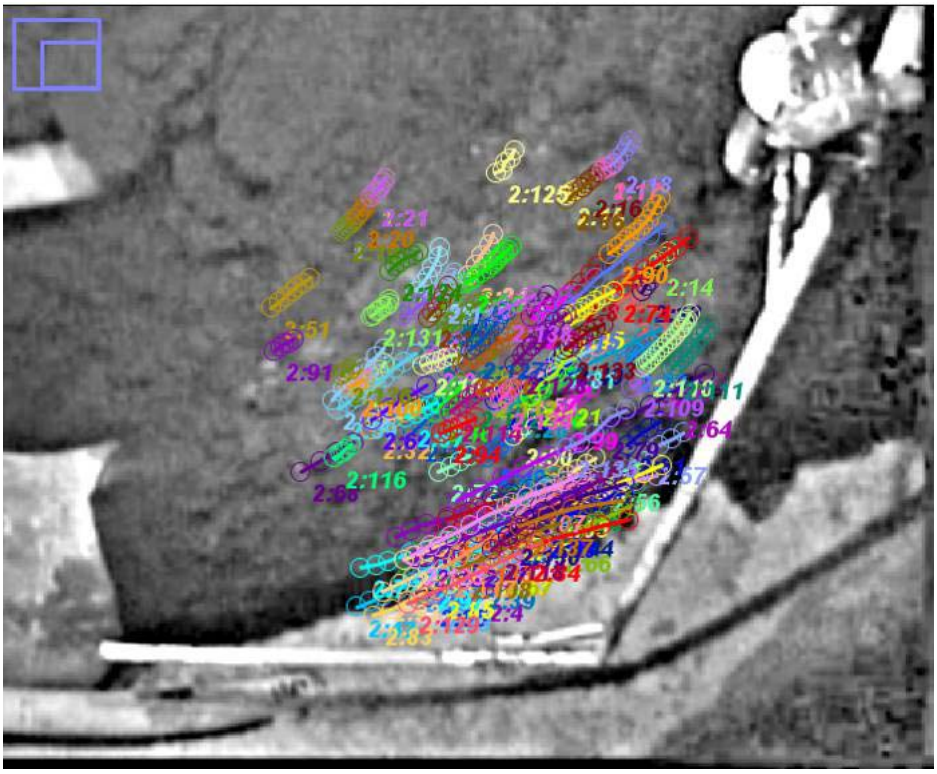

Figure 13: Feature tracks manually identified in the main jet of the Riser End Jet.

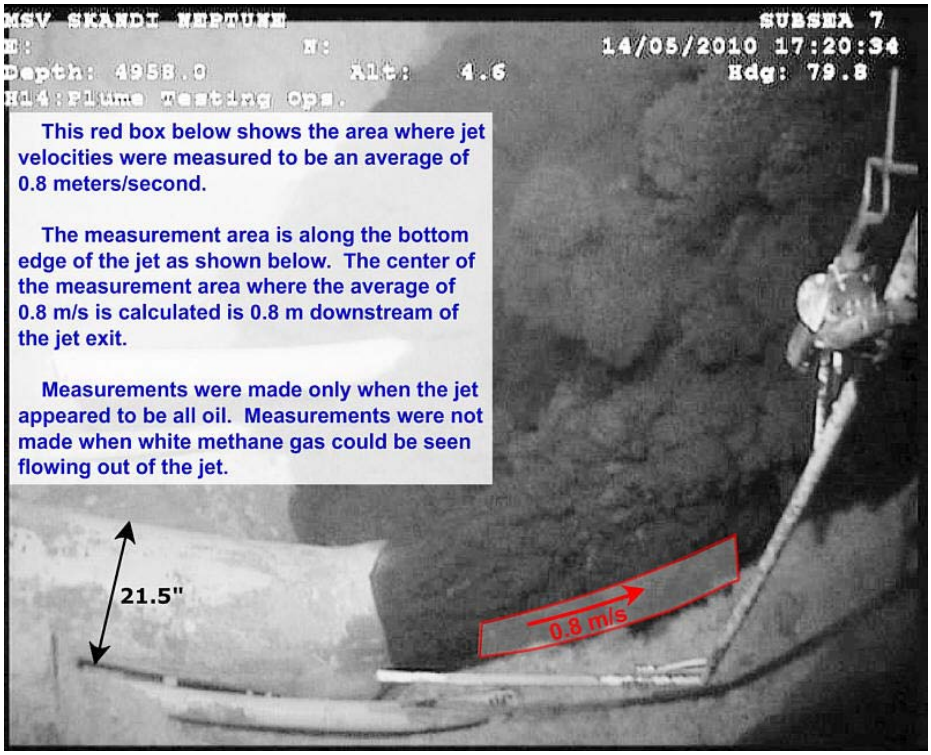

Figure 14: An enhanced view of the bottom edge of the Riser End Jet.

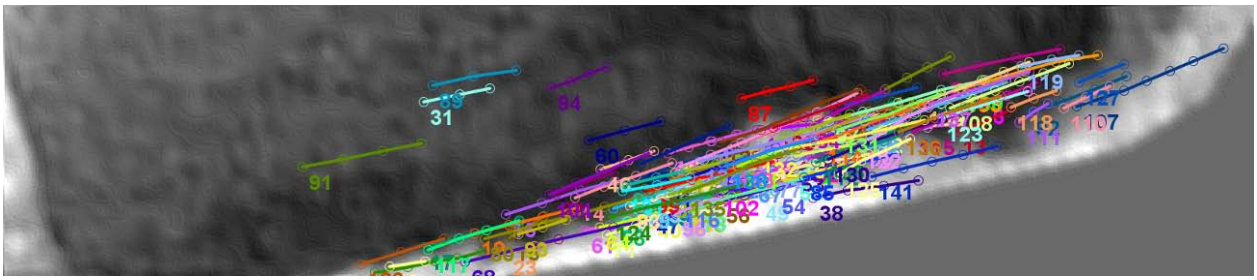

Figure 15: An enhanced view of the bottom edge of the Riser End Jet showing tracked features.

Figure 15 shows a magnified and enhanced view of the bottom edge of the jet. The light area on the far left of the image is the end of the riser. It was found that the shadow of the jet on the bright sea floor just below the jet provided a very high contrast image of the jet boundary. This allowed more accurate recognition and tracking of jet features. More than 500 velocity measurements were extracted from this video over a period of 250 seconds.

A total average velocity of 0.8 m/s was measured at the location 0.8 meters downstream of the Riser End Jet along the bottom edge of the jet. A total average velocity of 0.7 m/s was measured at the location centered at 1.5 meters downstream of the Riser End Jet exit.

Velocities Measured for Post Riser-Cut Jet

For the Post Riser-Cut Jet, the same manual FTV methodology described above was applied to frames 2810 to 3125 of the video TOPHAT_06-03-10_14-29-22.avi. More than 500 velocity measurements were made by manual FTV. The average distance downstream of the riser was 0.6 meters (about 1 jet diameter downstream). The average velocity measured was 1.5 meters per second. The plot below shows a histogram of the velocity measurements. Velocities measured with manual FTV were then used to estimate oil leak rates for each of the jets as described below.

Calculation of Total Oil Leak Rate using FTV Velocity Measurements

Once the velocity of the boundary of the jet has been measured with manual FTV, the oil flow/leak rate can be calculated. Several other pieces of information are needed to calculate oil flow rate. These include the radial velocity profile (or the total average velocity across the profile) of the jet at the location where velocity was measured, and the amount of water that has been entrained into the jet at the location where velocity was measured. Oil or methane gas flowed alternately from the Riser End Jet, so for the Riser End Jet an additional piece of information is needed: the fraction of the time oil flowed.

The equation used to calculate the total average oil leak rate, $\dot{Q}_{oil}$, from an oil leak jet is

$$\dot{Q}_{oil} = \overline{V}_{jet} A_{jet} X_{oil} (1 - X_{water}) \varepsilon_{oil} \pm U_{\dot{Q}_{oil}}$$

where

$\overline{V}_{jet}$ is the average jet velocity across the jet cross section at the location where the manual FTV measurements were made.

A_{jet} is the cross sectional area of the jet at the location where manual FTV measurements were made.

X_{oil} is the volume fraction of oil due to methane gas being dissolved into the oil.

X_{water} is the volume fraction of water in the jet due to water entrainment at the location where manual FTV was made.

ε_{oil} is the time oil is flowing versus the time gas is flowing from the Riser End Jet.

In this equation it is assumed that the effect of the ROV being at a small angle to the orthogonal of the jet is negligible. It is also assumed that parallax effects are negligible.

Measurement uncertainty of these manual FTV is primarily due to pixel resolution of the BP videos and subjective decisions by the user in tracking jet features that are changing with time. Other Plume Team members who did manual feature tracking assumed measurement uncertainty to be in the range of 20% to 40%. Professor Savas uses a value of 25% for measurement uncertainty (150 ±40 cm/s). So in this analysis, a value of 25% is used for measurement uncertainty. The calculation of oil flow rate for each of the oil leak jets is given below.

Total Average Oil Leak Rate from the Riser End Jet

As discussed above, manual FTV measured a total average velocity of 0.8 m/s at an average distance of 0.8 meters downstream of the exit of the Riser End Jet. This is about two jet exit diameters downstream. At this location the radial velocity profile is evolving from a top hat profile at the jet exit to a Gaussian profile far downstream of the jet exit. Other Plume Team members assumed that the average velocity across the entire jet diameter is 1 to 2 times the jet boundary velocity. Because the manual FTV method used in this analysis attempts to measure only higher velocities at the boundary of the jet core, the value of 1 is used in this analysis. This means that the average velocity across the jet cross section is equal to the velocity measured with manual FTV, i.e., $\overline{V}_{jet}$ = 0.8 m/s.

The diameter of the Riser End Jet at the location where manual FTV measurements were made was measured directly from the BP videos to be about 0.6 meters, giving a cross sectional area of 0.25 m^2. The assumption of the Plume Team is that all gas has separated out of the oil during transit between the BOP and Riser End Jet, so the value of $\overline{X}_{oil}$ =1. Other Plume Team members have measured the time intermittency factor to be $\overline{\varepsilon}_{oil}$ = 0.4, indicating that all oil was flowing out of the Riser End Jet for 40% of the time. The rest of the time gas was flowing out the Riser End Jet.

Entrainment of water into the Riser End Jet is estimated using the empirical analysis of B.J. Hill, 1972[8]. From Hill's paper, water entrainment is estimated to be 25% (X_{water} = 0.25) where velocity was measured. Another Plume Team (Leifer) also used a value of 25% for water entrainment at this location in the Riser End Jet using a different approach for estimating water entrainment.

The equation for oil flow rate from the Riser End Jet becomes

$$\dot{Q}_{oil} = 1.0 * 0.8 * 0.25 * 1 * 0.75 * 0.4 = 0.06 \, m^3/s$$

To convert this volumetric flow rate to barrels per day at the sea surface, conversion factors of 264.2 gallons/sec per m^3/s, 42 gallons per barrel of crude oil, and a 35% volume expansion of oil from the sea floor to the sea surface are applied.

The total average oil leak rate is calculated to be 44,000 barrels per day ± 11,000 barrel per day of oil for the Riser End Jet using Feature Tracking Velocimetry.

Total Average Oil Leak Rate from the Riser Kink Jets

The fluid mixture flowing out of the Riser Kink Jets appears to be a well mixed mixture of oil and methane gas. The volume fraction of oil in this mixture has been measured by BP to be 0.29 at the sea floor (0.4 at the sea surface). The diameter of the Riser Kink Jet at a distance of 0.6 meters downstream of the jet exit is measured to be approximately 0.25 meters. This gives a cross sectional area of 0.05 m^2.

The velocity profile at this location can be calculated in Analysis Approach 2 of this NETL report by Weiland and Richards. The following italicized section is from Weiland and Richard's Analysis Approach 2:

In momentum-dominated jets, the far-field ($x/d_0 > 15$, for our purposes) axial jet velocity profile, U(r), is known to follow a Gaussian profile:

$$U(r) = U_{cl} e^{-(r/\delta)^2 \ln(2)}$$

where U_{cl} is the centerline velocity, r is the radial distance from the centerline, and δ is the half-width of the jet, defined to be the location where the centerline velocity falls to half its value. The jet half

[8] "Entrainment in Turbulent Jets," B.J. Hill, Journal of Fluid Mechanics, Vol. 51, Part 4. pp. 773-779, 1972.

width increases linearly with x in the far-field, so the jet spreading rate is typically measured as δ/x as a constant. Incorporating this jet spreading rate, the jet centerline velocity can be estimated from a velocity measurement, U_{PIV}, at a radial location, R, and a downstream axial location, X, as:

$$U_{cl} = U_{PIV} e^{(R/X)^2 (x/\delta)^2 \ln(2)}$$

Using this equation gives a centerline jet velocity of three to four times the velocity measured at the jet boundary using manual FTV. Other Plume Team members assumed a Gaussian velocity profile with a ratio of centerline to measured velocity of about 1.5 to 3.0. In this analysis, the cross sectional *averaged* jet velocity is simply assumed to be twice the measured velocity with manual FTV. This is in reasonable agreement with Analysis Approach 2 of this report and with other velocity profiles used by the Plume Team.

Both Analysis Approach 2 of Weiland and Richards, and an external review by Yashuo Onishi of Pacific Northwest Laboratory (PNL), estimate water entrainment to be 85% in the J1 jet of the Riser Kink Jets at the location where velocity was measured. That means that 85% of the jet's volume at this location is water.

The Riser Kink Jets flow continuously (do not alternate between oil and gas), so the time intermittency factor is 1. So the equation for oil flow rate from the Riser Kink Jet becomes

$$\dot{Q}_{oil} = 2.0 * 1.7 * 0.05 * 0.29 * 0.15 * 1 = 0.0074 \, m^3/s$$

To convert this volumetric flow rate to barrels per day at the sea surface, conversion factors of 264.2 gallons/sec per m^3/s, 42 gallons per barrel of crude oil, and a 35% volume expansion of oil from the sea floor to the sea surface are applied.

Therefore, the total average oil leak rate from Riser Kink Jet J1 is calculated to be 5,400 barrels per day. Adopting the assumption of other Plume Team members that the total oil flow rate from all Riser Kink Jets is twice that of jet J1, **the total oil leak rate from the Riser Kink Jets is estimated to be 11,000 bpd ±2700 bpd.**

Total Average Oil Leak Rate from the Post Riser-Cut Jet

The total average jet velocity at the jet boundary was measured to be 1.5 m/s using manual FTV in this analysis at an average location of 0.6 meters downstream of the jet exit. The approach of other Plume Team members (Savas and Wereley) to handle effects of water entrainment and the actual cross section of the jet is adopted here. The cross sectional area of the jet at this location of the velocity measurement is assumed to be the same as the cross section of the riser exit without the internal pipes and without distortion of the riser, i.e., 0.19 m^2.

The fluid mixture flowing out of the Post Riser Cut Jet is assumed to be a well mixed mixture of oil and gas. The volume fraction of oil in this mixture has been measured by BP to be 0.29 at the sea floor (0.4 at the sea surface). So the equation for oil flow rate from the Riser Kink Jet becomes

$$\dot{Q}_{oil} = 1.5 * 0.19 * 0.29 = 0.083 \, m^3/s$$

To convert this volumetric flow rate to barrels per day at the sea surface, conversion factors of 264.2 gallons/sec per m^3/s, 42 gallons per barrel of crude oil, and a 35% volume expansion of oil from the sea floor to the sea surface are applied. **Therefore, the total average oil leak rate from Post Riser-Cut Jet is estimated to be 61,000 barrels per day.**

Total Oil Leak Rates

The total average oil leak rate *before the riser was cut* is simply the sum of flow rates from the Riser Kink Jets and the Riser End Jet. **This analysis estimates a total average oil leak rate of <u>55,000 barrels per day ± 14,000 barrel per day</u> from the BP Deepwater Horizon well site before the riser was cut.**

The total average oil leak rate after the riser was cut is simply the oil flow rate from the Post Riser-Cut Jet: <u>61,000 bpd ± 15,000 bpd.</u>

Additional Assumptions

It should be noted that this analysis does not include the effect of natural variability of the discharge rate from oil wells. According to one Plume Team members with expertise and experience with similar oil wells on the ocean floor, natural variability is significant and could change the estimate by a factor of 0.5 to 2.0.

Rather than guess the radial velocity profile in this FTV analysis, a better approach is to use established theory of turbulent jets to determine radial velocity profile. This is the subject of the next section.

Analysis Approach 2: Application of Turbulent Jet Theory

This analysis of the oil leak rates is analytical in nature. The vertical Riser Kink Jets and the horizontal Riser End Jet are analyzed by different methods. The Riser End Jet analysis is meant to be coupled to the feature tracking measurements described in the previous section of this report. The analysis of the main Riser End Jet was done as a stand-alone analysis.

General values used throughout the analyses are:

- Density of seawater, ρ_{water} = 1028 kg/m^3 (from: Bullard, Physical properties of sea water, http://www.kayelaby.npl.co.uk/general_physics/2_7/2_7_9.html)
- Density of oil at discharge, ρ_{oil} = 689 kg/m^3
- Density of gas at discharge, ρ_{gas} = 136 kg/m^3

It is emphasized that the jet exit diameter is a critical part of this analysis because the *square* of the diameter will control the volume flow for a given pressure drop. This is further confounded by the recognition that the physical hole is likely to be distorted since it was formed during the pipe bending. The effective diameter used above is consistent with image analysis. As seen later, a range of jet diameters is considered to bound this flow.

Theoretical Analysis of Riser Kink Jet J1

This jet is assumed to behave as a classical axisymmetric momentum-dominated turbulent jet. These types of jets generally behave very predictably with regard to mass entrainment, jet spreading, velocity profiles, and the like. For a given measurement of velocity at a location on the periphery of the jet, two things need to be known in order to make a reasonable estimate of the total oil flow rate: the amount of oil in the combined oil + gas + water jet at that location, and the jet velocity profile. These are addressed separately below.

For both of these analyses, the geometry and conditions assumed at the exit of the jet are:

- The jet exit is a circular hole, d_0 = 0.75" ± 0.25" in diameter, based on image analysis.
- The ratio of the volume of oil to the volume of oil + gas at the jet exit, $X_{o,exit}$ = 0.4, based on BP's measurement of the gas/oil ratio from captured samples. This gives a nominal density of combined oil + gas exiting the jet, $\underline{\rho_{exit}}$ = 357.2 kg/m^3

It is emphasized that the jet exit diameter is a critical part of this analysis because the *square* of the diameter will control the volume flow for a given pressure drop. This is further confounded by the recognition that the physical hole is likely to be distorted since it was formed during the pipe bending. The effective diameter used above is consistent with image analysis. As seen later, a range of jet diameters is considered to bound this flow.

Water Entrainment Scaling: The spreading of the oil/gas jet as it exits the hole in the riser kink is due in large part to entrainment of water into the jet. The theory used here does not account for the immiscible nature of the fluids; this would need to be included in a more detailed analysis. For momentum-dominated jets, this entrainment follows well-studied scaling laws that depend on the fluid density difference and distance downstream from the jet exit. Near to the exit of the jet, entrainment is nonlinear until the flow achieves self-similar scaling, after which mass entrainment is linear with downstream distance. The near-field region for an orifice can be characterized as the region less than 15 jet exit diameters downstream ($x/d_0 < 15$), while for other, better studied geometries such as the long pipe, this region can extend to 30 or more exit diameters from the jet exit (Nathan et al, 2006). Since velocity measurements were not made in this region, we will assume a constant mass entrainment, $C_{e,15}$, up to this location, $x/d_0 = 15$. The mass flow rate of entrained water, m_{water}, as a function of the mass flow rate of the jet exit fluid, m_{exit}, is expressed as:

$$m_{water} / m_{exit} = C_{e,15}(\rho_{water}/\rho_{exit})^{1/2}$$

Values for $C_{e,15}$ are taken from the literature. The ideal situation of a jet issuing from a sharp-edged orifice in a flat plate cannot be found in the literature, however, Hill (1972) found $C_{e,15} = 4$ for a contoured nozzle in a flat plate, while Mi et al (2007) found $C_{e,15} = 3.4$ for a sharp-edged orifice in a small plate ($d_0/d_{plate} = 0.38$). Using the best available data, we will assume an average value of $C_{e,15} = 3.7 \pm 0.3$. Based on these numbers, the mass of jet fluid (oil + gas) 15 jet diameters downstream of the jet exit is only 14.5% of the total jet mass, the rest is water.

In the far-field, beyond $x/d_0 = 15$, the local mass entrainment rate is proportional to distance per:

$$dm_{water}/dx = C_{el} * m_{exit}/d_0 * (\rho_{water}/\rho_{exit})^{1/2}$$

where C_{el} is the local entrainment rate, chosen to be $C_{el} = 0.32$ after Ricou and Spalding (1961) and Hill (1972), who both measured entrainment in a contoured nozzle from a flat plate. This value is consistent with the results of Mi et al (2007) and several others as well, and carries little uncertainty. Integrating this equation from $x/d_0 = 15$ on downstream and adding the effect of near field entrainment yields:

$$\frac{m_{water}}{m_{exit}} = \left(\frac{\rho_{water}}{\rho_{exit}}\right)^{1/2}\left[C_{e,15} + C_{el}\left(\frac{x}{d_0} - 15\right)\right]$$

Converting this to a volumetric basis and accounting for the ratio of oil to gas in the jet exit yields the following equation for the volume fraction of oil in the jet at a downstream location $x/d_0 > 15$ of:

$$X_{oil,jet}(x) = \frac{V_{oil}}{V_{oil} + V_{gas} + V_{water}} = \frac{X_{oil,exit}}{1 + \left(\frac{\rho_{exit}}{\rho_{water}}\right)^{1/2}\left[C_{e,15} + C_{el}\left(\frac{x}{d_0} - 15\right)\right]}$$

Using this equation, the oil volume fraction at the location of the FTV measurements above ($x = 0.6$ m) is just 6.4%, the gas volume fraction is 9.5%, and the remaining 84% is entrained water. As this analysis shows, lack of proper accounting for water entrainment can lead to an order of magnitude error in the estimate of the oil leak rate based on PIV measurements at a particular downstream location.

Velocity Profile Scaling: In momentum-dominated jets, the far-field ($x/d_0 > 15$, for our purposes) axial jet velocity profile, $U(r)$, is known to follow a Gaussian profile:

$$U(r) = U_{cl} e^{-(r/\delta)^2 ln(2)}$$

where U_{cl} is the centerline velocity, r is the radial distance from the centerline, and δ is the half-width of the jet, defined to be the location where the centerline velocity falls to half its value. The jet half width increases linearly with x in the far-field, so the jet spreading rate is typically measured as δ/x as a constant. Incorporating this jet spreading rate, the jet centerline velocity can be estimated from a velocity measurement, U_{PIV}, at a radial location, R, and a downstream axial location, X, as:

$$U_{cl} = U_{PIV} e^{(R/X)^2 (x/\delta)^2 ln(2)}$$

The velocity measurement occurs at the outer edge of the jet. The velocity profile in the interior of the jet can be accounted for with the expression for $U(r)$ above, and the total volumetric flow in the interior of the jet, Q_{jet}, can be determined by integrating that expression from the centerline to the radial point of measurement, R. Utilizing the expression for U_{cl} above, this integration yields:

This value is very sensitive to uncertainties in the values for R and X, as determined from the feature tracking measurements described in the previous section, and in particular to δ/x, which must be determined from the literature. Most values for δ/x in the literature are for jets from long pipes or contracting nozzles, though jet spreading rates from these configurations can vary significantly from those in sharp-edges orifices (Mi et al., 2001). Common values of jet spreading rate for contracting nozzles range from $\delta/x \approx 0.096$ (Quinn, 2006) to 0.113 (Richards and Pitts, 1993). For sharp-edged orifices, this rate ranges from $\delta/x \approx 0.098$ (Quinn, 2006) to 0.182 (Mi et al, 2001). Most of these values are for jets that do not issue from a flat wall, but rather the open atmosphere, where spreading rates can be 20% higher than for jets issuing from a wall (Abdel-Rahman et al, 1997). These values are independent of the density differences across the jet. As a conservative estimate, the value of 0.182 is chosen for these analyses, though from the above references it should be noted that very significant uncertainty is attached to this number. In particular, lower spreading rates can yield large and often unphysical jet centerline velocities, depending on the values used for X and R. Further investigation into the proper jet spreading rate is warranted in continued analysis of this problem, and may also turn out to be affected by the immiscibility of the two fluids.

The volume flow rate of oil out of the kink jet, based on a measurement of total average velocity at a particular jet location, can be made by multiplying the above expressions for Q_{jet} and $X_{oil,jet}$ together. In this manner, multiple estimates of the jet leak rate can be made from the plethora of averaged velocity measurements and locations attained, and statistics of probable maximum and minimum flow rates can be made. Uncertainties in d_o, $X_{o,exit}$, and the above constants from the literature should also be taken into account while calculating these estimated leak rates from the kink jet.

FTV measurements yield an average jet velocity of U_{PIV} = 1.7 m/s with an uncertainty of 10% at the jet periphery, a distance of X = 0.6 meters downstream of the jet exit. The average jet spread half-angle is measured to be 12.5 on the video, though this is roughly the location of the center of the turbulent vortices as they propagate downstream. The FTV measurements track the outer surfaces of these structures, which appear at a maximum spread angle of 15.5 for the largest structures. An appropriate average spread angle for these structures is taken to be 14° ± 1.5, to account for the tracking of the outer surfaces of the largest to the smallest structures in the shear layer. The peripheral FTV measurement location at an axial location of 0.6 m is therefore estimated to be at a radius of R = 0.15 ± 0.02 m. Applying these numbers to the theoretical analysis of the Riser Kink Jet J_1 yields a best estimate for the total average oil flow rate of 8,500 barrels per day of oil for the Riser Kink Jet using Turbulent Jet Theory**.**

The largest sources of uncertainty in this analysis come from the estimation of the jet exit diameter at 0.75" ± 0.25", the FTV measurement uncertainty of 10%, and the measurement uncertainty of the radius, R, at about 12%. Since this last uncertainty appears in the exponential in the above equation for Q_{jet}, the impact on this measurement on the jet velocity measurement is very large – this uncertainty alone yields a range of 6,700 to 15,000 bbl/day total oil flow rate from the jet. The remaining uncertainties combined using the sum of squares method roughly yield a 36% uncertainty, independent of the uncertainty of the R measurement location, yielding a range of 5,400 to 11,600 bbl/day leak rate. If the other jets are assumed to have a flow rate of the same amount as the main jet, J_1, (as discussed above), then the **total average oil flow rate from all Riser Kink Jets doubles to 10,800 to 23,000 bpd, for Turbulent Jet Theory, with a best estimate of 17,000 bpd**, independent of the uncertainty in R. Clearly this technique will require substantial refinement and reduction of uncertainties if another estimate of the kink jet flow rates is required. However, having accounted for water entrainment and the jet velocity profile, uncertainties in this measurement technique should be smaller than those that do not include these effects.

These estimates are very sensitive to the assumptions used in the analysis approach as well as the precision of evaluating the edge-velocity from the FTV measurement. As an independent check on the analysis, a much simpler calculation was made based on a knowledge of the pressure in the riser kink versus the ambient sea pressure. This approach uses the orifice equation that is found in handbooks such as Marks Standard Handbook for Mechanical Engineering, Eighth Ed. (1978) McGraw Hill, pp 61-64:

$$\text{Volume flow} = K^*\text{Area}^* (2^*\Delta P/\rho)^{1/2}$$

The flow coefficient K is estimated here as 0.6, which is typical of an orifice. The pressure drop is taken from information provided to the analysis team and is 400 psi between the interior of the riser and the sea environment. Assuming the same properties for density as used above, the calculated flow for the range of jet diameters (0.75+/- 0.25 inches) is:

0.5 inch	0.75 inch	1 inch
1940 bbl/day	4360 bbl/day	7760 bbl/day

This analysis suggests the estimates from the FTV and jet profile are substantially larger than an orifice flow prediction. This discrepancy may arise from the range of uncertain parameters that exist in the jet analysis and FTV measurement. Notably, the FTV measures come from a range of observed velocities that are statistically averaged, to provide an edge velocity. This process can lead to an *overestimation* of the flow. This is because the actual velocity profile may take on a shape that is not Gaussian, resulting in a lower flow rate than predicted from the FTV measurement and jet analysis. Thus, the FTV and jet analysis should be viewed as a *maximum* flow estimate from the J1 Riser Kinks, subject to the assumptions already presented. Likewise, the flows from the other jets in the kink area have not been analyzed due to their position, but appear to have similar orders of magnitude.

Theoretical Analysis of the Riser End Jet

Analysis of this jet involves buoyant jet flow from an inclined pipe similar to Peters and Gottgens (1991). They attained a set of differential equations for the jet trajectory in the presence of no ambient flow, which was analytically solved by Gore and Jian (1993) to yield an explicit jet trajectory. An attempt was made to match these theoretical studies to experimental observations of hydrogen and helium leaks into air by Kim et al (2009), with reasonable success. The basic geometry and nomenclature for the situation under study is shown in Figure 16, taken from Kim et al (2009):

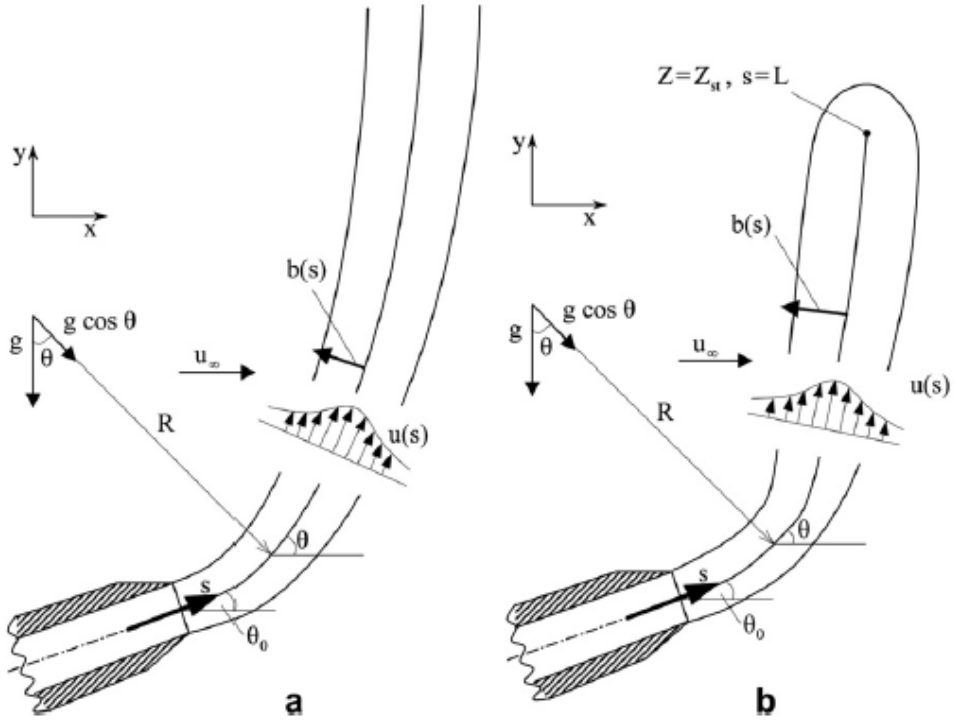

Figure 16: Schematic geometry and nomenclature used in the analysis of the Riser End Jet (from Kim et al, 2009).

In this analysis, s is the curvilinear coordinate of the jet centerline, b is roughly the jet half-width, and θ is the jet angle relative to the horizontal. The jet angle can be expressed as:

$$\tan\theta = \tan\theta_0 + \frac{1}{\sqrt{\rho_0/\rho_\infty}\cos\theta_0 Fr^*}\left[\left(\frac{s}{d}\right) + 2\beta\left(\frac{s}{d}\right)^2 + \frac{4}{3}\beta^2\left(\frac{s}{d}\right)^3\right]$$

where θ_0 is the initial jet angle relative to the horizontal, ρ_0 is the jet exit density, here assumed to be entirely oil ($\rho_0 = \rho_{oil}$), ρ_∞ is the ambient density, here equal to water ($\rho_\infty = \rho_{water}$), and d is the jet exit diameter. Photos of the end of the riser jet were provided by BP after the riser section was cut off. An estimated cross-sectional area of the riser exit can be attained from these photos, and a corresponding circular diameter of d = 0.35 m was used for this analysis. The term Fr^* is a modified Froude number:

$$Fr^* = \frac{u_0^2}{gd}\sqrt{\rho_0/\rho_\infty}\,\frac{\rho_\infty}{\alpha(\rho_\infty - \rho_{st})}$$

where u_0 is the bulk jet exit velocity, g is the gravitational constant, α is a fitting parameter, assumed by Peters and Gottgens to be equal to unity (α = 1), and ρ_{st} is a mixed density downstream from the jet exit at a location where the jet fluid and ambient fluid have mixed in stoichiometric proportions. One of the difficulties with this analysis is the fact that ρ_{st} has no meaning in an unreacting flow problem such as ours. In our analyses, we have chosen $\rho_{st} = \rho_{oil}$ as a reasonable approximation. Also, in the above equation, β is a jet spreading parameter such that $b = \beta s + d/2$ (Gore and Jian, 1993). This was determined in the original analyses to be $\beta = C_\beta(\rho_{st}/\rho_\infty)^{1/2}$, with a calculated value for the constant C_β = 0.23. Substitution of ρ_{st} for ρ_{oil} in this expression yields very good agreement with the observed jet spreading rate, however, the half-width b is roughly half of the centerline velocity, and not necessarily that at the edge of the jet as seen in the videos. Peters and Gottgens note that a more accepted value for the half-width of a constant-density jet is β = 0.085, though other appropriate values for the half-width could be used as well. We will conservatively choose C_β = 0.104 to yield β = 0.085 in this analysis, though larger values of C_β will certainly result in higher oil leak flow rates. This value of C_β is comparable to jet spreading rates of other studies (Richards and Pitts, 1993), and should be better representative of low velocity mixing in immiscible fluids, compared to the value C_β = 0.23. Given more time, a detailed analysis of experimental and CFD velocity profiles can be performed to significantly reduce the uncertainty attached to this value. A change in the value of C_β by 20% alters the estimation of the leak rate by only about 5% however, which is the conservative estimate of the flow rate uncertainty we'll attach to the uncertainty in C_β.

Another uncertainty in this analysis lies in the value of α = 1, where α is used to approximate the following integral (Peters and Gottgens, 1991):

$$2\int_0^\infty (\rho_\infty - \bar{\rho})r\,dr = b^2\alpha\,(\rho_\infty - \rho_{st})$$

where $\bar{\rho}$ is the time averaged density. Replacing ρ_{st} with ρ_{oil} in this equation yields α = 1 if the integral is evaluated at the jet exit, however, as $\bar{\rho}$ increases towards ρ_∞ with increasing downstream distance s and jet width b, it is expected that α would decrease under the substitution

of ρ_{st} for ρ_{oil}. As a result, the jet scaling above is expected to deteriorate at appreciable distances downstream from the jet exit. The current analysis is undertaken with a value of $\alpha = 1$, however, comparison with the riser jet profile and trajectory is weighted towards the near-field region closer to the jet exit, where this relationship is still valid. Improvement in the model could be made with more accurate fits for α to experimental or CFD modeling data, however, time constraints have excluded the possibility of this analysis at this time.

Application of the above analysis to the Riser End Jet involves making an estimate of the jet exit velocity, u_0, computing the modified Froude number using the above equation, and then computing the angle θ as a function of the curvilinear coordinate, s. This relationship can then be mapped to standard horizontal and vertical coordinates, and the resulting centerline trajectory can be compared against the actual jet trajectory from the BP videos. Additionally, the upper and lower jet boundaries can be calculated from the relationship $b = \beta s + d/2$ above, using $C_\beta = 0.23$, which can also be compared to the videos. Adjustments to the initial jet angle and jet velocity are performed iteratively to attain a good match to the observed jet profile.

Figure 17a below shows the result for an initial jet angle of $\theta_0 = 12°$ and a bulk jet exit velocity of 3.3 m/s, where, as noted above, the best fit is made to the initial portion of the jet, up to roughly 5 jet diameters downstream of the exit. The computed jet boundaries match the observed boundaries very well, and the resulting exit velocity yields a total flow rate of 172,000 barrels of oil per day with only oil flowing out of the riser. Multiplied by the intermittency factor of 0.4 to account for periodic gas flow, the estimated oil flow rate is 69,000 barrels of oil per day. Also shown in Figure 17b is a result using the image employed in the CFD analysis below.

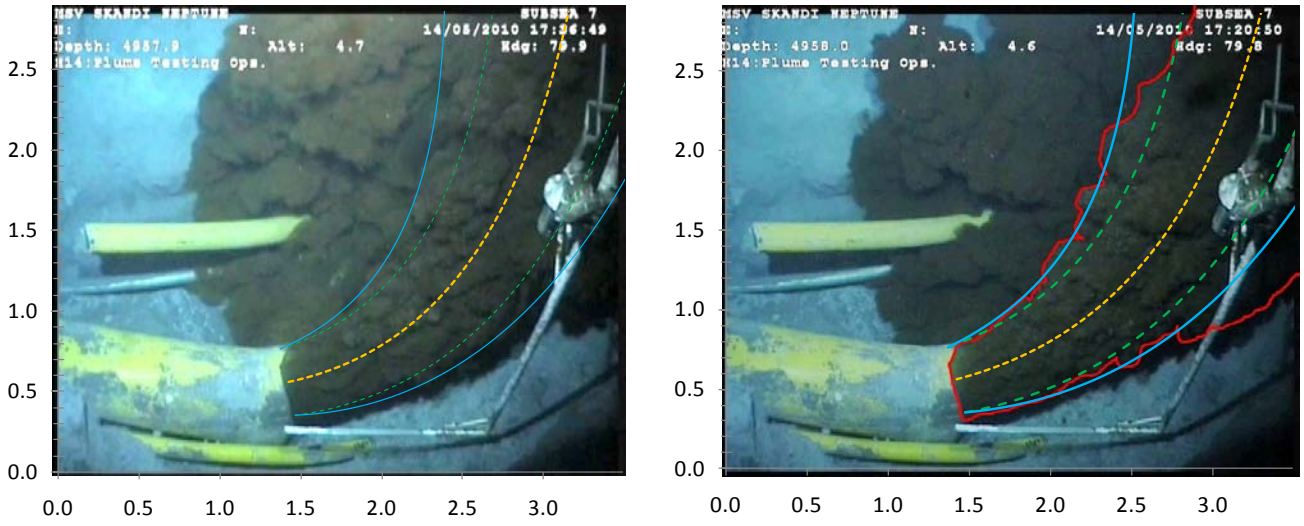

Figures 17a and 17b: Jet centerline, half width, and edge profiles predicted by theoretical analysis are shown as yellow, green, and blue lines, respectively. Notice that the jet is casting a shadow on the ocean floor, so the bottom edge of the jet is slightly above the bottom edge of the dark area.

The primary assumptions made in this analysis are:

- Only oil is flowing out of the riser in the analyzed videos.
- The pipe exit is a circular hole of 13.78 in diameter.
- There is no ambient flow of water in the immediate vicinity of the jet.
- The jet is unaffected by its proximity to the walls or floor of the trench in which it lies.
- The camera angle of the videos with respect to the horizontal is small.
- The analysis applies to immiscible fluids.
- The videos analyzed are representative of the average "oil-only" flow conditions exiting the pipe.
- And, as above, the fitting relationship $\alpha = 1$ applies in the near-field region of the jet.

As such, the fitting of the analytical relationships for the jet trajectory and boundaries is still somewhat subjective. Analysis of a range of u_0 and θ_0 that could be considered to produce an acceptable fit on a particular image yield an uncertainty estimate of ±25%. Further, it should be noted that "oil-only" riser flows can be observed to vary in flow rate in the videos. An accurate estimate of the true average flow rate can only be done by analyzing many jet plume images spanning several days and averaging their results, which is currently prohibitive given the time intensive nature of the task. In addition a true estimate of oil flow rates will require analysis of *all* of the video footage that has been recorded, beyond what limited footage has been supplied to date by BP. That said, we have averaged the estimated flow rates from the 6 video images we have analyzed to yield a best estimate oil leak rate of 72,000 bbl/day, and applied the standard deviation of 12% as the uncertainty on this average representing the true temporal average of the flow rates. Combined uncertainties were determined by the sum of the squares of the individual component uncertainties, including those for C_β (5%), the trajectory matching methodology (25%), the "time" averaging of the image results (12%). As such, the analysis conducted with the approach outlined above suggests that **the total time averaged oil flow rate is in the range of 51,000 to 93,000 bbl/day of oil for the Riser End Jet using Turbulent Jet Theory**.

Combined Total Average Oil Leak Rate

Combining the Approach 2 estimates for oil leak rate before the riser was cut, from the Riser Kink Jets and the Riser End Jet, yields a **best estimate total oil flow rate of 89,000 bbl/day, with a range of 62,000 to 116,000 bbl/day of oil using Turbulent Jet Theory.**

Analysis Approach 3: Computational Fluid Dynamics Simulations of the Riser End Leak Jet

The objective of the third analysis approach was to use Computational Fluid Dynamics (CFD) to estimate the total flow rate of oil being discharged from the Riser End Jet. The approach taken is to estimate an oil flow rate from the Riser End Jet by comparing the size, shape and trajectory of the simulated oil plume with the size, shape and trajectory of the oil jets seen in videos provided by BP of the Riser End Jet.

For this study, the Volume of Fluid (VOF) multiphase model, available in the commercial CFD software ANSYS FLUENT was selected. The VOF multiphase model has been widely used to model the flow of immiscible fluids, including those encountered in oil and gas industry (http://www.fluent.com/solutions/articles/ja127.pdf). Although the oil leak jets at the BP Horizon well site discharge both oil and gas into sea water, the Plume Modeling Team found the flow from the Riser End Jet alternated between all oil and all gas. The intermittency (fraction of time only oil flowed) was determined by the plume team to be 0.4. That is, 40% of time mostly oil is being discharged. Based on this observation by the Plume Modeling Team, the multiphase CFD simulations were only performed for two phases: oil and sea water. The oil plume simulated with CFD was visually compared to the oil plume seen in BP videos when only oil was being discharged from the Riser End Jet. The oil flow rate from the Riser End Jet was estimated by varying oil flow rate in the CFD simulations until the simulated oil plume profile was similar to the actual oil plume profile seen in BP videos. This oil flow rate was multiplied by the intermittency factor of 0.4 to yield the actual spill flow rate at the sea floor. Oil is known to expand in volume by 35% from the sea floor to the sea surface, so the oil flow rate at the sea floor was then multiplied by the oil expansion factor, 1.35, to yield oil flow rate at the sea surface in barrels per day.

The simulation considered the flow of oil through the riser and of the oil plume through sea water at the pressure and temperature conditions encountered in a region around the Riser End Jet. The compressibility of oil and sea water was assumed to be negligible because only a small region surrounding the riser jet was considered in the simulations. The Realizable K-ε turbulence model, with standard wall function was used to model the effect of turbulence. The default model constants for the Realizable K-ε turbulence model in FLUENT were used in this study. The value of y^+ (from wall to cell center) inside the riser pipe varied from 400 to 500. A wall function was used for the riser-wall boundary condition. A second order discretization scheme was used for the solution of momentum, energy, turbulence kinetic energy and turbulence dissipation transport equations. The Geo-Reconstruct scheme was used for the solution of volume fraction equation. The inlet boundary was selected to be a mass inlet, with oil flow rate being specified with a uniform inlet velocity profile. The simulations were conducted for different values of the oil flow rate. Since no information was available on the turbulence characteristic of oil flow inside the riser pipe, the default turbulence intensity of 10% was selected in FLUENT. The outlet boundary condition was set to a pressure outlet with the mixture gauge pressure set to zero. The sea floor was modeled as a no-slip wall. The symmetry boundary condition was selected for the four surrounding planes in the computational domain.

Figure 18 shows the computational domain used for the initial study. Oil flows through the last 8.382 m of the riser and discharges into a 16.76 m by 8.98 m by 17.77 m volume filled with sea water. Since the orientation of the broken riser with respect to the sea floor is not easily measured from the videos provided by BP (because the ROV's are floating at an unmeasured orientation), in the simulation, it is assumed that the broken riser lies parallel to the sea floor at a distance of 18 inches above the sea floor. Since the exact dimensions of the riser exit was not known, the exit was modeled as a sudden contraction from 19.5" to 13.78" as seen in Figure 19. At initialization, flow outside of riser pipe is set to be sea water and flow inside the riser pipe is set to be oil.

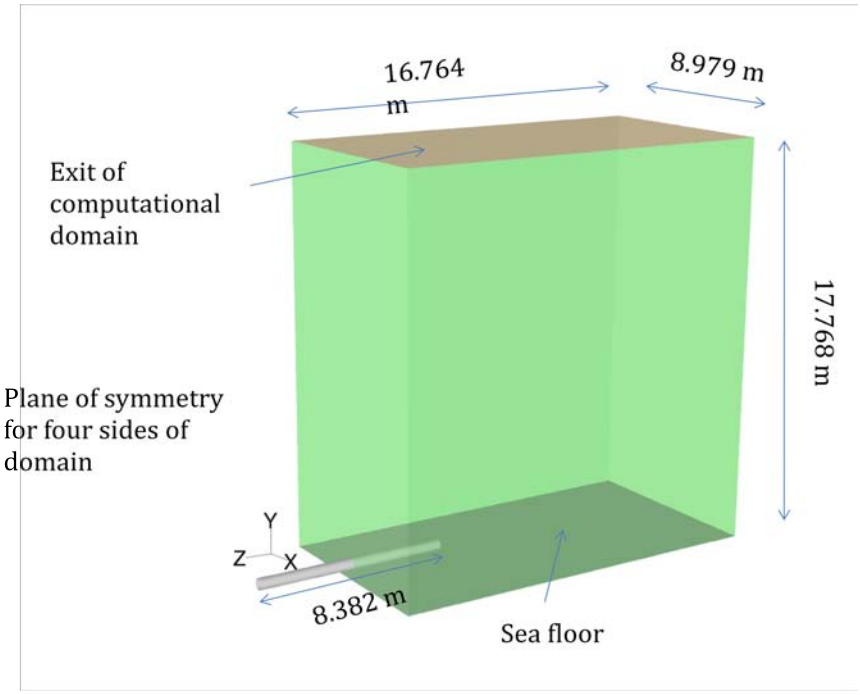

Figure 18: Dimensions of the computational domain.

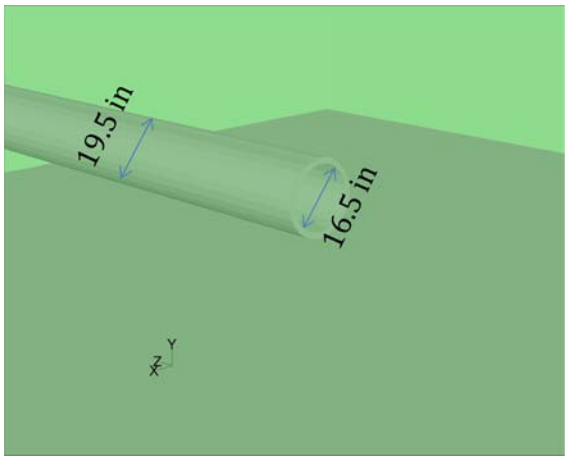

Figure 19: A close-up view of the exit plane of the broken riser.

The entire domain is at the temperature and pressure measured at a depth of 5000 ft in sea water. The input conditions to the model are:

Riser inner diameter = 19.5 in Riser diameter at exit = 13.78 in Ambient pressure = 2248 psi Sea water density = 1028 kg/m^3 Sea water temperature = 4 ^{o}C Sea water viscosity = 1.88E-03 Pa	Oil temperature = 110 ^{o}F Oil density = 688.8 kg/m^3 Oil viscosity = 0.00053 Pa-s Oil surface tension = 0.0167 N/m

The oil viscosity used in the simulations was that estimated at the well bottom hole, based on BP measurements. Due to the long horizontal distance (>200 meters) between the Riser Kink Jets and the Riser End Jet, the Plume Team assumes that all dissolved methane is released from the oil by the time it reaches the Riser End Jet. This produces a slug flow regime and the alternate oil/gas flow seen from the Riser End Jet. As a result, the viscosity of the liquid oil increases by about a factor of two. This should not significantly affect these preliminary CFD calculations.

In this CFD study, care must be taken to ensure the solution is not dependent on the grid size and the size of the domain chosen, especially the placement of the symmetry plane in front of the riser exit. Given the time frame available to perform the simulations, it was not possible to conduct a complete, comprehensive study to evaluate the effects of computational grid size and domain. Nevertheless, the approach outlined below was employed to ensure that the results are independent of the grid and domain size.

First, a computational domain consisting of 417,476 hexahedra mesh was chosen. The riser pipe is situated in the computational domain such that the upstream symmetry plane and the two side symmetry planes were at a distance of L/D=11 from the point of discharge. The downstream symmetry plane was located at a distance of L/D= 32 from the point of discharge.

Figure 20 illustrates the oil plume penetration into sea water at an oil flow rate of 100,000 bpd. It is evident from Figure 20 that a considerable portion of the computational domain is not affected by the oil plume. To optimize the mesh, a second simulation for an oil flow rate of 100,000 bpd was conducted with the symmetry plane upstream of the oil leak set right at the plane of riser exit, Figure 21. This reduced the number of computational cells in Figure 21 to 300,820 hexahedra mesh. A comparison of Figures 20 and 21 indicates that the location of the symmetry plane upstream of the oil plume does not affect streamwise penetration and lift of the plume. So the computational domain size in the second simulation was taken as adequate.

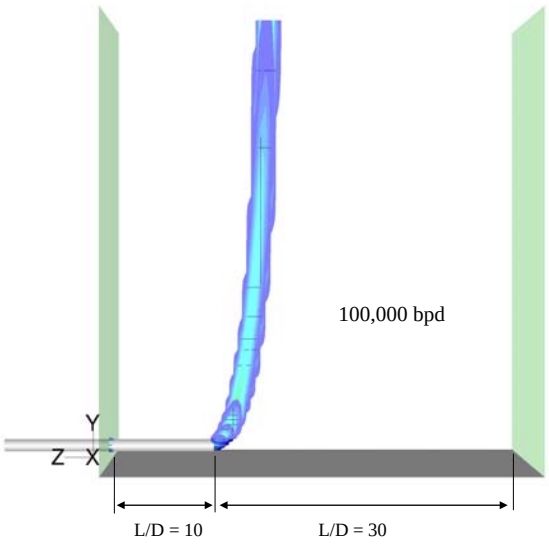

Figure 20: Oil plume released into sea water at a flow rate of 100,000 bpd.

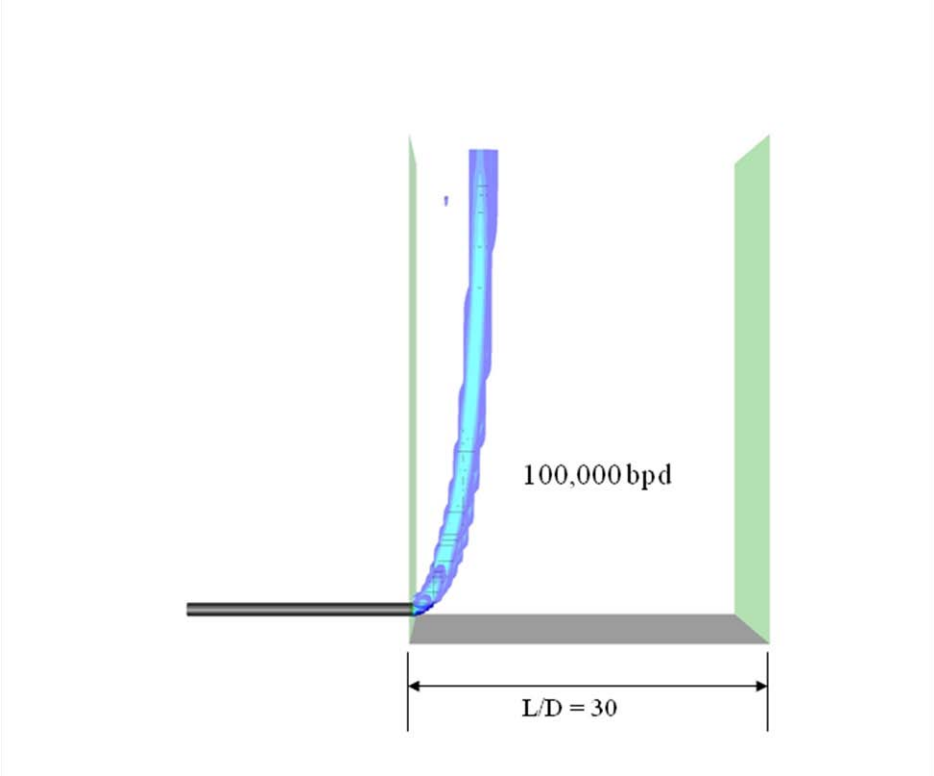

Figure 21: Oil plume released into sea water at a flow rate of 100,000 bpd.

Based on the findings described above, a new mesh was generated based on the computational domain shown in Figure 22. The domain in Figure 22 contains 902,464 hexahedra mesh.

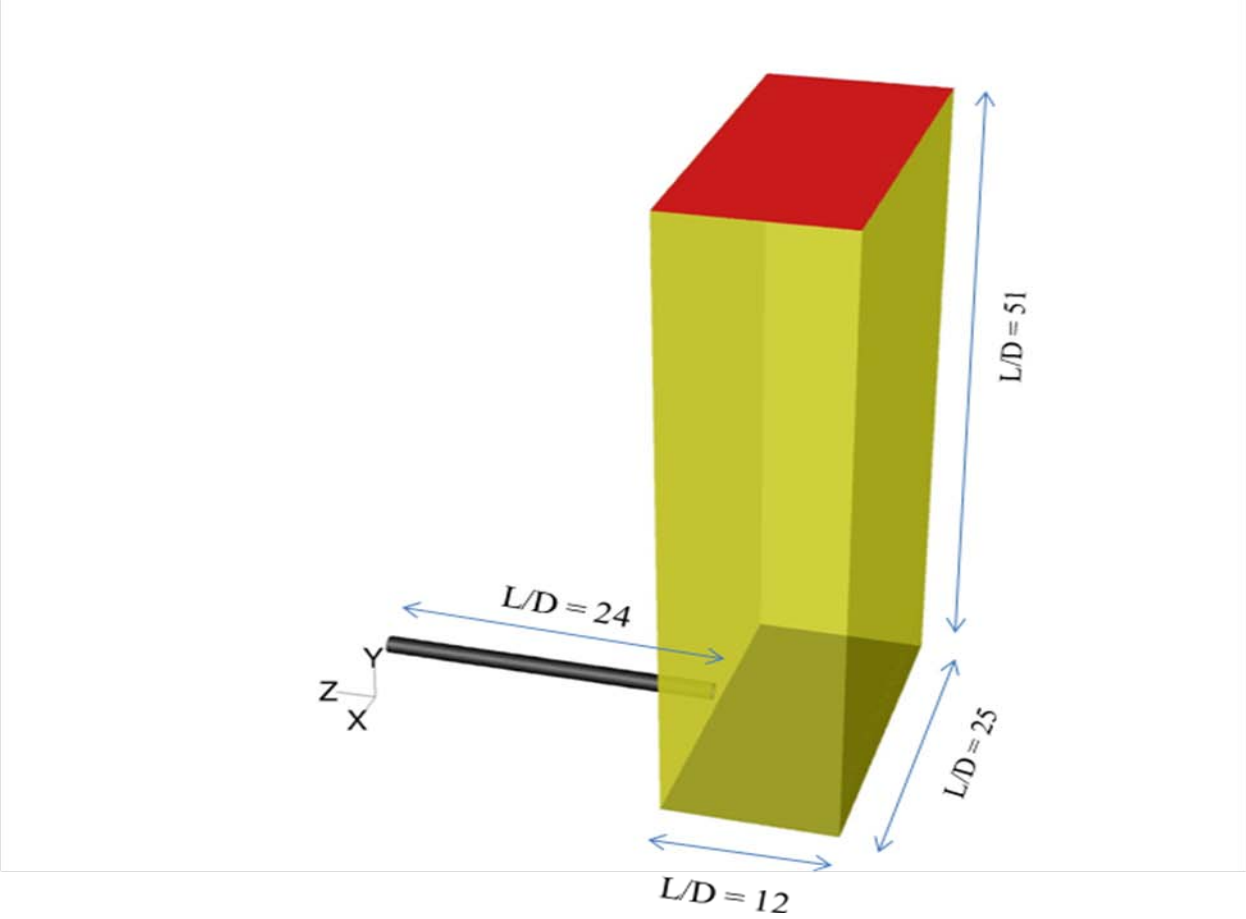

Figure 22: Dimensions of the computational domain.

A series of simulations were conducted at assumed oil flow rates of 19,000 bpd, 35,000 bpd, 100,000 bpd, and 130,000 bpd. Figures 23a-c illustrate oil flow velocity vectors at the riser exit plane. Velocity vectors indicate a predicted *inflow* of seawater into the riser pipe for flows rates of 19,000 bpd and 35,000 bpd. At a flow rate of 100,000 bpd, no seawater flow into the riser. A close inspection of the BP videos of the Riser End Jet indicates there is no flow of sea water upstream into the broken riser as the bottom boundary of the oil plume at riser exit is in contact with the riser wall. Based on this observation, it was concluded that flow rates of 19,000 bpd and 35,000 bpd of oil are not sufficient to prevent the sea water from moving upstream into the riser.

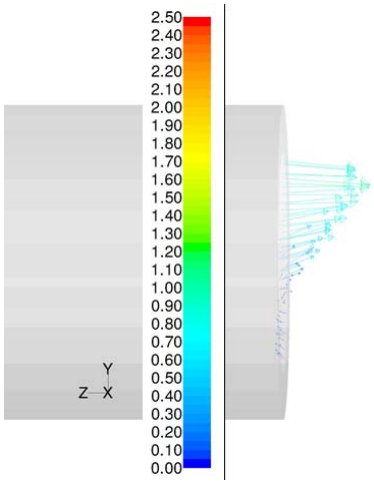

Figure 23a: Oil velocity vector at the riser exit at an oil flow rate of 19,000 bpd (before intermittency factor is applied) for riser exit diameter = 13.78 in.

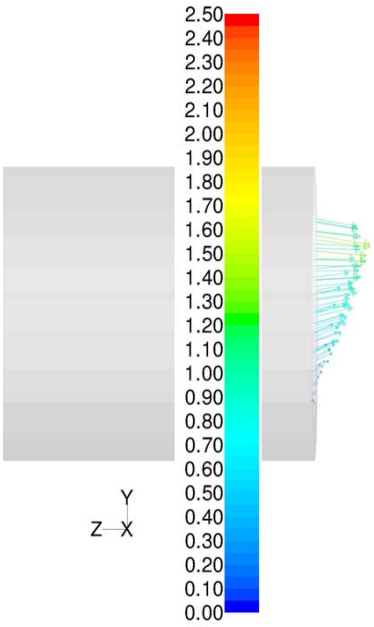

Figure 23b: Oil velocity vector at the riser exit at an oil flow rate of 35,000 bpd (before intermittency factor is applied) for riser exit diameter = 13.78 in.

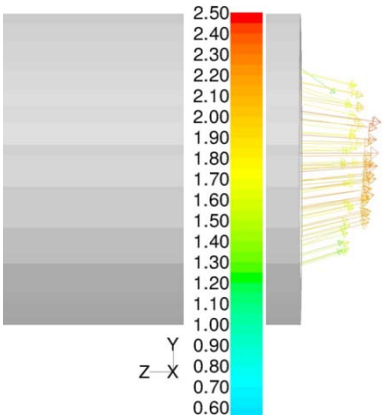

Figure 23c: Oil velocity vector at the riser exit at an oil flow rate of 100,000 bpd (before intermittency factor is applied) for riser exit diameter = 13.78 in.

Figure 24 shows the simulated plume shape and penetration at four different oil flow rates of (before intermittency factor is applied) 19,000 bpd, 35,000 bpd, 100,000 bpd and 130,000 bpd, for the restricted riser diameter of 13.78 inches. The plume shape is represented by coloring computational cells with an oil volume fraction between 0.01 and 1.0. A snap shot of the actual oil jet plume from the BP video is also shown, where the Riser End Jet plume has been isolated in the image. The oil plume shape and penetration at assumed flow rates between 100,000 bpd to 130,000 bpd (before the intermittency factor is applied) agree favorably with the actual oil plume shape and penetration seen in the BP video snap shot.

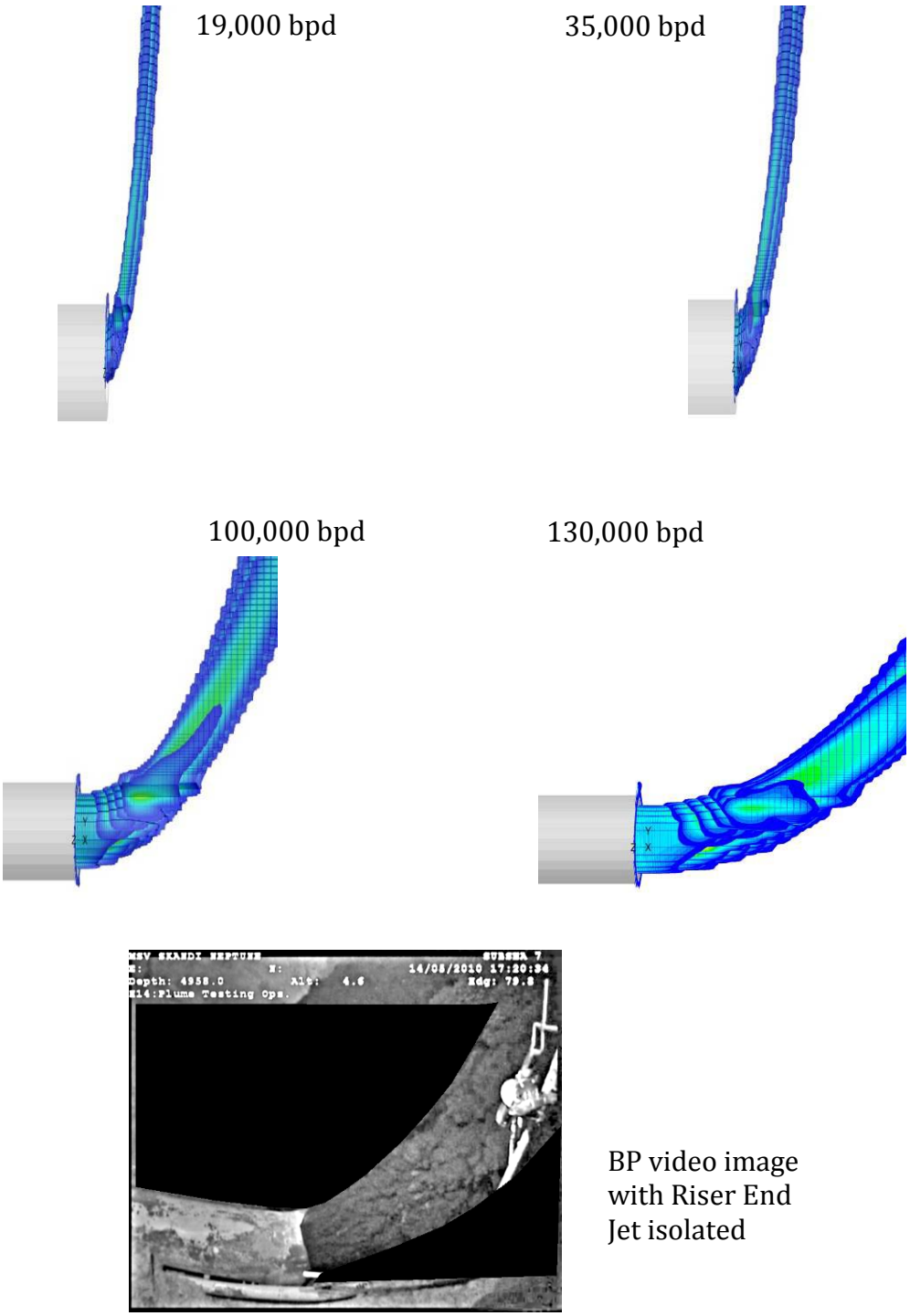

BP video image with Riser End Jet isolated

Figure 24: Simulated oil plume size and penetration for a restricted riser diameter of 13.78" at oil flow rates of 19,000 bpd, 35,000 bpd, 100,000 bpd and 130,000 bpd (before intermittency factor is applied).

Based on this plume shape and penetration comparison, the range of values between 100,000 bpd and 130,000 bpd was selected as the probable oil leakage range for the Riser End Jet.

As pointed out earlier, this simulation considers an oil-only flow into sea water. The intermittent change between total gas flow and total oil flow caused by the slugging behavior in the riser section was not modeled. Moreover, according to Plume Modeling Team, oil is expected to expand by about 35% moving from sea floor to the surface.

Therefore, applying an intermittency factor of 0.4 for the ratio of the time oil is flowing to the total time and factor of 1.35 for oil expansion from sea floor to sea surface, **the estimated total average oil flow rate at the Riser End Jet is between 54,000 barrels per day and 70,200 barrels per day** at standard conditions using Computational Fluid Dynamics. It should be noted that this estimate does not include the Riser Kink Jets, so this is not an estimate of the overall total oil leak rate of the BP Deepwater Horizon site.

Summary and Conclusions

The NETL has used three different analysis approaches by three different groups of researchers to produce estimates of total average oil flow rate from the BP Deepwater Horizon site. In addition to the assumptions denoted in the analysis descriptions above, the following assumptions apply to these three analyses:

- We have been provided video clips showing all oil leaks present in the system.
- The video clips provided by BP were representative of the total average flow behavior of the jets over long periods of time.
- The total period of video for which jet velocity was measured using Approach 1 was representative of the entire period covered by this analysis, which is from April 20, 2010, through July 10, 2010.
- There is no significant variability in oil leak rate over the period of analysis.

The results of these three analyses are summarized as follows:

Approach 1: Feature Tracking Velocimetry

The following oil flow rates were measured before the riser was cut:

- Riser Kink Jets Leak Rate- total average oil flow rate is 11,000 barrels per day ± 2,700 barrels per day.
- Riser End Jet Leak Rate – total average oil flow rate is 44,000 barrels per day ± 11,000 barrel per day.

Manual FTV estimates the following total average oil leak rates before and after the riser was cut:

- ***Before the riser was cut, the total average leak rate is 55,000 bpd ± 14,000 bpd.***
- ***After the riser was cut, the total average leak rate is 61,000 bpd ± 15,000 bpd.***

Approach 2: Turbulent Jet Theory

Turbulent jet theory was applied to estimate total oil leak rates only before the riser was cut. For the two leak jet areas in the riser before it was cut, the following oil leak rates are estimated:

- Riser Kink Jets: best estimate of total average oil flow rate is 17,000 with a range of 10,800 – 23,000 bpd
- Riser End Jet: best estimate of 72,000 with a range of 51,000 - 93,000 bpd

Turbulent jet theory estimates the following total average oil leak rates before the riser was cut:

- ***Combined Total Leak Rate before the riser was cut: 89,000 barrels per day, with a range of 62,000 -116,000 bpd***

Approach 3: Multiphase Computational Fluid Dynamics

CFD was applied to estimate total oil leak rate only from the Riser End Jet before the riser was cut. Oil leak rate was not estimated from the Riser Kink Jets before the riser was cut. Also, oil leak rate from the Post Riser-Cut Jet was not estimated.

> *CFD estimates the following total average oil leak rate from the Riser End Jet:*
> ***between 55,000 barrels per day and 70,200 barrels per day of oil***

Because most of the Plume Team relied on measurements of jet velocity using either automatic PIV or manual FTV, the NETL estimate using Approach 1, manual FTV, can be considered as NETL's estimate for use by the Plume Modeling Team.

It is recognized that the range of uncertainty for these analyses is large. The measurement uncertainty alone has been estimated by members of the Plume Team from NIST to be in the range of +/- 40%. Estimates for uncertainty were made for Approach 1 and Approach 2 and are reflected in the values above. Uncertainty estimates were not made for the CFD result of Approach 3.

References

Abdel-Rahman, A. A., Chakroun, W., and Al-Fahed, S. F., 1997. "LDA measurements in the turbulent round jet," *Mechanics Research Communications*, **24**:277-288.

Gore, J. P., and Jian, C. Q., 1993. "Analytical solution to the flame trajectory based on the analysis of "Scaling of buoyant turbulent jet diffusion flames" by N. Peters and J. Gottgens, *Combust. Flame*, **93**:336-337.

Hill, B. J., 1972. "Measurement of local entrainment rate in the initial region of axisymmetric turbulent air jets," *J. Fluid Mech.*, 51:773-779.

Kim, J. S., Yang, W, Kim, Y., and Won, S. H., 2009. "Behavior of buoyancy and momentum controlled hydrogen jets and flames emitted into the quiescent atmosphere," *Journal of Loss Prevention in the Process Industries*, **22**:943-949.

Mi, J., Kalt, P., Nathan, G. J., and Wong, C. Y., 2007. "PIV measurements of a turbulent jet issuing from round sharp-edged plate," *Exp. Fluids*, **42**:625-637.

Mi, J., Nathan, G. J., and Nobes, D. S., 2001. "Mixing characteristics of axisymmetric free jets from a contoured nozzle, and orifice plate and a pipe," *J. Fluids Eng.*, **123**:878-883.

Nathan, G. J., Mi., J., Alwahabi, Z. T., Newbold, G. J. R., and Nobes, D. S., 2006. "Impacts of a jet's exit flow pattern on mixing and combustion performance," *Prog. Energy Combust. Sci.*, **32**:496-538.

Peters, N., and Gottgens, J., 1991. "Scaling of buoyant turbulent jet diffusion flames," *Combust. Flame*, **85**:206-214.

Quinn, W. R., 2006. "Upstream nozzle shaping effects on near field flow in round turbulent free jets," *European Journal of Mechanics B/Fluids*, **25**:279-301.

Richards, C. D., and Pitts, W. M., 1993. "Global density effects on the self-preservation behavior of turbulent free jets," *J. Fluid Mech.*, **254**:417-435.

Ricou, F. P., and Spalding, D. B., 1961. "Measurements of entrainment by axisymmetrical turbulent jets," *J. Fluid Mech.*, 11:21-32.

Appendix 8: Flow Rate Estimation from Feature Tracking

Flow Rate Estimation from Feature Tracking on the Video of the Spill Sites based on Statistical Correlation Algorithms

Juan C. Lasheras and Juan C. del Álamo
University of California San Diego
Alberto Aliseda, Oscar Flores, and James Riley
University of Washington

Working as part of the Plume Team within the Flow Rate Technical Group

Preamble

This report is the result of the work of a team of researchers from the Universities of Washington and California, San Diego, named above. This work was performed to address the need to assess the flow rate of oil into the Gulf of Mexico from the site of the Deepwater Horizon Incident. It is based on the analysis of several hours of video that was made available to the Plume Team within the FRTG through a NOAA ftp server.

The authors got involved in this problem at the request from NOAA to attempt to estimate the flow rate of oil discharging from the broken riser of the oil well from video images taken by Remotely Operated Vehicles (ROVs). The UW-UCSD team was part of the Flow Rate Technical Group that was created under the direction of Dr. Marcia McNutt to address this critical need. The sole purpose of our study is to provide information to the National Incident Command, as requested by Dr. McNutt. This report is not intended to be used for any purpose other than that.

The circumstances that gave rise to the leak (Deepwater Horizon explosion and sinking), the depth at which the oil was leaking (5000 feet underwater at the bottom of the Gulf of Mexico, 25 miles off the coast of Louisiana) and the urgency under which this project developed made this study an incredibly difficult engineering endeavor, with no time or opportunity for the careful analysis that the authors always employ in their normal research activities. The measurement of the flow rate of a turbulent two-phase flow jet from video sequences taken at 30 frames per second presents enormous challenges. Owing the gravity of the situation, and the pressing need to have an estimated range to aid the response of the National Incident Command, the authors accepted the request from the Federal Government while recognizing the severe limitations imposed by this technique. The use of underwater video images from moving ROVs to measure velocities and estimate flow rates had never been tried before (to the best of our knowledge). This difficulty was coupled with the complex nature of the crude oil flowing through the broken riser, with a mixture of oil and gas of unknown compositions, and under constant phase changes. The urgent national need for an estimate to inform and guide the response effort needs to be taken into account to understand the conditions under which this group operated. All the work described in this report was carried out between May 13 and June 13, 2010.

The problem of estimating the flow rate of oil coming out of the riser pipe after the explosion and sinking of the Deepwater Horizon is broken into two parts. First we analyze the flow rate of crude oil discharged from two main sites before the riser pipe was cut on June 2nd. The primary discharge site was located at the open end of the riser pipe where oil and gas are coming out of a 21.5 in OD, 19.5in nominal ID pipe lying horizontally for several thousand feet on the bottom of the Gulf of Mexico (see Figure 1). The second site was located on top of the blow out preventer (BOP) were the riser pipe was bent as it fell from its vertical position, crimpled and formed several cracks through which an oil/gas mixture was observed escaping. A sketch of the overall setting, with the two areas of interest marked, is given in Figure 1. A trench was excavated around the open end of the riser area and video cameras on the ROVs conducted surveillance of the spill site. The ROVs also injected oil dispersant at the site from the time the trench was excavated to the time the riser was cut just above the Blow Out Preventer (BOP) on June 2nd. The second part of the report focuses on the estimation of the flow rate discharging after the riser pipe was cut. At that time, and until the LMRP was placed, the flow of crude oil was coming out only from a single site and the uncertainties associated with the presence of multiple leaks of unknown geometries was removed.

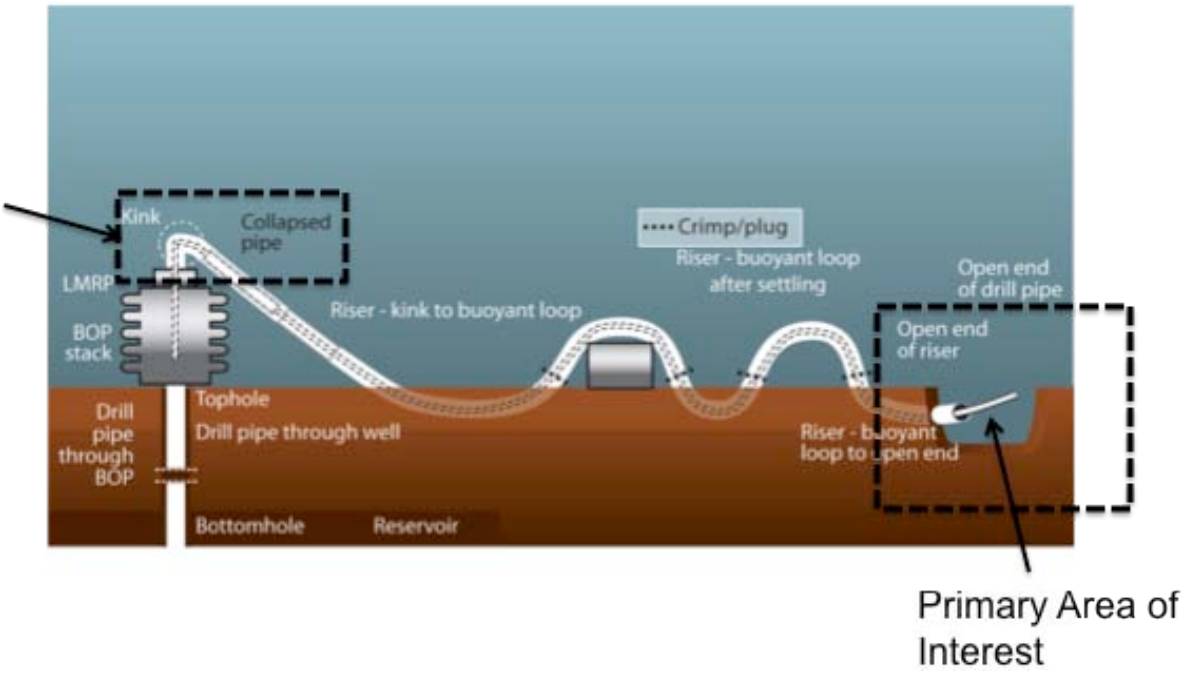

Figure 1: Sketch of the BOP and riser lying on the sea bed.

This second analysis is believed to provide a more accurate estimate of the current flow rate after the installation of the Top Hat Cap. If one assumes that the presence of the Top Hat cap on the cut riser installed later does not induce a significant change in the flow rate from the oil well (the back pressure produced by the cap is negligible compared to the hydrostatic pressure differences and the viscous losses associated with the flow from the reservoir to the cap), then the estimate of flow after the riser was cut and before the cap was installed is representative of the total flow once the cap was installed and operated (the sum of the flow going up the LMRP and the flow going out of the cap through vents and leaks between the cap and the flange it sits on).

Section 1: Estimate of the Oil Flow Rate Before the Riser Pipe was Cut on June 2nd

Before the riser pipe was cut on June 2nd, there were two leak sites: 1) a primary leak site was located at the open end of the riser pipe, and 2) second leak site was at the top of the Blow Out Preventer (BOP) where the riser pipe bent as it fell from its vertical position to the horizontal one resting on the bottom, crimpled and formed several cracks. The two subsections below estimate the oil flow rate coming out from each of these sites.

Section 1A: Estimate of the Oil Flow Rate at the Open End of Riser. Analysis of the Temporal Evolution of the Velocity and Composition.

This section analyzes the temporal evolution of the velocity and composition discharging from the open end of the riser. The results of this section are based on the analysis of three different videos:

- 5 minutes 051720101304crater.mpg of May 17th
- 30 minutes 20100514235708344@H14Ch1H264h.mov of May 14th
- 16 minutes 20100514220052312@H14Ch1H264h.mov of May 14th

These videos were found to be the more appropriate for the analysis, since they showed the end of the riser from the side, with the position of the ROV and the focus of the camera varying little in time.

General Observations: After the accident, the riser pipe sunk to the ocean floor and crude oil flowing through the riser pipe began to be discharge at its open end. Due to progressive cooling and condensation of heavy hydrocarbon fractions, the crude oil flow in the long riser pipe (> 1000 feet) resting on the sea floor segregates and formed a two-phase flow composed of a mixture of condensed hydrocarbons (oil) and gas flowing in the "slug flow" regime as shown in Figure 2.

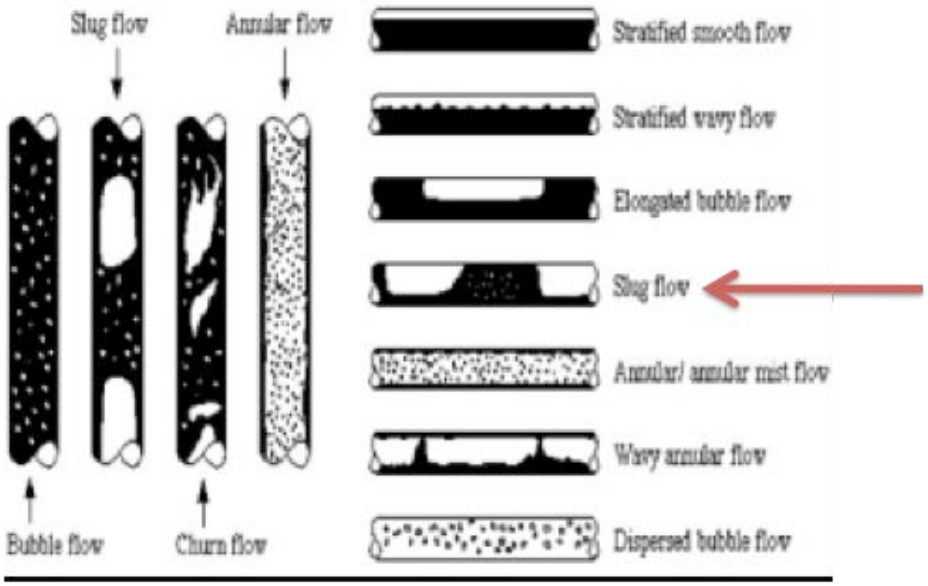

Figure 2: Different regimes for gas/oil flowing in a pipe.

As shown in Figure 3, the "slug flow regime" is characterized by the high intermittency of the flow, which shows different events including

- Events dominated by the discharge of almost pure gas. This regime is made evident not only by the sharp change in brightness, but more importantly, because the jet becomes "buoyancy-driven", showing a parabolic shape near the outlet and becoming completely vertical 3 to 4 diameters downstream (see Figure 3a).
- Events dominated by what appears to be the discharge of almost pure condensed oil. This regime is evident by the change to a mostly uniform dark color, and more importantly, because the jet is then mainly "momentum-driven" and discharges almost horizontally and has a very small parabolic curvature, consistent with smaller buoyancy effects (see Figure 3b).
- Events where a mixture of gas and oil is discharged simultaneously (see Figure 3c).

To be able to measure the oil discharged from the open end of the riser by digital image processing of these videos, it is essential to estimate with sufficient confidence the period of these events and the fraction of oil being discharged during each event.

a)

b)

c)

Figure 3: Frames from 20100514220052312@H14Ch1H264h.mov, showing the intermittency in the flow of gas and oil in the horizontal riser pipe.

Image Brightness Analysis: To characterize the temporal variability in the flow of oil and gas, a Region of Interest (ROI) that includes the pipe exit and the gas and oil plumes was chosen and digital image processing was applied on it to calculate the average image brightness for each frame of the movies that were studied. The ROI used for this analysis is shown in Figure 4. The average image brightness of each frame in a movie was normalized between 0 (minimal average intensity recorded in the movie) and 1 (maximal average intensity recorded in the movie). The normalized average image brightness is used as a surrogate for the relative concentration of gas and oil at the pipe's exit. Measuring the time variation of the normalized average brightness shows the intermittency of the gas/oil flow rate. Results from this analysis are shown in Figure 5.

Figure 4: Definition of the Region of Interest in the images from the riser pipe's exit.

In the movies we analyzed, we observed a cyclic repetition of a brightness pattern consisting of a gradual increase in the brightness level, followed by a sharp decrease. Visual observations of the frames indicate that at the peak of brightness level, the riser appears to be discharging mostly gas, while the lowest values correspond to the riser discharging what appears to be mostly oil. The time between successive ramps is approximately 3 min (see Figure 5). The standard deviation of the average brightness in the ROI shows the same 3 minute period (see Figure 6).

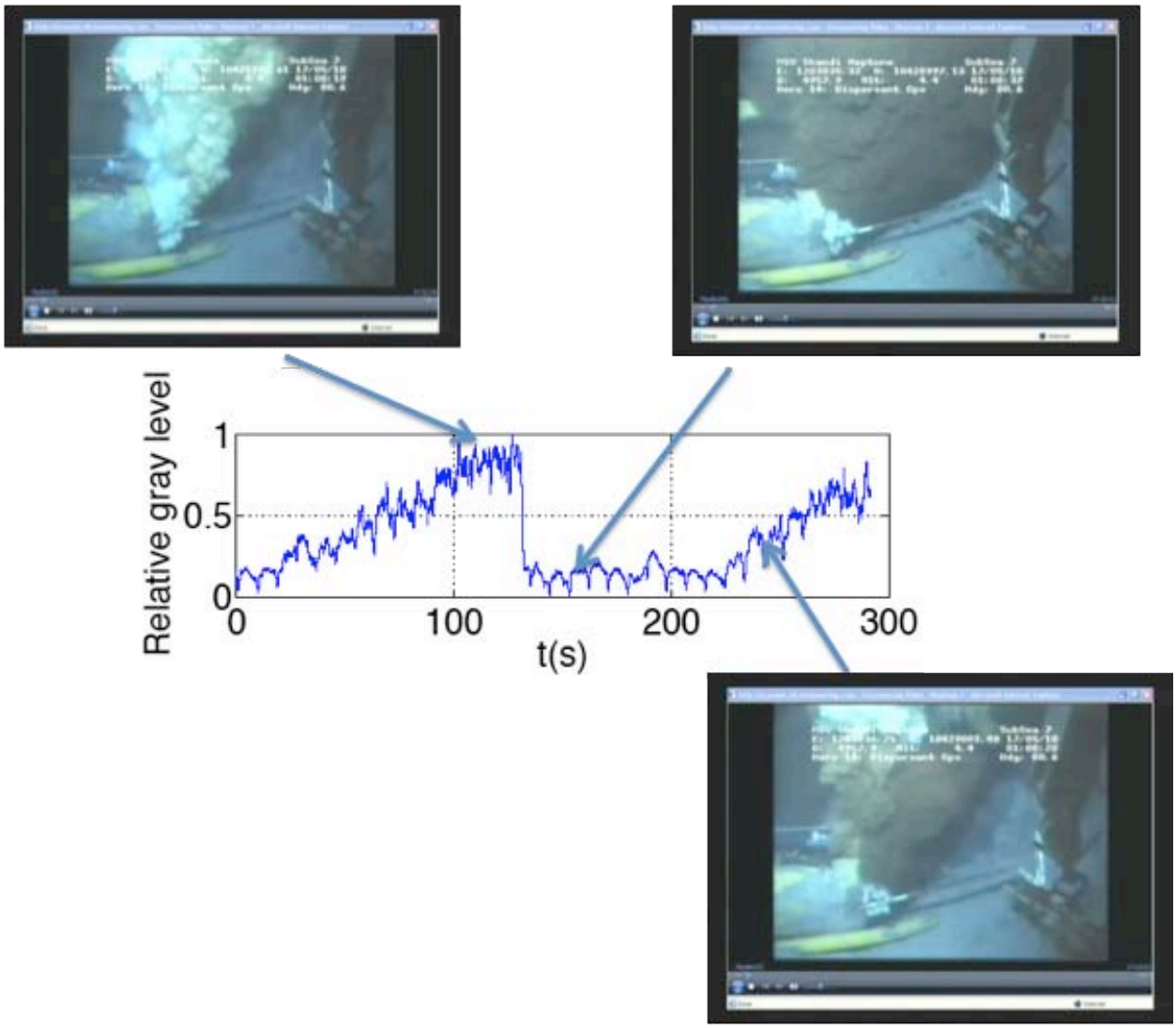

Figure 5: Time trace from 051720101304crater.mpg (5 minute clip from May 17th).

The analysis of the grey levels of two longer image sequences from May 14th (see Figure 7) confirms the "slug flow" regime found in the short 5 minute clip from May 17th. In both movies the gas slugs appear to come in pairs (uniformly spaced an average time T' approximately 70 s) and with a very well-defined time periodicity between the pairs of ≈ 200 s with a very well-defined time periodicity between the pairs of T≈ 200 s ≈ 3.3 minutes. Autocorrelation analysis of the time variation of the average brightness intensity (see Figure 8) confirms the periodic behavior of the oil/gas composition with two distinct peaks at 70s and 200s observed in Figure 7.

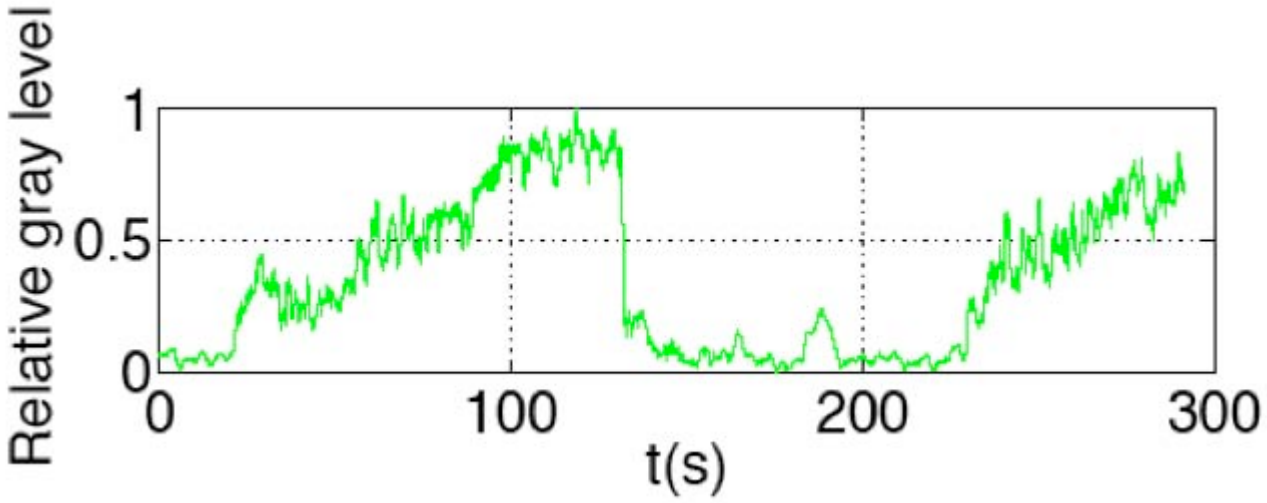

Figure 6: Standard deviation of image brightness (grey level) inside the ROI defined in image Time trace from 051720101304crater.mpg (5 minute clip from May 17th).

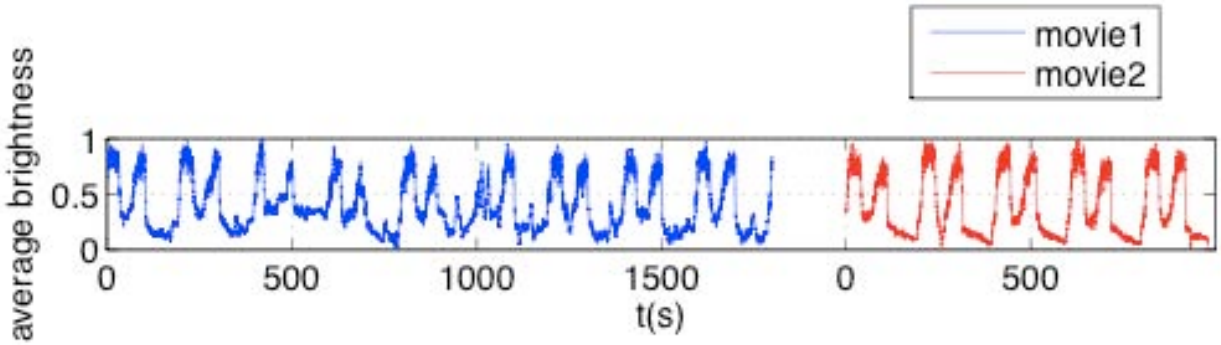

Figure 7: Temporal evolution of the average brightness in an ROI at the riser exit.

30 minutes 20100514235708344@H14_Ch1-H264h.mov of May 14th
16 minutes 20100514220052312@H14_Ch1-H264h.mov on May 14th

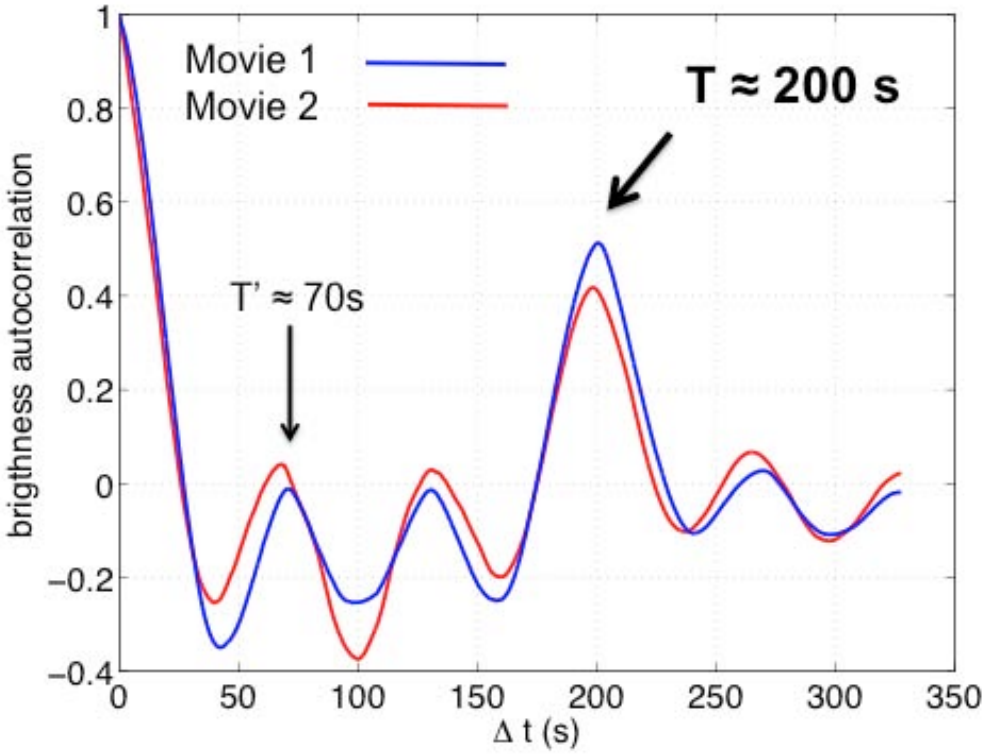

Figure 8: Temporal autocorrelation of the average brightness in an ROI at the riser exit.

30 minutes 20100514235708344@H14_Ch1-H264h.mov on May 14th
16 minutes 20100514220052312@H14_Ch1-H264h.mov on May 14th

Assuming that the concentration is directly proportional to the normalized average brightness, one can estimate the fraction of time that is occupied by gas and oil, by integration in time of the above signal:

20100514235708344@H14_Ch1-H264h.mov
GAS/OIL time fraction = 38/62

20100514220052312@H14_Ch1-H264h.mov
GAS/OIL time fraction = 40/60

Note that the above estimated gas to oil ratio from the integration of the average brightness represents an upper bound since we have assumed that there is only condensed oil being discharged when the normalized average pixel intensity in the ROI is minimum and pure gas when is maximum. This assumption is rather restrictive since one can observe in the videos that there is always a small fraction of oil flowing at the bottom of the riser pipe when the brightness is at a maximum and a similarly small amount of gas flowing at the top of the pipe when the intensity is at a minimum.

Cross Correlation Image Velocimetry (PIV): Three independent measurements have been carried out using two different PIV correlation algorithms. UCSD used segments from 20100514224719234@H14_Ch1-H264h.mov (17:47:17 -> 17:56:59). UW used 2 consecutive image sequences totaling 44:50 minutes, 20100514220052312@ H14_Ch1-H264h.mov and 20100514221717125@H14_Ch1-H264h.mov (17:00:49->17:45:39).

Figure 9 shows the geometry of the riser pipe end with the different lengths used for spatial calibration of the images and areas used to compute the flow rate.

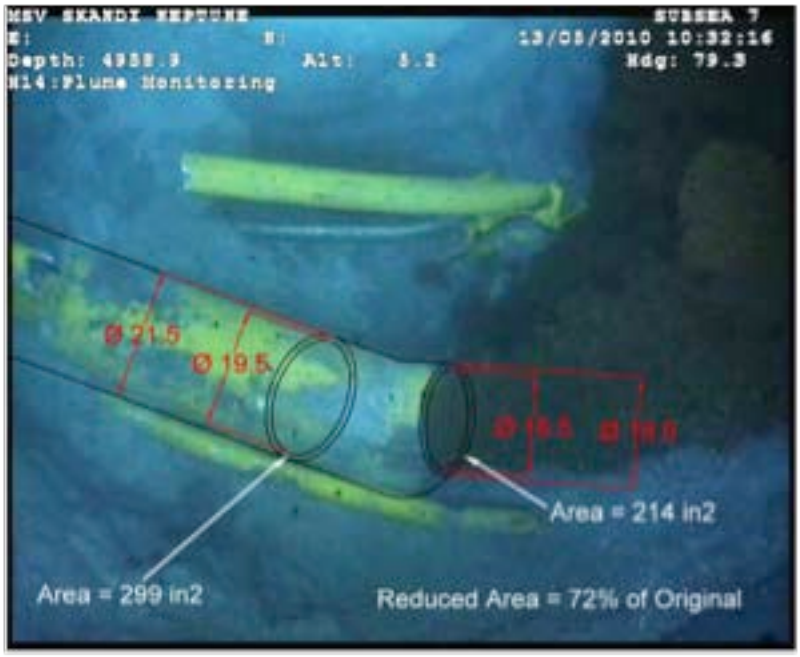

Figure 9

The result of analyzing, with an Ensemble PIV algorithm, 100 consecutive frames over 4 seconds in sequence 20100514224719234@H14_Ch1-H264h.mov is shown in Figure 10. This 4 second segment was chosen as representative of the time when the image brightness is very low associated with an outflow composed mostly of oil. Prior to processing, image brightness was inverted in all frames so that dark features in the movie were tracked as bright features by the image correlation in the PIV algorithm. In order to estimate the flow rate, it is important to measure as close as possible to the pipe exit, so that we are in the potential cone, and the horizontal velocities of the surface features can be related to the velocities at the pipe exit. However, the surface features are still not clearly visible and that prevented us from measuring immediately downstream of the exit. Thus, we masked out the first quarter diameter of the jet from the PIV algorithm. The PIV results show that one diameter downstream of the exit, the maximum horizontal velocities are of the order of 0.2 m/s. To remove operator bias, the same sequence was analyzed, using a different PIV software and operator and a different mask, yielding the same result (see Figure 11).

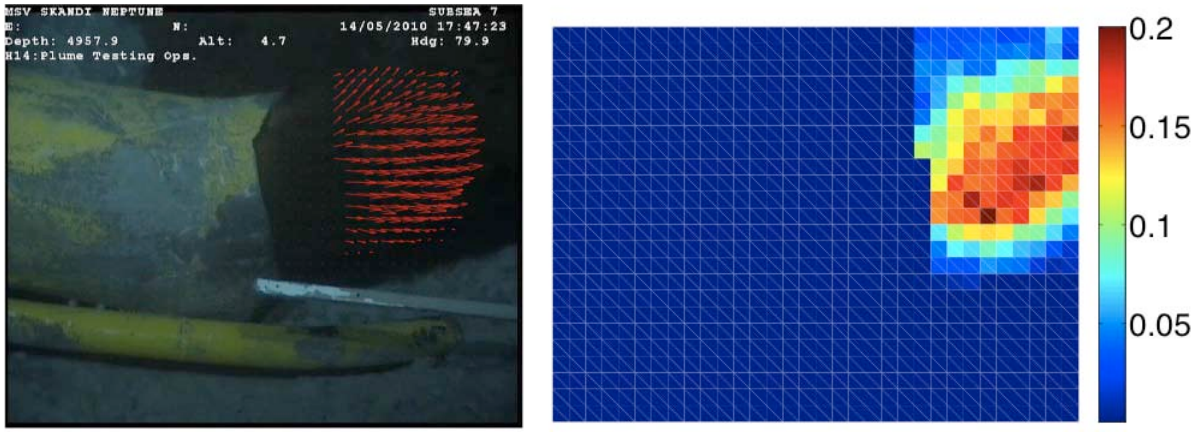

Figure 10: Velocity vectors (left panel) and color map of the horizontal velocity component in m/s (right panel) obtained by applying a PIV algorithm to the images of the jet outflow from the riser pipe.

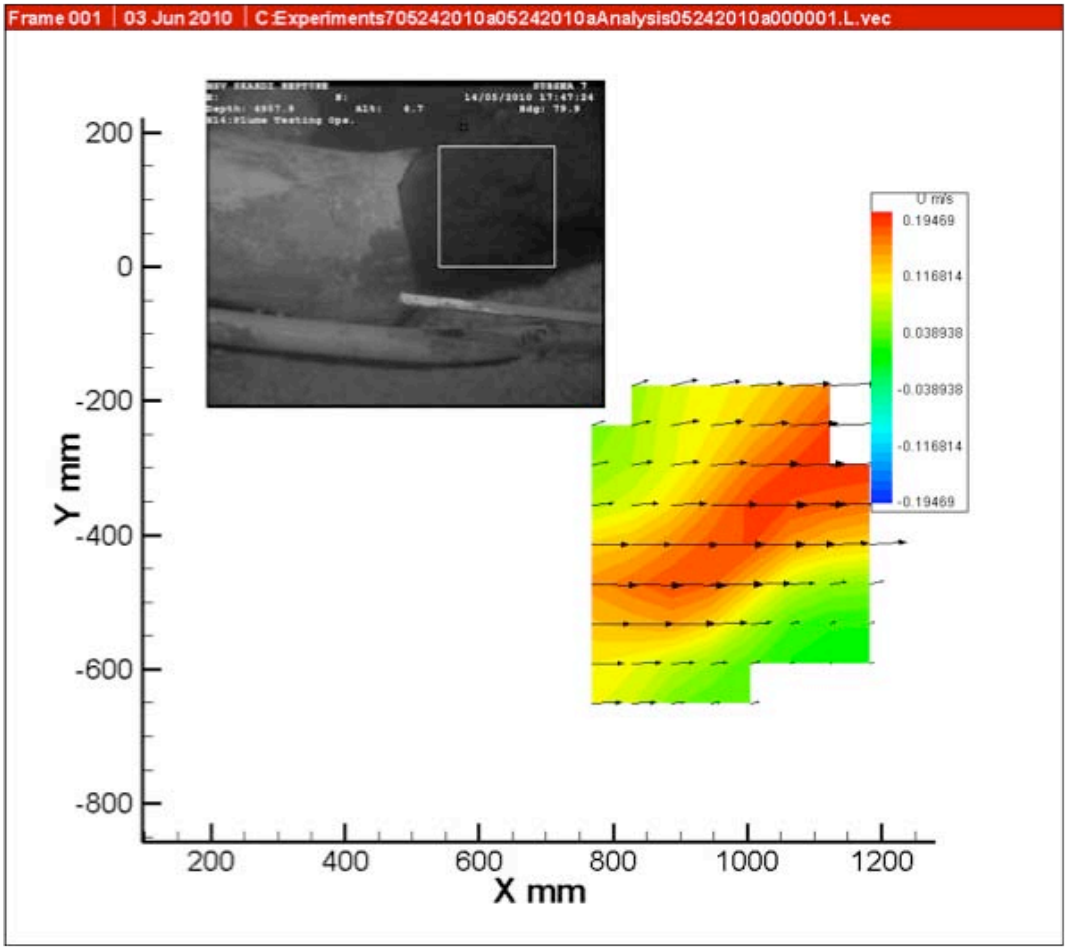

Figure 11: Alternative PIV analysis of the same time segment shown in Figure 10.

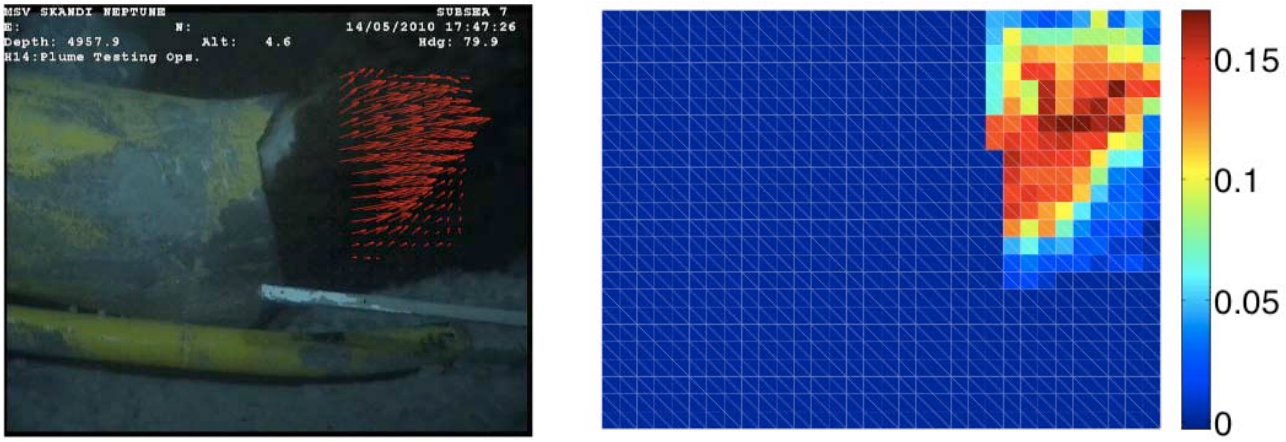

Figure 12: Velocity vectors (left panel) and color map of the horizontal velocity component (right panel) from image correlation with a PIV algorithm at a time when the flow is transitioning from mostly oil to mostly gas.

Figure 12 shows the result of applying the ensemble PIV algorithm to 100 consecutive images over 4 seconds at the initial stages of the formation of a gas slug (20100514224719234@H14_Ch1-H264h.mov). Note that the jet becomes more buoyant, but the horizontal component of velocity remains almost the same as in the previous case.

Estimate of the Oil Discharging from the Open End of Riser:

ESTIMATES 1 (UCSD)

We know that

- the peak magnitude of the velocity of the surface features measured in the ensemble records is 0.2 m/s (Figures 10 to 12);
- the mean velocity of the surface features measured in the ensemble records is 0.12 m/s (Figures 10 to 12);
- the cross sectional area of the pipe is 214 in^2;

and consider that

- the average Gas/Oil temporal fraction is 40/60, as measured from the analysis of the time variation of the average brightness intensity.

Using these data, different assumptions of the relation between the measured convection velocities of the surface features (V_{conv}) and the average bulk velocity of the potential core of the jet ($V_{bulkjet}$) lead to the following estimates for the flow rate:

- If we assume that $V_{bulkjet}$ is approximately 1.5 of the maximum V_{conv} measured, we estimate ≈ **14000 bbl/day** of condensed oil.
- If we assume that $V_{bulkjet}$ is approximately 2 times the maximum V_{conv} measured, we estimate an oil flow rate ≈ **18000 bbl/day**.

- If we assume that $V_{bulkjet}$ is approximately 1.5 the average V_{conv} measured, we estimate an oil flow rate ≈ **8000 bbl/day**.
- If we assume that $V_{bulkjet}$ is approximately 2 times the average V_{conv} measured, we estimate an oil flow rate ≈ **11000 bbl/day**.

The resulting range of estimates is **8000-18000 bbl/day flowing at the open end of the riser.**

ESTIMATES 2 (UW)

Combined Grey Level – Feature Tracking Velocimetry

We measure the relative oil/gas concentration from the grey level along the blue line shown in Figure 13. Unlike the UCSD technique described above, this is a pointwise estimate of the local concentration, no averaging is performed inside an area or along the measurement line.

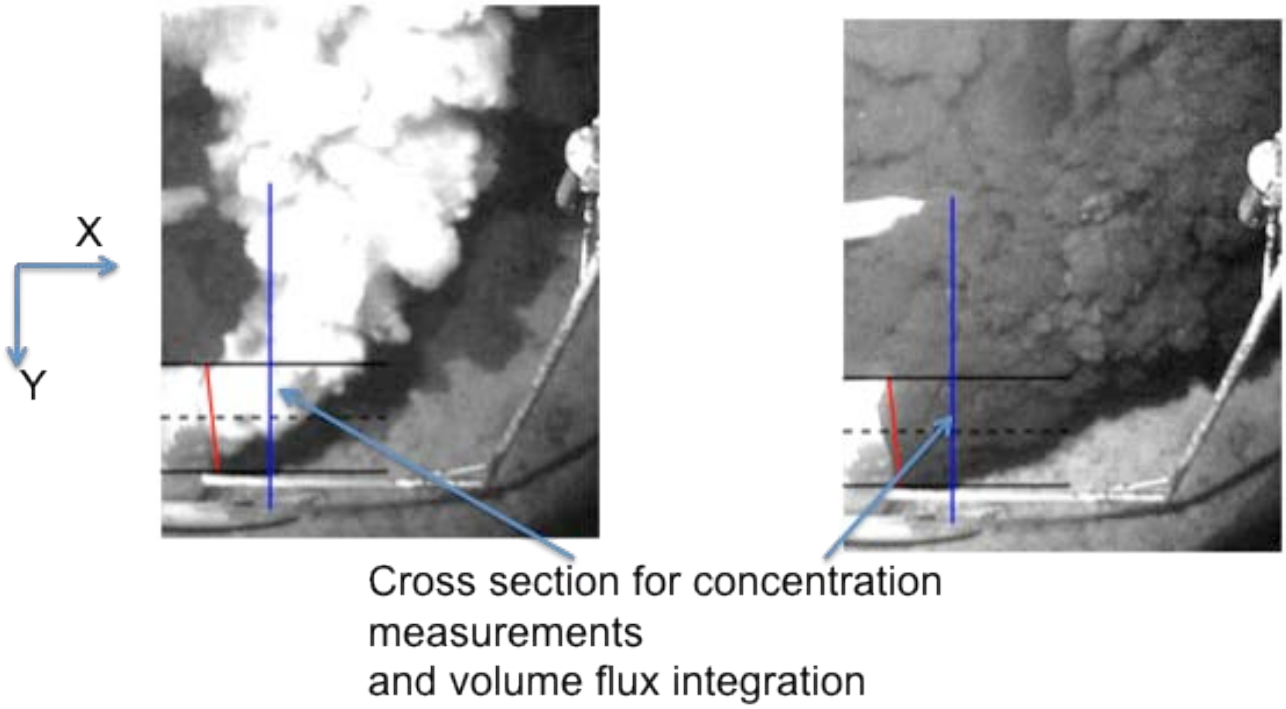

Figure 13: Sketch of the geometry used for the velocity and concentration measurements for estimate 3.

We apply the PIV algorithm on the whole image. Measurements from 100 image pairs are averaged, weighted by the signal to noise ratio at each measurement window. Time dependent flow rate integrated along the cross section of the jet in 2 different ways:

- Q = Area * 2 max(V_x) * mean(c) (black line in lower panel of Figure 14)
- Q = Area * 2 max (V_x * c) (red line in lower panel of Figure 14)

As observed in Figure 14, the differences between both expressions are minimal.

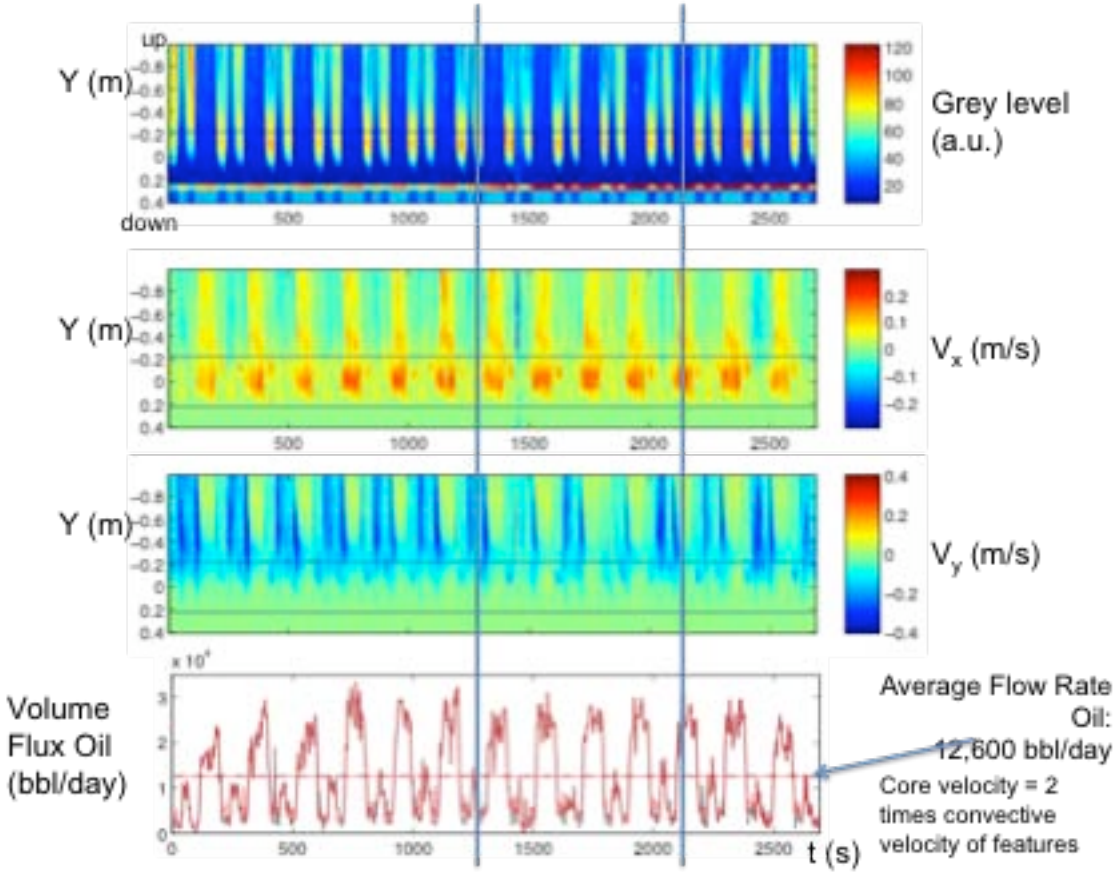

Figure 14: Results from image analysis showing the relative gas/oil concentration, horizontal and vertical velocities and the integrated oil flow rate.

The factor of 2 in the expressions for the flow rate is obtained by assuming that the convective velocity of the features measured by the PIV algorithm is around ½ of the maximum velocity of the jet. Figure 14 shows the flow rates computed with that factor, giving an averaged flow rate of **12600 bbl/day**. When the factor of 1.5 proposed by UCSD is used in the calculations, the averaged flow rate is reduced to **9450 bbl/day**. It is worth noting that in both of these analyses, the calculations yield a flow rate of oil in the condensed phase measured at the location of the spill. If this is to be converted to liquid oil at the surface, a conversion factor would have to be used to account for the phase change that is associated with the temperature and pressure changes between the two states.

Conclusions from Section 1A

- The gas/oil mixture discharging from the open end of the riser is a highly intermittent slug flow.
- There are two well defined periods (70s, 200s) over which the flow oscillates between mostly gas to apparently (annular flow of oil around a gas core) mostly oil. However, there may be even longer periods of gas-oil flow fluctuation in the range of hours or even as long as days that must be characterized.
- Analysis of time histories of the grey level signal from the fluid leaving the exit of the pipe flow was done assuming this quantity to be directly proportional to the gas/oil fraction. The average gas/oil fraction measured in this way was ≈ 40/60. UCSD used this value to correct the average flow rates obtained from velocity measurements. UW integrated the instantaneous product of the velocity and estimated gas/oil fraction, obtaining similar results.
- Based on Feature Tracking Velocimetry and concentrations measurements, and using the assumptions indicated above, we estimate the condensed oil flow rate from the open end of the riser to be between 8,000 bbl/day and 18,000 bbl/day.

Section 1B: Estimate of the Oil Flow Rate Discharging from the Leaks at the Kink on the Top of the Blow Out Preventer

The jets emanating from the various holes in the kink of the riser pipe located on top of the BOP is momentum-dominated. We have measured the spreading half-angle and it is ≈ 13.5 degrees (Figure 15), which is the spreading angle of high Re number turbulent jets in the absence of buoyancy forces. Therefore we are confident that buoyancy does not play a dominant role in the development of the jet at the relative short distances where the measurements are performed. Estimating the total flow from the several leaks in the kink at the top of the BOP is more challenging than the flow of the riser pipe because we have been able to measure only the larger jet located at the center of the kink. It is very difficult to measure the flow rate of the other additional two smaller jets, one which impinges directly on an auxiliary line (see Figure 15), which makes it necessary to extrapolate the flow rate of those leaks from the main leak that is the only one where measurements can be performed. Furthermore, it is impossible to perform measurements at or near the leak orifices. This is due to their small size and the high speed of the jets coming out of them, combined to the limited temporal and spatial resolution of the images, which causes the image of that near field region to be blurry.

Figure 15: Sketch of the location of PIV measurements in the main leak on the kink at the top of the BOP. The jet is still momentum dominated (buoyancy effects not considered).

We analyzed images from sequential movies: H14 BOP Plume May 15 1915-1920.asf (5 minutes) and H14 BOP Plume May 15 1920-1945.asf (25 minutes). Velocity measurements were made at a cross section about 25 Diameters downstream of the exit (the leak orifice is estimated to be about 1.2 cm in width). At this point the diameter of the jet is 0.21 m (100 pixels). According to a recent study on the dynamics of light jets (Foisy et al. 2010. IJHFF 31, 307–314) the entrainment at that point makes up about half the volume flux in the jet. Using these measurements and estimates about entrainment from the literature on light jets, we can evaluate the flow rate from the leak with several simple assumptions, namely that the jet velocity is axisymmetric and has a Gaussian radial profile, and the ratio of maximum velocity to measured velocity is equal to 2 (see Figure 16). We avoid the need to accurately assess the orifice diameter and the virtual origin of the jet. These two quantities are very difficult to evaluate and they have an enormous influence on the outcome of a possible flow rate calculation that depends on them (the flow rate goes like the ratio of diameters squared and approximately like the inverse of the ratio of virtual origins).

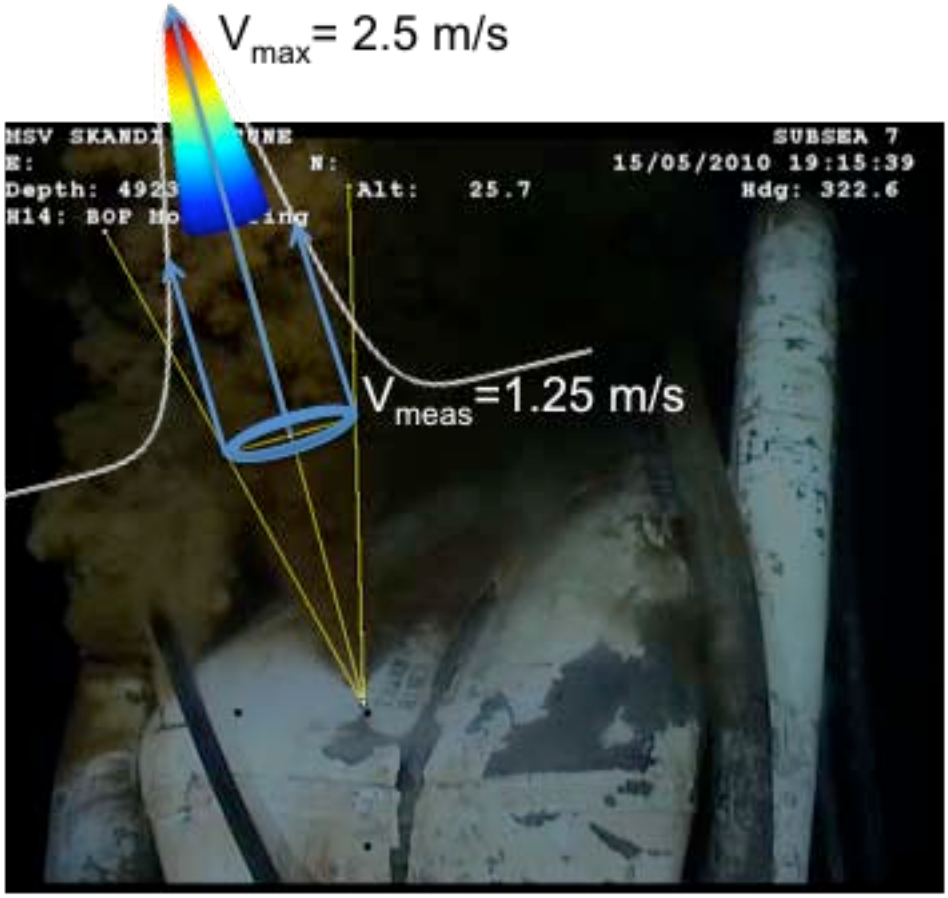

Figure 16: Sketch of the model used to relate the velocity measurements to the oil flow rate at the kink jet.

Considering the entrainment and assuming a 75/25 gas to oil ratio, we get **6,000 bbl/day**. If we assume a 59/41 gas to oil ratio, based on the latest data on the collection from the LMRP system that started on June 3rd, we get **10,000 bbl/day.** Considering the other two jets, we will assume that they discharge half of the amount measured in the stronger central jet. Therefore the total flow rate from the kink is estimated to be between **9,000 bb/day** and **15,000 bbl/day**. We have used measurements of the gas to oil ratio measured at the surface to estimate the amount to barrels of liquid oil at the surface as fraction of the total flow rate at the spill. To do this, we use conservation of mass and the known densities of oil and gas at both surface conditions and spill site conditions. $x \cdot \rho_{oil}^{surface} + y \cdot \rho_{gas}^{surface} = z \cdot \rho_{oil}^{depth} + (1-z) \cdot \rho_{gas}^{depth}$, where x=1 barrel of oil, y=3000 scf of gas, the densities of oil and gas at the spill site were reported by BP to be 44.4 lb/ft^3 and 12.3 lb/ft^3, and the densities of oil and gas at the surface were extracted from tables for sweet Louisiana crude and methane respectively. Values reported by BP from sampling before the incident happened were 3000 standard cubic feet of gas per barrel of oil at the surface. That yielded the value of z=0.25 barrels of liquid oil at the surface per barrel of volume flow rate at depth. The results from the capture with the LMRP cap installed on June 3rd yielded an average gas to oil ratio of approximately 2200 scf of gas per barrel of liquid oil at the surface, which turns into z=0.41 barrels of liquid oil at the surface per barrel of flow rate at depth.

Conclusions from Section 1B

- The analysis of the leaks at the kink on top of the BOP has significantly higher uncertainty than the estimates of the riser's end, due to
  - The existence of several leaks, some of which cannot be measured
  - The small size of the orifices and fast speed of the jets coming out of them, combined to insufficient temporal and spatial resolution of the movies analyzed.
- The jet emanating from the kink is momentum-dominated.
- Velocity measurements made 25 Diameters downstream one orifice, together with
  - an estimated entrainment of half the volume flux in the jet taken from the literature of compressible jets,
  - assumed 75/25 or 59/41 gas/oil ratios,
  - axisymmetric Gaussian velocity profile in the jet,
  - maximum to measured velocity equal to 2,
  - assumed that the total flow from all the leaks is equal to 1.5 times the flow estimated from the main leak,

  lead to a total flow rate from the kink between 9,000 bb/day and 15,000 bbl/day.

Conclusions from Section 1

Analysis of the measured time histories of the grey level signal from the fluid at the open end of the riser reveals gas/oil temporal fraction of 40/60. However, there may be even longer periods of gas-oil flow fluctuation in the range of hours or even as long as days that must be characterized.

Based on Feature Tracking Velocimetry and concentrations measurements, and using the assumptions indicated above, we estimate the condensed oil flow rate

- from the open end of the riser = 8,000 bbl/day to 18,000 bbl/day
- from the kink on top of BOP = 9,000 bbl/day to 15,0000 bbl/day

TOTAL ESTIMATE = 17,000 to 33,000 bbl/day

Section 2: Estimate of the Oil Flow Rate After the Cut of the Riser

The geometry of the riser pipe after the cut just above the Blow Out Preventer is shown in figure 17. We use 19.5 inches as the interior diameter of the pipe and assume that the exit is round and neglect the effect of the drilling pipe inside the riser and the metal flap across the section resulting from the uneven cut. The resulting cross sectional area used in the calculations is 0.1927 m^2.

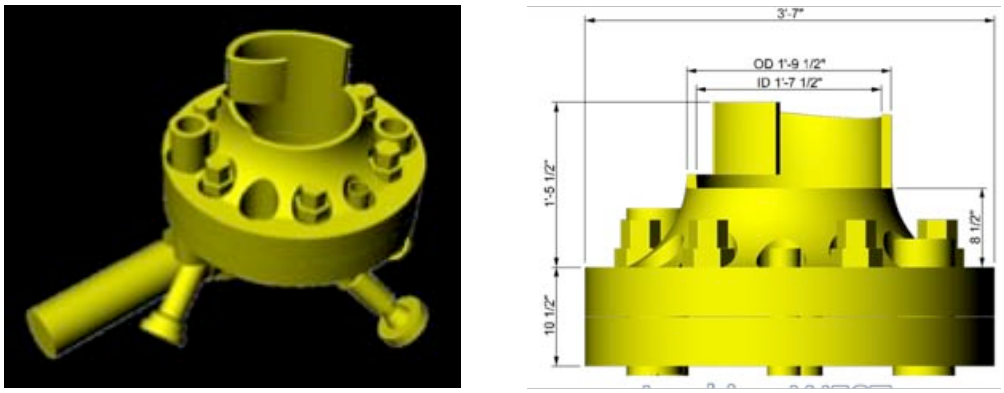

Figure 17: Sketch of the geometry of the riser pipe after the cut just above the flange on top of the BOP.

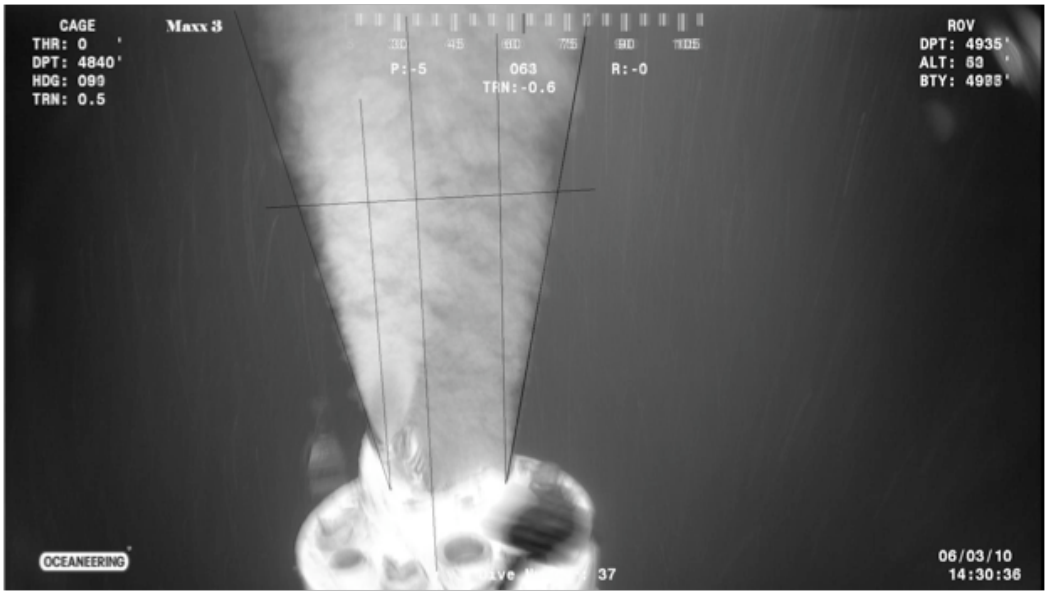

Figure 18: Time averaged black and white image intensity.

Observation of the flow coming out of the cut riser shows that the jet discharging from the riser is "momentum-driven" up to at least 3 jet diameters downstream, after which it starts to be strongly influenced by buoyancy. The regime is that of a continuous bubbly gas/oil uniformly mixed as opposed to the intermittent slug flow observed at the open end of the riser discussed in Section 1. Figure 18 is obtained by superposition of a sequence of 50 images averaging the grey level at each pixel. The instantaneous features are washed out, but the average shape of the jet is brought to the forefront, showing the 13.5° half angle for the spreading characteristic of momentum driven jets.

Section 2A: Results from UCSD Analysis

We performed ensemble PIV measurements of two sequences of the movie TOPHAT_06-03-10_14-29-22.avi. The first sequence was from 14:30:46 to 14:30:48 (50 frames, 49 pairs, Figure 19 left panel), while the second sequence was from 14:30:35 to 14:30:36 (30 frames, 29 pairs, Figure 19 right panel). These measurements showed that the maximum velocity of the coherent structures of the jet immediately downstream of the outlet is ≈ 0.5 m/s and that this velocity decreases to ≈ 0.4 m/s approximately one diameter downstream of the outlet.

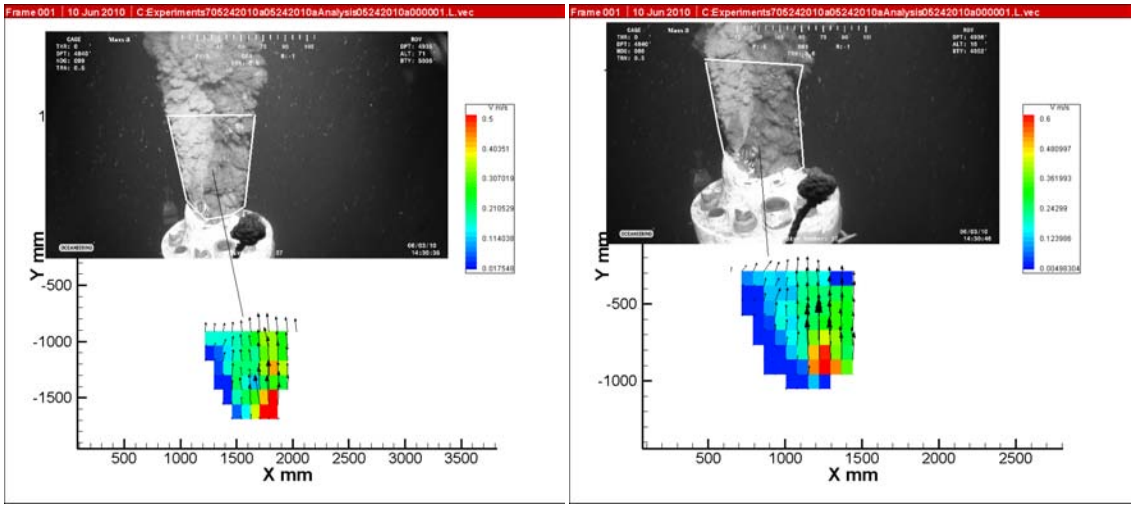

Figure 19: Velocity measurements from the correlation of image pairs through the PIV algorithm. The images come from two sequences of the movie TOPHAT_06-03-10_14-29-22.avi. The first sequence was from 14:30:46 to 14:30:48 (50 frames, 49 pairs, Figure 19 left panel), while the second sequence was from 14:30:35 to 14:30:36 (30 frames, 29 pairs, Figure 19 right panel).

Using these measurements of the convection velocity of the coherent structures, the only step necessary to estimate the flow rate is to relate the measured velocity to the jet exit velocity. Because we are taking our measurements next the jet's exit, we are within the potential cone and therefore the centerline velocity of the jet is still equal to the jet exit velocity. Analysis of the literature from uniform density mixing layers suggests a value for that ratio of 1.6. This value was estimated by considering that the coherent turbulent structures in a shear flow propagate with an advection velocity equal to the mean of the streamwise velocity that they sample in their interior (Townsend 1976), which has been tested successfully for wall turbulence (del Álamo and Jiménez, 2009). We apply this idea to the shear layers surrounding the potential cone of the jet (see Figure 20), which were characterized by Wygnanski and Fiedler (1970). The level of intermittency in the shear layer, γ, is used as a fiduciary indicator of the presence of turbulent coherent structures, so that the average of the mean streamwise velocity weighted with γ provides an estimate of the convection velocity of the jet turbulent structures, which yields a ratio of 1/0.62 ≈ 1.6 between the velocity of the jet coherent structures measured by PIV and the bulk flow velocity at the potential cone of the jet.

We use the factor estimated above to convert the velocities measured with PIV next to the pipe exit (≈ 0.5 m/s) into estimated bulk velocities at the potential cone of the jet A conservative

factor of 2.5 by multiplying 1.6 times the square root of the density ratio between the surrounding fluid and the jet ($\approx 1.6 \times \sqrt{1030/415}$) is applied as we move downstream of the exit, where the velocities measured by PIV are ≈ 0.4 m/s. This is done following Dahm and Dimotakis, (1987) to account for the effect that the difference in density between the jet's fluid and the entrained fluid has in the overall flux of momentum downstream as entrainment becomes more important (Measurements of Entrainment and Mixing in Turbulent Jets . Authors: Dahm, WJA; Dimotakis, PE. Source: AIAA Journal, Volume 25, Issue 9, Pages 1216-1223. Published: Sep 1987). We use a ratio of flow of oil at the surface/total flow at depth equal to 0.41 as evaluated above from the values of gas to oil ratio reported by BP from the LMRP collection data. The cross-sectional area the jet exit deduced from the geometry of the pipe after the riser cut (see Figure 17). The range of possible values for the estimated oil volume flow rate that comes out of the riser is shown in Table 1. The most plausible value of the flow rate, **Q ≈ 35000 bbl/day**, is outlined in the table.

Table 1: Flow rate estimates from the movie TOPHAT_06-03-10_14-29-22.avi after the riser pipe was cut above the BOP.

Correction Factor	PIV Velocity (m/s)	Area (m^2)	Oil/Gas	Flow Rate (bbl/day)
1.6	0.4	0.1927	0.41	28000
2.5	0.4	0.1927	0.41	43000
1.6	**0.5**	**0.1927**	**0.41**	**35000**
2.5	0.5	0.1927	0.41	54000

Results from UW Analysis

1. Video segment: TOP_HAT_060310_14:30:35_37.

Ensemble averaged over 54 image pairs (Frames 2203 to 2258).

This is the original sequence that we compared in the first group discussion of the FRTG on Thursday, June 10, 2010. We have resolved the inconsistency in the PIV measurements by focusing on the same very near region of the jet development, closer than 1 diameter to the riser pipe's end. The results are shown in Figures 20 and 21. We all measure a maximum velocity of V_max ≈ 0.58 m/s (UCSD, UW, and Purdue). The maximum velocity is always found very close to the rim, less than 0.25 D downstream.

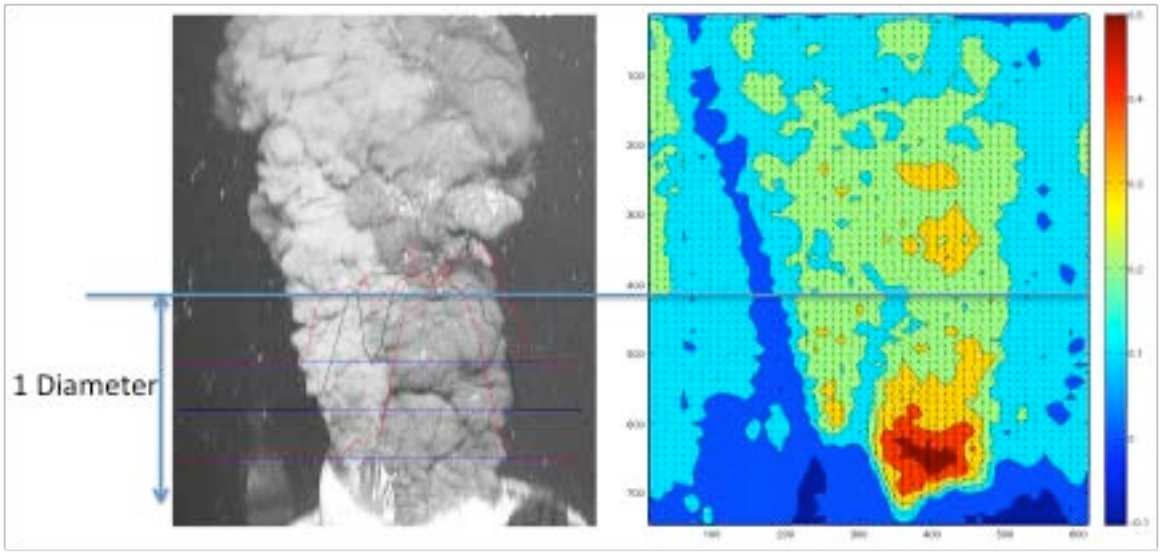

Figure 20: Image of the riser pipe outflow (left) and correlation velocity measurements (right) with the locations at which the flow rate is evaluated marked.

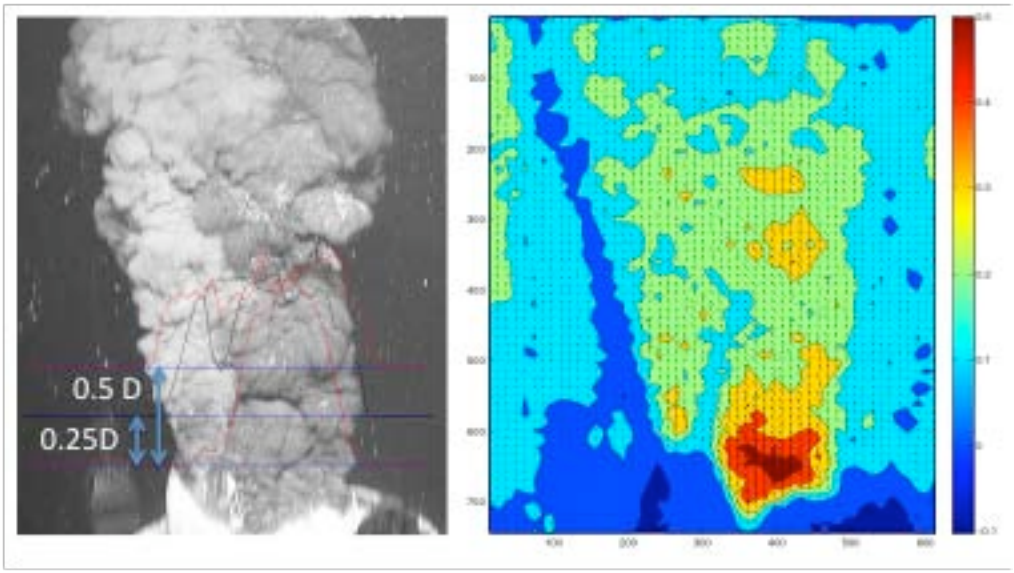

Figure 21: Side by side presentation of the riser outflow and the velocity measurements with the three cross sections used to calculate the flow rate (right at the nozzle, 0.25 D and 0.5D downstream).

Because the highest velocity is found near the jet exit, we apply a factor of 1.6 to calculate the core velocity and the flow rate. Conservative factors of 2 and 3.15 ($\approx 2 \times \sqrt{1030/415}$) are applied as we move downstream. Note that further downstream the coherent structures have more time to develop and the density ratio between the density of the jet and the entrained fluid can play a role. With these assumptions, we obtained the following results from this image sequence:

- At section z=0.5D, V_max=0.3498 m/s with a factor of 3.15 we get **Q=46,688 bbl/day**.
- At section z=0.25D, V_max=0.4157 m/s with a factor of 2 we get **Q=35,746, bbl/day**.
- At section z=0, V_max=0.5773 m/s and with a factor of 1.6 we get **Q=39,710 bbl/day.**

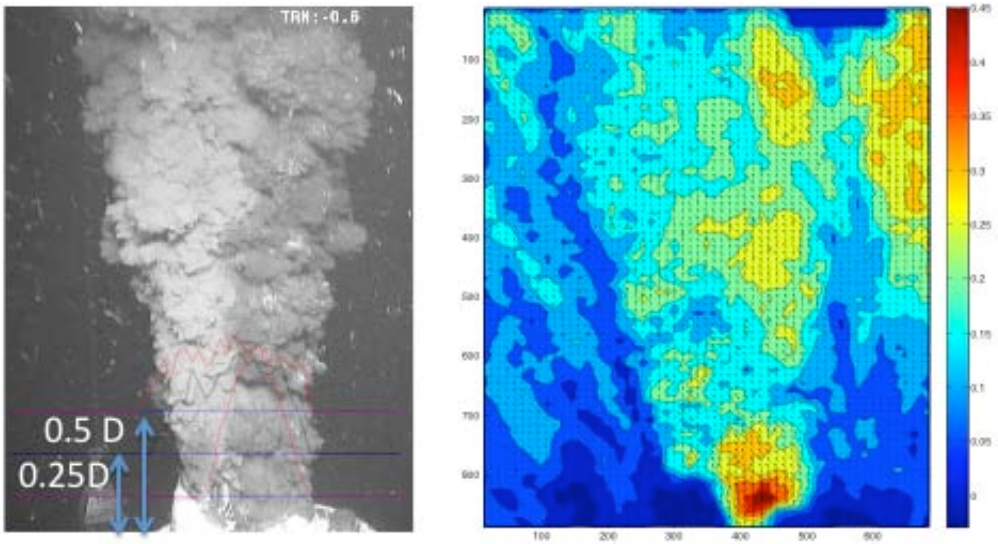

Figure 22: Image and velocity measurements from image sequence 14:30:33 to 35.

2. Video Segment: TOP_HAT_060310_14:30:33_35.

Ensemble averaged over 50 frames.

In this sequence the maximum velocity is V_max ≈ 0.50 m/s. The maximum velocity is always found right on the rim, away from the pipe flap that wrap around the light jet. With these assumptions, we obtained the following results from this image sequence:

- At section z=0.5D, V_max=0.2579 m/s with a factor of 3.15 we get **Q=34,422 bbl/day**.
- At section z=0.25D, V_max=0.3385 m/s with a factor of 2 we get **Q=29,105 bbl/day**.
- At section z=0, V_max=0.4913 m/s and with a factor of 1.6 we get **Q=33,794 bbl/day**.

3. Video Segment: TOP_HAT_060310_14:30:47_49

Ensemble averaged over 76 frames.

In this sequence the maximum velocity is V_max ≈ 0.50 m/s. The maximum velocity is always found right on the rim, away from the pipe flap that wrap around the light jet (see Figure 23). With these assumptions, we obtained the following results from this image sequence:

- At section z=0.5D, V_max=0.3451 m/s with a factor of 3.15 we get **Q=46,601bbl/day**.
- At section z=0.25D, V_max=0.3385 m/s with a factor of 2 we get **Q=31,934bbl/day**.
- At section z=0, V_max=0.4913 m/s and with a factor of 1.6 we get **Q=33,602 bbl/day**.

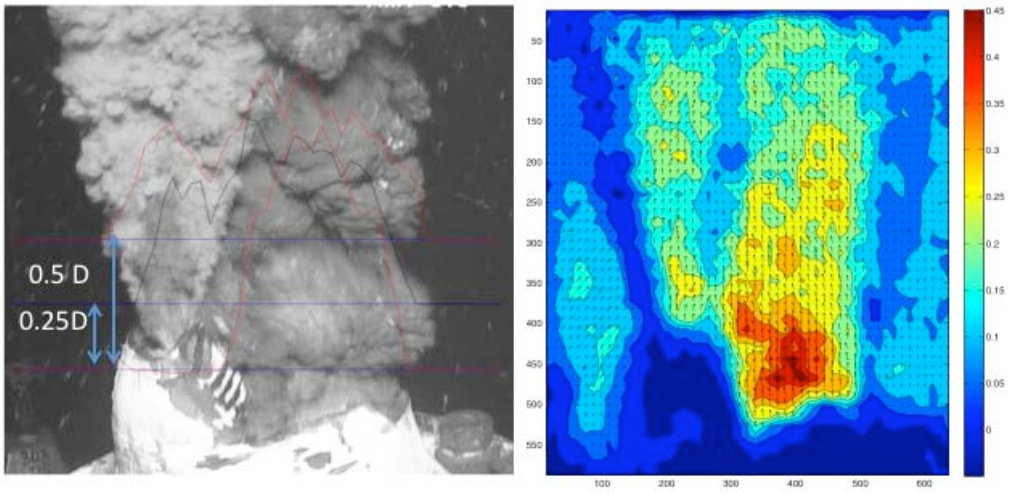

Figure 23: Sketch of the measurement region on the flow image and the velocity measurements at the third video sequenced analyzed.

4. Video Sequence: TOP_HAT_060310_14:31:35_41

Ensemble averaged over 180 frames.

This sequence is focused on the jet carrying lighter fluid which dominates the image in Figures 24 and 25. The velocity of the light grey jet is always smaller than the main, dark jet. In this sequence the maximum velocity is V_max ≈ 0.40 m/s. The maximum velocity is always found right on the rim, away from the pipe flap that wraps around the light jet. With these assumptions, we obtained the following results from this image sequence:

- At section z=0.5D, V_max=0. 2729 m/s with a factor of 3.15 we get **Q=36,424 bbl/day.**
- At section z=0.25D, V_max=0. 2546 m/s with a factor of 2 we get **Q=21,891 bbl/day.**
- At section z=0, V_max=0. 4137m/s and with a factor of 1.6 we get **Q=28,457 bbl/day.**

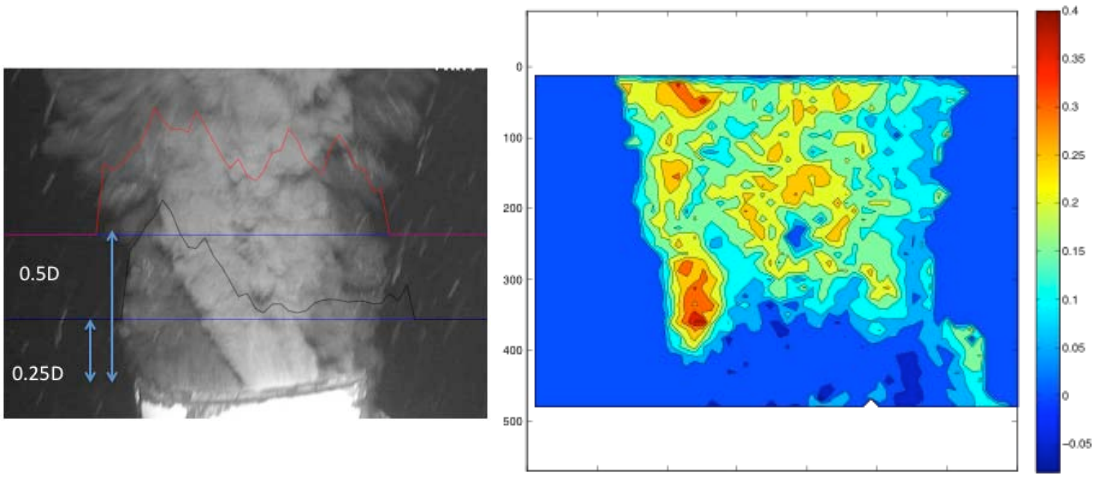

Figure 24: Zoomed in image of the outflow from the riser pipe's end, with the lighter jet in the front of the image. Velocity measurements show a very low velocity of the lighter jet, but maximum velocities close to the rim and away from the lighter jet.

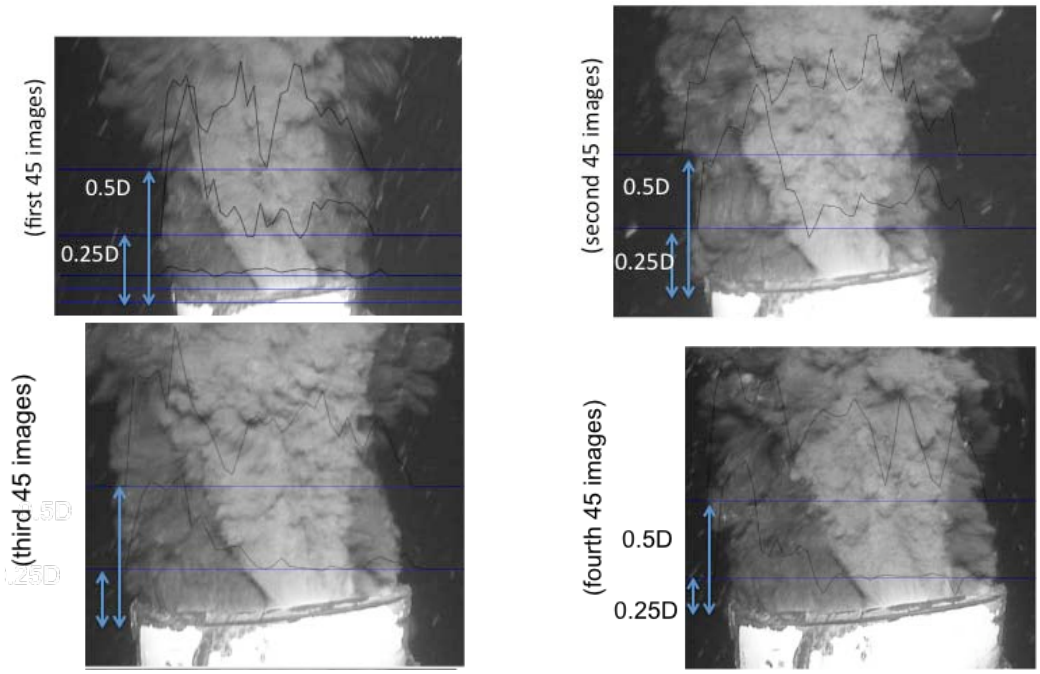

Figure 25: Four images from the 180 frame sequence showed in Figure 24, with the superimposed velocity profiles from ensemble averages in four subsequences of 45 frames each.

The range of flow rate estimations obtained from the four videos is summarized in Table 2 below.

Table 2: Flow rate estimates from the videos taken on 06032010 after the riser pipe was cut above the BOP. The lighter cells at the top represent the minimum flow rate calculations, the intermediate part of the table represents the averages and the bottom part (darker) has the maximum values. The absolute minimum, best estimate and absolute maximum are marked in bold.

Correction Factor	Velocity (m/s)	Oil/Gas	Flow Rate (STB/day)
1.6	0.41	0.41	28000
2	**0.25**	**0.41**	**22000**
3.15	0.26	0.41	35000
1.6	**0.49**	**0.41**	**34000**
2	0.35	0.41	30000
3.15	0.31	0.41	41000
1.6	0.58	0.41	40000
2	0.42	0.41	36000
3.15	**0.35**	**0.41**	**47000**

Conclusions from Section 2

- Image correlation techniques (PIV) provide consistent velocity measurements across different sequences, algorithms and users.
- The main source of uncertainty lies in the relationship between measured velocity of turbulent coherent structures in the outer interface of the jet and the velocity at the potential cone of the jet (developed vs. developing flow, coherent structures, entrainment with different density, etc.). This introduces a variability in the estimations of up to 300%.
- Secondary sources of uncertainty are:
  - temporal fluctuations,
  - use of mean or averaged velocity,
  - cross sectional area of the pipe at exit,
  - constant vs. inhomogeneous oil volume fraction (0.41),
  - ROV velocity

FINAL ESTIMATE = Best estimate of 34,000 bbl/day with a range of between 22,000 to 54,000 bbl/day.

Appendix 9: Plume Team Biographies

Dr. Alberto Aliseda is an Assistant Professor of Mechanical Engineering at the University of Washington. His research and teaching focuses on fluid mechanics with applications to Energy, Environmental and Biomedical Flows.

Dr. Paul Bommer is a Senior Lecturer in Petroleum Engineering at the University of Texas at Austin. He teaches courses in drilling, production, artificial lift, and facilities. He also spent twenty-five years in private practice, specializing in drilling and production operations and oil and gas appraisals.

Dr. Pedro I. Espina serves as Program Analyst at the Office of the Director of NIST. Dr. Espina served as the International Liaison of the International Bureau of Weights and Measures. Dr. Espina also served a Scientific Advisor at the Chemical Science and Technology Laboratory of NIST, and is the former Leader of the NIST Flow Metrology Group.

Dr. Oscar Flores is a Research Associate in the Department of Mechanical Engineering at University of Washington. His primary area of research is fluid mechanics, with emphasis on wall-bounded turbulent flows and on density-stratified turbulent flows.

Dr. Juan C. Lasheras is Stanford S. and Beverly P. Penner Professor of Engineering and Applied Sciences Distinguished Professor of Mechanical and Aerospace Engineering and Bioengineering at University of California at San Diego. He is Chairman of the American Physical Society/Division of Fluid Dynamics. His research interests include turbulent flows, two-phase flows, and bio-medical fluid mechanics, and biomechanics.

Dr. William (Bill) J. Lehr is Senior Scientist at the Office of Response and Restoration of the National Oceanic and Atmospheric Administration (NOAA). He was previously Spill Response Group Leader for the same organization, technical analyst with NASA Jet Propulsion Laboratory and held a joint appointment with the Research Institute and Mathematical Science Department at the University of Petroleum and Minerals. Dr. Lehr is an expert in the field of hazardous chemical spill modeling and remote sensing of oil spills.

Dr. Ira Leifer is an Associate Researcher at the University of California at Santa Barbara. His research projects include a simulation of a subsurface oil spill by a hydrocarbon seep, and an estimate of the release points of oil slicks in the ocean using the natural laboratory of the Santa Barbara Channel.

Dr. Antonio Possolo is Division Chief (Statistical Engineering) at National Institute of Standards and Technology. He holds a Ph.D. in Statistics from Yale University.

Dr. James J. Riley is Paccar Professor of Engineering at the University of Washington and former Chairman of the American Physical Society/Division of Fluid Dynamics. He is a pioneer in the development and application of direct numerical simulation to transitioning and turbulent flows. His current research emphasizes turbulent, chemically-reacting flows, as well as waves and turbulence in density-stratified flows and rotating flows.

Dr. Omer Savas is a Professor with the Department of Mechanical Engineering at the University of California at Berkeley. His research interests include fluid mechanics, aircraft wake vortices, biofluid mechanics, boundary layers, instrumentation, rotating flows, transient aerodynamics, turbulent flows, and vortex dynamics. He is a fellow of the American Physical Society, an Associate Fellow of American Institute of Aeronautics and Astronautics, and A.D. Welliver Fellow of The Boeing Company

Franklin Shaffer is a Senior Research Engineer with USDOE National Energy Technology Laboratory. For 25 years he has led the development of new high speed particle image velocimetry (PIV) tools to study particle flow dynamics of energy processes. He has received numerous national and international awards for development of new high speed imaging tools, including the R&D 100 Award and the Federal Laboratory Award for Excellence in Technology Transfer.

Dr. Steven Wereley is an Associate Professor of Mechanical Engineering at Purdue University. His research interests include biological flows at the cellular level, and electrical and optical manipulation of particles and fluids. He is on the editorial board of Microfluidics and Nanofluidics Journal and Experiments in Fluids and is an Associate Editor of ASME's Journal of Fluids Engineering.

Dr. Poojitha D. Yapa is a Professor of Civil and Environmental Engineering at Clarkson University. His research interests include modeling of deep-water oil and gas jets and plumes, modeling of the fate of oil spills and related oil spill processes, and oil shoreline interaction. He is past associate editor of hydraulic journals of American Society of Civil Engineers (ASCE) as well as the International Association of Hydraulic Research (IAHR).

Appendix 10: Expedited Peer Review Report

While there was not sufficient time to conduct a complete and formal peer review of this report, the following scholars agreed to undertake an expedited review.

Dr. Ronald Adrian	Arizona State University
Dr. Edward Cokelet	Pacific Marine Environmental Laboratory
Dr. Peter Cornillon	University of Rhode Island
Dr. John Kim	UCLA
Dr. Robert Moser	University of Texas
Dr. Yasuo Onishi	Pacific Northwest National Laboratory

Their comments, without attribution or editing, are provided below, plus any responses from the Team. In certain cases their suggested revisions were included in a revised individual report. This may not be acknowledged in all cases.

Reviewer 1

This reviewer was asked to evaluate the report entitled "Deepwater Horizon Release Estimate of Rate by PIV" by the Plume Calculation Team, led by Bill Lehr at NOAA. The team undertook 5 independent analyses of the Deepwater Horizon oil discharges, at three different locations: at the kink in the riser, at the riser outlet, and after the riser was cut off, at the cut location above the blowout preventer. Below are some general comments followed by comments on these 5 analyses.

General Comments: There is some consistency among several of the groups regarding feature velocity estimates at the riser exit (around 0.17-0.19 m/s from Purdue, UCSB, UCSD/UW,) and after the riser cut-off (around 0.5 m/s from Purdue, UCSD/UW). It is not clear why the velocities from other groups that reported them are significantly different. It would be good to track these issues down. The estimates for the oil release rates are not as consistent, because of the numerous assumptions that needed to be made. The assumptions are generally reasonable though they are usually not well justified by the authors; they are mostly a matter of expert opinion, necessarily based on incomplete information and experience. In general, it would be useful if the authors provided as much justification for their assumptions as possible. This is the major reason for large uncertainties in the estimates. The consensus estimates cited in the conclusions (page 13) appropriately reflect these uncertainties. Despite the limitations of the analyses discussed below, they appear to reflect the best possible estimates based on the data available, for these two situations. A big concern remains as to how representative the data examined is of the long-time behavior of the well.

There is much less consistency in the estimates for the jets issuing from the kink. The velocities are larger, requiring that they be measured far from the outlets, also requiring that even more assumptions be made regarding the entrained fluid and buoyancy effects. The velocity estimates are also not consistent among the groups. The result is a huge variation among the authors regarding an estimate for the flow rate from the kink region (1200 to 31,000 bbl/day). These bounds are almost certainly too broad. The best documented estimates, with what appear to this reviewer to be reasonable assumptions is that by the UCSD/UW group, which has a narrower range (9,000-15,000 bbl/day) for the kink flow, though there are presumably more uncertainties than have been accounted for (e.g., in the flow from the unobserved jets).

The separate analyses are described in the appendices of the report as listed below:

Appendix 4: Omer Savas, U. California at Berkeley

This analysis is the most detailed for the multiple small jets at the riser kink. However, in the end Savas makes the same assumptions that others do, that the aggregate flow from all the kink jets is about double that of the one jet (J1) whose velocity can be measured in the videos.

Several different analyses are pursued, the first relies on the similarity expressions for a momentum driven jet, and a guess by the author of the Reynolds number. It seems that there is little basis for such a guess, so this reviewer finds the analysis unconvincing.

The flow in J1 is estimated based on feature tracking in the images, to estimate the velocity of visible features (about 3 m/s). This is much higher than velocities estimated for this jet by other groups, and it is not clear why. Also, the method used to back out flow rate by projecting back to the discharge hole is very sensitive to assumptions about the geometry (diameters, virtual origin etc). The result is quite high estimates of the flow from the riser kink of 12,600-31,400 bbl/day. Savas does not put forward a reliable estimate for the riser exit plume.

After the riser cut, velocity estimates based on features tracking, tracking "stability waves" at the exit and PIV analysis are used. These estimates vary from better than 1m/s to less than 0.3 m/s. A factor to convert feature velocity to bulk velocity is needed (appear to use 1 for feature tracking and PIV and 2 for wave tracking), and were assumed without cited justification. I am concerned if a factor of 1 was really used here, as this is almost certainly incorrect. The overall oil discharge rate is estimated to range from 29,000-45,000 bbl/day.

Appendix 5: Steve Wereley, Purdue

In this analysis, the author noted concerns regarding inconsistencies in the framing rate of the movies analyzed and considerable compression artifacts. This issue was not noted by other analysts, and it may be worth clarifying in general. However, the difference (25 Hz vs. 30Hz) would introduce a 20% error, which is modest relative to most other analysis uncertainties.

At the riser exit, a flow is estimated by estimating a velocity via PIV (~0.19 m/s). Oil discharge rates are estimated using the local plume diameter, an assumed oil/gas ratio (0.29 to 0.5) and an assumed ratio of bulk velocity to feature velocity (1.5 to 2.0). These seem reasonable, but are justification is not cited. Also, no account is taken for entrainment or buoyancy, which may be OK, since the measurement plane appears to be just a diameter or two downstream. The estimated release rate is then 13,800-31,700 bbl/day.

The flow rates from the leaks at the kink are estimated similarly (velocity of 0.17m/s), with similar shortcomings. Ignoring entrainment is more problematic here, because measurements are presumably made many diameters downstream (it is not reported). The resulting flow rate is 1200-2800 bbl/day. Total discharge rate (adding to riser exit flow) is then estimated at 15,000-34,500 bbl/day.

Post riser cut-off, similar analysis was done, with velocities measured at 0.5m/s, at a position quite close to the outlet. The growth of the jet is ignored and the riser ID is used to determine area (as in the other analyses). A rather low oil to gas ratio is used (29%) compared to other analyses, which is again not justified in the text. An overall flow rate of 30,000-40,000 bbl/day is estimated.

Appendix 6: Ira Leifer, U. California, Santa Barbara

For analysis of the riser exit, a time series analysis of the plume brightness as a surrogate for the gas (light) and oil (dark) flows is performed. Results show an intermittent flow of mostly gas and mostly oil. A flow estimate was made based on a similarity analysis with reference to previously measured cases. There does not appear to be enough information to evaluate precisely what analysis was performed here. It will not be considered further.

Feature tracking was used to estimate a velocity (0.17 m/s) oil release rates were estimated based on assumed ratios of core velocity to feature velocity (1.4 to 2.6, the last estimated from entrainment of an eel floating by), and 30-50% oil duty cycle. The result is a release rate of 14,500-45,000 bbl/day, with the author strongly favoring the later (range expanded to the low end by the reviewer to account for the authors' stated variations). The author also notes some oil discharges during the gas flow phase, perhaps increasing the oil discharge to as high at 50,000 bbl/day.

The author notes that estimates for the kink flow rate are needed, but none are provided.

Post riser cut-off analysis was done using hand tracking of features, due to strong turbulence near the outlet. Velocities of 1.3m/s and 1.8 m/s are observed in the first several diameters of the jet. This is used to estimate oil release rates of 50,000-62,500 bbl/day. Here the ratio of bulk velocity to feature velocity is assumed to be 1.2 without cited justification, and the oil to gas ratio is taken as 0.4, apparently from BP's analysis of produced fluid. Note that the feature velocities here are significantly larger than those estimated by other analysts (0.5 m/s), for unknown reasons.

The author notes a number of major uncertainties, but notes that by far the largest is that arising from extrapolating the small video samples available to long times. He therefore does not provide a final estimate. He does suggest, however, that experiments to more directly measure the oil release rate be conducted.

Appendix 7: F. Shaffer, N. Weiland, M. Shahnam , M. Syamlal, G. Richards, US DOE NETL

This group performed three independent analyses of the pre riser cut-off configuration. They use feature tracking, a similarity analysis and computational fluid dynamics.

Feature Tracking Analysis: At the kink jet, a feature velocity of 1.7 m/s was estimated far down stream of the exit (0.6 m). Close to the riser exit (0.8 m, or about 1.6 jet diameters) the plume velocity is estimated to be 0.8m/s (when oil is flowing). This velocity for the riser exit is much higher than the other estimates (~0.2 m/s) for unknown reasons. Flow rates are estimated based on the areas of the jets (both riser exit and kink jets) at the measurement location, 29% oil fraction (at the kink) and 50% oil duty cycle at the riser exit.

There are several problems with these calculations. These include, neglect of the differences between bulk velocity and feature velocity, the neglect of entrainment of water in the kink jets, the inconsistent and perhaps erroneous velocity in the riser outlet plume, and the neglect of almost all sources of uncertainty resulting in a claimed 10% uncertainty. Together, these problems cast significant doubt on the reliability of the estimates.

Similarity Analysis: For the kink jet flow rate, this analysis attempts to eliminate some of the problems described above by using the feature velocity measured in a self-similar jet solution. However, the authors are left guessing at important sensitive parameters such as R, the result appears no more reliable than before.

For the riser exit jet, a theory for buoyant jets is used, which looks to be inapplicable. The analysis used was apparently based on gas mixtures (hydrogen and helium in air), and depends on an estimate of the density at stoichiometric conditions, which is certainly meaningless in this case. The estimated exit jet velocity from this analysis (3 m/s) is totally inconsistent with observations, even the anomalously large velocity estimates of the authors' analysis above. This purely theoretical jet analysis does not provide a reliable flow rate estimate, and is essentially invalidated by the observations.

CFD Analysis: The authors undertook a CFD analysis to try to determine the flow rate that would be required to produce results that were qualitatively similar to the images. Unfortunately, these simulations also appear to be unreliable. The authors provide no indication of the grid resolution or its adequacy, except to say that a coarse mesh that allowed the computations to be done quickly enough was used. It is common in CFD to get qualitatively incorrect results with inadequate resolution, and without evidence to the contrary, this must be considered as a significant possibility here. Also, no mention is made of turbulence models, which should be necessary here, the validity of the multi-phase models used, or the validity of the turbulence models for this case. In short, this is a complex computational modeling problem, and computational results cannot be relied on without significant verification and validation.

Appendix 8: J. C. Lasheras, J. C. del Alamo, U. California, San Diego
A. Aliseda, O. Flores, J. Riley, U. Washington

The analysis by this group starts by evaluating the oil/gas duty cycle of the plug flow in the riser. They analyze the time history of plume brightness (light for gas, dark for oil), and conclude that the aggregate gas fraction (in time) is of order 40%. This is based on an assumption that gas fraction is proportional to normalized brightness. This assumption introduces unevaluated uncertainty into the conclusion, and the authors suggest it is an upper bound on the gas fraction.

Feature velocities at the riser outlet (approximately a diameter downstream) were estimated using several PIV algorithms by different analysts at UCSD. Both maximum and average feature velocities were determined (0.2 m/s and 0.12 m/s). Using estimates for ratio of bulk to feature velocity (1.5 or 2, no cited justification), and the average oil duty cycle (0.6), estimates ranging from 8000-18000 bbl/day of oil release were determined. The UW team also used a different analysis, in which local brightness was assumed to correlate with local gas concentration, which appears to have not made a significant difference. The independent UW analysis is consistent with the UCSD analysis and the range quoted above was reported.

At the riser kink, the observable jet (J1) was analyzed, with feature velocities estimated at about 30cm from the leak (about 1.25 m/s). Flow rate was estimated by assuming a jet profile, a ratio of peak velocity to feature velocity (2), a fraction of entrained fluid (50%), the jet diameter (estimated from images as 1.2cm), the gas/oil ratio (75/25 or 59/41) and the contributions from the other jets (factor of 2). As in the other analyses these assumptions are made without citing justifications. The fraction of entrained flow appears to be based on an analysis or application of the results of Foisy et al, but the details are not provided (it would be good if they were). The flow rate estimates from this analysis are 9,000-15,000bbl/day.

Analyses of the plume after the riser was cut off are based on the observation (from the spreading angle) that the flow is a momentum dominated jet close to the outlet. Feature velocities ranging from 0.31 m/s to 0.58 m/s are cited, depending on the down-stream location (higher velocities close to the exit). The ratio of bulk to feature velocity (1.6) is determined based on intermittency estimates. A more conservative value is this (or 2) times the square root of the density ratio (with no cited justification). Oil fraction is taken to be 0.41, as determined by BP from the produced fluid. The resulting flow rate estimates are 22,000-54,000 bbl/day.

Reviewer 2

This report of the Plume Calculation Team of the Deepwater Horizon Flow Rate Technical Group was written quickly and under duress as the authors strived to estimate the Deepwater Horizon oil spill flow rate for the sole purpose of assisting the response effort. The report's purpose is to present the results of eight teams who worked more or less independently to estimate the oil outflow from three separate leaks from the Deepwater Horizon runaway oil well in the Gulf of Mexico. The first two leaks were from the Riser End Jet and the Riser Kink Jets of the bent riser pipe on the sea floor. The third and later leak was from the Severed Riser Jet above the blowout preventer (BOP) after an ROV (remotely operated vehicle) tool intentionally severed the riser on 3 June 2010. Deducing the oil volume flux of a three-component (gas + oil + water) turbulent fluid from video images alone is an incredibly difficult task. The teams primarily used particle image velocimetry (PIV) applied to ROV-derived video images to measure the flow rate at the edge of each jet. To compute the volume flux, they made various assumptions about the ratio of oil to total (oil + gas + water) flow volume, flow intermittency, multi-component fluid density, the relationship between the jet edge-velocity to its core or average velocity, and the number of jets. As these assumptions imply, complications arose because the ROV was not always stationary during filming, the relative volume of oil to gas was unknown and varying, and the video images could only track the slower outer edge of each jet because the faster core was obscured by the opaque fluid. Besides PIV techniques, some groups used knowledge or assumptions about the flow conduit, Darcy's Law for flow through porous media, pressure measurements, the effect of bubble and hydrate formation and dissolution, analytical and computational fluid dynamics calculations for turbulent jets, and measurements of flow color and intermittency.

The first 13 pages of the report are an introduction with summary conclusions. In what follows I will refer to that as the Overview. The Overview precedes eight independent technical appendices from the team sub-groups and a ninth appendix of brief Principal Investigator biographies.

Overall the work is first rate. However the report is difficult to comprehend at first reading owing to the eight separately authored appendices, each of which is essentially a compressed technical report. Suggestions to improve that are as follows:

- Use consistent naming for the leaks, e.g., Riser End Jet, Riser Kink Jets, and Severed Riser Jet.
- Use consistent names, definitions, and abbreviations throughout and provide a list of abbreviations. For example, one can find the following to designate barrels of oil: bo, boe, bopd, bbl, stb, STB, etc.
- Use consistent units throughout. Presently both metric and American engineering units are used in separate sections.
- State when gas volumes are evaluated at sea-floor and sea-surface pressures. Give the equations and assumptions that allow one to move between the two frames of reference.

The Overview attempts to tie the eight technical appendices together, but it could be improved with some more work. It would be worthwhile to expand the Overview to pull in the results from some of the Appendices, thus shortening or eliminating some and focusing their results. For instance, the Overview could start out with possible oil and gas pathways from the reservoir to the seafloor using the diagrams and suppositions of Appendix 2. It could employ some of the diagrams and explanations of bubble, slug, churn, annular, etc. flow from Appendix 8 to give the reader some idea of the complicated flows within the well and riser before the fluids reach the ocean. It could bring in the qualitative ideas of Appendix 3 to set the stage for how gas-oil-hydrate mixtures might behave in the ocean. It would be helpful to include a multi-row table giving the best estimate and the range of each group's (and sub-group's) flow rates for four quantities: (1) the Riser End Jet, (2) the Riser Kink Jets, (3) the sum of the two, and (4) the Severed Riser Jet. The results of Appendix 1 could be brought in at this stage to give what is essentially the result of a statistical poll of the various estimates.

As for specific points about the Overview, Table 1 is impossible to read because the typeface is too small. Its dates are in European format (dd/mm/yyyy) instead of formats like dd mmm yyyy and yyyy/mm/dd used elsewhere. Table 2 has undefined units and unspecified purple highlights. All the figures should be numbered and have captions. Those on p. 4 and 14 are not. The figure on p. 14 needs to be cropped and zoomed to remove extraneous contours and reveal the annotations. I do not recall this map being referred to, but it should be.

Appendix 1 is an attempt to weight statistically the various flow estimates to come up with a consensus with error bars. Below the first table (unlabeled) it gives a formula for a multiplicative factor of 0.988. Where did that come from? This Appendix would be better incorporated into the Overview.

Appendix 2 contains new information (to this reviewer) by an author familiar with the oil drilling. It shows a well schematic and in-well pressure and phase distributions. This could go into the Overview's Background or Introduction. This would leave room here to explain better the Darcy's Law results and make this appendix more parallel to the others.

Appendix 3 is qualitative and very informative. It would be better served in the Overview's Background or Introduction.

Appendix 4 gives a useful description of the complications of the Riser Kink Jets. (Equation (1) is incomplete in my manuscript copy.) The image analysis section gives a Riser Kink Jet velocity estimate of 85 m/s that is much higher than any in the other appendices. If this is not a misprint, then more explanation is required here. It would be useful to convert the flow rate from m3/d to bbl/d as do the other authors. Symbols for variables such as volume flux, diameter, distance downstream, velocity, pressure, density, etc. should be consistent throughout the entire report. The relationship in Equation (9) needs explanation and a reference. It is critical but seems snatched out of the air. The table at the end of Appendix 4 has but one row; the rest are missing in my copy of the manuscript. Without it, the author's points are dulled. The author explains his PIV results succinctly using diagrams and tables.

Appendix 5 is clear and succinct. This author introduces factors to his PIV measurements to account for gas in the flow and how it changes at sea-surface pressures as do later appendix authors. The laying out all the numbers in his formulae make his assumptions easy to follow.

Appendix 6: The video intensity study of Appendix 6 provides a clear way to quantify the flow intermittency owing to slugs of gas and oil. Reference to the Coal Oil Point seep provides useful background. The response of a hapless eel gives a new perspective to the flow field outside the jet. The paragraph on p. 77 about size scaling is instructive. As with Appendix 5, juxtaposing the numbers in formulae with their short word explanations is helpful as is the lengthy exposition on the Severed Riser Jet.

Appendix 7: The authors of Appendix 7 use three different methods to measure the oil flux: feature tracking (akin to PIV), theoretical analysis and computational fluid dynamics. They do a very competent job, and like some of the other appendices, their results could stand in for the entire report (but credible results from other groups reinforces the results and shows their spread).

Appendix 8 is another very complete study. The Preamble sets the stage for the work, and could be used profitably in the Overview. Unfortunately my version of the manuscript has text missing on p. 114 in the General Observations section. Figure 2 showing the possible gas-oil flow regimes would be useful in the Overview. The image brightness study is similar to the intensity study of Appendix 6 and demonstrates the flow intermittency. The PIV work is complete and convincing. The graphics and the changing velocity profiles at three levels very near the leak sources give new insight into those flows.

In conclusion, I think the work in the Appendices is first rate. The fact that many independent teams provided flow estimates strengthens the statistics of the final results. As mentioned earlier, I would like to see each set of results presented in one final table in the Overview.

Reviewer 3

Comments on DOE NETL CFD Simulations of the Riser End Jet

This review is regarding the CFD simulations of the riser end jet reported in Appendix 7 (Analysis Approach 3 by the DOE NETL team). CFD simulations were performed using the ANSYS FLUENT code. Several simulations at different flow rates were performed, and then the flow rate that produced the best result, matching the shape and trajectory of the oil jet seen in the videos provided by BP, was assumed to be the right flow condition. I have several concerns, some serious and some minor, as described below.

1. First and utmost, although a commercial code, such as the Fluent code used here, can provide some insight into complex flow phenomena, one has to be cautious in interpreting its quantitative information. Furthermore, it was difficult to assess the validity of the present results since the author did not provide sufficient information in the report. If this report were to be led as an official government report, the authors are recommended to provide more detailed information, some of which are mentioned below, so that anyone who wishes to do so could repeat the same or similar simulations.

2. Considering the Reynolds number involved (and as confirmed in the video images), the entire flow must be turbulent, but the authors did not specify how their simulations were performed. Were their simulations performed in DNS/LES/DES/RANS? I assumed that they performed coarse LES's. If this was the case, was Fluent's sub-grid scale model capable of predicting two-phase turbulent flows with confidence?

3. No information on the numerical grids (\a reasonable ` worst case' course (typo?) mesh was employed" does not belong to a technical report) was given. Assuming, again, it was LES, was the wall region in the riser pipe properly resolved? In other words, was it a wall-resolved LES or was a wall-function used instead? At the minimum, the total number of grid points in each direction and the grid information inside the riser pipe (preferably in terms of wall units) must be given so that the readers, if necessary, can make their own judgment on the accuracy of the numerical results. Plus, the flow inside the riser pipe could have been used as a validation of their simulations (see below).

4. Boundary conditions were too vague. At the inlet (inside the riser pipe), it was stated that a volume flow rate was specified. What mean pro le? What turbulence fluctuations? Were the results insensitive to the inlet conditions? At the exit of the computational domain, the ambient pressure was prescribed. It is not clear how this was implemented since for incompressible flows, pressure itself does not enter into the problem, and boundary conditions for the velocity components need to be specified. Also, how was the sea-floor treated? If the no-slip condition was used, was the wall layer adequately resolved or modeled through a wall function? The use of a symmetry condition for the left and right planes (from the view of Fig. 14) seems to be somewhat odd. In particular, did they examine the affects of the symmetry condition at the left plane on the computed results?

5. The diameter of the riser pipe suddenly decreases at the end, forming a nozzle-like shape (Fig.4 in this report and according to other images I have seen). It is not clear from the report how this was modeled. It looked like that they treated it as a tapered pipe (Fig. 14 in the earlier report submitted on June 15, 2010). This could be a critical point since they used the amount of back flow as one of their primary diagnostics. The nozzle-like shape at the end would have caused a stronger jet (known as the thumb e ect as one would put a thumb at the end of a hose to get a water jet reaching further), which could have significantly affected the nature of the back flow at the exit of the riser pipe.

6. Did they perform any grid independent test? This is a must if we want to accept any quantitative information from CFD simulations, especially from a commercial code, which, in general, is known to be robust but less accurate. I am particularly concerned with the possibility that a lack of adequate resolutions in the wall region of the riser pipe could have led to an under-prediction of the wall shear (a typical symptom in a coarse LES), which in turn would have affected the nature of the back flow. One validation they could have done was to examine whether the flow inside the riser pipe was well predicted. Considering the long length of the riser pipe, it can be assumed that the flow was a fully developed pipe flow. Given a flow rate, it is easy to check whether the computed results, such as the skin-friction, mean and turbulence fluctuation profiles, agree with known results. If these were not correctly predicted (most likely due the lack of proper resolution in the riser pipe), which provided the inflow conditions for the jet, the jet flow downstream of the pipe cannot be trusted either.

7. It is my understanding that the jet flow was a mixture of oil and gas, periodically alternating between mostly oil and mostly gas and probably sometime in between a mixture of the two, it seems to be a rather crude approximation to estimate the total oil flow rate based on the simulation of a single phase oil flow (not counting the surrounding water into which the oil jet is discharged) by multiplying an intermittency factor.

In conclusion, I would be extremely cautious in interpreting the CFD simulations results, in part due to the lack of appropriate information, and in part because they may have been carried out without proper conditions (grid resolution, boundary conditions, riser exit geometry, and possibly the subgrid-scale model and numerical accuracy of the code itself). Understandably, the time was rather limited to perform these simulations, but it would require much more careful simulations and validations before these CFD results could be considered as a relevant source for an estimation of the oil leak.

Reviewer 4

General Comments

The Plume Calculation Team (PCT) conducted high quality work within a very short period of time, in spite of needing to use less than ideal quality videos provided by British Petroleum (BP), especially those made before the cutoff of the riser above the Blow Out Preventer (BOP) on June 3, 2010. There are at least two valid approaches for estimating the oil discharge coming out from the Deepwater Horizon broken pipeline and its riser, using BP videotapes. One method is to estimate the exit velocity directly with the use of the Particle Image Velocimetry (PIV). The second method is to use a buoyant plume analysis to determine the exit velocity. The PCT used both of these methods.

The PIV method focuses on phenomena in a very small local area where the mixture of oil and gas is being released to the Gulf of Mexico. The oil-gas mixture generates several difficulties that the PCT needed to account for when applying the PIV method. Estimates of the oil discharge by five PCT members after the riser cut are quite consistent with each other, ranging 24,000 to 42,000 bbl/day for low estimates, and 40,000 to 49,000 bbl/day for the high estimates, as shown in Appendix 1 of the PCT report.

These estimates have some uncertainties. The fact that it is difficult to see the inside structure of the oil-gas plume is a primary uncertainty. Another uncertainty is the velocity field in the local area, which varies significantly from one instance to another, necessitating the assumption that the phenomena shown on the videos are representative of the average condition. Some of the intensive turbulent-looking appearance of the plume may come from the fact that the oil and gas move upward at different velocities due to the different buoyancy, rather than solely from the turbulence of the jet flow itself. Vigorous interaction between gas and oil alters each phase's pathline. However, this interfering effect may not be significant. It is because at the kink location just above the BOP, Jet J1 is more dominated by the inertia force than the buoyancy force, based on my estimate of the J1 jet's densimetric Froude Number being 42, as discussed later. At the end of the riser, the oil/gas mixture coming out from the end of the riser is horizontal, thus the inertia force is horizontal and buoyancy force is vertically upward. Therefore, plumes of oil and gas have separate flow paths caused by buoyancy differences of within the plumes and ambient water, when there is not strong mixing between the oil and gas. As Appendix 6 states, the flow coming out at the end of the riser has three distinct mixtures; mostly oil alone, mostly gas alone, and a mixture of oil and gas, resulting in significant variation of the oil and gas ratio. As the PCT report correctly states, the much longer duration is needed to obtain the accurate averaged velocity of the oil plume.

Because the PIV method estimates the velocity near the outer edge of the buoyant plume, the estimated velocity at the plume edge needs to be related to the velocity averaged over the plume cross section. For a free homogeneous jet, there are two distinct flow regions: the zone of the flow establishment, and the zone of the established flow. The total length of the zone of the flow establishment is expected to be around 6.2 times the nozzle diameter, but a buoyant plume has a shorter distance of this zone (Baumgarter and Trent 1970). Some of the PIV measurements were conducted within this zone, and the flow distribution is expected to be more like a top-hat shape, representing jet core and shearing areas. In the subsequent zone of the established flow, the normal (Gaussian) distribution is expected, as discussed in Appendix 7. For a single-phase buoyant plume (gas or oil alone), a normal (Gaussian) distribution is generally accepted for lateral distributions of the longitudinal velocity and the diluted concentration in the zone of the established flow (Stolzenbach and Harleman 1971). Although there are some uncertainties associated with the multi-phase oil-gas flow, it is possible to estimate the plume velocity averaged across the plume cross-section with the velocity of the plume edge estimated by the PIV method. The PCT members assigned the ratio of the average velocity to the plume edge velocity to be between 1.5 and 3. This assumption is probably reasonable in light of many other uncertainties associated with the velocity estimates with the PIV.

A second valid approach to estimate the oil plume exit velocity, thus the oil discharge rate, is to use a buoyant plume analysis (e.g., trajectory and width analyses) with and without the use of computational fluid dynamics codes. Appendix 7 shows the usefulness of this approach to estimate the oil discharge rate. This approach uses the overall behavior of the buoyant plume, as compared to the PIV method using a local plume velocity field.

There have been a large number of field measurements, laboratory hydraulic flume/basin experiments, and numerical models for a buoyant plume trajectory and mixing analysis associated with heated water and sewage/industrial waste effluents released to surface waters (Abraham1963, Fan and Brooks 1969, Sharazi and Davis 1972). Although there are some recent studies, most of the cited studies have been conducted in 1960s to mid 1970s. One caution when using this approach to estimate oil discharge rate, is that the plume trajectory is very sensitive to the ambient flow. Although there may be some intermittent ambient flows in this depth, it is reasonable to assume (at least initially) that the ambient flow velocity at the bottom of the Gulf of Mexico at 5,000 ft deep is almost zero. However, Appendix 6 indicates that the ambient velocity there may be 0.1 ~ 0.2 m/s due to the existence of the trench. If the actual ambient flow is horizontal, the computed plume trajectory with the assumption of a stagnant ambient flow would significantly overestimate the plume inertia at the end of the riser to match the observed oil plume trajectory. This leads to the significant overestimation of the plume exit velocity, thus, the oil discharge rate. If the actual ambient flow is more vertical, the computed plume trajectory with a stagnant ambient flow significantly overestimates the plume buoyancy to match the observed oil plume trajectory. This leads to the significant underestimation of the plume exit velocity, thus, the oil discharge rate. Beside plume exit velocity measurements suggested in Appendix 6, velocity measurements of the ambient flow may also be needed.

A computational fluid dynamics code must include all major mechanisms of the oil transport and fate, if it is to be applied to the oil plume dispersion in a wide area for long transients. These phenomena include the rising of oil droplets of multiple sizes (with the use of oil dispersant) and oil emulsion.

It is generally better to use various different approaches to estimate the oil discharge rate, because each has its own limitations and uncertainties. I added some additional ways to evaluate the oil discharge rate.

As I stated at the beginning, the PCT has conducted a credible job by employing various assessment methods within the short period of time with the materials supplied to them.

Specific Comments

Appendix 4: Subsection 2.2.1 of this appendix states that the estimated centerline jet velocity is 3 m/s at 70 cm away from the 2.4-cm diameter opening. By using Equation 6 of Appendix 4, the plume exit velocity is calculated to be 85 m/s, assuming the plume is homogeneous. This leads to the oil discharge of 3,400 m3/day, as reported in the appendix.

The centerline velocity is usually expressed as (Wiegel 1964)

$$\frac{U_C}{U_0} = 6.2\frac{D}{x} \qquad (1)$$

where,

U_C = centerline jet velocity
U_0 = jet nozzle velocity
D = nozzle diameter
x = downstream distance.

Equation 1 with the centerline velocity of 3 m/s at 70 cm away yields the jet nozzle velocity of 14 m/s, not 85 m/s. Please clarify this point.

Subsection 3.3 states that the flow is inertia dominated because of the estimated high Reynolds Number. As I will discuss later in this review write-up, the oil plume at the end of the riser (at least what I saw briefly) appears to be a strongly buoyant plume, although the inertia force of the oil plume may still be somewhat greater than the buoyancy force with the estimated densimetric Froude Number being greater than one.

Appendix 6 describes the proposed experiment. I support that well thought-out field measurements will be conducted at the oil spill site to reduce a large amount of uncertainties described in the PCT report.

Appendix 7: In this appendix, for the velocity estimate using the PIV method, the velocity at the edge of the plume is assumed to be the average velocity across the plume cross-section. With this assumption, the oil discharge rate at the end of the riser was estimated to be 55,000 bbl/day. This estimate is very conservative as the maximum oil discharge estimate. Other PCT members used the plume average velocity to be 1.5 to 3 times the velocity estimated at the plume edge. The distance from the riser end was reported to be 0.8 m, which is 2.3 times the 13.75-inch diameter of the riser. Thus, this location is likely to be in the zone of the flow establishment of this plume jet, and I expect that the average velocity to be closer to 1.5 times the velocity of the plume edge than 3 times. With the average velocity to be 1.5 times of the velocity estimated at the plume edge, it would be 83,000 bbl/day, instead of 55,000 bbl/day, as reported in Appendix 7. This is also true for the oil discharge estimate at the kink location based on the velocity estimate at 60 cm downstream. If the J1 jet opening diameter is 1.9 cm, as Appendix 7 indicates, this location is 32 times the jet exit diameter from the opening. Thus, it is in the zone of the established flow, and the velocity distribution is expected to a Gaussian distribution, as Appendix 7's Approach 2 also indicates. Thus, the ratio of the average jet velocity across the plume cross-section to the plume edge velocity is closer to 3 than 1.5.

Appendix 7 also assumes that the total oil flow rate from the riser kink jets to be twice of the oil discharge of the J1 jet. Subsection 3.1 of Appendix 4 states that the jets J and J2 are stronger than J1. Is it better to assume that the total oil discharge is about three times the J1 discharge?

These two points imply that the oil discharge estimates reported under Approach 1 of Appendix 7 seem very conservative as maximum oil discharge estimates.

I strongly support a plume analysis to be a part of the oil spill assessment, as performed under Analysis Approaches 2 and 3 of Appendix 7. It should cover both the close proximity of the BOP/the end of the riser in a short-term, and regional-scale in the longer time frame. Analysis Approach 2 of Appendix 7 describes three different methods; the first method is based on the ambient flow entrainment, the second method uses the pressure drop across the kink, and the third is based on the plume trajectory angle. The first method led to a conclusion that the oil-gas mixture is diluted by 6.7 times by the ambient water, and its plume width is 30 cm (16 times the kink opening diameter of 1.9 cm) at 60 cm downstream (32 times the kink opening diameter). These values at 60 cm downstream are consistent with the dilution and the plume width I estimated with different approaches, as discussed here.

The rise and mixing of a buoyant effluent discharged through a submerged outfall in stagnant, non-stratified ambient water is governed by the buoyancy and inertia forces of the effluent, and is commonly expressed as a function of the following densimetric Froude Number:

$$F_D = \frac{U_0}{\sqrt{\frac{\rho_a - \rho_J}{\rho_a} gD}} \qquad (2)$$

where,

- D = Effluent outlet nozzle diameter
- F_D = Densimetric Froude Number
- g = Gravitational acceleration
- U_0 = Effluent nozzle velocity
- ρ_a = Ambient water density
- ρ_J = Effluent density at the nozzle.

With D = 1.9 cm, U_0 = 14 m/s, ρ_a = 1028 kg/m3, ρ_J = 413 kg/m3 (a 50-50 mixture of oil and gas indicated in Appendix 7), the densimetric Froude Number, FD is 42. Thus, the jet is driven mostly by the inertia force, not much by the buoyancy force. Thus, this plume is close to a homogeneous free jet.

Predicted dilution of a jet discharged vertically into a stagnant non-stratified ambient water is presented in Figure 1 (Sharazi and Davis 1972).

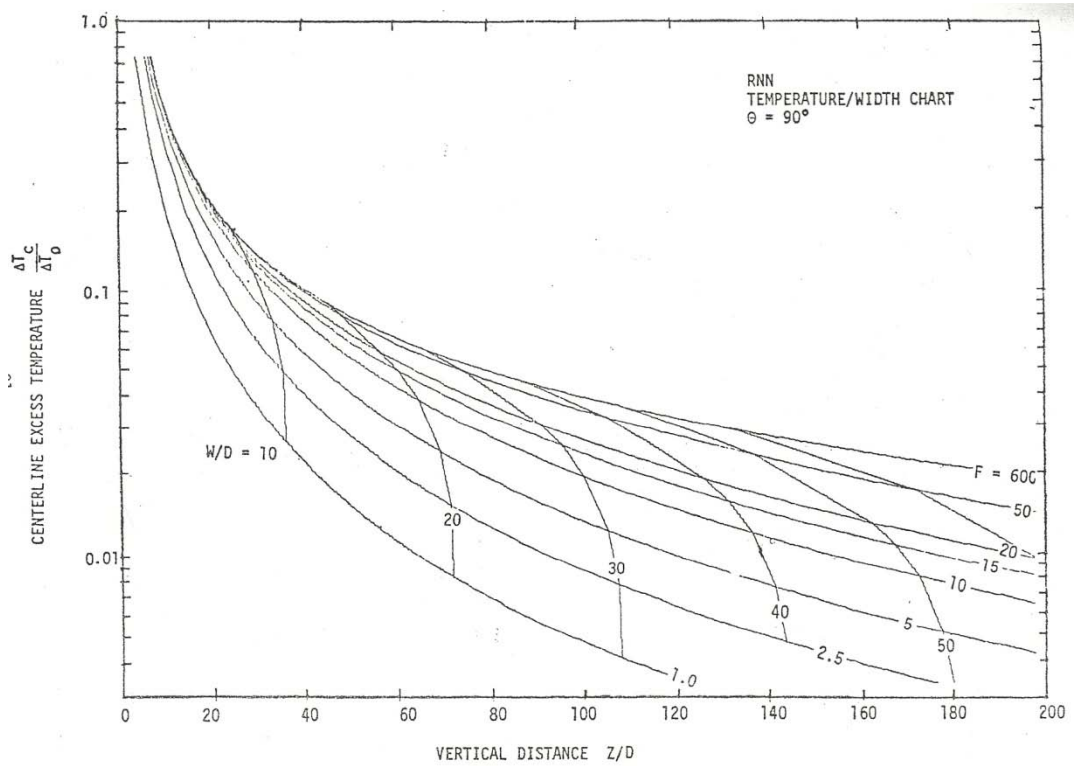

Figure 1: Vertically Injected Buoyant Plume (Sharazi and Davis 1972)

In this figure, the values of 1.0, 2.5, 5, etc., shown in the right part of the figure are the densimetric Froude Number values, and W/D is the width to the diameter ratio. The $\Delta T_C/\Delta T_0$ in the figure expresses the degree of effluent mixing with the ambient water,

$$\frac{\Delta T_C}{\Delta T_0} = \frac{T_C - T_a}{T_J - T_a} \qquad (3)$$

where,

T_a = Ambient water temperature
T_C = Temperature at the plume centerline
T_J = Effluent temperature at the nozzle exit.

At the vertical distance 60 cm (Z/D = 32) and the densimetric Froude Number, FD of 42, Figure 1 shows that the W/D ≈ 15, and $T_C/T_0 \approx 0.15$. Thus, the plume width is 15 times the diameter of 1.9 cm and is 29 cm. $T_C/T_0 \approx 0.15$ corresponds to 6.7 times the dilution. The estimated dilution of 6.7 and plume width of 29 cm at 60 cm above the kink opening, are basically the same values as what Appendix 7's Method 1 predicted.

Another method I used is as follows:

The Densimetric Froude Number of 42 indicates that the J1 jet is marginally buoyant, and could be approximated as a homogeneous jet. For a three-dimensional circular free homogeneous jet, the dilution is expressed as (Weigel 1964)

$$\frac{Q}{Q_0} = 0.32\frac{Z}{D} \qquad (4)$$

where,

Q = Flow rate at distance Z
Q_0 = Jet discharge at the nozzle exit.

Thus, at Z = 60 cm (Z/D = 32), the discharge of the diluted jet is 10 times greater than the initial plume discharge. Thus, the dilution is 10 times.

These values, using the two methods I employed here, are similar to the values reported in Appendix 7.

Method 2 used under Analysis Approach 2 of Appendix 7 depends on the value of the pressure drop across the JI jet opening. Unless 400 psi pressure drop used in the analysis was actually a measured value across the J1 jet opening, there is a large uncertainty on the pressure drop estimate of 400 psi. There is a large uncertainty on the pressure drop through a well from the oil reservoir to the sea bottom. Thus, I consider Method 1 based on the plume entrainment assessment has a greater probability of being more accurate than Method 2 based on the pressure drop.

Method 3, Analysis Approach 2 of Appendix 7, uses somewhat similar approach to what I used, as described below. The modified Froude Number defined in Appendix 7 is different from more common definition of the densimetric Froude Number shown in Equation 2 here. Please define parameters, ρ_0 and ρ_∞ of the modified Froude Number. The left plot of Figure 13 in Appendix 7 shows a reasonable match between the actual plume and the predicted plume trajectory. However, the estimated oil discharge of 86,000 bbl/day is much greater than what I estimated as described below. The actual plume rise shown in this plot rose less sharply than the one I saw on Yahoo.com and used. Thus Appendix 7's oil discharge estimate is much greater than my estimate. This discrepancy may be a reflection of the temporal variability of the plume coming out from the end of the riser.

Analysis Approach 3 of Appendix 7 describes an application of the commercially available computational fluid dynamics code, FLUENT, showing a good match between the observed and predicted plume dispersion.

FLUENT has been widely used to solve a wide range of fluid dynamic problems. However, I anticipate that an FLUENT application to this oil spill condition in a regional-scale and longer term may face a strong challenge to handle multiple-size oil droplets by simultaneously solving a multiple set of Navier Stokes Equations for oil droplets of each size and the ambient flow, and simulating the momentum exchange among each of these oil droplets and ambient water.

Appendix 8 states that the Jet J1 is a main jet coming out at the kink riser above the BOP. Please see my above comment of Jets, J, J2 and J1.

Independent of the PCT effort, I estimated the possible oil flow discharge rate at the end of the riser with a plume trajectory analysis and a video I saw on yahoo.com, as I will briefly described here. My estimate provides a rough estimate of the oil discharge rate for comparison with the PCT report information.

The mixing trajectory of a buoyant plume discharged horizontally through a submerged outfall in stagnant, non-stratified ambient water is governed by the buoyancy and inertia forces of the effluent, as shown in Figure 2 (Sharazi and Davis 1972):

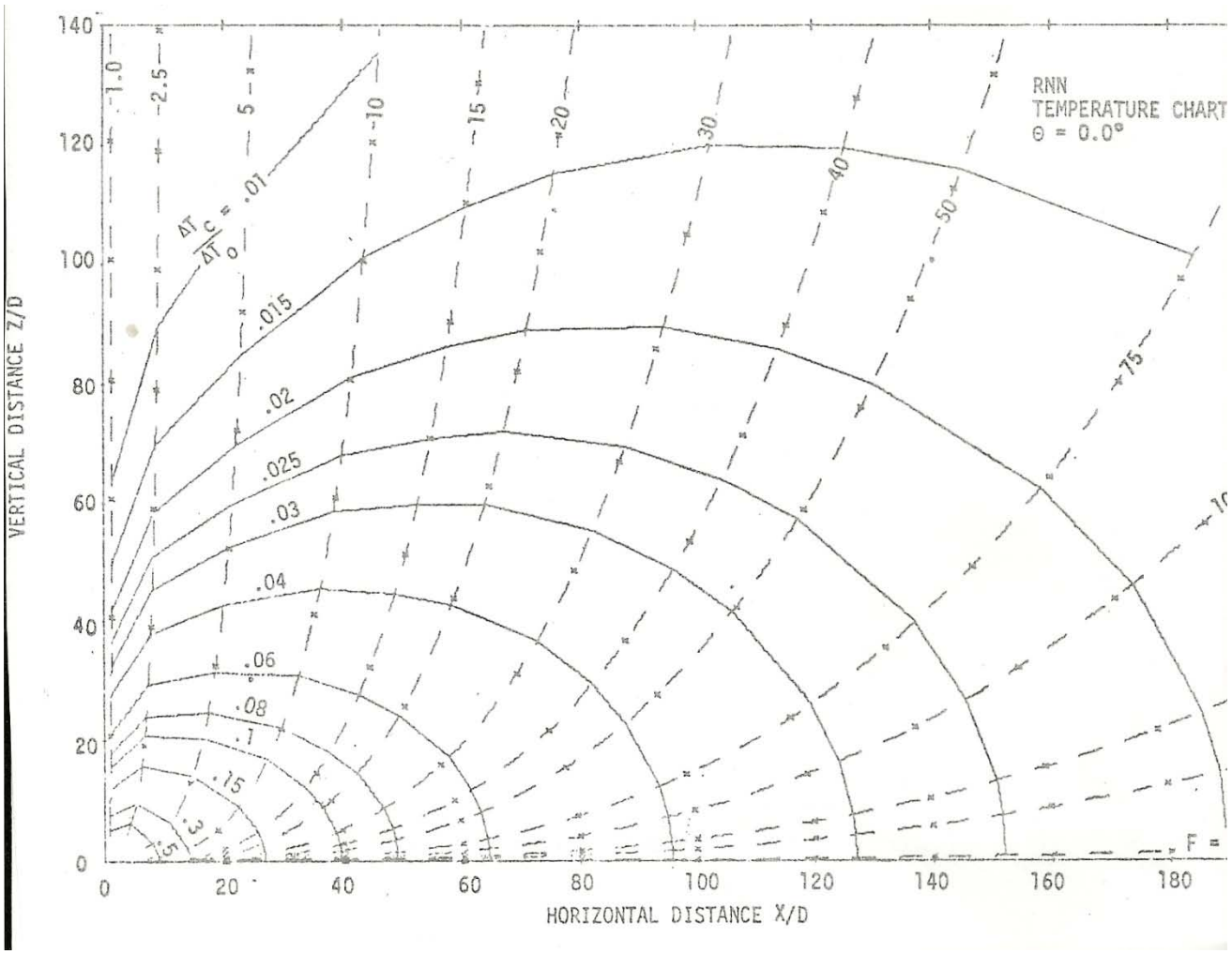

Figure 2: Horizontally Injected Buoyant Plume (Sharazi and Davis 1972)

In this figure, the values of 1.0, 2.5, 5, etc., shown in the upper part of the figure are the densimetric Froude Number, while the $\Delta T_C/\Delta T_0$ expresses the effluent degree of mixing with the ambient water.

These buoyant plume trajectories shown in Figure 2 are compared with the trajectory of the oil horizontally coming out from the end of the riser. A BP video of a buoyant plume shown in yahoo.com was used for this plume trajectory analysis. The video reveals that the plume is a strongly driven by buoyancy. Immediately after the mixture of oil and gas was discharged into the bottom of the sea, it separated into oil and gas plumes. The oil and gas plumes have their own separate trajectories, reflecting the buoyancy difference between oil, gas, and ambient water. Thus, there were basically two, two-phase plumes, instead of one multiphase plume, supporting this plume trajectory approach. The oil plume was immediately rising at approximately 45° angle from the discharge point.

Comparison of the oil and thermal plumes (See Figure 2) implies that the densimetric Froude Number of the oil plume appeared to be greater than 1.0, but a little less than 2.5. NETL used general values for key properties and these values are used here, specifically the oil density to be 0.689 g/mL. The PCT report also states in Appendix 4 that estimates of oil volume fraction at the bottom of the sea range from 25 % to 76 %, and that they selected 41% for their analysis. Assuming densities of the oil and sea water to be 0.689 and 1.028 g/mL, the oil-gas mixture to be 41 vol% oil and 59 vol% of gas, Equation 2 provides the oil velocity coming out of the 13.75-inch diameter riser. Calculated exit velocity and discharge of oil at the end of the riser are shown in Table 1.

Table 1: Calculated Oil Exit Velocity and Discharge at the End of the Riser

Densimetric Froude Number	1	2.5
Exit Velocity, m/s	0.85	2.1
Discharge, bbl/day	18,000	46,000

Table 1 indicates that the very rough estimate of the oil discharge out of the end of the riser is around 46, 000 bbl/day. This assumes that the densimetric Froude Number is 2.5, based on the single videotape. If the densimetric Froude Number is 1.0, the average oil discharge from the end of the riser is approximately 18, 000 bbl/day.

The estimates of oil release rate from the end of the riser are very rough and have many uncertainties, including:

- The video shows only the short distance of the plume trajectory out of the end of the riser.
- The plume of oil outside of the riser was assumed to be a single-phase.
- The ambient flow was assumed be stagnant in the immediately vicinity of the riser.
- No ambient stratification was assumed near the riser.
- The plume model predictions are for heated water, and industrial and municipal wastes. Heated water mixes relatively easily with water. However, industrial and municipal wastes are more difficult to mix with water, and are somewhat similar to oil in this respect.
- The mixture of the oil and water change the viscosity of the mixture much more than heated water does.

References

Abraham. G. 1963. "Jet Diffusion in Stagnant Ambient Fluid," Delft Hydraulics Publication No. 29, Delft Hydraulic Laboratory, Delft, The Netherlands.

Baumgarter, D.J., and D.S. Trent. 1970. "Ocean Outfall Design Part 1. Literature Review and Theoretical Development," U.S. Department of the Interior, federal Water Quality Administration, Northwest Region, Pacific Northwest Water Laboratory, Corvallis, Oregon.

Fan, L-N and N.H. Brooks. 1969. "Numerical Solution of Turbulent Buoyant Jet Problems," Technical Publication No. KH-R-18, W.M. Keck Laboratory of Hydraulics and Water Resources, Division of Engineering and Applied Sciences, California Institute of Technology, Pasadena, California.

Shirazi, M.A. and L.R. Davis. 1972. "Workbook of Thermal Plume Prediction, Volume 1. Submerged Discharge," EPA-R2-72-005a, The U.S. Environmental protection Agency, Pacific Northwest Water Laboratory, National Environmental Research Center, Corvallis, Oregon.

Stolzenbach, K.D., and D.R.F. Harleman. 1971. "An Analytical and Experimental Investigation of Surface Discharges of Heated Water," Report No. 135. Ralph M. Parsons Hydraulic Laboratory, Massachusetts Institute of Technology, Cambridge, Massachusetts.

Wiegel, R.L. 1964, Oceanographical Engineering, Prentice-Hall Inc., Englewood Cliff, New Jersey.

Reviewer 5

General Comments

First, I only had time to carefully read the report and Appendices 1-6, with particular attention on Appendices 4-6. My comments are based on these.

Second, I found the report itself to be very weak. Basically, it relies on the reader to sort through all of the appendices to understand the numbers presented. Specifically, it is not clear where the numbers presented in the Executive summary and in the body of the report come from nor what they mean. Furthermore, the numbers presented in the report are not consistent with one another. Had the report presented a coherent summary of the work presented in the appendices it would have been a lot easier to read and a lot more believable.

Executive Summary

3rd paragraph, 1st line: "Most of the experts" is a vague statement, not appropriate in a document such as this. Thirteen members are listed as members of the Plume Calculation Team. How many of these are considered to be experts? How many of these "have concluded that..."?

3rd paragraph: In addition to the comment above, this paragraph is very weak. It should state a range with clarity. As written it has two ranges, suggests that some experts don't agree and complains about the lack of data and time. Furthermore it is not clear what the ranges really mean. Is one an absolute range? Is the other a range with a confidence of 75%, 95%, 99%…? What does "best estimate" mean? Also, I do not understand what "as little as" and "as large as" means. See comment related to the 50,000 bbl/day number in the following paragraph.

4th paragraph: This paragraph suffers from the same problems as the previous one. I do not understand what "as little as" and "as large as" means. "[A]s large as 50,000 bbl/day" sounds like an absolute upper bound, so the 60,000 bbl/day upper bound in the last sentence of this paragraph is not consistent with this. Is the phrase "as large as" to be interpreted as an absolute upper bound, an upper bound that includes uncertainty in the analysis of the examined videos plus uncertainty associated with poor temporal sampling of the videos, gas/oil ratio, etc? If not, what does it mean? If it is an absolute upper bound then how is this reconciled with the 60,000 bbl/day in the next sentence? Also, the range in the next sentence should read bbl/DAY. My sense is that the report should present either absolute upper and lower bounds (which isn't really possible; there will always be some uncertainty) or (preferably) a 95% confidence (or confidence at some other value, 99%, 90%...) upper and lower bounds.

The Body of the Report

As mentioned in the introductory comments, it is not clear where the numbers used came from. A table listing the volume estimates made, the speeds obtained, the videos used, etc would have been invaluable in reading this report. Appendix 1 does list some post cut-off numbers, but I don't believe that it lists all of them and it is not clear where these numbers came from either. In Appendix 4 by Savas, the author stated that the [RFTG] members agreed on a 220 frame section of the video to examine. This should be stated in the report.

Conclusions

Many of the same comments here as made for the Executive Summary. In addition:

1st paragraph, line 6: "[T]he Team assumed that average flow between the start of the incident and the insertion of the RITT was relatively constant…" On what information was this assumption based and when was this assumption made?

2nd paragraph, 2nd line: "the best estimate of the average flow rate…" On how many video segments is this "best estimate" based?

3rd paragraph: Where do the numbers in this paragraph come from?

4th paragraph: I'm puzzled by what convinced the Plume Team that their upper bound of 50,000 bbl/day was too low.

Appendix 4: Savas, Supplemental Report

Large eddy tracking - major point: I am a bit perplexed with regard to why an effort was not made to estimate the speeds near the pipe exit. (Savas may have indicated this and I may have just missed it.) My impression was that it was because the flow was too fast, but the instability wave tracking gave a speed of .35 cm/s which is quite a bit smaller than the 1 m/s found at 1.5 jet diameters with the eddy tracking. Is it because there were no evident eddies near the outflow. Figure 8 (should be Figure 9) seems to show some. What am I missing here?

Page 48, 10 lines into the paragraph beginning "I see two…", discussion of the window size - a minor point: Don't you really have to look at the correlation fields to say this? I agree that a visual comparison suggests that a 32x32 pixel interrogation will not work, but I would feel more comfortable seeing the correlation fields for a few regions.

Page 50, reference to Fig. 8 in paragraph beginning "I have visually…" - minor point:: This figure does not have a figure number. Subsequent figures are misnumbered.

Page 52, paragraph under Table 2, 2nd line - significant point: I assume that the cross sectional area give here is for the id of the pipe. Is this the case? If so this may lead to a significant underestimate of the flow rate. Specifically, the diameter of the plume appears to increase by ~60% from the pipe exit to the point at which eddy speeds were measured, ~1.5 jet diameters. This corresponds to a cross sectional area that is 2.6 times that used; hence these flow rates would be a factor of 2.6 low. I think that I am missing something here.

If the diameter of the plume was calculated in another fashion, the method used should be described. For example, if the flow rate estimates were made based on the diameter of the plume in the vicinity of the speed estimates precisely what diameter was used. The diameter of the plume appears to increase by about 22% from the location at which tracking started (the top of the vertical white line, near the middle of the image) in the left hand frame of Figure 7 to the location at which tracking ended (the top of the vertical white line) in the right hand frame. This would correspond to an increase in cross sectional area of 50%.

As an aside, it would be interesting to estimate the speed of turbulent eddies at several distances from the pipe exit. I realize that water is entrained as the plume rises and the speed as a function of radial distance from the plume center will also likely change with distance, but an estimate of speed as a function of downstream distance might provide insight into these variations.

Page 52, paragraph under Table 2, 4th line - significant point: Assuming that the cross sectional area estimate is for the entire plume I think that an estimate of the speeds in both the gas dominated and oil dominated flow should be made as they may be different. Which was used in the results presented in Table 2?

Page 52, last paragraph, 1st line, Table 2 - minor point: I think that you mean Table 3.

Page 54, Figure 9 - major point: I am very confused by this figure. The velocity vectors suggest speeds outside of the plume to be similar to those inside the plume. The fact that the speeds are near zero where there are fixed objects (such as the well head) suggests that the velocities are not due to motion of the camera. Is the entire flow in the region moving up? There is something incongruous about this image. Also, the velocity field obtained here is very different from that obtained by other investigators. My sense is that the others are more reasonable.

Appendix 5 - Wereley

Page 57-58, flow rate calculation - major point: I do not understand why the pipe cross sectional area is used for the flow rate calculation as opposed to the diameter of the plume at the point at which the speeds were calculated. The diameter here appears to be about 60% larger than that of the pipe which would give rise to a cross sectional area approximately 3 times as large hence a flow rate 3 times as large as well. You do note that you used the pipe diameter and that this would give you a conservative estimate, but it seems that it would be conservative by a lot and you don't include the full factor of 3 in plume cross section in your error estimates. I see that you use the plume diameter in the calculations made on the high resolution images later. You might want to mention in this section that you address the cross sectional area in more detail in the next section. You do mention that this section is "a bit of history", but it is not clear where the history ends.

Page 59, 3rd line from end of 1st paragraph - major point: You use ratios of 0.29 to 0.5 but you also comment that the period examined is one of large oil fraction. Is the GOR a function of time or a mixture at one instant in time? If the former, then you are OK, if the latter then you should not be multiplying your numbers by these factors; i.e., you are underestimating the flow of oil by doing this. Again, you may be OK here, but I think that you might want to check with BP about what their GOR numbers mean and if it is an average over time you should probably clarify this here. Leifer, Figure 2, suggests that at least for the videos that he analyzed, the oily to gassy periods are very regular with the oily phase occupying about 47% of the period, the gassy phase, 27%, and the mixed phase the remainder, 26%. These numbers suggest that the 29% number is a time average with the oily phase still containing some gas.

Page 61, Table 1 - minor point: Column labels would help here.

Appendix 6 - Leifer

Page 70, Figure 2 - major point: You assert that the change in intensity is due to a change in composition of the flow. This is indeed possible; however an alternative explanation is that the location of two components of the flow is changing as the flow leaves the pipe so that the oil portion moves in front of the gas portion. Is there any evidence of rotation of the two flows with time? My guess is that this is in part happening, but that the ratio of the flows is changing as well with the two correlated. A two camera view at one point or another might help answer this question. I looked at one of the video for 11/05/10 23:33:42 to 23:34:10 (a later period on the same day that you analyzed, but all that I had, sorry). It appears that the oily portion of the flow moves in front of the gas flow while also mixing some with it, but there is still a remnant of the flow, evident at the top of the pipe exit (also seen in Fig. 9) and in plume in the upper portion of the image. The billowing plume goes partially white at times, such as around 23:34:02, in the upper part of the video, suggesting that a gas jet still exists behind the oil jet. Unfortunately I do not have a longer segment than this so can't see what happens later in the video.

Page 72, 1st paragraph, 1st line - major point: How was the buoyancy flow of 400 L/s calculated? If explained elsewhere in the appendix, it should be referenced here. If not, there should be an explanation for how this number was determined.

Page 72, 3rd paragraph, 2nd line - major point: How was the gas flux of 400 L/s converted to an equivalent oil flux to get 33,500 bbl of oil per day? I understand the 50:50 factor, but the gas flow of 400 L/s of the first paragraph yields a daily volume flux of gas of about 233,000 bbls. I'm assuming that this was converted to a liquid equivalent at depth to get the oil volume. How was this done?

Page 74, equation - major point: A factor of 0.8 is used for the oil ratio. I assume that this is the oil to gas ratio. Why is 0.8 used as opposed to the 25% number cited earlier? Is this because the region/time being examined is in the oil phase? This raises the question of whether the 25% is a temporal average of oil to gas or an instantaneous value. My understanding is that it is a temporal average in which case it should be used for the oil phase. This would reduce this estimate by at least a factor of 2. What am I missing here?

Page 76, above Fig. 10 - major point: I was a little surprised by the comment that the eel accelerated toward the main plume. In the segment that I mentioned above, I noticed a number of small particles drifting through the field of view. The first is a dark particle (with a shadow on the pipe suggesting that it was quite close to the pipe) that appears around. It was entrained into the flow at the exit of the pipe accelerating significantly around time xx being entrained into the flow in a few frames. In contrast, a white particle, probably a hydrate, flows OUT of the plume around 23:33:59 and slowly drifts away from it. There is a bulge in the plume under this point that flows out with the particle for a few frames but then it retracts while the particle continues to move away from the plume. It is not clear how strong the entrainment by the plume is from these particles. It would be interesting to look at a number of such particles in the higher resolution videos to see what their motion is like. My concern with the eel observations is that fish and eels swim often with very little apparent motion of their bodies/fins hence one could easily confuse an acceleration due to entrainment with one due to self advection.

Page 79, above Fig. 13 - minor point: This figure is a bit difficult to interpret. First, the labels above the figures get a bit mixed up. Second, and more importantly, it is not clear what is being tracked from one frame to the next. I'm assuming that the yellow lines indicate features that were tracked. A caption explaining the figure would help.

Page 83, discussion of the difference between HDIV and manual tracking - major point: The author notes that the HDIV and manual tracking differ substantially with the HDIV providing regions of very low velocity along with other anomalies. It may be that the manual tracking was drawn to well defined feature which may have biased these observations to quickly moving features in that the eye will tend to pick these out. It might be of interest to plot the manually tracked velocities on the HDIV field of Fig. 14.

Reviewer 6

The body of the report gives a fair and accurate summary of the separate and independent studies conducted by the several investigators on the Team. The conclusions accurately state the results. The statistical study is a useful method of combining sometimes disparate results and presenting a leavened assessment of the flow rate. It gives an answer that passes the sanity tests.

Hereafter, my review is restricted to the investigations that measured the flow rate by image analysis.

Appendix 4-Dr. O. Savas

2.1 The 'guess' for the Reynolds number stated in Eq. (4) of Savas' report is not justified by any fact relevant to the oil release, and the subsequent estimate of 3,700 m^3/day is based directly on this assumption. I recommend it be deleted from the report.

2.2.1 The inverse decay law for jets is not valid in the first 10-15 jet diameters from the exit because of the non-similar initial condition of the jet as it exits the pipe. Therefore extrapolations based on 1/x behavior should not be trusted, especially if they are used to estimate velocity close to the (unknown) location of the virtual origin.

2.2.2 The discussion of PIV seems to generalize from Dr. Savas' experience with his 'in-house' PIV/ALPT system to all PIV systems when he extrapolates the fact that that he could measure "only a handful of independent vectors" to all PIV systems. It would be more prudent to restrict his conclusions to the measurement system that he dealt with.

Appendix 4 Supplemental Report- Post-cut analysis

In this analysis the velocity of fluid is measured in the jet plume issuing from the riser after the damaged pipe had been cut off. The flow in this plume is simpler than the leaks from the broken pipe, and it is more amenable to analysis.

Three methods of image motion analysis were used:

1. Direct visual tracking of large eddies,
2. Direct visual tracking of instability waves at the exit of the tube, and
3. Conventional PIV correlation on the **green** channel of the TIFF images.

The table presented in the Supplemental Report indicates relatively close agreement between the three methods:

Table 5: Supplemental report summary.

Method	Oil Discharge Rate (m^3/day)	Remarks
Large Eddy tracking	7,100	Most likely
Instability wave tracking	4,600	Conservative minimum
Image velocimetry @ 32×32	6,400	Maximum from Table 4
Image velocimetry @ 64×64	5,900	Maximum from Table 4
Image velocimetry @ 128×128	5,900	Maximum from Table 4

The difference between PIV and large eddy tracking is much less than the difference between min and max of large eddy tracking. Hence, PIV speed = large eddy tracking speed to within the error bar. This is reassuring.

Why does Figure 9: Sample PIV result.... show velocity in the seawater surrounding the jet that is almost as large as the jet velocity, itself?

Appendix 5-Dr. S. Wereley

The analysis is straight-forward. EDPIV, a custom software analysis that was developed in-house. the final calculation of daily leakage uses 29% oil, instead of 41%, as used in the other investigations.

Appendix 6-Dr. I. Leifer

The post-cut plume was analyzed by hand, yielding velocities of 130+_20 cm/s and by hierarchical deformation image velocimetry, yielding 20-30 cm/s, apparently when averaged over the plume. The HDIV measurements were considered to be too low and were not used. Could the low value have resulted from averaging over the whole plume? This appendix emphasizes that "The largest uncertainty is the extrapolation from 3 seconds of data to a daily rate. Natural seep systems can vary by orders of magnitude on short time scales from minutes."

Appendix 7- Dr. F. Shaffer, et al.

This Team estimated the maximum leak rate using three different methods:

- "The first analysis approach was to measure oil jet velocities using Feature Tracking Velocimetry, which is similar to Particle Image Velocimetry (PIV) using NETL's proprietary high speed PIV software (Patent Pending, U.S. Patent Application No. 12765317); this analysis was applied to one jet at the riser kink and to the jet at the riser end.
- The second analysis approach analyzed the trajectory of the buoyant jets and estimated the flow rate based on the established theory of turbulent jets; this analysis was applied to the same plumes as the FTV analysis (namely, one jet at the riser kink and the jet at the riser end).
- The third analysis approach involved computer simulations of the multiphase jet at the riser end using computational fluid dynamics (CFD); the comparison of jet profiles from these simulations with profiles seen in the ROV images of the riser-end jet provided confirmatory observations for the range of the maximum potential flow rate."

This team preferred to use manual feature tracking, but no review comments are offered because the report did not contain their analysis of the post-cut plume.

Appendix 8- Dr. J. Lasheras, et al.

A significant contribution of this team's effort is that they "have resolved the inconsistency in the PIV measurements by focusing on the same very near region of the jet development, closer than 1 diameter to the riser pipe's end. The results are shown in Figures 20 and 21. We all measure a maximum velocity of V_max ≈ 0.58 m/s (UCSD, UW, and Purdue)." Given this consistency, the greatest uncertainty is the ratio of the bulk velocity of the jet to the velocity measured at the oil-seawater interface.

Review Summary

There are uncertainties in the measured velocity at the exit of the post-cut riser of approximately +/- 30%. The range of 35,000 to 60,000 bbl/day stated in the report allows for additional errors associated with factors other than velocity measurement. The latter uncertainties that cannot be resolved without further research. They are:

1. The ratio of the measured velocity at the oil-seawater interface is unknown. Estimates in the report range from 1.2 to 2.9, implying a =/- 42% error in the inferred flow rate. This uncertainty can be resolved by laboratory experiments.
2. The percent oil is estimated to be between 29% and 41%. The majority of investigators used 41%, and it will be difficult to improve much on this number.
3. The flow rate varies significantly in time, and measurements of the necessarily short periods during which videos are available do not suffice to document this variation.

The approach of the USGS in obtaining independent estimates from a number of investigators is probably the best way to place error bounds on the best estimate of oil leakage per day, given the available data and the intended purposes of the answer.

Replies to Reviewers

Background - Lehr

I would like to thank the six reviewers who provided their assessment of this report. As was the case with the Plume Team itself, the reviewer list was chosen to meet the two criteria of professional excellence and diversity of viewpoint. Their assessments indicate that both have been met. Because of the emergency nature of this work, reviewers and authors suffered under extreme time constraints. Yet, none that were asked refused to participate or failed to meet their commitments. My gratitude to all of them.

This report will hopefully provide a valuable resource to future spill scientists and responders as the Nation prepares for the inevitable next big spill. However, the nature of the document should not be misunderstood. It was not intended as a comprehensive research study similar to those produced by the National Academy of Science. There will perhaps be such a study in the future and this report will provide important background material. Instead, this report tries to capture the methods and thoughts of the Team as it reached consensus to advise the National Incident Command on the oil flow rate. For this reason, I must take exception to some comments by reviewers 2 and 5. The introductory background material was not intended to be a summary of the individual appendices, but rather to provide a basic explanation of the PIV method and to record the consensus results. This consensus was reached prior to the documenting material in the appendices and changing the section to include them would not accurately represent the process. Appendix 1, however, does provide statistics on the individual estimates based upon the most recent individual reports.

Appendix 4 –Savas

General Remarks to FRTG Reviewers' Report

Due to possible communications problems during the switch-over of our email server, I received the Reviewers' report late on Thursday, July 15, 2010. Because of this time constraint, I will only write some generals remarks about my report, for responding to specific comments from the Reviewers requires careful considerations, hence require more time.

The flow estimate from the end of the riser before it was cut-off is the most difficult, which I have shunned. The reason is that it is a semi-confined multiphase (oil, gas, hydrates) jet flow, whose discharge profile is uncertain. My very first estimate of the flow rate there is reproduced below from an email I sent to Prof. Juan Lasheras (President of APS/DFD) on May 14, 2010

"*Using the celerite[sic] of the large eddies at the edge of the plume to estimate the mean discharge flow velocity (80 cm/s, underestimates), and assuming a fill factor of 1/3 for oil (from the video), I come up with oil discharge rate of 5100 m3/day or (43,000[sic][9] barrels/day) for the 21-inch diametr[sic] pipe.*"

[9] 5100x8.6 =43,000 dry barrels, 5100x6.3=32,000 bbl

This estimate, though highly uncertain, is closer to the CFD estimates than the PIV estimates carried out by the group members.

After the riser was cut-off at the BOP, the flow estimation task became less uncertain.

The features near the exit plane can be actually tracked with PIV. But they are not flow velocities, but the phase speeds of the instability waves. The connection of the phase velocity to fluid velocity is clear only if the profile behind them is uniform. In our case, the velocity profile has at least one valley and two peaks, most likely a gorge and two ridges due to the drill pipes (2) in the bore. Further, the lighter color jet from the drill pipe is faster, therefore, anything claimed to have been measured on it is just noise. Actually, PIV shows (both the group's and mine) slower velocities at the jet discharging from the drill pipe. PIV application there is trying to capture eddy sizes, not displacements. Any connection between the waves and the flow through idealized profiles is tenuous. The PIV results are shown to illustrate that a wide range of numbers can be obtained depending on particular choices one makes.

Buoyancy effects are visible in the jet after the cut-off, as its lateral spread is slower than that of typical momentum dominated jet. For this reason, I was carful in extrapolating the large eddy velocities to the discharge velocity at the exit plane of the jet.

Ömer Savas
July 16, 2010

Appendix 7 - Shaffer

This section contains responses to external reviewers' comments on the three separate analysis approaches used by the USDOE National Energy Technology Laboratory. The responses are separated based on the analysis approach. Reviewer *comments are italicized and colored blue*.

Responses to External Reviewers' Comments on Analysis Approach 1: Manual Feature Tracking Velocimetry

The Reviewers mention that there were large differences in velocity values measured by different Plume Team members. The reasons for the differences in velocity measurements are a critical issue and must be resolved and understood. The difference in measured jet velocities are summarized in the table below for the two measurement techniques (automatic PIV and manual FTV) for all three oil jets.

	Automatic PIV						Manual FTV		
	Alisedo	Lasherus	Wereley	Savas	Leifer		Leifer	Savas	Shaffer
Riser Kink Jet		**1.25 m/s** at 0.45 m downstream	**0.18 m/s** at 0.5 m downstream					**1.5 m/s** at 0.7 meters from exit	**1.7 m/s** at 0.6 meters from exit
Riser End Jet	**0.12 m/s** at 0.5 m downstream	**0.12 m/s** at 0.5 m downstream	**0.19 m/s** at 0.5 m downstream of exit				**1 m/s**[1]	**1 m/s**[1] near jet discharge	**0.8 m/s** at 0.8 m downstream
Post Riser -Cut Jet	**0.25-0.58 m/s** at < 0.5 m downstream	**0.4- 0.5 m/s** at 0-1 m downstream	**0.51 m/s** at 0.3 m downstream of exit	**0.03-0.35 m/s** at < 0.2 m downstream from exit	**0.2-0.3 m/s**		**1.3 m/s** at 0.5-1.0 m downstrea m of exit	**1.1 m/s** at < 1.5 meters from exit	**1.5 m/s** at 1 m downstream

It is clear that automatic PIV produces much lower velocity values than manual FTV. For the Riser End Jet, automatic PIV measurements are more the five times lower than manual FTV. For the Post Riser-Cut Jet, automatic PIV measurements are two to three times lower than manual FTV.

All automatic PIV measurements are in good agreement for the Riser End Jet and the Post Riser-Cut Jet. However, there is some disagreement in velocity values for the Riser Kink Jet. All manual FTV measurements are in reasonable agreement for all jets.

Three of the six Plume Team members (Leifer, Savas and Shaffer) abandoned the use of automatic PIV software for their estimate of oil leak rate because they considered automatic PIV software to be unreliable this application. They also believe, as stated in their reports, that automatic PIV software will produce unrealistically low values of jet velocity.

It is my opinion that the velocity values from automatic PIV measurements are too low. Automatic PIV software was not designed for this application (measurements using videos of oil jets) and has not been tested or proven reliable for this application. Automatic PIV software was designed to detect the motion of high concentrations of very small particles (about 10 micron in diameter) in a transparent fluid that is being illuminated with a thin sheet of laser light. In this application, the fluid is completely opaque, there are no seed particles, and the flow the entire flow field is illuminated with white light. Automatic PIV software is being applied to try to track the motion of visible features in these oil jets (usually vortices or turbulent eddies), but unlike small solid particles, these features are continually changing in size and shape. These jet features are also many orders of magnitude larger than 10 micron particles.

Even if automatic PIV software can track features in the BP videos of oil jets, the jet features seen in these videos could lead to unrealistically low velocity values. For example, vortices often appear to stop moving in the BP videos, but the core of the oil jet is continuous and steady. It is likely that the paused vortices are either momentarily moving in the direction of the camera, or have momentarily detached from the jet core. Automatic PIV software will measure the motion of slow or paused vortices, thereby biasing the average velocity towards lower values. Also, vortices in such jets exhibit reverse spin. This too could lead to unrealistically low velocity values. These jets also have instability waves that are being detected by automatic PIV software, and the instability waves are moving much slower than the fluid velocity.

The difference in velocity values produced by automatic PIV and manual FTV are critically important because oil leak rate is directly proportional to jet velocity. More study is needed to determine why velocity values are so different, and which are correct.

Specific Responses to External Reviews

Below are my responses to each comment by external reviewer 1 regarding my work, which is Analysis Approach 1, use of manual feature tracking to estimate oil leak rate. The comments made by Reviewers are *colored blue and italicized*.

Reviewer 1- I agree with Reviewer 1's general comments that the discrepancy in velocity measurements by different team members should be explained. I also agree that the assumptions made by each individual team member in the calculation of oil leak rate should be compared and better explained.

Reviewer 1 made the following comments about my analysis:

Comment: *"Feature tracking analysis: At the kink jet, a feature velocity of 1.7 m/s was estimated far down stream of the exit (0.6 m). Close to the riser exit (0.8 m, or about 1.6 jet diameters) the plume velocity is estimated to be 0.8m/s (when oil is flowing). This velocity for the riser exit is much higher than the other estimates (~0.2 m/s) for unknown reasons. Flow rates are estimated based on the areas of the jets (both riser exit and kink jets) at the measurement location, 29% oil fraction (at the kink) and 50% oil duty cycle at the riser exit.*

There are several problems with these calculations. These include, neglect of the differences between bulk velocity and feature velocity, the neglect of entrainment of water in the kink jets, the inconsistent and perhaps erroneous velocity in the riser outlet plume, and the neglect of almost all sources of uncertainty resulting in a claimed 10% uncertainty. Together, these problems cast significant doubt on the reliability of the estimates."

Response: I do not agree with the judgments of Reviewer 1 that my velocity measurements are "*inconsistent and perhaps erroneous in the riser outlet plume,"* nor do I agree that with the judgment that *"these problems cast significant doubt on the reliability of the estimates."*

The judgment that my manual FTV measurements are *"inconsistent and perhaps erroneous"* is made without any explanation. My velocity measurements of around 1 m/s (0.8 m/s at 0.8 meters downstream from the jet exit) at the Riser End Jet are in good agreement with manual feature tracking estimates by two other Plume Team members (Leifer and Savas). Measurements with automatic PIV software (Alisedo, Lasherus, Wereley) do produce much lower velocities, around 0.12 m/s for the Riser End Jet.

The discrepancy between automatic PIV measurements and manual feature tracking measurements is a very important issue. I have revised my section of NETL's final report (Appendix 7) to better explain why I abandoned automatic PIV and how I conducted my manual FTV measurements.

Comment: *"Flow rates are estimated based on the areas of the jets (both riser exit and kink jets) at the measurement location, 29% oil fraction (at the kink) and 50% oil duty cycle at the riser exit."*

Response: This is correct. The values are different because at the Riser Kink Jet oil and gas are mixed (gas is dissolved into the oil). In the long horizontal length of pipe between the Riser Kink Jet and the Riser End Jet, all gas separates out of the oil. So only time intermittency needs to be taken into account when calculating oil flow rate from the Riser End Jet.

The issue of the correct value for oil volume fraction at the Riser Kink Jet and Riser End Jet was largely unresolved at the time team members submitted their sections of the Plume Team final report. This issue was clarified during a meeting with Secretary of Energy Chu's team on June 14. During this meeting, the Plume Team was informed that the volume expansion of oil from the sea floor to the sea surface had to be taken into account in the calculation of total oil leak rate. Oil expands by 35% in volume when brought from the pressures at the sea floor at the BP Horizon well site to the sea surface. The Plume Team is now using a value of 0.4 (or 0.41) for oil volume fraction when calculating total oil leak rate at the sea surface. The NETL report has been revised to consistently 0.29 for oil volume fraction at the Riser Kink Jet and Post Riser Cut Jet, and 0.4 for time intermittency at the Riser End Jet. Calculations of oil flow rate at the sea surface must take into account a 35% volume expansion of oil from sea floor to sea surface. The NETL report has been revised accordingly.

Comment: "*There are several problems with these calculations. These include, neglect of the differences between bulk velocity and feature velocity, the neglect of entrainment of water in the kink jets,…"*

Response: It is correct that I did not discuss the issues of jet velocity profile and water entrainment in the calculation of oil leak rate from the Riser Kink Jet and Riser End Jet. However, these issues were not ignored. My report has been revised to better explain these issues.

When I did my estimate using manual FTV, I did have access to NETL's Analysis Approach 2 which is based on jet theory. Values for velocity profile and water entrainment are calculated in Analysis Approach 2. I did not include these issues in my Analysis Approach 1 for two reasons: (1) these effects offset each other and do not significantly change my oil leak rate estimate and (2) to avoid confusion and redundancy with Analysis Approach 2, I did discuss these issues in my Analysis Approach 1. I have revised my analysis to discuss and include the effects of velocity profile and water entrainment.

Comment: *"and the neglect of almost all sources of uncertainty resulting in a claimed 10% uncertainty."*

Response: Reviewer 1 does not give any explanation or justification for the statement that I *"neglect almost all sources of uncertainty."*

Like many issues during the Plume Team's work, the issue of uncertainty was an ongoing issue and the approach to handle uncertainty changed throughout the Plume Team's operation. It was my understanding that NIST was handling the issue of total uncertainty in velocity measurements and individual Plume Team members were not to do a full uncertainty analysis. At the time this final report was written (around June 12), the issue of how to handle uncertainty was still not clear to me. So I included an estimate of measurement uncertainty in my analysis. I could have explained my uncertainty estimate better, and with adequate time I would have, but the Plume Team's estimate was done (as stated at the beginning of the Plume Team final report main body) without enough time and information.

I have revised my section of the NETL report to better explain my estimate of measurement uncertainty. The estimate was based on a combination of all measurement uncertainties in a manual FTV measurement using established principles for calculating measurement uncertainty. The most significant uncertainty arises from video pixel resolution (704 x 576 pixels for pre riser cut jets). Velocity values were based on tracking a flow feature for an average of 20 to 40 pixels. The pixel resolution leads to a measurement uncertainty of +/- 1 pixel. For a distance of 20 pixels, this results in an uncertainty of +/- 5%. I increased my estimate of measurement uncertainty to +/- 10% to account for user subjectivity in detecting the location of flow features.

My estimates of the sources of measurement uncertainty for velocity measurements are too far from other team members' estimates. For example, Professor Savas also uses the same value of +/- 1 pixel for measurement uncertainty due to pixel resolution. His total measurement uncertainty is 25% (e.g., 150 cm/s +/-40cm/s). Professor Wereley uses a total uncertainty of +/- 20%. Dr. Leifer estimates measurement uncertainty to be 20% to 40%.

I have increased my estimate of measurement uncertainty from 10% to 25%. This is in good agreement with all other team members' estimate of measurement uncertainty for jet velocity.

Reviewer 2

Comments: *"The authors of Appendix 7 use three different methods to measure the oil flux: feature tracking (akin to PIV), theoretical analysis and computational fluid dynamics. They do a very competent job, and like some of the other appendices, their results could stand in for the entire report (but credible results from other groups reinforces the results and shows their spread)."*

Response: I agree.

Reviewer 3 -Reviewer 3 only addressed NETL's CFD analysis. All other analyses by all other Plume Team members, including mine, were ignored.

Reviewer 4

Comment: *"It is generally better to use various different approaches to estimate the oil discharge rate, because each has its own limitations and uncertainties. I added some additional ways to evaluate the oil discharge rate."*

Comment: *"A second valid approach to estimate the oil plume exit velocity, thus the oil discharge rate, is to use a buoyant plume analysis (e.g., trajectory and width analyses) with and without the use of computational fluid dynamics codes. Appendix 7 shows the usefulness of this approach to estimate the oil discharge rate. This approach uses the overall behavior of the buoyant plume, as compared to the PIV method using a local plume velocity field."*

Comment: *"I strongly support a plume analysis to be a part of the oil spill assessment, as performed under Analysis Approaches 2 and 3 of Appendix 7."*

Response: I am in complete agreement with these statements. Given the national importance of this estimate, and given that automatic PIV has not been tested and proven for this application, and given that there are large discrepancies between velocity values measured with automatic PIV and manual FTV, it is imperative to use alternate analysis methods for estimation of oil leak rate.

This is why NETL used three independent analysis approaches. When a primary analysis method (automatic PIV) is untested and unproven for an application, it is always prudent to find alternate methods to verify the credibility of the primary analysis method

Below are the specific comments of Reviewer 4 regarding my Analysis Approach 1 using manual FTV.

Comment: *"In Appendix 7, for the velocity estimate using the PIV method, the velocity at the edge of the plume is assumed to be the average velocity across the plume cross-section…. This estimate is very conservative as the maximum oil discharge estimate… This is also true for the oil discharge estimate at the kink location based on the velocity estimate at 60 cm downstream."*

Response: I agree with Reviewer 4's comment that I did not include a velocity profile in my estimates of oil leak rate from the Riser Kink Jet and Riser End Jet. As I explained in my response to Reviewer 1, for the Riser Kink Jet the issues of velocity profile is discussed in NETL's Analysis Approach 2. I have revised my report to include and discuss the effects of velocity profile and water entrainment.

Comment: *"Appendix 7 also assumes that the total oil flow rate from the riser kink jets to be twice of the oil discharge of the J1 jet. Subsection 3.1 of Appendix 4 states that the jets J and J2 are stronger than J1. Is it better to assume that the total oil discharge is about three times the J1 discharge?"*

Response: This is a valid point. But the entire Plume Team adopted the estimate that the total oil leak rate from the Riser Kink Jets is twice that of jet J1. I used the same assumption that the rest of the Plume Team used.

Reviewer 5- Reviewer 5 did not review my analysis or other NETL analyses. Reviewer 5 did make the following comments on the entire Plume Team report:

Comment: *"…I found the report itself to be very weak. Basically, it relies on the reader to sort through all of the appendices to understand the numbers presented. Specifically, it is not clear where the numbers presented in the Executive summary and in the body of the report come from nor what they mean. Furthermore, the numbers presented in the report are not consistent with one another. Had the report presented a coherent summary of the work presented in the appendices it would have been a lot easier to read and a lot more believable."*

Response: I agree.

Reviewer 6-Reviewer 6 did not comment on my report.

Responses to External Reviewers' Comments on Analysis Approach 2: Application of Turbulent Jet Theory

by Nate Weilend and Geo Richards

Reviewer 1

Comment: *Similarity analysis: For the kink jet flow rate, this analysis attempts to eliminate some of the problems described above by using the feature velocity measured in a self-similar jet solution. However, the authors are left guessing at important sensitive parameters such as R, the result appears no more reliable than before.*

Response: Admittedly, the crux of this analysis lies in the analysis of the velocity profile across the jet. Due to the exponential expression in the Gaussian profile, the results are very sensitive to the radial measurement location, *R*, which cannot be determined with any better accuracy with the available videos and methods. Regardless, this analysis quantifies this uncertainty rather than assuming a centerline to measurement velocity ratio, as other analyses have done, hence, it is expected that this analysis of the kink jet should yield lower uncertainty than other analyses where this has not been considered. In the larger scheme, the total oil from the kink jets are about 20% of the total oil leak rate, so large uncertainties here are less important in the overall oil leak rate calculation.

Comment: *For the riser exit jet, a theory for buoyant jets is used, which looks to be inapplicable. The analysis used was apparently based on gas mixtures (hydrogen and helium in air), and depends on an estimate of the density at stoichiometric conditions, which is certainly meaningless in this case. The estimated exit jet velocity from this analysis (3 m/s) is totally inconsistent with observations, even the anomalously large velocity estimates of the author's analysis above. This purely theoretical jet analysis does not provide a reliable flow rate estimate, and is essentially invalidated by the observations.*

Response: The analysis is applicable to any mixture of fluids in which there are density differences. That it has previously been applied to helium/hydrogen jets does not invalidate its usefulness in the current approach. While the density at stoichiometric conditions (typically the lowest density in the system) does not apply, the jet exit density is a suitable replacement, being the lowest density present in the current analysis.

The larger velocities of 3 m/s are not completely inconsistent with the observations, which are only seen on the outer edge of the riser end jet, where the interior (unseen) velocity can be much larger than those at the edge. The CFD simulations in Approach 3 support this claim.

Reviewer 2

No comments.

Reviewer 3

No comments.

Reviewer 4

Comments: *A second valid approach to estimate the oil plume exit velocity, thus the oil discharge rate, is to use a buoyant plume analysis (e.g., trajectory and width analyses) with and without the use of computational fluid dynamics codes. Appendix 7 shows the usefulness of this approach to estimate the oil discharge rate. This approach uses the overall behavior of the buoyant plume, as compared to the PIV method using a local plume velocity field.*

There have been a large number of field measurements, laboratory hydraulic flume/basin experiments, and numerical models for a buoyant plume trajectory and mixing analysis associated with heated water and sewage/industrial waste effluents released to surface waters (Abraham1963, Fan and Brooks 1969, Sharazi and Davis 1972). Although there are some recent studies, most of the cited studies have been conducted in 1960s to mid 1970s. One caution when using this approach to estimate oil discharge rate, is that the plume trajectory is very sensitive to the ambient flow. Although there may be some intermittent ambient flows in this depth, it is reasonable to assume (at least initially) that the ambient flow velocity at the bottom of the Gulf of Mexico at 5,000 ft deep is almost zero. However, Appendix 6 indicates that the ambient velocity there may be 0.1 ~ 0.2 m/s due to the existence of the trench. If the actual ambient flow is horizontal, the computed plume trajectory with the assumption of a stagnant ambient flow would significantly overestimate the plume inertia at the end of the riser to match the observed oil plume trajectory. This leads to the significant overestimation of the plume exit velocity, thus, the oil discharge rate. If the actual ambient flow is more vertical, the computed plume trajectory with a stagnant ambient flow significantly overestimates the plume buoyancy to match the observed oil plume trajectory. This leads to the significant underestimation of the plume exit velocity, thus, the oil discharge rate. Beside plume exit velocity measurements suggested in Appendix 6, velocity measurements of the ambient flow may also be needed.

Response: The ambient flow, in the case of the riser end jet, is likely induced by water entrainment into the jet. Since the theoretical analysis does include water entrainment by accounting for jet spreading, a flow induced ambient velocity is not entirely outside the scope of the theory. Further, ambient flows of 0.1 – 0.2 m/s are only about 5% of the estimated jet velocity using this analysis, and are not likely to affect the analysis as significantly as some of the other sources of uncertainty. For these reasons, the ambient flow velocity is not included in this analysis, but may serve to reduce the overall flow estimate somewhat as suggested above.

Comment: *Appendix 7 also assumes that the total oil flow rate from the riser kink jets to be twice of the oil discharge of the J1 jet. Subsection 3.1 of Appendix 4 states that the jets J and J2 are stronger than J1. Is it better to assume that the total oil discharge is about three times the J1 discharge?*

Response: It may be better to assume 3x the J1 discharge, but NETL has followed the lead of other FRTG members in conservatively estimating a doubling of the J1 flow rate.

Comment: *I strongly support a plume analysis to be a part of the oil spill assessment, as performed under Analysis Approaches 2 and 3 of Appendix 7. It should cover both the close proximity of the BOP/the end of the riser in a short-term, and regional-scale in the longer time frame. Analysis Approach 2 of Appendix 7 describes three different methods; the first method is based on the ambient flow entrainment, the second method uses the pressure drop across the kink, and the third is based on the plume trajectory angle. The first method led to a conclusion that the oil-gas mixture is diluted by 6.7 times by the ambient water, and its plume width is 30 cm (16 times the kink opening diameter of 1.9 cm) at 60 cm downstream (32 times the kink opening diameter). These values at 60 cm downstream are consistent with the dilution and the plume width I estimated with different approaches, as discussed here.*

Comment: *Method 2 used under Analysis Approach 2 of Appendix 7 depends on the value of the pressure drop across the JI jet opening. Unless 400 psi pressure drop used in the analysis was actually a measured value across the J1 jet opening, there is a large uncertainty on the pressure drop estimate of 400 psi. There is a large uncertainty on the pressure drop through a well from the oil reservoir to the sea bottom. Thus, I consider Method 1 based on the plume entrainment assessment has a greater probability of being more accurate than Method 2 based on the pressure drop.*

Response: Agreed. The 400 psi pressure drop is attained from Appendix 2, where no uncertainty estimates accompany this number.

Comment: *Method 3, Analysis Approach 2 of Appendix 7, uses somewhat similar approach to what I used, as described below. The modified Froude Number defined in Appendix 7 is different from more common definition of the densimetric Froude Number shown in Equation 2 here. Please define parameters, ρ_0 and ρ_∞ of the modified Froude Number. The left plot of Figure 13 in Appendix 7 shows a reasonable match between the actual plume and the predicted plume trajectory. However, the estimated oil discharge of 86,000 bbl/day is much greater than what I estimated as described below. The actual plume rise shown in this plot rose less sharply than the one I saw on Yahoo.com and used. Thus Appendix 7's oil discharge estimate is much greater than my estimate. This discrepancy may be a reflection of the temporal variability of the plume coming out from the end of the riser.*

Response: Definitions of the various Froude number densities are already included in the report. The flow rate in our analysis has been decreased 20% by using a more accurate measurement of the flow intermittency of 0.4, similar to that used by the other FRTG members. Finally, of the 6 images analyzed, one was from a video with a noticeably lower (i.e., more buoyant) oil flow rate. It is uncertain whether or not this is the video that the reviewer was analyzing, but the choice of the 6 images analyzed is roughly consistent with the amount of time each flow regime was observed in the videos supplied.

Reviewer 5

No comments.

Reviewer 6

No comments.

Responses to External Reviewers' Comments on Analysis Approach 3: Application of Computational Fluid Dynamics Simulation of the Riser End Jet

by Mehrdad Shahnam and Madhava Syamlal

Reviewer 1

Comment: *CFD Analysis: The authors undertook a CFD analysis to try to determine the flow rate that would be required to produce results that were qualitatively similar to the images. Unfortunately, these simulations also appear to be unreliable. The authors provide no indication of the grid resolution or its adequacy, except to say that a coarse mesh that allowed the computations to be done quickly enough was used. It is common in CFD to get qualitatively incorrect results with inadequate resolution, and without evidence to the contrary, this must be considered as a significant possibility here. Also, no mention is made of turbulence models, which should be necessary here, the validity of the multi-phase models used, or the validity of the turbulence models for this case. In short, this is a complex computational modeling problem, and computational results cannot be relied on without significant verification and validation.*

Response: The case and data files of the simulations containing complete information about the simulations have been archived and will be made available as necessary to other investigators. Information on grid and turbulence model has been now added to the report and a grid independence study has been reported.

The reviewer is right that computational results cannot be relied upon without extensive verification and validation. That is one reason we relied on the commercial code FLUENT, which undergoes extensive verification tests to prove that the solution given by the code is indeed the correct solution of the mathematical equations. In the validation step one shows that the mathematical equations represent physical reality. FLUENT volume of fluid model (the multiphase model used in this study) has been used for simulating various two-phase flows, including the simulation of oil spill cleanup using boom (http://www.fluent.com/solutions/articles/ja127.pdf).

Reviewer 3

Comments on DOE NETL CFD Simulations of the Riser End Jet

This review is regarding the CFD simulations of the riser end jet reported in Appendix 7 (Analysis Approach 3 by the DOE NETL team). CFD simulations were performed using the ANSYS FLUENT code. Several simulations at different flow rates were performed, and then the flow rate that produced the best result, matching the shape and trajectory of the oil jet seen in the videos provided by BP, was assumed to be the right flow condition. I have several concerns, some serious and some minor, as described below.

Comment: *1. First and utmost, although a commercial code, such as the Fluent code used here, can provide some insight into complex flow phenomena, one has to be cautious in interpreting its quantitative information. Furthermore, it was difficult to assess the validity of the present results since the author did not provide sufficient information in the report. If this report were to be led as an official government report, the authors are recommended to provide more detailed information, some of which are mentioned below, so that anyone who wishes to do so could repeat the same or similar simulations.*

Response: All the additional information requested by this reviewer and others has been added to the report. In addition, the case and data files of the FLUENT simulations containing complete information about the simulations have been archived and will be made available as necessary to other investigators.

Comment: *2. Considering the Reynolds number involved (and as confirmed in the video images), the entire flow must be turbulent, but the authors did not specify how their simulations were performed. Were their simulations performed in DNS/LES/DES/RANS? I assumed that they performed coarse LES's. If this was the case, was Fluent's sub-grid scale model capable of predicting two-phase turbulent flows with confidence?*

Response: We did not use an LES model. We used a volume of fluid model, including a two-phase (sea water, oil) realizable k-ε turbulence model, with standard wall functions. No subgrid-scale turbulence model was required as we did not use LES.

Comment: *3. No information on the numerical grids (\a reasonable ' worst case' course (typo?) mesh was employed" does not belong to a technical report) was given. Assuming, again, it was LES, was the wall region in the riser pipe properly resolved? In other words, was it a wall-resolved LES or was a wall-function used instead? At the minimum, the total number of grid points in each direction and the grid information inside the riser pipe (preferably in terms of wall units) must be given so that the readers, if necessary, can make their own judgment on the accuracy of the numerical results. Plus, the flow inside the riser pipe could have been used as a validation of their simulations (see below).*

Response: Grid information has been added to the report, including the Y^+ inside the pipe. We did not say 'worst case' mesh. The typo (course instead of coarse) has been corrected. We did not use LES model and a wall function was used with the realizable k-ε turbulence model. See the rebuttal to comment #6 regarding the last comment about validation.

Comment: *4. Boundary conditions were too vague. At the inlet (inside the riser pipe), it was stated that a volume flow rate was specified. What mean profile? What turbulence fluctuations? Were the results insensitive to the inlet conditions? At the exit of the computational domain, the ambient pressure was prescribed. It is not clear how this was implemented since for incompressible flows, pressure itself does not enter into the problem, and boundary conditions for the velocity components need to be specified. Also, how was the sea-floor treated? If the no-slip condition was used, was the wall layer adequately resolved or modeled through a wall function? The use of a symmetry condition for the left and right planes (from the view of Fig. 14) seems to be somewhat odd. In particular, did they examine the affects of the symmetry condition at the left plane on the computed results?*

Response: Additional information on boundary conditions has been added to the report. At the inlet a flat velocity profile was used and sufficient pipe length (L/D= 24) to allow the flow to develop. The turbulence intensity specified was 10%, which is the default value in FLUENT and a standard value used in absence of exact knowledge of the turbulence intensity as in the present case. We did not study the sensitivity of the results to this parameter, which we do not expect to be high.

The specified pressure outlet boundary condition is indeed the appropriate condition in the present case, and velocity components cannot be specified at the outlet. The reviewer is correct that the absolute value of pressure does not matter, in the incompressible simulation we conducted. We specified an absolute value for the pressure in our simulations because we were expecting to conduct compressible three phase simulations (sea water, oil, gas), when the absolute value of pressure would matter. This does not cause any error in our incompressible computations, however.

The sea floor was modeled as a no-slip wall and the wall layer modeled with a wall function.

The symmetry condition is indeed the appropriate boundary condition for the problem. The only question is how large a domain should be used for the simulations. We want the symmetry walls to sufficiently far away from the region of interest where the oil jet shoots into sea water. We took care to impose the symmetry condition sufficiently far away from the jet exit. One study was done with the upstream symmetry plane at L/D=10 and the downstream symmetry plane at L/D=30. A second study was done with upstream symmetry at L/D=0 (right at the point of oil jet exit) and the downstream symmetry plane at L/D=30. No difference was seen in the plume penetration and lift as the result of moving the upstream symmetry plane right at where oil jet is being discharged. So the domain size (as governed by the location of the symmetry walls) considered in our simulations is adequate.

Comment: *5. The diameter of the riser pipe suddenly decreases at the end, forming a nozzle-like shape (Fig.4 in this report and according to other images I have seen). It is not clear from the report how this was modeled. It looked like that they treated it as a tapered pipe (Fig. 14 in the earlier report submitted on June 15, 2010). This could be a critical point since they used the amount of back flow as one of their primary diagnostics. The nozzle-like shape at the end would have caused a stronger jet (known as the thumb effect as one would put a thumb at the end of a hose to get a water jet reaching further), which could have significantly affected the nature of the back flow at the exit of the riser pipe.*

Response: The riser exit was modeled as an abrupt change in the diameter from 19.5" to 13.78". That's all we know about the riser exit geometry even today. We agree that the exact exit geometry would influence the sea water back flow, which we used as a criterion to rule out the especially low oil flow rates. But we expect that the important effect is that of the exact area of the exit, which we have captured in our simulations.

Comment: *6. Did they perform any grid independent test? This is a must if we want to accept any quantitative information from CFD simulations, especially from a commercial code, which, in general, is known to be robust but less accurate. I am particularly concerned with the possibility that a lack of adequate resolutions in the wall region of the riser pipe could have led to an under-prediction of the wall shear (a typical symptom in a coarse LES), which in turn would have affected the nature of the back flow. One validation they could have done was to examine whether the flow inside the riser pipe was well predicted. Considering the long length of the riser pipe, it can be assumed that the flow was a fully developed pipe flow. Given a flow rate, it is easy to check whether the computed results, such as the skin-friction, mean and turbulence fluctuation profiles, agree with known results. If these were not correctly predicted (most likely due the lack of proper resolution in the riser pipe), which provided the inflow conditions for the jet, the jet flow downstream of the pipe cannot be trusted either.*

Response: We had not conducted a grid independency study at the time the reviewed version of the report was written. So we used a grid resolution based on the time limitations. We have now conducted a study to demonstrate grid independency of the results, which is reported in a revised version of the report.

We used a wall function for the riser wall. We did not check whether a fully developed profile was predicted because we do not know whether the flow will become fully developed before the exit. (We know that models in FLUENT have been validated to predict fully developed flows for pipe flows.) In the present case, a buoyant jet issues from the riser exit into sea water and lifts off vertically. There is really no basis for assuming that such a flow is fully developed. We specified sufficient pipe length before the exit to ensure that the flat velocity profile specified at the entrance does not influence the shape of the plume.

Comment: *7. It is my understanding that the jet flow was a mixture of oil and gas, periodically alternating between mostly oil and mostly gas and probably sometime in between a mixture of the two, it seems to be a rather crude approximation to estimate the total oil flow rate based on the simulation of a single phase oil flow (not counting the surrounding water into which the oil jet is discharged) by multiplying an intermittency factor.*

Response: We actually simulated a two-phase flow (sea water, oil) and not a single phase flow. The logic of not considering the gas flow is as follows. The plume team, from hours of observation of the videos, found that intermittently the flow became oil-only and stayed oil-only for a period of time. The simulation considered only that time period and the simulation results were compared only with videos from that time period. So from CFD we are only expecting to predict the oil flow rate accurately during that time period. The actual oil flow rate is then calculated by multiplying the flow rate calculated from CFD with the intermittency factor. This is not a CFD approximation, and is in fact an assumption made in other plume analyses as well.

Comment: *In conclusion, I would be extremely cautious in interpreting the CFD simulations results, in part due to the lack of appropriate information, and in part because they may have been carried out without proper conditions (grid resolution, boundary conditions, riser exit geometry, and possibly the subgrid-scale model and numerical accuracy of the code itself). Understandably, the time was rather limited to perform these simulations, but it would require much more careful simulations and validations before these CFD results could be considered as a relevant source for an estimation of the oil leak.*

Response: The lack of appropriate information is indeed an issue for CFD simulations, just as it important with other analysis techniques used by the Plume Team. We focused on conducting the best possible CFD analyses based on the available information and time.

The questions about grid resolution and symmetry boundary conditions have been resolved by conducting additional simulations with different grid resolutions and domain sizes. The questions about other boundary conditions and riser exit geometry have been answered in the rebuttal and by adding the required information in the report. No sub-grid scale model was required because we did not do an LES simulation.

The numerical accuracy of the code itself is the least of our concerns because the code used in this case (FLUENT) is the most widely used commercial code for CFD simulations by industry and academia. The code is thoroughly tested by the developers by running numerous verification test cases. Many validation studies and application cases using FLUENT have been reported in journal articles and are available from FLUENT website. For example the VOF multiphase model has been used in the past for simulating oil cleanup using a boom (http://www.fluent.com/solutions/articles/ja127.pdf). The analysts that conducted the present CFD study have many years of experience in CFD, especially in using FLUENT as the analysis software.

Appendix 8 - Aliseda

We have included a warning that the calculation of the flow rate from the end of the riser is done in barrels of oil at depth, and not equivalent liquid barrels at the surface as is done in the rest of the calculations. I have also included how the values of 0.25 and 0.41 for the ratio of oil flow rate at the surface to total flow rate at depth were calculated. And finally, I have added the reference for Dimotakis' paper from which we extract the value of square root of the density ratio to modify the factor between the surface velocity and the core velocity in the jet. On the editorial side, I repeated a figure by mistake in the report and I have now eliminated the repeated figure and included the right one.